ISBN 0-315-56320-6

STRUCTURAL RESPONSE OF CURVED BOX GIRDER BRIDGES

A Comparison Study between Model Test Results and Finite Element Predictions

By

Hachem Mahmoud Hachem

A thesis
presented to the University of Ottawa
in partial fulfillment of the
requirements for the degree of
Master of Applied Science
in
Civil Engineering

DEPARTMENT OF CIVIL ENGINEERING
UNIVERSITY OF OTTAWA
OTTAWA, ONTARIO
October. 1988

UNIVERSITÉ D'OTTAWA
UNIVERSITY OF OTTAWA

Abstract

Horizontally curved box girder bridges have become increasingly popular in the light of the complex geometric alignments required in modern highway systems. Their popularity however, is also attributed to other factors such as the modern emphasis on esthetic considerations, their cost effectiveness and their superior structural advantages in comparison with other types of bridges.

The curvilinear nature for this type of structure along with the complex deformation patterns and stress fields developed for different boundary and load conditions have encouraged designers to employ approximate and conservative methods of analysis in designing such structures. Unfortunately, only a small amount of experimental work has been done to determine the response of model or prototype structures and to verify the accuracy of existing methods of analysis.

The Cyrville road bridge spanning the Queensway underpass east of Ottawa, Ontario, was selected as the prototype bridge for the current model study. The prototype structure is a continuous two span concrete box girder bridge having a total circumferential length of 102.4 meters and a horizontal angle of curvature of 16.8 degrees between abutments centerlines. It consists of four 1.83 meter deep box girders supporting the 12.8 meter wide bridge deck which includes two traffic lanes and two pedestrian side walks. The bridge was designed for ASHTO design truck load HS20-44 and was built in 1973 by the Ministry of Transportation and Communication.

The model bridge was designed by Shao R. Guang of Nanjing Institute of Technology and constructed at the University of Ottawa by adopting a linear scale of 1:24. Unlike the prototype, the model structure is of composite construction consisting of four aluminum box girders supporting a 20 mm thick micro concrete bridge deck. Its horizontal angle of curvature follows that for the prototype bridge. The model is supported by two concrete columns at the abutments and by a single solid aluminum shaft at the central section.

In this investigation, the response of the curved bridge model subjected to OHBD design truck loads was examined experimentally and confirmed analytically using the finite element method. The experimental study was confined to the linear elastic

structure behavior whereas the finite element analysis was carried one step further to predict the bridge model response at overloads and ultimate limit states. For the latter, analysis pertained only to material nonlinearity and hence the assumptions of small displacements and small strains were retained. In conducting the analytical study, the general purpose finite element program ADINA was employed.

Case studies on well known curved and straight box girder bridges verified the successful application of the ADINA program in predicting elastic and inelastic behavior of such structures. It was evident that ADINA's isoparametric thin shell element is quite versatile for modelling the various structural components of which the curved box girder bridge is made. Analysis indicated that such structures when subjected to eccentric point loads may require finer discretization in reaching accurate response than those subjected to concentric loads. When modelling bridge transverse boundary conditions, the assumption of stiff diaphragm in-plane action at support sections proved to be influential in terms of both displacement and stress fields. For the cases considered, maximum displacement can be overestimated by as much as a factor of 4 if diaphragm action is ignored.

For the seven eccentric design truck loading conditions employed in the elastic analysis, the ADINA model predictions for maximum displacements and maximum longitudinal normal stresses compared fairly well with the corresponding experimental values. The average percentage errors for maximum normal stress in ADINA's model was 21 % while that for maximum deformation was 35 %. In predicting deformation, the analytical solution has always underestimated the corresponding experimentally measured response. As such, the finite element model was stiffer than the physical bridge model.

The case study on a straight simply supported single box girder bridge subjected to a uniformly distributed load indicated that the absence of end diaphragm elements may not influence the elastic structure response. However, nonlinear analysis indicated erroneous structural response at ultimate limit states if end diaphragm action was ignored. It was evident, at least for the cases investigated, that the ultimate load carrying capacity of the girder can be underestimated by as much as 22 %.

The materially nonlinear analysis for the curved bridge model was carried out using the ADINA program for positive and negative moment load scenarios. The aluminum components of the strucutre were assumed to follow elastic-plastic material behavior, whereas an elastic multilinear-plastic material model was employed for the concrete deck. It was evident that one way longitudinal bending action dominated the response at critical positive moment sections while two way bending action combined with torsion was observed at the negative moment section over the central column support.

Under the positive moment load scenario, the ADINA model predicted failure due to excessive deformation at a total load of 556 KN (125 Kips). Analysis also indicated the formation of two plastic hinges over the critical positive and negative moment sections at failure. For the negative moment load scenario, analysis indicated that a collapse mechanism for the bridge would occur at a total load of 959 KN (216 Kips) as a result of the formation of three plastic hinges, two at the positive moment sections and one at the negative moment section over the central column support.

Acknowledgements

The author expresses sincere gratitude to his supervisor Professor Simon F. Ng for his patience, guidance, and support throughout the course of this study. The financial support from the Natural Science and Engineering Research Council of Canada is gratefully acknowledged.

The financial support and constructive criticism provided by Professor Moe Cheung is greatly appreciated. Sincere thanks are also expressed to Professor Guang R. Shao for his extensive contributions in the design and the testing stages of the experimental program.

The technical staff of the structural laboratory of the University of Ottawa provided excellent workmanship in constructing the physical curved bridge model.

Many thanks to Ms. Elizabeth Sullivan, system analyst of the Academic Computing Center, for her prompt support on the ADINA software.

The author is indebted to his colleagues: Mr. Z. Wasiewicz, Mr. W. Li, Mr. B. Morse and Mr. M. Y. Chan who unselfishly contributed their time and energy in discussing various aspects of this project and gave constructive comments.

To all professors, graduate students and friends who contributed their help and support the author expresses his sincere appreciations.

Dedication

This thesis is dedicated to my parents Mahmoud and Fatima.

Notations

$[B]$	=	Strain–displacement matrix.
$[C]$	=	Material constitutive law matrix.
D_r	=	Radial flexural rigidity per unit circumferential length.
D_θ	=	Angular flexural rigidity per unit radial width.
$D_{r\theta}$	=	Radial torsional rigidity per unit circumferential length.
E	=	Young's modulus.
$\hat{E}$	=	Young's modulus scale factor.
E_a, E_c	=	Young's moduli for aluminum and concrete.
E_t	=	Strain hardening modulus.
F	=	Equivalent OHBD parallel trucks load.
$\hat{F}$	=	Force scale factor.
F^t_{total}	=	Total trucks force applied at time step t.
F_{unit}	=	Unit trucks force.
F_y	=	Yield stress.
I	=	Moment of inertia about the beam neutral axis.
$\hat{I}$	=	Moment of inertia scale factor.
J'_2	=	Second deviatoric stress invariant.
$[K]$	=	Global stiffness matrix.
$[K^e]$	=	Stiffness matrix on the element level.
$\hat{L}$	=	Linear scale factor.
M	=	Longitudinal bending moment.
P	=	Jack force applied to the parallel trucks assemblage.
R	=	Radius of bridge horizonal curvature.
$\{R\}$	=	External load vector.
$\{R^e\}$	=	load vector on the element level.
$\{U\}$	=	Nodal displacement vector.
V^k_n	=	Normal vector for the shell element at node k.
Y_{ep}	=	Distance between neutral axis and elastic-plastic boundary measured in direction perpendicular to original beam axis.
c	=	Distance between neutral axis and extreme fibre.
e_s, e_t	=	Unit vectors along the shell neutral coordinates axes s, t.
$e_{\hat{r}}$, $e_{\hat{s}}$	=	Unit vectors along the cartesian shell-aligned axes r, s.

f'_c	=	Compressive strength of concrete.
f'_{ct}, f'_t	=	Tensile splitting strength of concrete.
f_{cy}	=	Concrete stress at onset of elasto plastic action.
f_{cu}, f_u	=	Ultimate strength of concrete.
f_{ult}	=	Ultimate strength of aluminum.
f_Y	=	Yield strength of aluminum.
l	=	Length of simply supported beam.
r^2	=	Coefficient of determination.
u_k, v_k, w_k	=	Translational degrees of freedom at node k.
x_e	=	Distance from support to edge plastic zone.
Δ_{max}	=	Maximum deflection at mid-span of simply supported beam.
Δ_e	=	Elastic portion of beam mid-span deflection.
Δ_{ep}	=	Elastic-Plastic portion of beam mid-span deflection.
$\Psi(x)$	=	Longitudinal curvature function of a beam.
$\Omega(t)$	=	Load level at time step t.
α_k, β_k	=	Rotational degrees of freedom of the shell element at node k.
γ	=	Shear modulus.
ϵ	=	Element strain vector.
ϵ_L, ϵ_D, ϵ_T	=	Strain components of the rosette strain gage.
ϵ_E	=	Energy convergence tolerance.
ϵ^m, ϵ^p	=	Normal strain for the model and the prototype bridges.
ϵ_{c1}	=	Concrete strain at onset of full plasticity.
ϵ_{c2}	=	Concrete strain at compression failure.
ϵ_{cy}	=	Concrete strain at onset of elasto-plastic action.
ϵ_u	=	Concrete ultimate strain.
${}^t\bar{\epsilon}^P$	=	Accumulated effective plastic strain.
$d\epsilon^p_{ij}$	=	Plastic strain increments.
ζ	=	Displacement increment vector.
η	=	Out-of-balance loads increment vector.
ν_a	=	Poissons's ratio for aluminum.
ν_c	=	Poissons's ratio for concrete.

$\{\sigma\}$	=	Element stress vector.
σ	=	Longitudinal normal stress.
σ_e	=	Standard of error.
σ^m, σ^p	=	Normal stress for the model and the prototype bridges.
σ_{max}	=	Maximum normal stress at beam mid-span.
σ_y	=	Yield stress of the material.
σ_{xx}, σ_{yy}, σ_{zz}	=	Normal stress components in the cartesian coordinate system.
σ_{rr}, $\sigma_{\theta\theta}$	=	Normal stress components in the cylindrical coordinate system.
τ	=	Shear stress.
τ_{xy}, τ_{xz}, τ_{yz}	=	Shear stress components in the cartesian coordinate system.
$\tau_{\theta r}$, $\tau_{\theta z}$	=	Shear stress components in the cylindrical coordinate system.
ω	=	Uniformly distributed load.

Contents

List of Tables

List of Figures

Chapter 1

Introduction

1.1 General

Horizontally curved bridges have become a major feature of highway systems in the past two decades. Elevated freeways and multilevel interchange structures are very common in densely populated cities. A natural outgrowth of such tight geometric restrictions is that modern highway bridges could hardly be constructed without curved alignments.

Among the wide spectrum of bridge types, it is usually those of cellular cross-section that are selected. In addition to their low material content, low weight and high longitudinal bending stiffness, box girder bridges are favored for their high torsional rigidity when compared with open sections. This property in straight bridges leads to nearly uniform transverse distribution of longitudinal flange stresses for eccentric distributed loads. In curved bridges the high torsional moments and deformations are of great importance even for centric loadings and the use of curved box girders seems to have significant advantages.

A typical curved box girder bridge consists of a top and bottom plate connected by curved or conical webs to form the closed structure. The cross-section may be composed of one or a few large cells which are either contiguous or separated. Usually interior cell shape is rectangular while edge cells often have trapezoidal cross-sections with inclined or rounded outside webs.

Transverse diaphragms are commonly used in curved box bridges to improve their torsional characteristics. They are used at end and intermediate support points; however, in some cases, such as bridges with relatively large horizontal curvatures, additional interior diaphragms are justified. The use of diaphragms in curved box girders would not only reduce the transverse bending moment, but also, would restrain the movements, caused by the differential displacements between webs, over the regions influenced by the diaphragms.

Small to medium span concrete box girder bridges are popular both as simple span and continuous structures. They are usually cast in situ or precast in segments which are erected on falsework or launching frame and prestressed. Steel box girders are frequently constructed as segmented cantilevers, but in some cases they are prefabricated in long lengths and lifted into position by climbing jacks and connected together. The slabs could be of steel battledeck or the more popular concrete composite construction and are often added after torsion boxes are in place.

Problems encountered in the fabrication and erection of curved girder bridges are, in most cases, similar to those encountered with straight girder bridges. However, certain problems, such as the fabrication of the curved girders, are unique for this type of construction. For the case of steel plate girders, two methods of fabrication have been employed [1]. One method involves prefabrication of a straight girder followed by either cold-bending or heat-curving to achieve the required curvature. In the second method, the curved flanges are cut from straight plates and welded to the webs which are curved by cold-bending.

Although curved box girder bridges came into existence due to tight geometric restrictions, their popularity is also attributed to other reasons. They form a very beautiful and aesthetically pleasing bridge for an elevated highway with their broad unbroken soffit when viewed from beneath. The interior column supporting the continuous bridge gives a graceful appearance to the structure when sighted from a distance.

In the current pro_ :t the static response for a curved box girder bridge is evaluated by means of detailed experimental and analytical studies. Analysis is based on the finite element method using the general purpose program ADINA. Among other available methods of analysis, the finite element approach seems to be the only approach capable of including most of the important factors influencing box girder behavior.

1.2 Objectives

The objectives of the present project are:

1. To Compare the analytical with the experimental linear static response of a four box curved girder bridge model;
2. To predict the ultimate load carrying capacity of the bridge model and to examine the materially nonlinear structure response.

1.3 Scope

1. A review of the analysis methods recommended by OHBD code for curved box girder bridges and a summary of their limitations.
2. To conduct an experimental study on the curved box girder bridge model within the elastic range of the material behavior.
3. Linear test case study on a twin box curved girder bridge.
4. Elastic analysis of the physical bridge model using the general purpose finite element program ADINA.
5. Comparison of the ADINA model predictions with the experimental response of the physical bridge model for seven load cases.
6. Nonlinear test case study on a single box straight girder bridge.
7. Inelastic analysis of the physical bridge model using ADINA for positive and negative moment load scenarios.

The usual assumptions of small deflections, homogeneous and isotropic material behavior are adopted. Loads are applied at a very slow rate such that the structure response pertains to static analysis only. For inelastic analysis, only material nonlinearity is considered and infinitesimally small strains are assumed.

1.4 Outline

The thesis first presents a review of the recommended OHBD code methods of analysis for the subject bridge(Chapter 2). A detailed description of the four box curved girder physical bridge model and the experimental program are given in chapter 3. Chapter 4 details the application of the finite element method in modelling curved box girder bridges using the ADINA program. A case study on a twin box curved girder bridge is presented. Comparison between experimental results and finite element predictions is presented in Chapter 5. The nonlinear structure response is examined analytically in Chapter 6. The conclusions and recommendations from this study are presented in Chapter 7.

Chapter 2

Literature Review

2.1 Introduction

The fundamental aspect, prior to analysis, in bridge design lies in the proper or most realistic structural idealization of the actual prototype in terms of its geometry, material, boundary conditions, as well as applied loads. In the analysis phase the mathematical idealization is further simplified by means of assumptions which establish the relation between the behavior of single elements in the integrated structure. The structural responses carried by any given component is assumed to be carried by the portion or portions of the structure for which the given component is analogue. Furthermore the combined response of these single components is assumed to represent the response of the whole structure. The accuracy of such solutions depends on the validity of the assumptions made.

Since the behavior of horizontally curved box bridges is always linear elastic under service loads, all methods of linear structural analysis may be applied. The methods of virtual work, conjugate beam, stiffness, flexibility, folded plate, finite strip, and orthotropic plate theory have all been used to analyze the behavior of curved girder systems. A comprehensive bibliography compiled by Mcmanus, Nasir, and Culver [1,2] in 1969 may prove to be a valuable source of reference for literature review on an international level. In this report, the author shall restrict the review to methods of analysis which have been recommended by the OHBD code in Canada:

namely,

- Grillage analogy methods.
- Orthotropic plate theory methods.
- Folded plate methods.
- Finite strip methods.
- Finite element methods.

In this chapter a brief outline of the aforementioned methods is presented. A detailed description of these methods is beyond the scope of this thesis. Instead, the various assumption and limits of applicability of each method are emphasized.

2.2 Grillage Analogy Methods

Most of the work done on curved bridges grid analysis involves curved bridges with open girders. However the grillage analogy methods are equally applicable to multi-cell or multi-spine curved box girder bridges. OHBD code limits the applicability of these methods to voided slab and box girder bridges in which the number of cells is greater than two [3].

In these methods the multi-cellular superstructure is idealized as a grid assembly. The continuous plated prototype structure is represented by a system of discrete curved I-beams intersecting orthogonally with straight transverse or cross beams. Part of the slab is assumed to act with the curved beams by adopting an effective width concept. In this concept the slab width is replaced by a reduced *effective* width, over which the stress is considered to be uniformly distributed. The different stiffnesses D_r, D_θ, $D_{r\theta}$ of the continuum are dislocated and hence lumped orthogonally along the boundaries of the beam elements. The stiffness representing the coupling of the two orthogonal bending curvature due to Poisson's ratio effect is usually neglected [4,5].

The problem of assigning the effective width of the slab to include shear lag effects has been studied by many researchers. However, most of the studies were limited to straight girder bridges. Hasebe et al. [6] in 1985 presented a detailed analytical study based on a refined beam theory by Kano et al. [7] to examine the influence of various parameters on the effective width of curved girders. The analysis was limited to simply supported structures consisting of a single box section or the open channel section. It was evident that the ratio of the effective width to the flange width is sensitive to many factors such as bridge horizonal curvature, distribution of applied loads, ratio of flange width to span length, and cross section dimensions. They concluded that the worst combination of these parameters occurs when the girder has high curvature, small flange width to span length ratio, deep webs especially for box sections subjected to concentrated point type of loads.

Another difficulty in the grillage analogy methods lies in the representation of torsional stiffness of the closed cells. It has been established by Evans and Shanmugam [8] that a satisfactory representation can be achieved in modelling the torsional stiffness of a single closed cell by an equivalent I-beam torsional stiffness. However, the results of their modelling technique may only be used as an approximate method of analysis [8,9].

Typical methods which have been used for the solution of grid systems are: the slope deflection method and the usual stiffness method [10]. The major advantage of the grillage analogy method lies in its simplicity. It enables a quick and economical solution to be obtained and hence it may be used for the repeated analysis required at the design stage.

2.3 Orthotropic Plate Theory Methods

The basic theory of orthotropic plates is based on the following Poisson-Kirchoff assumptions [11]:

- The orthotropic plate under consideration is assumed to be thin and have uniform thickness.
- Plate deflections are small compared to its thickness.
- Plate material is perfectly elastic, homogeneous and possesses different elastic properties with respect to the two in plane orthogonal directions.

- Middle plane of plate remains neutral during bending and particles on a plane perpendicular to the neutral plane remain normal to the deflected neutral surface. Furthermore normal stresses transverse to the plane of the plate are assumed to be small and hence neglected.

In the equivalent orthotropic plate method the stiffness of the flanges and girders are lumped into an orthotropic plate of equivalent stiffness. Cheung [12], Sawko and Merriman [13], and Coul and Das [14] suggested this method for multi-girder curved bridges with high torsional rigidity. Determination of representative flexural and torsional stiffness parameters D_r, D_θ, $D_{r\theta}$ lumped for the equivalent orthotropic plate is one major difficulty in this approach. Another difficulty in this method is the evaluation of slab and girder stresses in the final results.

In the orthotropic plate and beam assembly approach the interaction between the orthotropic deck and the curved girders is considered and the stiffness of the diaphragms is distributed over the girder length. Bell and Heins [15] solved such a model using the slope deflection technique and expressed their solution in terms of fourier series. Similar technique was adopted by Tung [16] for the analysis of twin box girder bridges. While Tung's method of analysis considers the interaction between the two girders it neglects the interaction between the annular flanges and the cylindrical webs. Later it was shown [17,18,19] that Tung's solution proved to be unreliable since it neglected the fact that curved box girders are composed of sections of plates and shell elements which interact together and with the top flange.

2.4 Folded Plate Methods

The method utilizes the plane stress elasticity theory and the classical two-way plate bending theory to determine the membrane stresses and slab moments in each folded plate member. The folded plate system consists of an assemblage of longitudinal annular plate elements interconnected at joints along their longitudinal edges and simply supported at the two ends.

Solutions for simply supported straight or curved box girder bridges is obtained for any arbitrary longitudinal load function by using the direct stiffness harmonic analysis. Pinjarker [20] was the first to apply the folded plate theory to simply supported curved box bridges consisting of longitudinal annular plates and vertical cylindrical shell elements. He assumed an isotropic material, no intermediate diaphragms and ignored coupling between in-plane and bending deformations in the cylindrical shell elements.

The method has been applied to continuous structures by using the standard force method [21]. However, it was evident that the method is complicated and time consuming. Furthermore, the OHBD code restricts this method for bridges that have support conditions closely equivalent to line supports, at both ends of the bridge and in the case of multi-span bridges at intermediate supports. A major drawback in this method is that it does not allow for any change in the elastic or geometric properties of the bridge longitudinally.

2.5 Finite Strip Methods

The finite strip method may be regarded as a special form of the displacement formulation of the finite element procedure. In principle, it employs the minimum total potential energy theorem to develop the relationship between unknown nodal displacement parameters and the applied loading.

In this method the box girders and plates are discretized into annular finite strips running from one end-support to the other and connected transversely along their edges by longitudinal nodal lines. A basic difference between the finite element method and the finite strip method originates from the assumed displacement interpolation functions. In the finite element method the displacement functions assumed take the form of two-way polynomial functions for a plate or shell element. The displacement functions for the corresponding finite strip are assumed as a combination of harmonics varying longitudinally and polynomials varying in the transverse direction.

The harmonic functions are selected such that end support conditions for the finite strip are satisfied. It is well established that the higher the number of harmonics used, the better is the solution accuracy. The unknown coefficients in the polynomial functions are determined by applying the compatibility conditions between the strips along the nodal line. Once the total potential energy function is expressed in terms of the assumed displacement function, the principal of minimum total energy is invoked and hence the unknown coefficients of harmonics are obtained.

Cheung [22] applied the finite strip method for cylindrical curved bridges with vertical webs. Meyer and Scordelis [23], however, considered the general case of inclined webs. The method is well established and is a powerful technique within its scope of application. The basic advantages of this technique may be listed as follows:

1. It requires small computer storage and relatively little computer time.
2. It accounts for the warping and distortion of the box girder.
3. The method permits any arbitrary longitudinal variation of both surface and joint loadings.
4. Any condition of imposed displacement and force boundary condition along the nodal line can be used.

For general purposes the application of the finite strip method may be limited as follows:

1. For extreme end-support conditions other than simple line support it is no longer valid to use simple harmonic functions. The use of more complicated harmonics may result in uncoupled harmonic terms. Consequently, a large set of simultaneous equations has to be solved [24]. Hence the method is limited to simply supported prismatic structures. For multi-span bridges, the OHBD code restricts the method to those which have interior supports closely equivalent to line supports. In this case the standard force method may be used, however, the method becomes very complicated and time consuming and convergence of the series solutions is no longer assured.
2. The method does not allow for any change in material and geometric properties of each strip of the bridge along its length.

2.6 Finite Element Methods

During the past two decades, the finite element method of analysis has rapidly become a very popular technique for the computer solution of complex problems in engineering. At present, the method represents one of the most general analysis tools and is used in practically all fields of engineering analysis. In structures, the method can be regarded as an extension of earlier established analysis techniques, in which a structure is represented as an assemblage of discrete elements interconnected at a finite number of nodal points.

Development of the finite element method has followed three main lines:

- Displacement-based formulation.
- Force-based formulation.
- Hyprid formulation.

The force-based finite element formulation can be understood as an extension of the flexibility method whereas the displacement-based formulation can be regarded as a continuation of the displacement method in structural analysis both of which had been used for many years in the analysis of beam, truss and framed structures. Although many of the concepts which pertain to the force-based formulation are, in many cases directly applicable to the displacement formulation, the latter approach seems to be more popular in the literature [25,26,27,28]

In the displacement formulation, the basic steps in the analysis can be summarized as follows:

1. The structure is modelled using suitable finite elements by subdividing its solution domain into discrete elements. Element type must be selected such that its structural response in terms of strains and deformation reflects, realistically, the components of the actual prototype. In case of box girder structures, plate bending or shell elements are usually selected. Furthermore, in this step one must decide upon the number, size and the arrangement of the elements in the discretized structure.

2. Since the displacement solution cannot be predicted exactly one must assume a suitable displacement function within the element to approximate the unknown solution. The assumed functions must be simple and should satisfy certain convergence requirements such as compatibility and completeness. The former requirement implies that the displacements within the elements and across the element boundaries must be continuous. The latter requirement ensures that the element can represent the rigid body displacements and the constant strain states [25]. In general, the interpolation displacement function is taken in the form of polynomials which merely describes the solution displacements at any point in the element space in terms of the nodal displacements.

3. From the kinematics of the problem at hand, element strains are obtained by using the appropriate strain-displacement relations. Moreover, element stresses are evaluated, depending on material model selected, by using appropriate stress-strain relations. Once these relations or matrices are established, the stiffness matrix $[K^e]$ and load vector $\{R^e\}$ on the element level are to be derived by using either equilibrium conditions or a suitable variational principle such as the minimization of total potential energy.

4. Since the structure is composed of several finite elements, the individual element stiffness matrices and load vector are to be assembled in a suitable manner taking into consideration any transformation of element local coordinates into the structure global coordinates. Hence the overall equilibrium equation can be formulated as follows:

$$[K]\{U\} = \{R\} \tag{2.1}$$

   where $[K]$ denotes the assembled or global stiffness matrix and $\{U\}$, $\{R\}$ denote structure nodal displacement and external force vectors respectively.

5. In this step, one modifies the overall equilibrium equations by imposing the boundary conditions and hence one solves for the unknown displacement vector.

6. Once the nodal displacements are known, one can solve for the element strains and stresses by using the elements strain-displacement and stress-strain matrices respectively.

In the earliest work on the analysis of curved box girder bridges by the finite element method, the curvilinear boundaries were approximated by a series of straight ones: In most cases, the structure was idealized by rectangular elements for the webs and quadrilateral elements for the flanges.

Anija and Frederic [29] divided their one-cell single span curved box girder into 240 panels. The flange elements were treated as flat plate elements with curved boundaries, whereas the webs, which are cylindrically curved plates, were treated as flat rectangular elements. Comparison between the finite element results and the experimental findings showed poor agreement and they concluded that flat elements cannot adequately represent the behavior of curved structures.

Willam and Scordelis [30] in 1972, presented a linear elastic analysis and computer program *CELL* for cellular structures of constant depth with arbitrary geometry in plan view. The multi-plate structure was idealized by means of improved quadrilateral or triangular elements containing both membrane and flexural stiffness. The special elements were developed using both mixed and displacement formulations. They tested their elements for a two-cell simply supported straight and a continuous highway bridge and concluded that the mixed formulations yielded more accurate results than the displacements-based models.

Bazant and El Nimeiri [31] in 1974 attributed the problems associated with the neglect of curvilinear boundaries of the curved box beam to the loss of continuity at the end cross sections of two adjacent elements meeting at an angle. The presence of such discontinuity violates the assumptions of the classical bending theory that cross sectional planes are normal to the beam longitudinal axis. No attempt was made to remedy this problem by using curvilinear element boundaries. Instead, they developed the skew-ended finite element with shear deformation using straight elements and adopted a more accurate theory which allows for transverse shear deformations and hence does not require the cross sections to be normal to the beam axis.

Although curvilinear boundaries may be idealized by straight edges, the number of the elements must be high enough to achieve a satisfactory solution. Such an approach is impractical especially for highly and moderately curved box bridges. The advantages of curved flat and shell elements have been demonstrated by Fam and Turkstra [32] both at the element level and at the three dimensional structural level. In 1975, Fam and Turkstra [33] described a finite element scheme for static and free vibration of box girders with orthogonal boundaries and arbitrary combinations of straight and horizontally curved sections. The curved top and bottom flanges of the box were idealized by a 4-node plate bending annular element with two straight radial boundaries. To idealize the general case of inclined web members in the curved box, conical elements were used. The analysis included in-plane, bending and coupling action as well as anisotropic element properties. They tested their elements against results from folded plate theory and finite strip methods with sufficient harmonics for a twin-cell simply supported curved box girder bridge and reported good agreement.

The versatility of the finite element method have eluded the attention of many researchers [34,35,36,37,38] to analyze the complex mechanics of an arbitrary girder-diaphragm-cross-beam system. The numerical effectiveness as well as the flexibility of the method in linear, nonlinear, static or dynamic-types of analysis attracted many investigators to use this technique as the basis of theoretical analysis in model studies of the multi-plate curved box structure. The only major shortcoming of the finite element method lies in its requirements for large amounts of computer core and processing time. This renders the technique less popular as a suitable design tool particularly for simple box structures.

Chapter 3

Experimental Study

3.1 Introduction

Due to the complex structural behavior of multi-cell curved box girder bridges, designers tend to shy away from this problem in one way or another. It is only natural to find that grillage analogy methods seem to be the most common technique in design offices. This is not surprising when one considers that the grid work approach belongs to the next level of complexity above the traditional straight beam solution[38]. Researchers on the other hand, tend to further simplify existing methods of analysis to enhance the repetitive nature of design procedures. The dilemma goes on; a simple approximate method of analysis resulting in a conservative design versus a more refined method with less conservative and hence less expensive design.

On a research scale, the literature on curved box girder bridges dictates that analytical development in the various methods of analysis, approximate or refined, outbalances the experimental investigation. Unfortunately, few authors [34,35,36,39]have undertaken experimental studies to investigate the accuracy of existing methods and the influence of the assumptions on the general solution of the problem. Full scale experimental investigation would result in very high costs. Model testing is the second best indispensable tool to verify analytical predictions of structure response.

Most experimental model studies involve geometrically simple models subjected to idealized single point loads. In general they lack one or a combination of the following features:

- Multi-Cell box girder as a typical cross section.
- Multi-Span continuous structures.
- Diaphragms.
- Design Truck Loads.

Curved box girder bridges having the aforementioned features are not uncommon in practice. Cyrville road over the Queensway underpass in east Ottawa sets a good example of such structure and hence it was selected as the prototype for the current model study. The structure is 102.4 meter long, 12.8 m wide and consists of two spans with a 16.8° horizontal angle of curvature between extreme end supports. A typical cross-section consists of four contiguous cells 1.83 m deep with prestressed diaphragms two of which are located at the extreme end supports and one intermediately located over the single column support. The bridge was designed for ASHTO design truck Load HS20-44 by The Ministry of Transportation and Communication and was built in 1973.

In this chapter a detailed description of the bridge model is presented. This includes model geometry, material properties, loading system, support details as well as instrumentation and loading setup. An outline of test procedure is then listed. The last part of this chapter presents experimental data interpretation and reduction into a proper form required for comparison study purposes.

3.2 Object of Experimental Study

The objectives of the current experimental study are:

1. To establish accurate experimental data for checking the prediction by computer analysis for structures of this type.

2. To obtain sufficient data related to the elastic response of curved box girder bridges under severe eccentric loading conditions applied by OHBD Truck from which general trends of behavior could be studied.

3.3 Bridge Model Description

3.3.1 Model Geometry & Construction

The bridge model was composite construction of micro-concrete deck with aluminum bottom plate and cylindrical webs. After preliminary consideration a linear model scale of 1/24 was adopted. The center line radius of curvature of the model was 14.554 m. Longitudinally, tangent to the center line, the model spans 4.268 m through the small angle of curvature (16.8°). The model was 490 mm wide and 133 mm deep as shown in Figures 3.1, 3.2.

A typical cross section of the model consists of four rectangular box girders of the contiguous type. Aluminum C-channels were used as transverse diaphragms. Two of the diaphragms were placed at the extreme end supports and one intermediate diaphragm was placed directly above the single center column support. The bridge model was supported at the ends by rockers to allow horizontal movement. Details of the model center and end sections are given in Figure 3.2.

To form the box girder, the curved webs were clamped in position and then they were welded to the bottom plate. Spot welds were used in order to minimize the amount of possible warping due to the heat released as a result of welding. The box girders were first closed using stay-in-place false work supported by transverse bars extended to the web flanges as shown in Figure 3.3. Temperature and shrinkage reinforcement consisting of $1'' \times 1'' \times 16$ WWF (Welded Wire Fabric) mesh was placed over the false work and then the micro concrete deck was poured. In order to have the slab acting as an integral part of the box girder, aluminum shear connectors 8 mm in diameter were connected to the top flange of the webs at 80 mm c/c spacing.

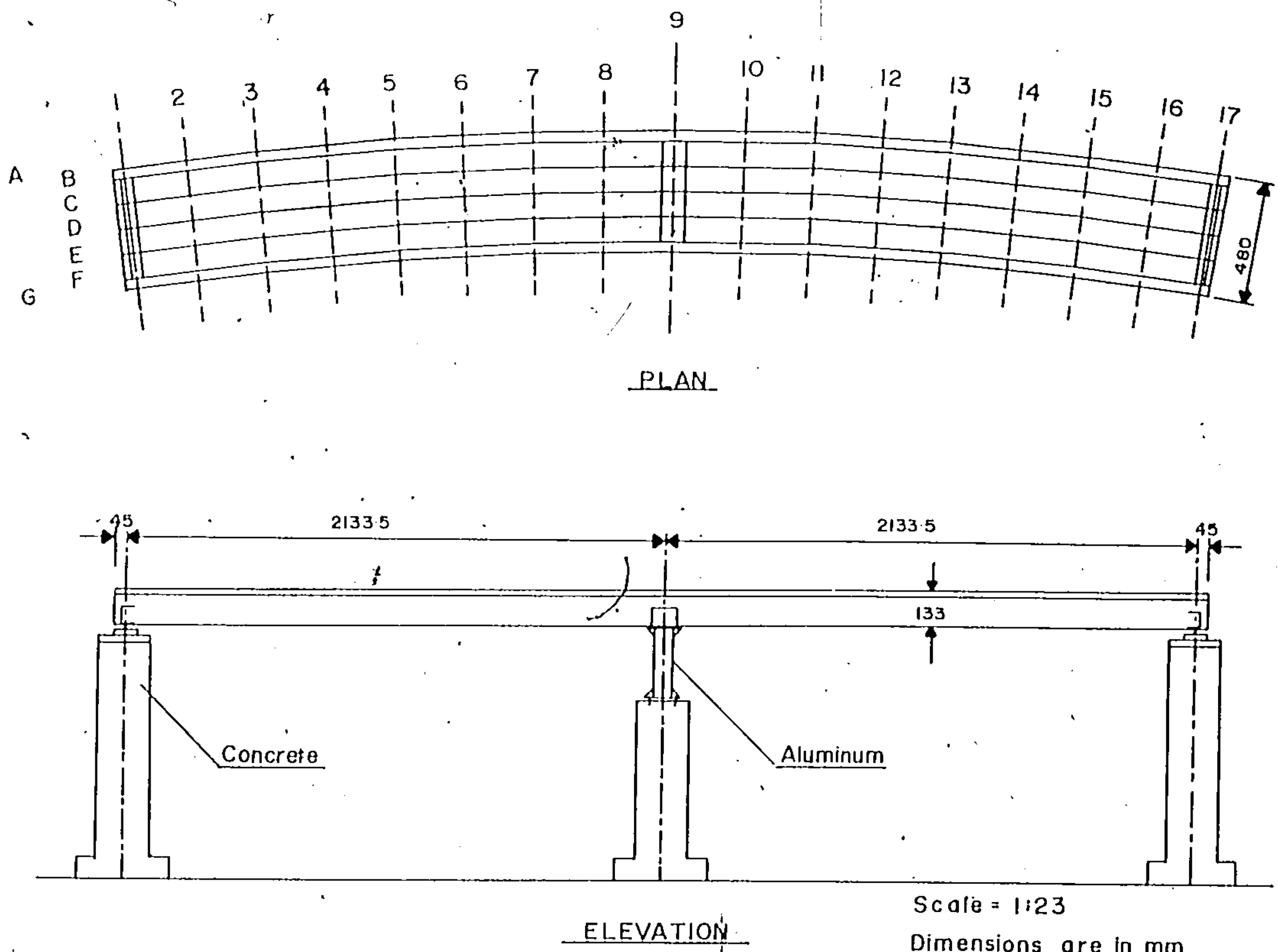

Figure 3.1: Geometry of curved box girder bridge model.

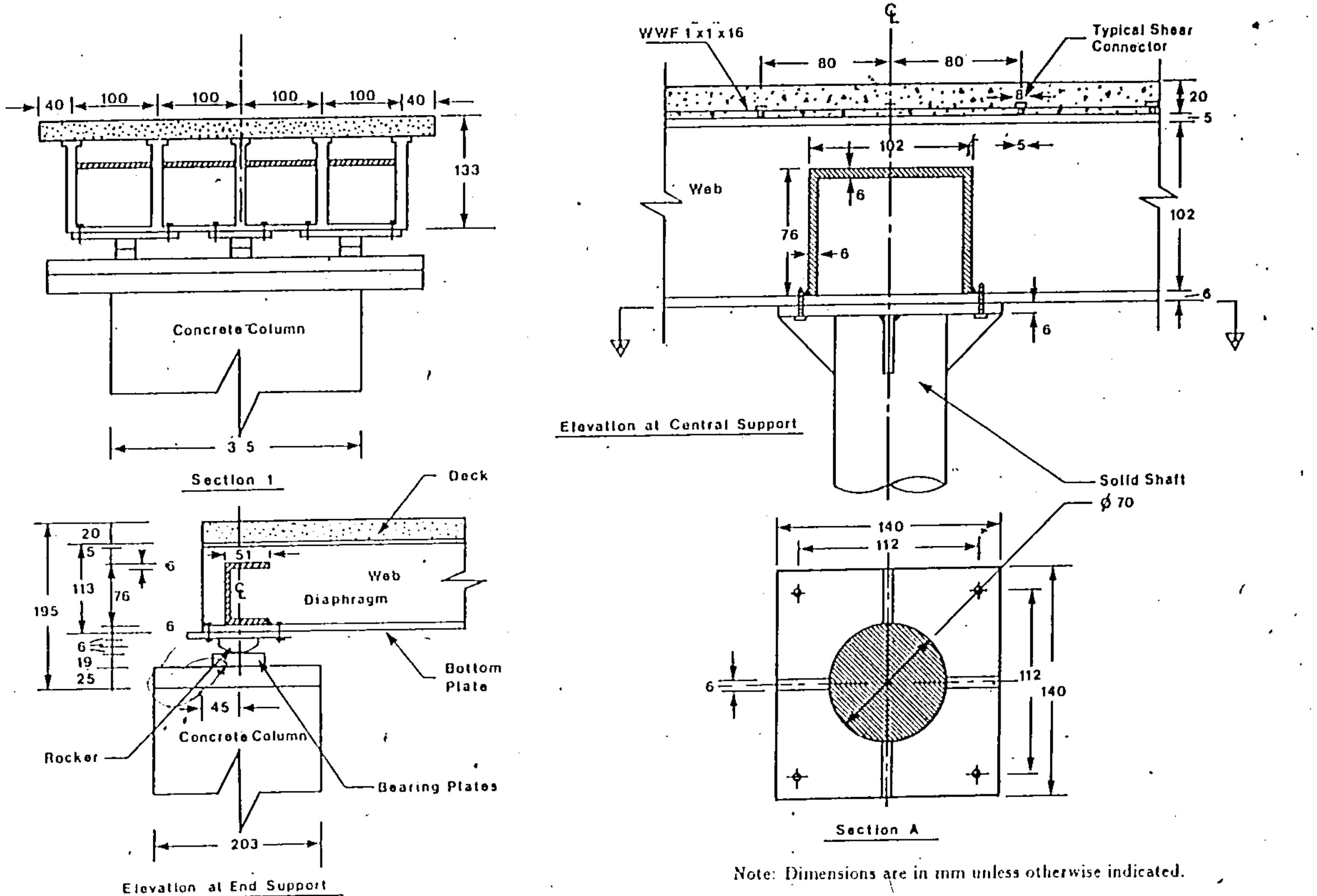

Note: Dimensions are in mm unless otherwise indicated.

Figure 3.2: Details of bridge model at supports.

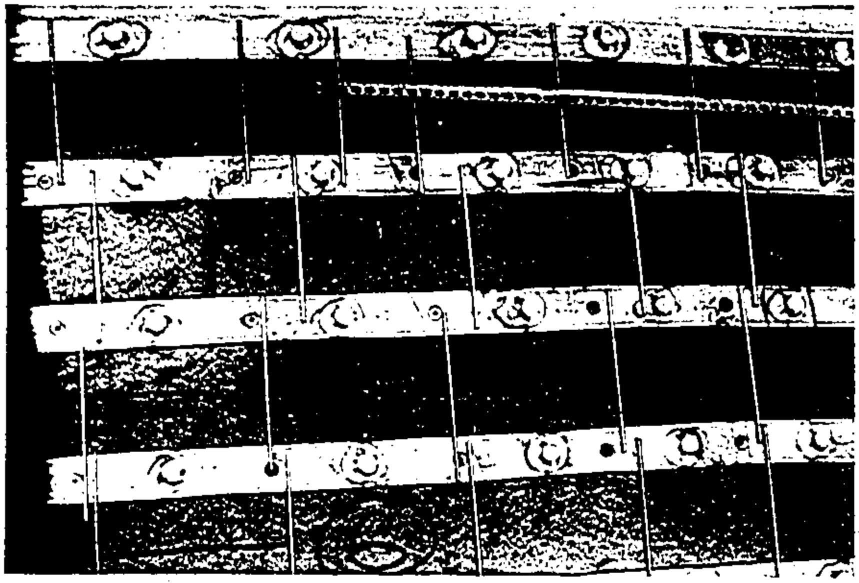

Figure 3.3: Stay-in-place false work under bridge deck.

3.3.2 Material Properties

The object of the experimental investigation dictates that the current model study is of the indirect type. In direct model tests the model is built such that all its properties are as similar as possible to those of the prototype but on a reduced scale. Since it was not intended in this study to model a particular design and develop a one to one correspondence between the model and the prototype responses, the main criteria used in the choice of model material was the practical aspects involved in fabrication, instrumentation and testing technique.

Concrete would have been an excellent choice for the model; however, preliminary studies showed that only a micro concrete deck can be modeled at 1/24 model scale. Moreover, a larger scale must be used in order to model the webs and the bottom plate. Considering the advantages and disadvantages of other material choices such as aluminum, steel, and plexiglass, the aluminum alloy was selected to model all the other components of the bridge for the following reasons:

1. The most serious disadvantage of plexiglass is that its material properties are time dependent, hence making it difficult to take measurements while the model is deforming. One could avoid this difficulty by selecting aluminum or

Table 3.1: Micro concrete mix details.

Mix ID	Cement (Kg)	Water (Kg)	Aggregates (Kg) #4	#8	#16	#30	#50	w/c (-)
A	22.378	9.000	9.846	11.19	8.952	9.398	5.370	0.402
B	9.324	4.662	4.923	5.594	4.476	4.699	2.685	0.500
Design	46.4	19.0	24.5	27.9	22.3	23.4	13.4	0.409

steel.

2. The problem of temperature rise at strain gage locations is magnified when adopting plexiglass. This is mainly due to the combined effect of the low thermal conductivity of the plexiglass and to the heat generation due to the current in the electrical resistance strain gages.

3. The problems associated with heat generation in the welding process could be minimized by proper clamping and stabilization before welding and by careful utilization of spot welds. Furthermore, damages to the strain gages which have to be installed on the interior webs could be avoided by installing them once all the welding needed is over and before casting the micro-concrete deck.

4. Aluminum is lighter and easier to machine than steel.

Micro Concrete

The thin design slab thickness (20 mm) for the bridge model reflects the reason for which a micro concrete, instead of regular concrete, had to be used for the model. Hence aggregates passing sieve No. 4 were chosen to be the maximum aggregate size.

Two trial concrete mixes were considered and a total of 24 ($3'' \times 6''$) concrete cylinders were cast and tested. Uniaxial compressive strength test results after 6, 18. 28 and 46 days from casting are given in Table A.1, Appendix A. Details of both trial mixes along with the design mix used for the deck are presented in Table 3.1 High early strength cement was used in the design mix. The bridge deck was cast on Aug. 25^{th}, 1986 along with 30 cylinders ($3'' \times 6''$) of which 12 cylinders were tested.

Table 3.2: Micro concrete compressive strength.

Specimens ID	$f'_c\,(MPa)$		
	7 days	14 days	28 days
A	27.3	40.0	46.3
B	39.0	39.5	46.3
C	33.2	40.2	43.9
Average	36.1	39.9	45.5

Table 3.3: Summary of micro concrete properties.

Property	Symbol	Magnitude
Compressive Strength (MPa)	f'_c	45.5
Tensile Splitting Strength (MPa)	f'_{ct}	5.19
Modulus of Elasticity (MPa)	E_c	31300
Poisson's Ratio	ν_c	0.15

The compressive strength of the cylinders tested after the $7^{th}, 14^{th}, 28^{th}$ day from casting are given in Table 3.2.

In order to determine Young's modulus of the micro concrete, specimens tested on the 28^{th} day were instrumented with two strain gages each. Hence, while under uniaxial compression, load and strain readings were recorded. The average strain value at each stress level are listed in Table A.2, Appendix A. The average Young's modulus for the three specimens was taken to be 31300 MPa.

The last set of 3 cylinders were tested, at 28^{th} day, for tensile splitting strength. The average strength value was computed as 5.19 MPa.

In summary the mechanical properties of the micro concrete used for the model deck are listed in Table 3.3

Table 3.4: Summary of aluminum properties.

Property	Symbol	Magnitude		
		Set A	Set B	Average
Ultimate Strength (MPa)	f_{ult}	327	306	317
Yield Strength (MPa)	f_Y	316	285	301
Modulus of Elasticity (MPa)	E_a	70277	72000	71100
Poisson's Ratio	ν_a	0.379	0.379	0.379

Aluminum

The Aluminum alloy reference[1] No. 6061-T6 was essentially used for all components of the bridge model excluding the deck. Two sets of aluminum samples were tested: namely, set A used as the bottom plate aluminum and set B representing the webs. A summary of the various properties and strength values for each set as well as the average is listed in Table 3.4.

3.3.3 Support Details

The bridge model was supported under its own dead weight by three rockers at each end and by a single column support at the mid-span section. The central column support consists of a single solid aluminum shaft 70 mm in diameter welded to top and bottom bearing plates. The bottom bearing plate was connected to a concrete pier by four screws grouted in the concrete. The top bearing plate connected the shaft to the bottom plate of the bridge by means of four (unbolted) screws. It is anticipated that this support would simulate the pin type with some degree of fixity but the support cannot be considered as totally fixed. Details of the column support are shown in Figure 3.2

All rockers were machined from 25.4 mm thick steel rings having an outer diameter of 108 mm and were connected to 6.5 mm steel bearing plates. The latter were then connected to the bottom plate of the box girder at the appropriate locations, thus making the rockers part of the structure. With a total of six rockers, the bridge was

[1] Magnesium and Silicon wrought alloy.

supported at each end section by steel bearing plates resting on a concrete column. A typical end support section is also shown in Figure 3.2

Prior to any loading it was observed that not all rockers were in contact with the bearing plate. Additional thin plates had to be inserted where necessary in order to adjust the elevation of the supporting columns.

In a preliminary test for bridge global stability, a considerable torsional rotation was observed for a relatively small eccentric loading. At such loads the bridge was supported by only one rocker at each end. Moreover, a gap of about 2 mm was observed between the top bearing plate of the center column shaft and the bottom plate of the model indicating the presence of torsional moments around the center column support. These observations may be attributed to the fact that the ratio of dead load to live load of the model was less than unity. This further reflects the fact that the dead weight of the prototype was not simulated in the current model.

In order to prevent the global instability of the model, it was decided to restrain the bridge against torsional movements by means of reaction beams at the extreme end sections of the bridge. These modifications for the end supports are shown in Figure 3.4. As for the center column support, it was decided to restrain any uplift movement within the vicinity of the connections. This was accomplished by using a hydraulic jack applying a constant downward force aligned vertically with the axis of the shaft. The jack was also reacted upon by a reaction beam as shown in Figure 3.5. Moreover, a load cell was installed between the jack and the reaction beam in order to control a constant jack load of 2000 lbs throughout the testing period. The pictures given in Figure 3.6 show the final setup used at the supports.

3.3.4 Model Loading System

The second objective of the experimental study dictates that the bridge model is to be loaded by an equivalent OHBD truck load. In the various loading conditions considered in this study, two parallel trucks loading was assumed to act simultaneously along the outer lane, producing severe eccentric truck loading. In order to design the loading system, one must first establish the equivalent OHBD truck load. Here one makes use of the laws of similitude and dimensional analysis.

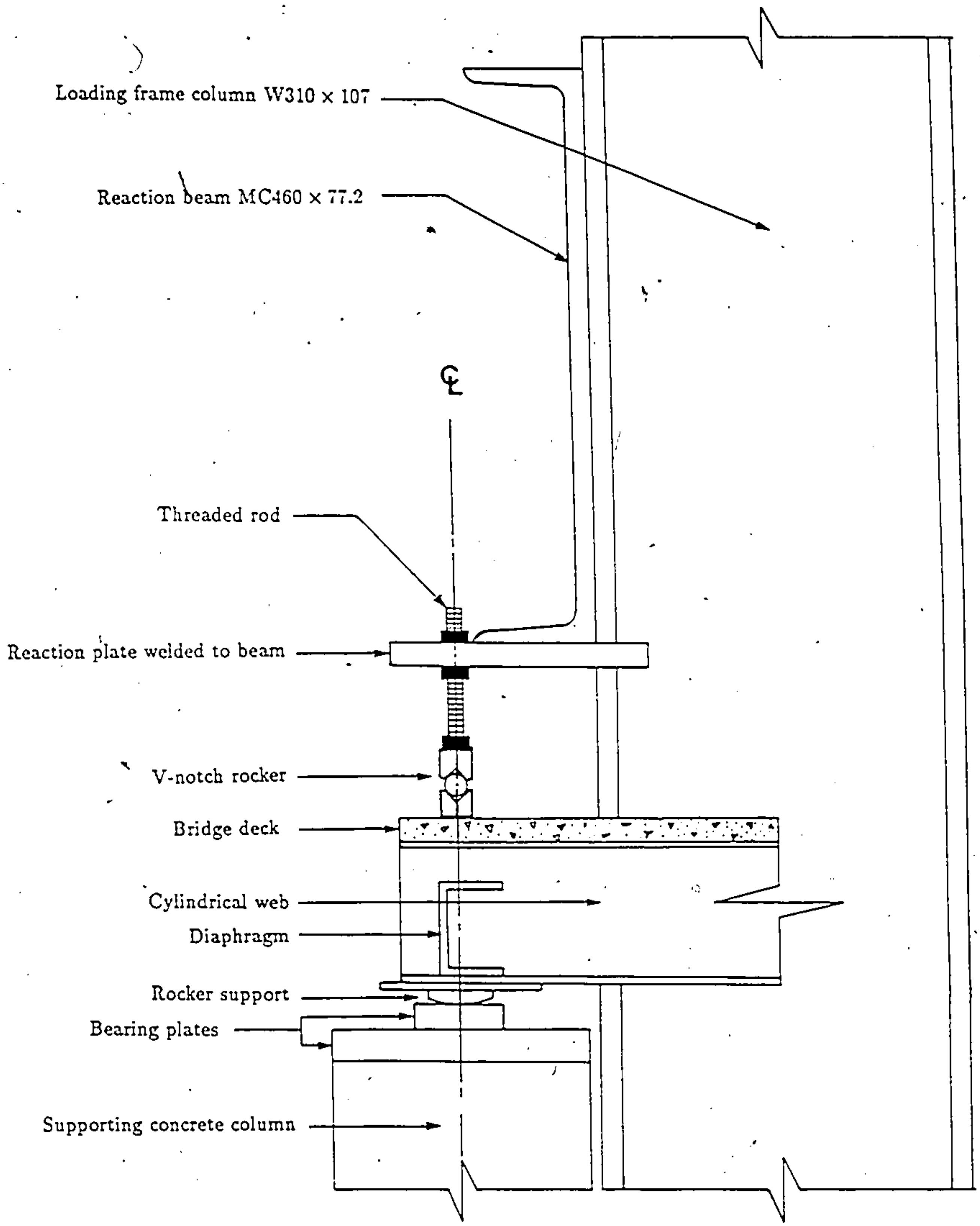

Figure 3.4: Details of bridge model at abutments.

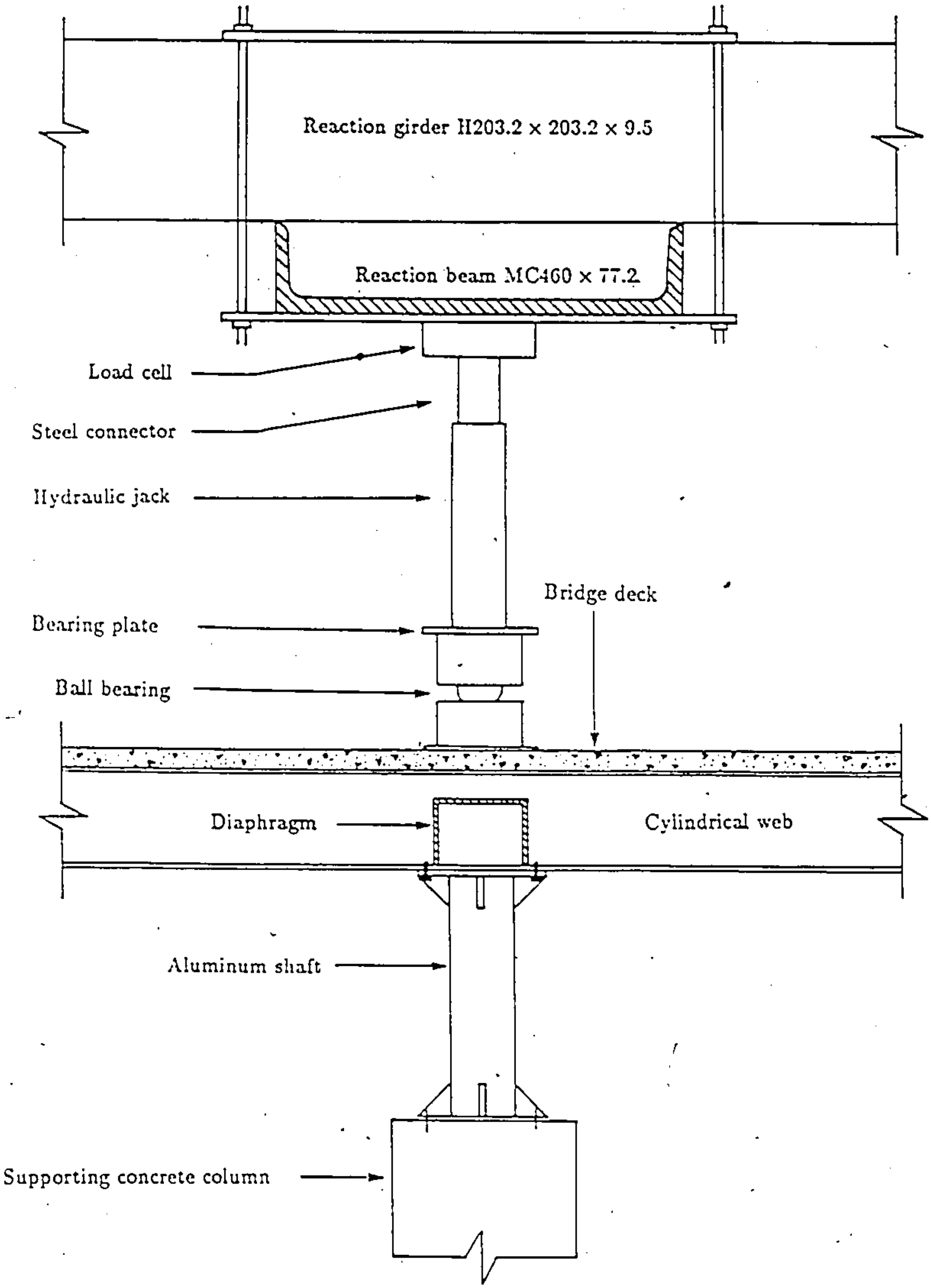

Figure 3.5: Details of bridge model at mid-span.

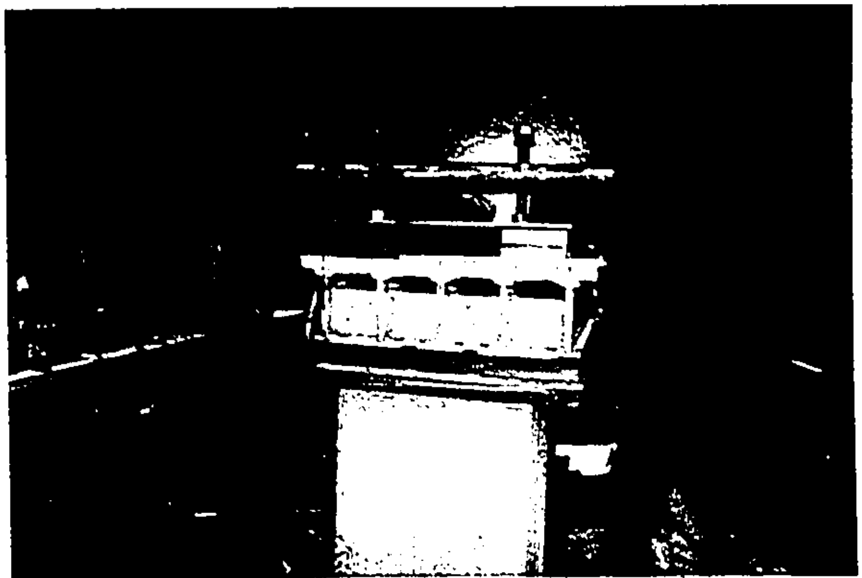
End support

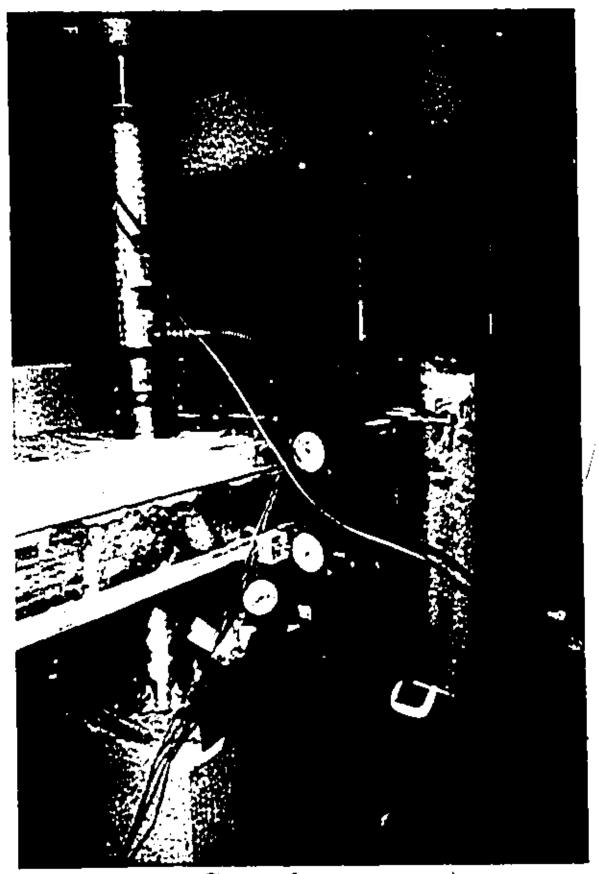
Central support

Figure 3.6: Pictures of bridge model at supports.

The basic type of similitude used in this analysis was that which simulate the normal longitudinal strains. In other words, the equivalent truck load in the model must be such that it would produce normal longitudinal strains (ϵ^m) in the model, that are equal to those longitudinal strains (ϵ^p) which would be produced by **OHBD** truck load in the prototype structure. Hence, the fundamental similitude equation is given as:

$$\epsilon^m = \epsilon^p \tag{3.1}$$

If we ignore Poisson's ratio effects then one may write:

$$\frac{\sigma^m}{E^m} = \frac{\sigma^p}{E^p} \tag{3.2}$$

where E, σ denote Young's Modulus and longitudinal bending stress respectively. Superscripts m, p denote the model and the prototype respectively. From elementary beam theory, normal stress at a section is given by:

$$\sigma = \frac{M\,Y}{I} \tag{3.3}$$

where: M denotes the bending moment at the section.
Y denotes distance from the neutral axis.
I denotes moment of inertia of the section about neutral axis.

Moreover, one may express the bending moment as the product of force (F) and a linear dimension along the longitudinal axes of the structure (X).

$$M = F \times X \tag{3.4}$$

Substituting Eq. 3.4 into Eq. 3.3 and applying the result of σ into Eq. 3.2 one gets:

$$\frac{F^m\,X^m\,Y^m}{E^m\,I^m} = \frac{F^p\,X^p\,Y^p}{E^p\,I^p} \tag{3.5}$$

or:

$$F^m = \frac{E^m}{E^p}\,\frac{I^m}{I^p}\,\frac{X^p}{X^m}\,\frac{Y^p}{Y^m}\,F^p \tag{3.6}$$

For the current bridge model a constant linear scale($\hat{L}$) was used for the two linear dimensions X,Y. If we let:

$$\hat{L} = \frac{X^p}{X^m} = \frac{Y^p}{Y^m} \tag{3.7}$$

$$\hat{I} = \frac{I^p}{I^m} \tag{3.8}$$

$$\hat{E} = \frac{E^p}{E^m} \tag{3.9}$$

Then equation 3.6 can be written as follows:

$$F^m = \frac{\hat{L}^2}{\hat{E}\hat{I}} F^p \tag{3.10}$$

or;

$$F^p = \hat{F} \times F^m \tag{3.11}$$

where $\hat{F}$ is given by:

$$\hat{F} = \frac{\hat{E}\hat{I}}{\hat{L}^2} \tag{3.12}$$

Equation 3.11 defines the relation between prototype force (F^p) and the equivalent model force (F^m) which satisfies normal strain similarity. The static, linear force scale ($\hat{F}$) is defined by Eq. 3.12. The stiffness properties used in the calculations of the force scale factor are listed below:

$I^p = 310520100\ cm^4$
$I^m = 2871\ cm^4$
$E^p = 27700\ MPa$
$E^m = 71100\ MPa$

Hence with a linear scale factor $\hat{L} = 24$, the resulting force scale factor $\hat{F}$ was computed to be:

$$\hat{F} = 73 \tag{3.13}$$

Using this factor the model truck load simulating a single OHBD tuck load was computed and is given in Table 3.5. A plan view of OHBD truck geometry is shown in Figure 3.7

Lumping the loads of the two axles, 2 & 3, into a single axle loads would simplify the truck model significantly. This is more so when considering that two parallel trucks model loading will be acting on the bridge in all load cases. Figure 3.8 shows the schematics of the two parallel trucks model employed for the design of trucks loading system.

Shao (1986)[40] in his report on the Design and Manufacturing of the Bridge Model presented a detailed description on the design of the parallel trucks loading system.

Table 3.5: OHBD Truck Load.

Axle No.	Load (KN)	
	Prototype	Model
1	60	0.822
2	140	1.918
3	140	1.918
4	200	2.740
5	160	2.192
Gross Load	700	9.590

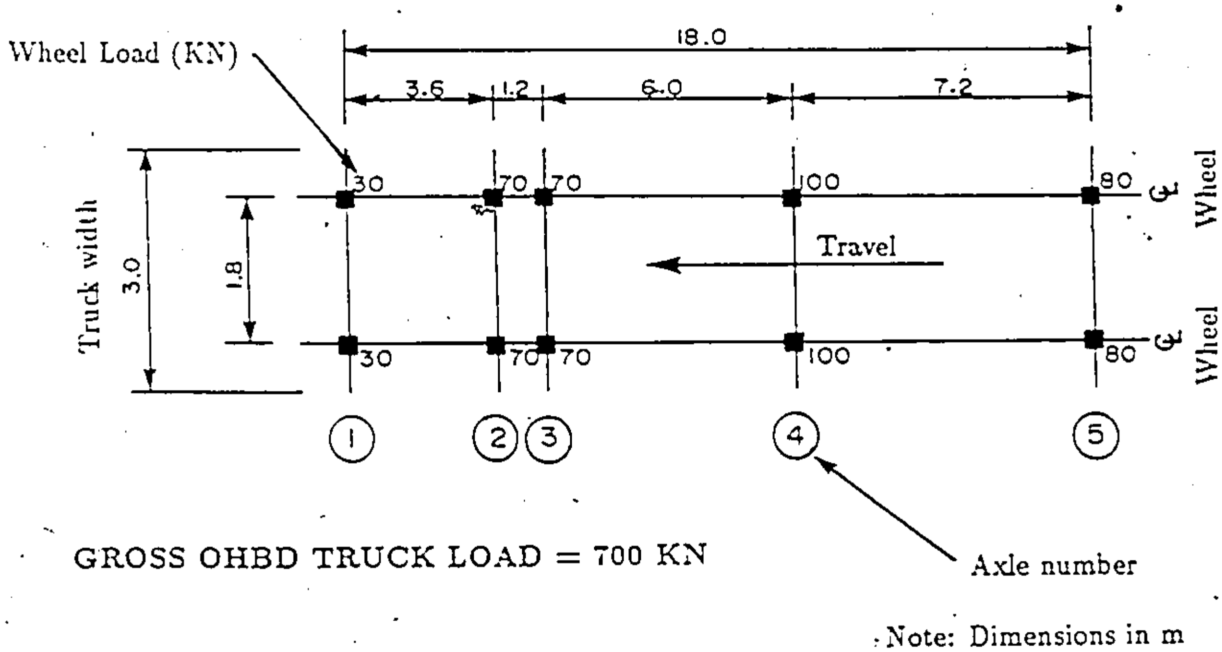

Figure 3.7: OHBD Truck Load.

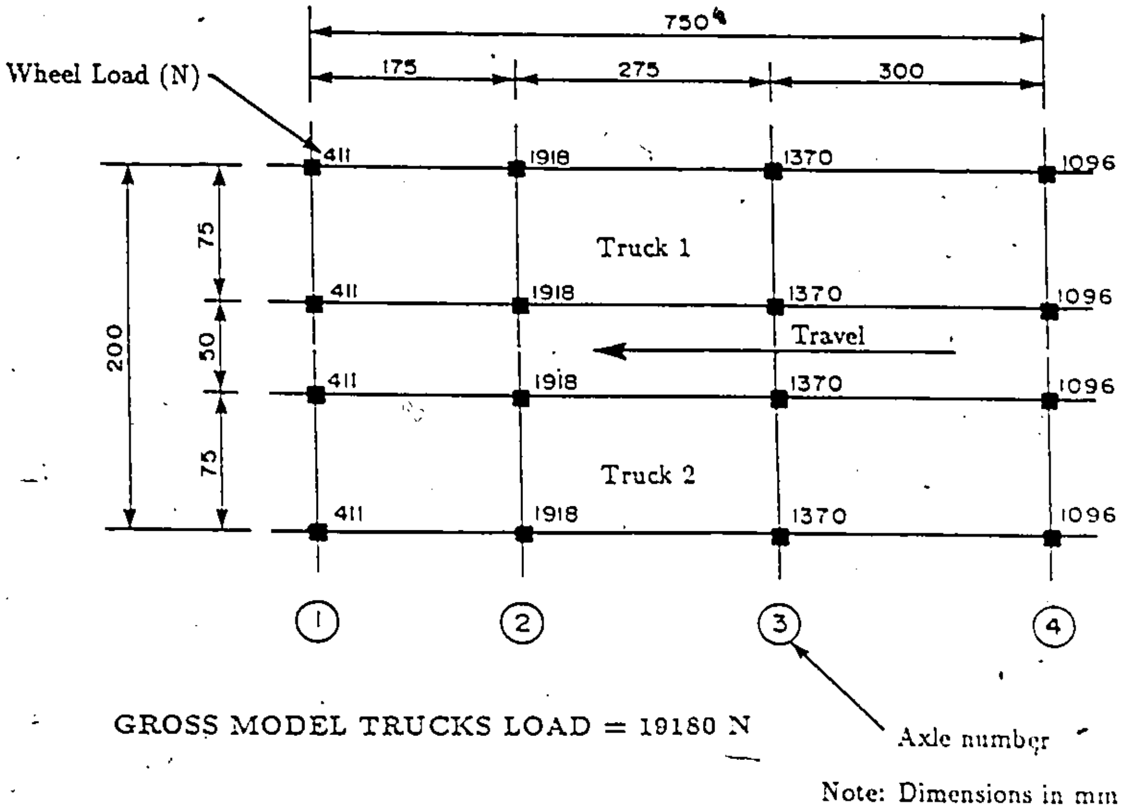

Figure 3.8: Schematics of parallel trucks model.

In brief, it consists of a combination of steel beams constructed one on top of another using steel disks as wheels. The beams are assembled such that when a concentrated jack load P is applied to the assemblage, it is distributed between the four axles and the various wheels in the same manner as the model trucks load is distributed in Figure 3.8. The total weight of the assemblage was 40 Kg (392 N). The gross model load equivalent to two OHBD trucks load is: $F = 2 \times 9590$ N. Therefore the required jack load P should be :

$$P = 2(9590) - 392 = 18788\ N\ (1915\ Kg)$$

Details of the beams assemblage are shown in Figure 3.9. For a given jack load P, the wheel loads at the four axles can be shown to be given by the following formulae:

$$F_1 = \frac{321}{15330} P + \frac{1657}{1400} \tag{3.14}$$

$$F_2 = \frac{3103}{30660} P + \frac{3313}{1400} \tag{3.15}$$

$$F_3 = \frac{1169}{16425} P + \frac{9981}{3000} \tag{3.16}$$

$$F_4 = \frac{931}{16425}P + \frac{9369}{3000} \quad (3.17)$$

where: P denotes the applied jack load (Kg).
F_i denotes a wheel load (Kg) at axles $i = 1, 2, 3, 4$.

3.3.5 Load Cases

The model loading reflects a distinct feature of the current experimental investigation. In that the **OHBD** truck load was used instead of a single point load. Moreover, the various load cases considered have been selected such that the maximum internal stresses would occur at a particular critical section. In order to determine the trucks location, longitudinal and transverse influence lines for various internal response quantities were first established. This was done by Shao (1986)[40] using a finite element program for the longitudinal influence lines and the grillage method for the transverse ones.

A total of 7 distinct load cases were considered for this study. Figures 3.10, 3.11 show the trucks location for each load case. Eccentric parallel trucks loading on the outer lane of the bridge was common to all load cases.

3.3.6 Instrumentation

Three types of foil strain gages were used in the experiment, viz. a 45° three-gage rosette and two uniaxial (linear) gage elements. The micro concrete deck surface was instrumented with linear strain gage type EA-06-500GB-120, whereas the aluminum surfaces were instrumented with linear gages type KEC-5-C1-11 or rosette gages type EA-13-125RA-120. All strain gages had a gage factor of about 2.10 and were cemented to the aluminum or concrete surfaces by means of Micro-Measurement M-Bond 200 adhesive. The procedure recommended in ref.[41] for strain gage installation and wiring was used.

The strain gages were installed at the four radial sections 2,5,8,9. Strain gages located on the interior webs were installed and water-proofed after the welding of

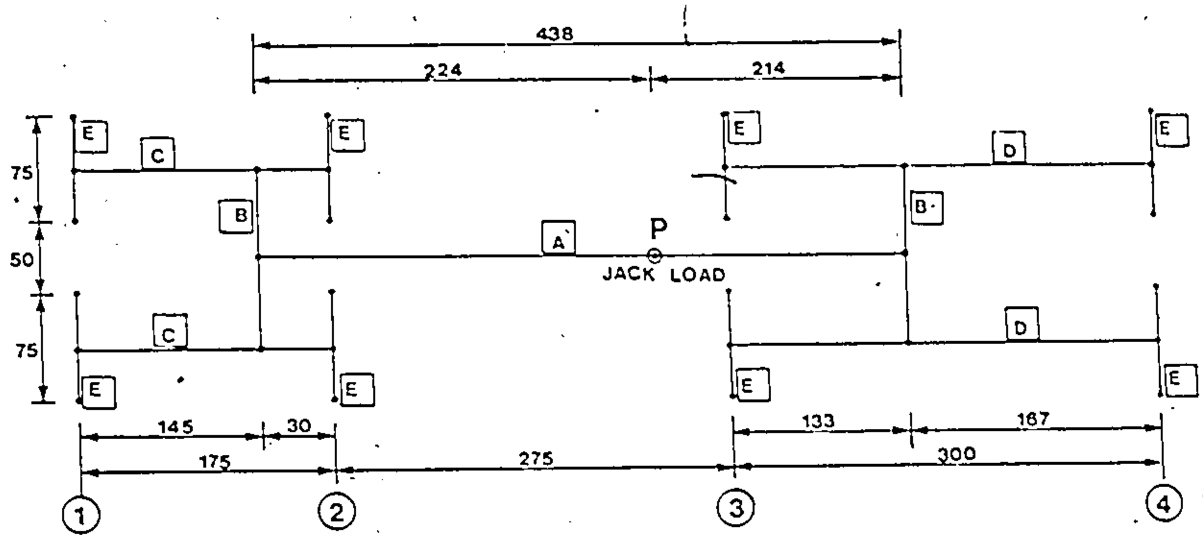

Beam ID.	Mass/beam (Kg)	No. of beams	Mass (Kg)
A	11	1	11
B	1.7	2	3.4
C	2.5	2	5.0
D	8.3	2	16.6
E	0.5	8	4.0
Total mass of trucks			40.0 Kg

○ Axle number

□ Beam ID

Note: Dimensions in mm

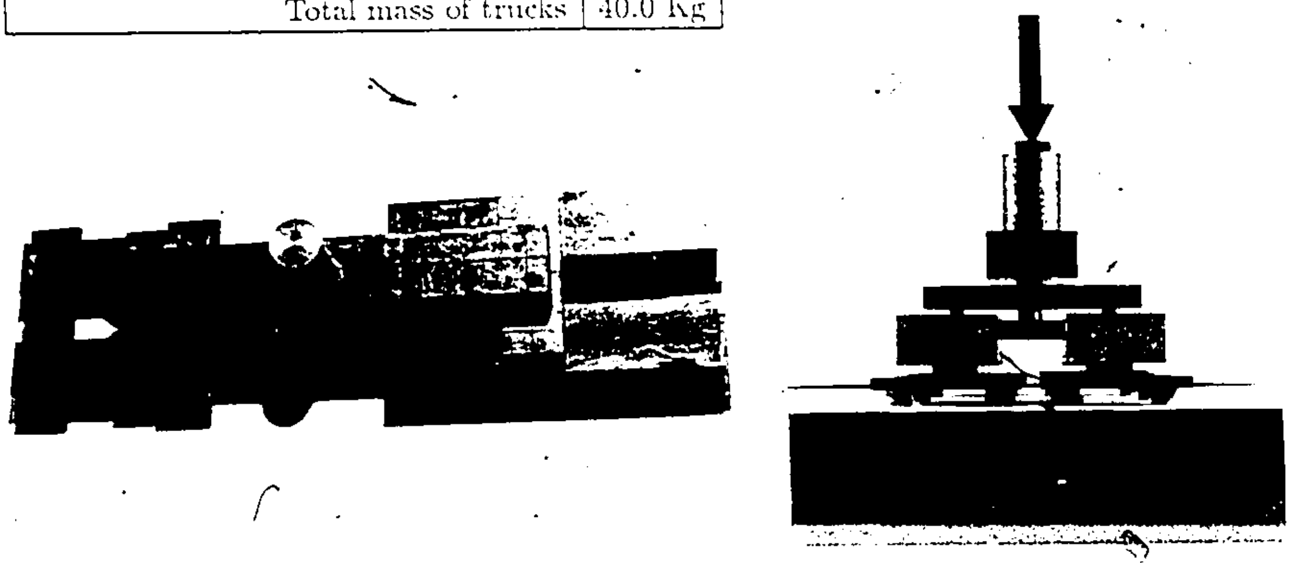

Figure 3.9: Parallel trucks loading system.

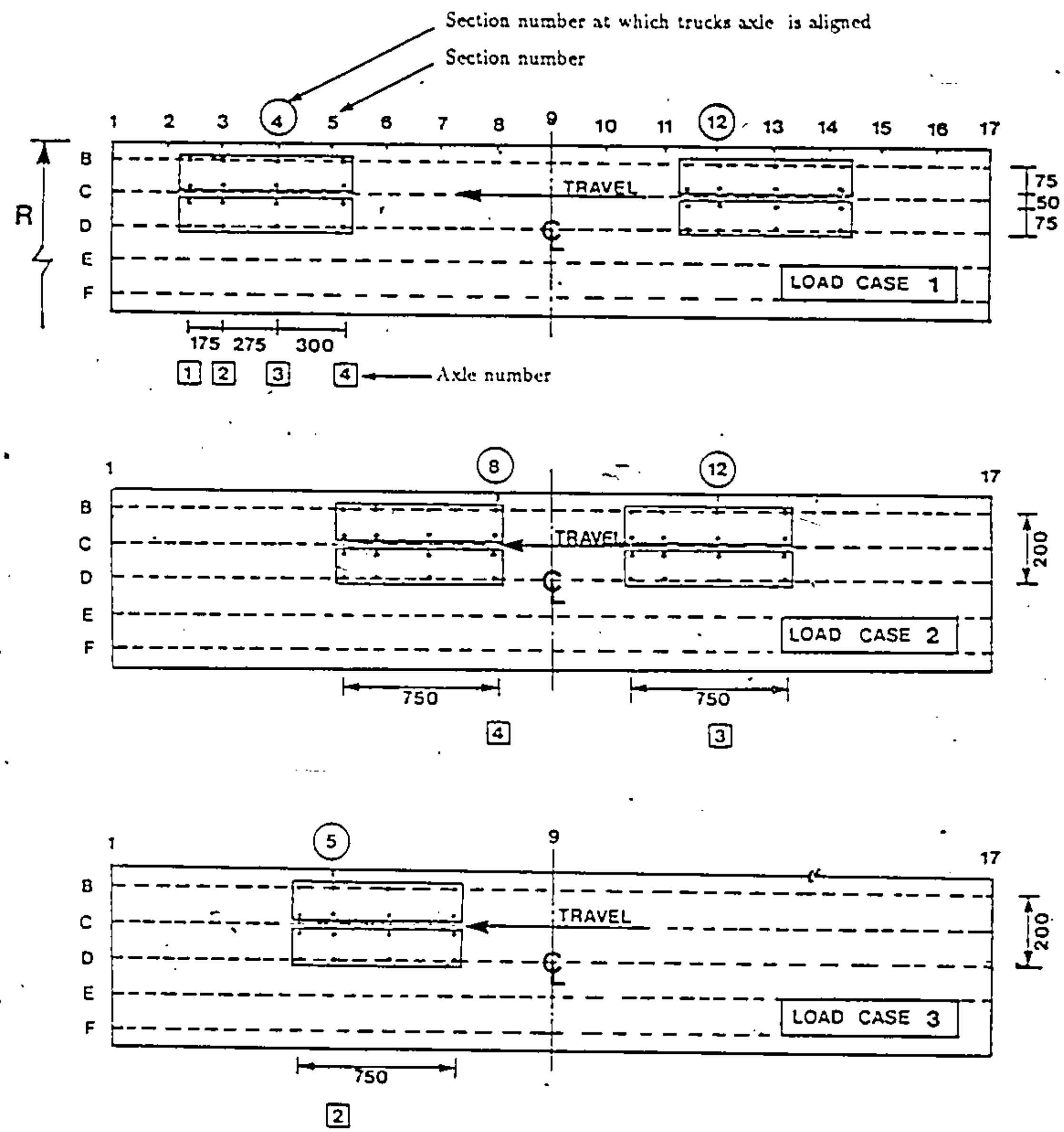

Figure 3.10: Trucks locations for load case 1,2,3.

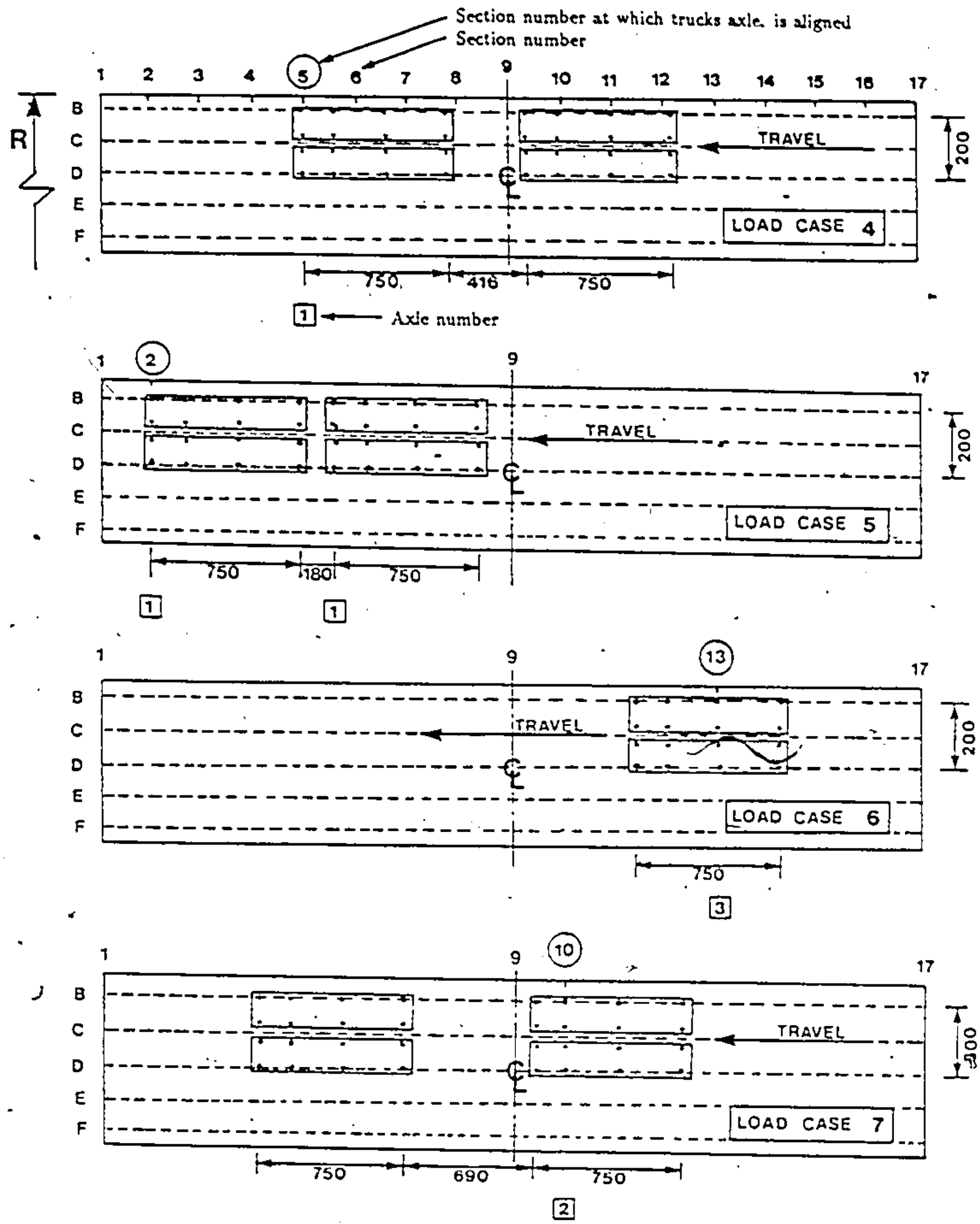

Figure 3.11: Trucks locations for load case 4,5,6,7.

aluminum components and before casting the deck to minimize initial straining and damage to the gages. A total of 48 strain gages were used . Ten linear gages were cemented on the micro-concrete deck surface, six rosettes were installed on the outer surface of sections 5,8 and 32 linear gages were cemented on other aluminum surfaces as shown in Figure 3.12

The identification symbol for each strain gage is given below:

C_{ij}^{L} denotes a linear strain gage located on a concrete surface at section j;
i denotes gage No. within section j.

A_{ij}^{L} denotes a linear strain gage located on aluminum surface at section j;
i is defined as above.

A_{ij}^{Rx} denotes a 45° Rosette gage located on aluminum surface at section j;
i is defined as above.
x denotes the axis in the plane of the rosette and is defined below:
x=L denotes longitudinal axis of the bridge.
x=T denotes perpendicular axis to L in rosette plane.
x=D denotes the 45° axis between L and T.

For instance A_{45}^{L} identifies the 4^{th} linear strain gage on aluminum surface at section 5.

Dial gages of sensitivity 0.01 mm were mounted vertically under the webs centerlines as well as in the top and bottom planes of the model at sections 5 and 9. The dial gages were supported by threaded rods bolted to steel angles. Once the dial gages were at the proper location, the angles were clamped onto a separate steel frame underneath the model.

To establish easy identification for dial gages position, the model was divided transversely in seven distinct tangential lines. Five of these lines, B,C,D,E,F, represent the centerlines of the webs. The remaining two lines A,G, represent the extreme edges of the concrete deck; namely, the outer and the inner tangential edges respectively.

A total of 24 dial gages were used in the experiment. They were classified into two groups in terms of their purpose. In one group, denoted by ϕ, the dial gages were used to read vertical deflection of the bottom plate of the box girder. The other group of dial gages, denoted by ψ, were employed to read lateral displacements.

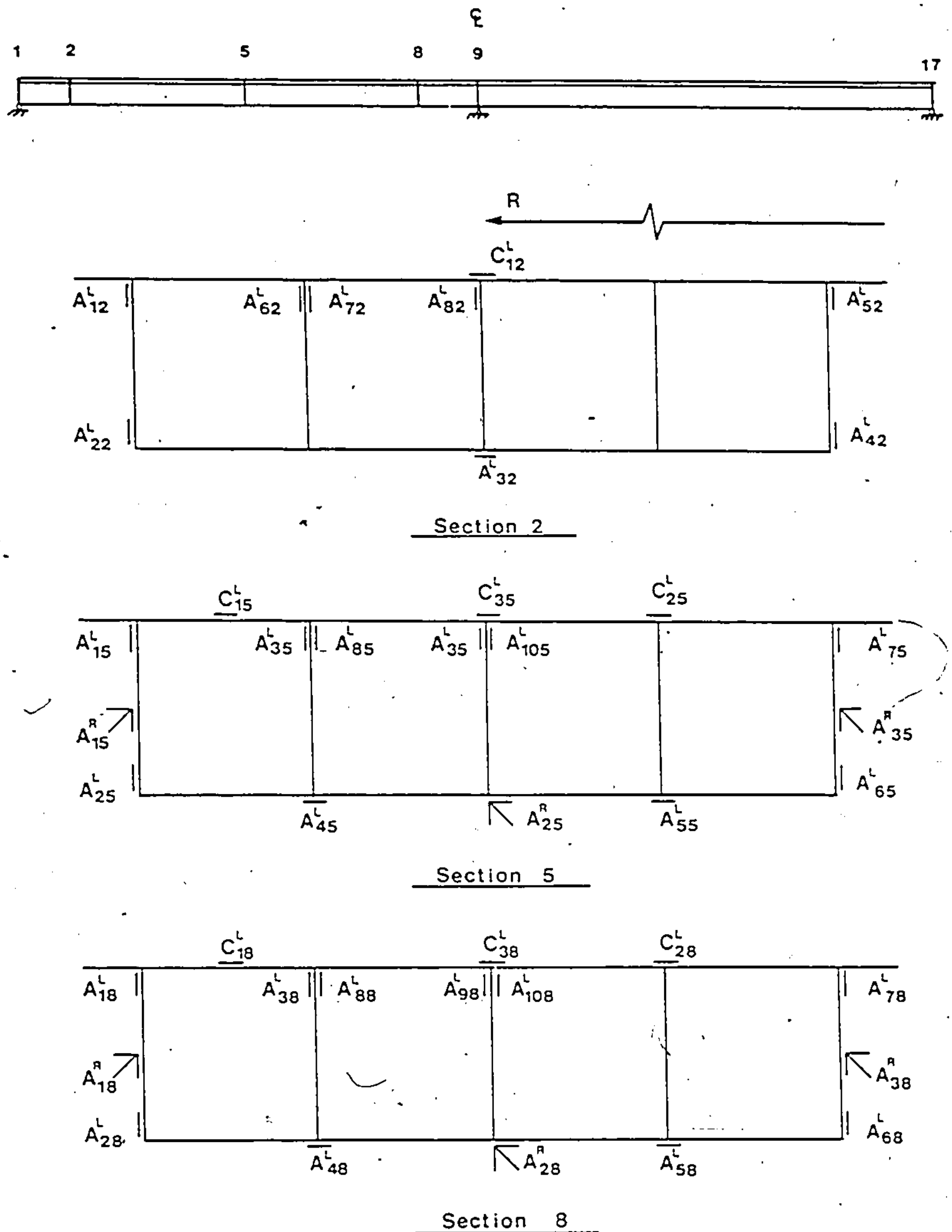

Figure 3.12: Strain Gages Location.

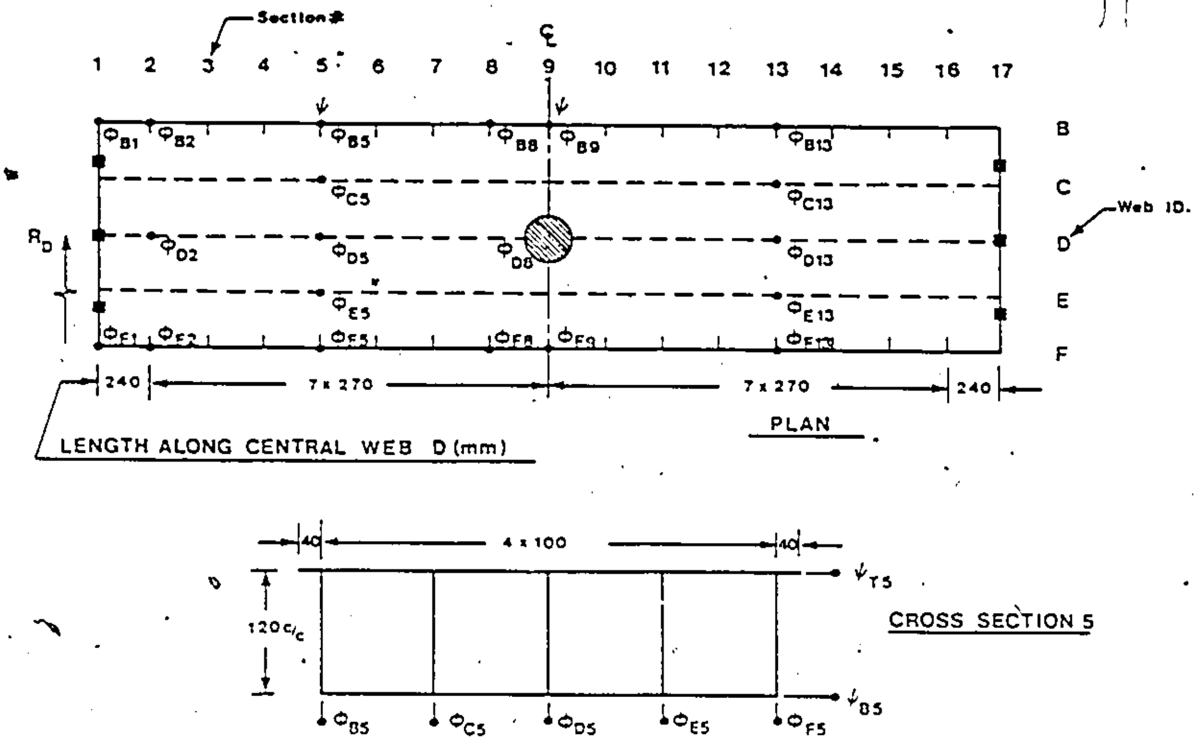

ϕ_{C5} : DEFLECTION DIAL GAGE UNDER WEB C AT SECTION 5

ψ_{B5} : ROTATIONAL GAGE IN BOTTOM PLATE AT SECTION 5

Figure 3.13: Dial gages location.

The location of the various dial gages are shown in Figure 3.13. Typical dial gage identification symbols are given below:

ϕ_{B5} denotes dial gage located underneath web B at section 5.
ψ_{T9} denotes dial gage in the top plane of the box girder at section 9.

3.3.7 Test Setup

In a typical test setup strain gage wires were grouped into six bundles. The group representing the concrete strain gages were connected to a single switch box and a Vishay strain indicator. The remaining aluminum strain gage wires were connected to five, 10-channel, switch and balancing units (BLH Model 1225). Normally each switch and balancing unit would be connected to a single digital strain indicator (BLH Model 1200B). Since there were only three strain indicator units, three switch and balancing units were connected in series with a single strain indicator unit. The remaining two were connected to a separate strain indicators.

In order to verify the performance of the series connection, an initial test on a simply supported beam was conducted. It was observed that to switch from one switch and balancing unit to another a minimum of 5 minutes must be allowed in order for the electric current to stabilize and hence to obtain a constant reading. However, when switching from one channel to another within a single switch unit, the reading were consistent from the instant of switching. This observation was taken into account while testing. The lag time required for a certain box in this series was used to take gage readings from an independent strain indicator unit.

Loading the bridge model was done by using 10 ton capacity hydraulic jacks (Model HSR-104T) along with load cells to control the applied jack loads. The load cells were instrumented between the jacks and the reaction beams. Once the parallel trucks loading system was assembled at the proper location, the reaction beam was aligned such that the axis of the jack passes through the center of gravity of the trucks loading system. The pictures given in Figure 3.14 show typical test setup and the loading system.

Jack loads were applied in increments of 440 *lbs.* for all load cases except load case 2 where increments of 880 *lbs.* was used. In any load case the target load on each set of trucks was 4400 *lbs.* This target load is about the equivalent of two OHBD truck loads. Strain and dial gage readings were taken for each load increment. This procedure should provide sufficient experimental data to establish accurate representation of the bridge response.

The seven load cases were tested during the second week of November 1986. Test duration averaged about 8 to 10 hours per load case.

3.4 Test Procedure

The test procedure for a typical load case was divided into three stages; namely, prior to loading stage, loading stage and unloading stage. Procedure details of each stage were as follows:

Figure 3.14: Test set-up and loading system.

1. Prior to loading stage:

   - Strain gages and load cells wiring was checked and gage factors were set to their appropriate values. In addition, dial gages were checked for proper locations.
   - A load of 2000 *lbs*. was applied and kept constant over the center column support.
   - Zero reading for strain and dial gages were taken.
   - Parallel trucks loading system was assembled at the proper location according to load case Number. The jacks were then aligned vertically over the center of gravity of the trucks loading system.

2. Loading stage:

   - While maintaining the 2000 *lbs*. over the center support a 440 *lbs*. load increment was applied on each set of loading trucks.
   - Strain & dial gage readings were then taken and recorded. This loading cycle was repeated until the jack load reached the target load of 4400 *lbs*.. It should be noted, however, the 2000 *lbs*. over the center column was maintained throughout the cycle.

3. Unloading stage:

   - The model was unloaded by releasing the jack loads on the trucks and clearing the bridge deck.
   - While maintaining the jack load over the center column, the bridge was allowed to creep for 30 minutes.
   - Zero readings were recorded and then the 2000 *lbs*. over the center column was released.

This procedure was followed for all load cases except for load case 2. Load case 2 was the first test that was performed and the only deviation from the aforementioned procedure was the 880 *lbs*. load increments. The experimental dial gages and strain gages data are presented in Appendix B, Tables B.1 to B.21.

3.5 Reduction of Experimental Data

3.5.1 Displacements and Strains

The ten load increments through which the total load have been applied, provides 10 sampling points for each strain gage and dial gage measurements. Since at any time the total applied load was within the elastic range of material response, one would expect a linear relationship between load and deformation. Experimental data, however, do not exhibit perfect linear relationship. This is due to various sources of experimental errors. The use of linear regression analysis proves to be a valuable tool. Through this type of analysis, one can establish the best line that fits load-deformation data. Once the linear function is known, it must be corrected for zero load by ignoring the constant parameter in the best fit line.

For the seven load cases considered in the experiment, both dial gage and strain gage readings were linearized by the least square method. The coefficient of determination (r^2) given in Eq. 3.18 was used as a measure of the goodness of fit.

$$r^2 = \frac{\sum_{i=1}^{N}(G(x_i) - \overline{f})^2}{\sum_{i=1}^{N}(f(x_i) - \overline{f})^2} \tag{3.18}$$

where $G(x_i)$ and $f(x_i)$ denote the predicted and measured values respectively and $\overline{f}$ denotes the mean value of measured or predicted data. Moreover, the standard of error (σ_e) given in Eq. 3.19 was also employed as a measure of experimental error.

$$\sigma_e = \sqrt{\frac{\sum_{i=1}^{N}(f(x_i) - G(x_i))^2}{N - M}} \tag{3.19}$$

where N is the total number of data points and M is the number of regression coefficients which is 2 in this case.

While the coefficient of determination (r^2) may provide a good measure of the correlation between the dependent and the independent variable for the linear functional approximation, this statistical measure suffers from a rather significant limitation. A given data set may show a good linear trend and yet the data could deviate significantly from the approximated linear function. In this case r^2 can be very close to 1.0 indicating excellent correlation and unless the data are plotted one cannot establish just how much the data deviate from the best fit line. The standard error

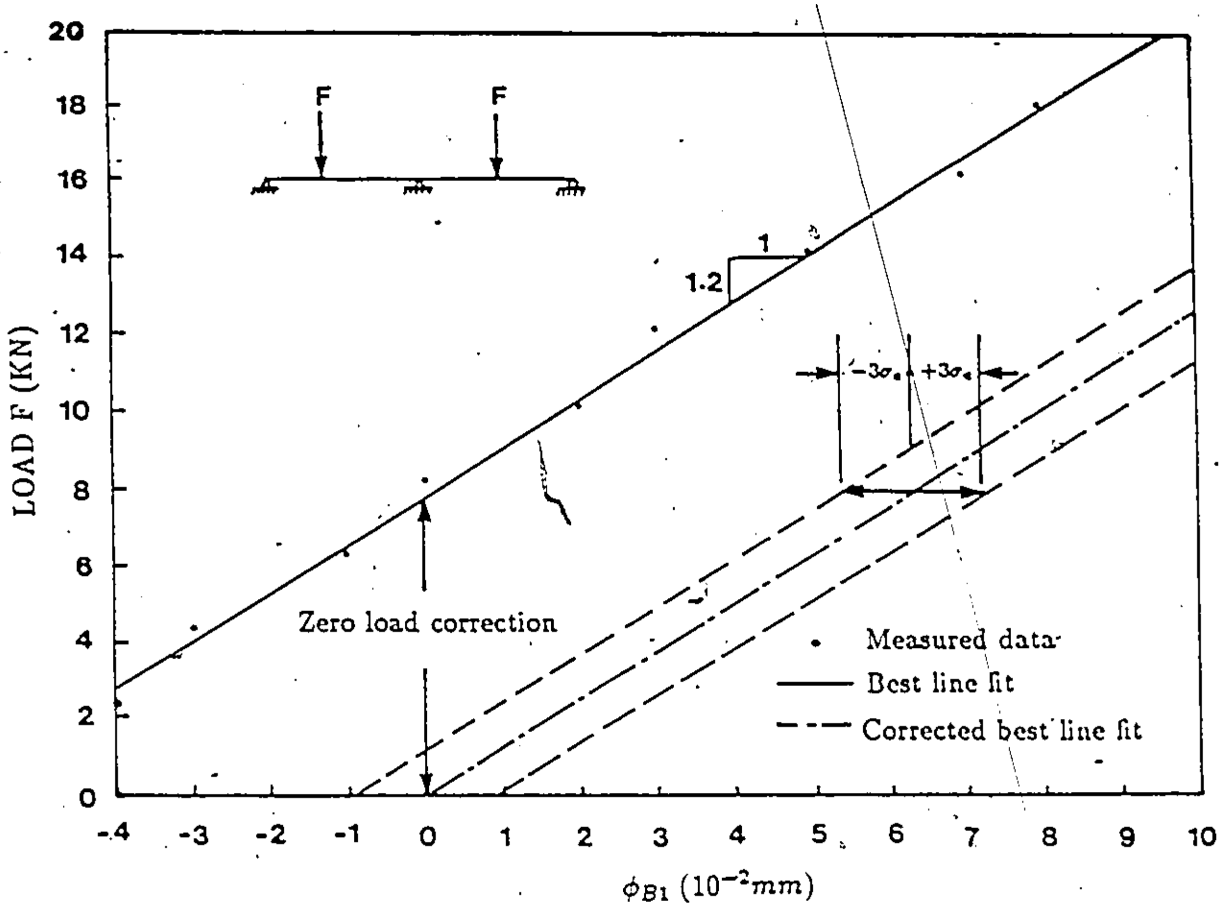

Figure 3.15: Reduction of experimental data

of estimate is an excellent measure for this matter and hence it was used in assessing experimental data reliability. This measure permit us to evaluate what certainty we can attach to the derived function. In that sense, it is similar to the standard deviation of random data. For a 67 % certainty, the predicted experimental data would fluctuate between $\pm 2\sigma_e$. The experimental error for dial gages and strain gages data were computed based on $3\sigma_e$. In this way there is 99.9 % certainty of the predicted experimental data when computed using an approximation function.

The aforementioned data reduction scheme is presented in Figure 3.15 for a typical dial gage data set (ϕ_{B1}) in load case 1.

A similar scheme was used to reduce strain gages data. The results of linear regression analysis are tabulated in Appendix B, Table B.22 to Table B.42 for both deflection and strain measurements. In these tables symbols a and b are the regression parameters representing the y-intercept and the slope of the approximated function respectively. Symbols ϕ^* and ϵ^* denote the predicted experimental values of deflection and strain at the equivalent OHBD parallel trucks load ($F = 2 \times 9590 = 19180 N$). The percentage error column is the experimental error associated with the prediction of the deflection or strain values for a 99.9 % certainty. The predicted experimental data at the equivalent OHBD trucks load are tabulated in Tables 3.6 and 3.7 for displacements and strains respectively.

Table 3.6: Displacement data at OHBD trucks load.

Section #	ϕ $10^{-2}mm$	Load Case 1	2	3	4	5	6	7
1	ϕ_{B1}	15	22	14	11	30	3	13
	ϕ_{F1}	-7	-20	-4	-9	-9	-5	-10
2	ϕ_{B2}	71	82	70	47	133	-16	49
	ϕ_{D2}	49	49	56	29	101	-20	32
	ϕ_{F2}	29	20	44	14	72	-23	16
5	ϕ_{B5}	140	224	198	131	322	-57	136
	ϕ_{C5}	122	191	184	112	296	-60	119
	ϕ_{D5}	99	152	163	89	264	-66	99
	ϕ_{E5}	78	109	145	68	232	-69	77
	ϕ_{F5}	62	76	130	49	203	-71	57
	ψ_{T5}	27	51	23	30	44	7	27
	ψ_{B5}	-8	-10	-13	-5	-19	9	-7
8	ϕ_{B8}	51	142	87	79	148	-17	81
	ϕ_{D8}	16	49	53	30	88	-31	32
	ϕ_{F8}	-19	-26	31	-11	43	-46	-8
9	ϕ_{B9}	47	122	30	62	61	25	63
	ϕ_{F9}	-18	-47	-13	-24	-28	-13	-25
	ψ_{T9}	28	68	20	35	36	17	34
	ψ_{B9}	9	20	7	10	12	6	9
13	ϕ_{B13}	170	274	-45	96	-79	292	86
	ϕ_{C13}	154	240	-55	73	-87	196	68
	ϕ_{D13}	135	201	-57	57	-96	178	51
	ϕ_{E13}	112	155	-63	38	-104	158	33
	ψ_{F13}	94	121	-68	23	-112	144	17

Table 3.7: Strain data set (a) at OHBD trucks load.

Section #	ϵ 10^{-6}	Load Case 1	2	3	4	5	6	7
2	C^L_{12}	-52	-44	-23	-17	-71	10	-22
	A^L_{12}	-44	0	-20	5	-45	9	-10
	A^L_{22}	41	15	17	15	115	-9	9
	A^L_{32}	73	62	44	36	150	-8	31
	A^L_{42}	34	27	30	18	68	-6	17
	A^L_{52}	-64	-57	-56	-18	-198	159	-61
	A^L_{62}	-47	-30	-32	-15	120	15	-14
	A^L_{72}	-	-	-	-	-	-	-
	A^L_{82}	-50	-29	-32	-13	122	12	-14
5	C^L_{15}	-	-	-	-	-	-	-
	C^L_{25}	-60	-78	-65	-42	-108	24	-36
	C^L_{35}	-34	-44	-47	-20	-87	-21	-21
	A^L_{15}	-112	-135	-129	-69	-154	51	-80
	A^L_{25}	90	133	149	83	232	-33	86
	A^L_{35}	-103	-125	-151	-69	-	48	-86
	A^L_{45}	138	221	233	119	311	-52	124
	A^L_{55}	115	180	198	108	277	-46	87
	A^L_{65}	38	123	99	52	149	-	68
	A^L_{75}	-90	-114	-139	-65	-203	50	-77
	A^L_{85}	-	-	-	-	-	-	-
	A^L_{95}	-86	-121	-147	-61	-142	46	-75
	A^{RL}_{15}	-19	-42	-34	-27	145	17	-24
	A^{RD}_{15}	114	-82	-71	-37	118	-21	-30
	A^{RT}_{15}	-15	-40	-48	-22	121	-14	-56
	A^{RL}_{25}	122	177	207	97	275	-58	108
	A^{RD}_{25}	12	-28	35	-16	58	-39	-19
	A^{RT}_{25}	-71	-86	-94	-53	-116	11	-62
	A^{RL}_{35}	-24	-28	-32	-21	-46	10	-26
	A^{RD}_{35}	11	31	12	10	24	12	12
	A^{RT}_{35}	-8	0	-8	-44	18	-18	-8

In order to assess the reliability of the predicted response at the equivalent OHBD trucks load, error-frequency diagrams were plotted for each load case. Percentage frequency diagrams for deflection data and for strain data are given in Figures 3.16 and 3.17 respectively.

It is evident from figures that among the seven load cases, the predicted data in load case 2 seems to have the lowest error frequency for both deflection and strain data. For this load case more than 90 % of the deflection data had percentage error less than 5 %. Unfortunately strain data did not perform as good. About 45 % of the strain data had errors less than the 5 % limit. There are two distinctive features for load case 2; it was the first load case performed and unlike the remaining load cases, only five sampling points instead of ten points were employed in the regression analysis. When comparing deflection frequency diagrams with strain frequency diagrams for each load case, it is obvious that most of the deflection data fall within 0 to 15 % error range while strain data fall within a much wider error range. In addition to individual load case frequencies, Figures 3.16 and 3.17 show the frequency diagram for all of the load cases. As shown, about 60 % of deflection data have error less than 5 % while less than 20 % of strain data have the same error limit.

The high reliability of deflection data relative to that of the strain data can also be observed in Figure 3.18 and Figure 3.19. In these figures, cumulative frequency polygons are plotted for each load case and for all the load cases. The steeper the curves in these diagrams the higher is the reliability of the predicted data. Imposing a 20 % maximum error limit on the predicted response would result in discarding 5 % of the predicted deflection data and about 45 % of predicted strain data. An upper limit of 10 % would result in discarding over 60 % of strain data. This implies that more than 50 % of the strain gages did not record linear strain within the ten loading increments. However, this does not mean that the structure response was materially-nonlinear since displacements data showed excellent linear response. It is believed that the wide variations of the experimental strains is mainly attributed to the strain-measuring instruments.

Table 3.7: Strain data set (b) at **OHBD** trucks load.

Section #	ϵ 10^{-6}	Load Case 1	2	3	4	5	6	7
8	C^L_{18}	53	33	21	34	23	42	28
	C^L_{28}	112	156	17	69	19	97	129
	C^L_{38}	13	-53	0	-18	-10	13	-10
	A^L_{18}	131	157	33	76	16	98	42
	A^L_{28}	-82	-78	15	-501	33	-34	-50
	A^L_{38}	120	148	34	75	134	78	75
	A^L_{48}	-155	-163	-26	-70	-28	-100	-81
	A^L_{58}	-	-	-	-	-	-	-
	A^L_{68}	-84	-106	-14	-38	-28	-55	-43
	A^L_{78}	90	135	11	54	27	70	94
	A^L_{88}	-	-	-	-	-	-	-
	A^L_{98}	113	127	30	57	122	82	57
	A^{RL}_{18}	42	54	22	29	38	36	-50
	A^{RD}_{18}	44	101	66	54	71	12	31
	A^{RT}_{18}	6	-5	20	5	20	8	-28
	A^{RL}_{28}	-149	-168	-28	-77	-34	-98	-76
	A^{RD}_{28}	-72	-92	8	-48	22	-63	-52
	A^{RT}_{28}	49	83	766	151	-	153	47
	A^{RL}_{38}	9	13	-9	0	30	6	7
	A^{RD}_{38}	18	78	22	32	41	11	35
	A^{RT}_{38}	-14	13	15	8	20	3	12
9	C^L_{19}	13	-38	-21	-10	-23	-17	-14
	C^L_{29}	53	-263	14	17	-9	18	122
	C^L_{39}	-	-	-	-	-	-	-
	A^L_{19}	283	569	163	263	204	167	231
	A^L_{29}	288	567	161	244	221	174	212
	A^L_{39}	-	-	-	-	-	-	-
	A^L_{49}	-	-	-	-	-	-	-
	A^L_{59}	235	420	119	184	172	136	154
	A^L_{69}	236	425	126	175	190	130	162

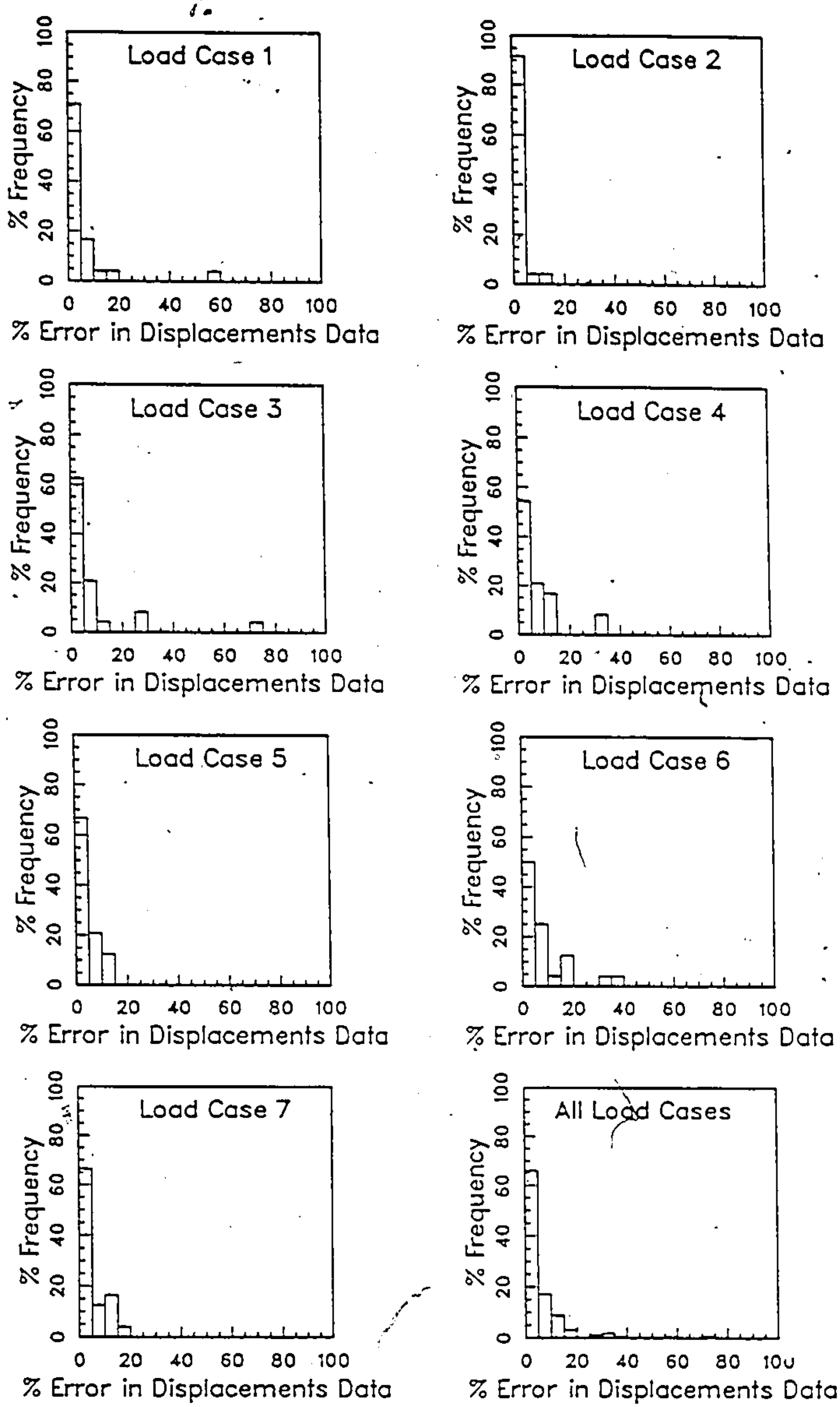

Figure 3.16: Frequency diagrams for predicted deflection data.

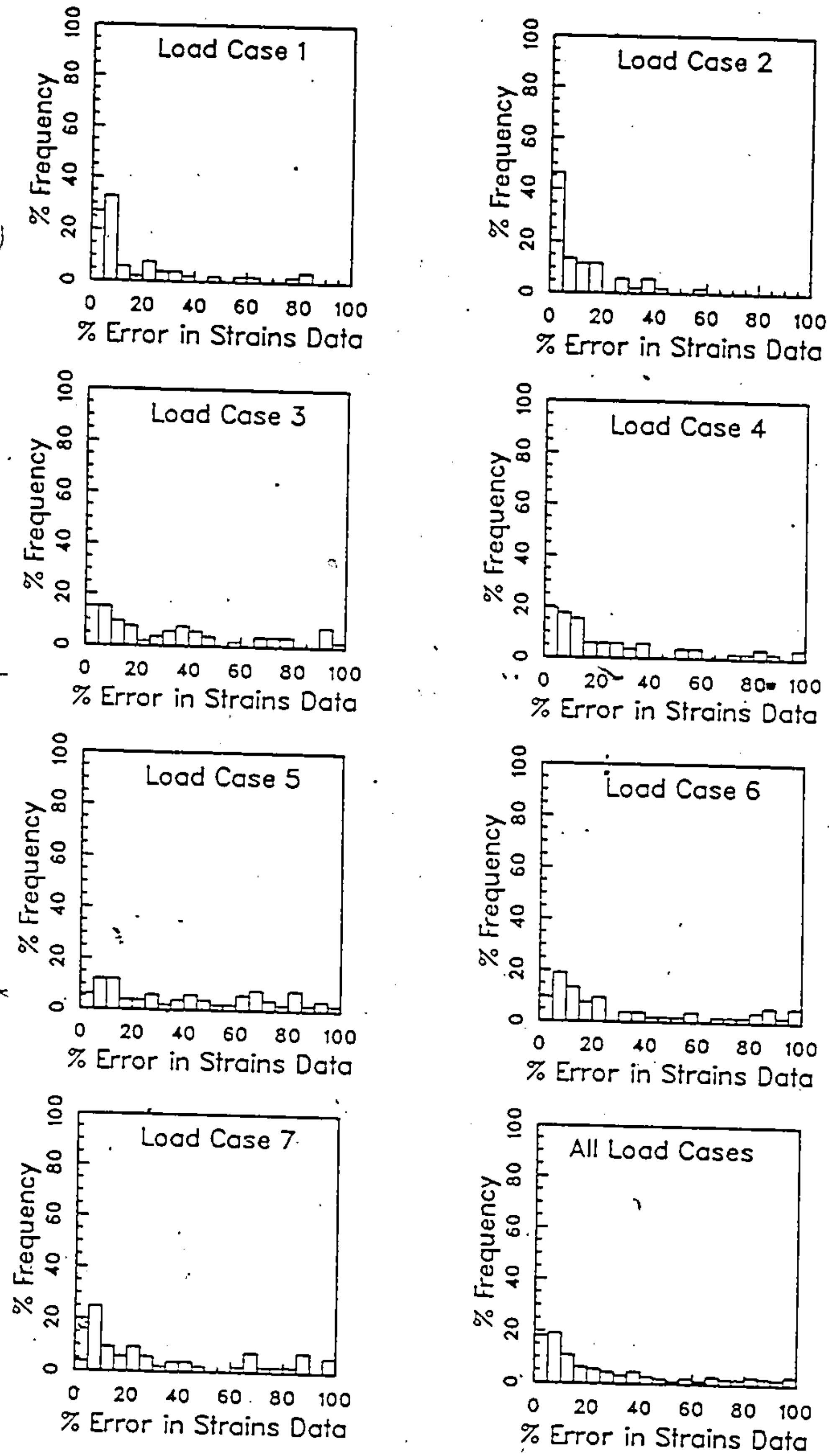

Figure 3.17: Frequency diagrams for predicted strain data.

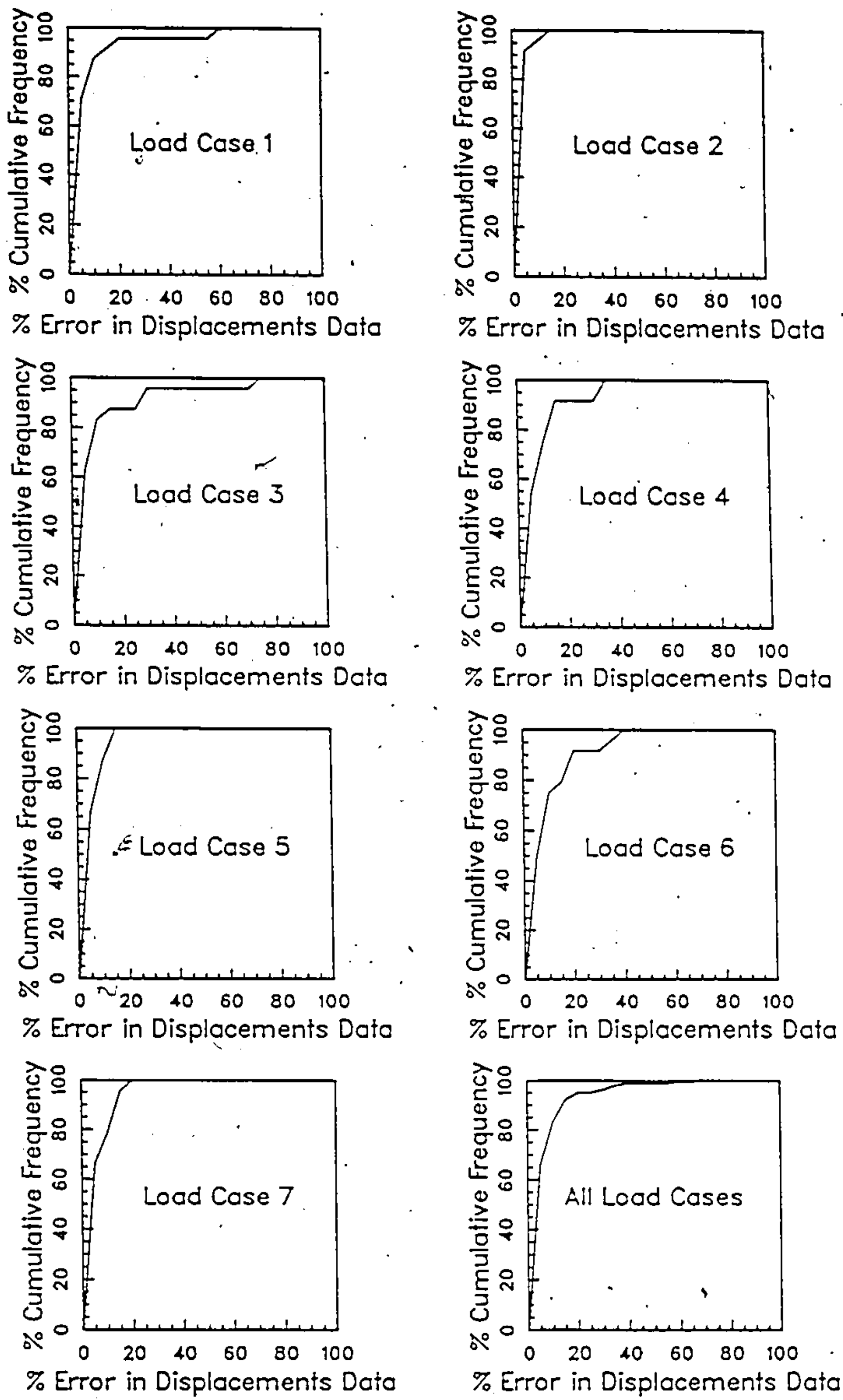

Figure 3.18: Cumulative frequency diagrams for predicted deflection data.

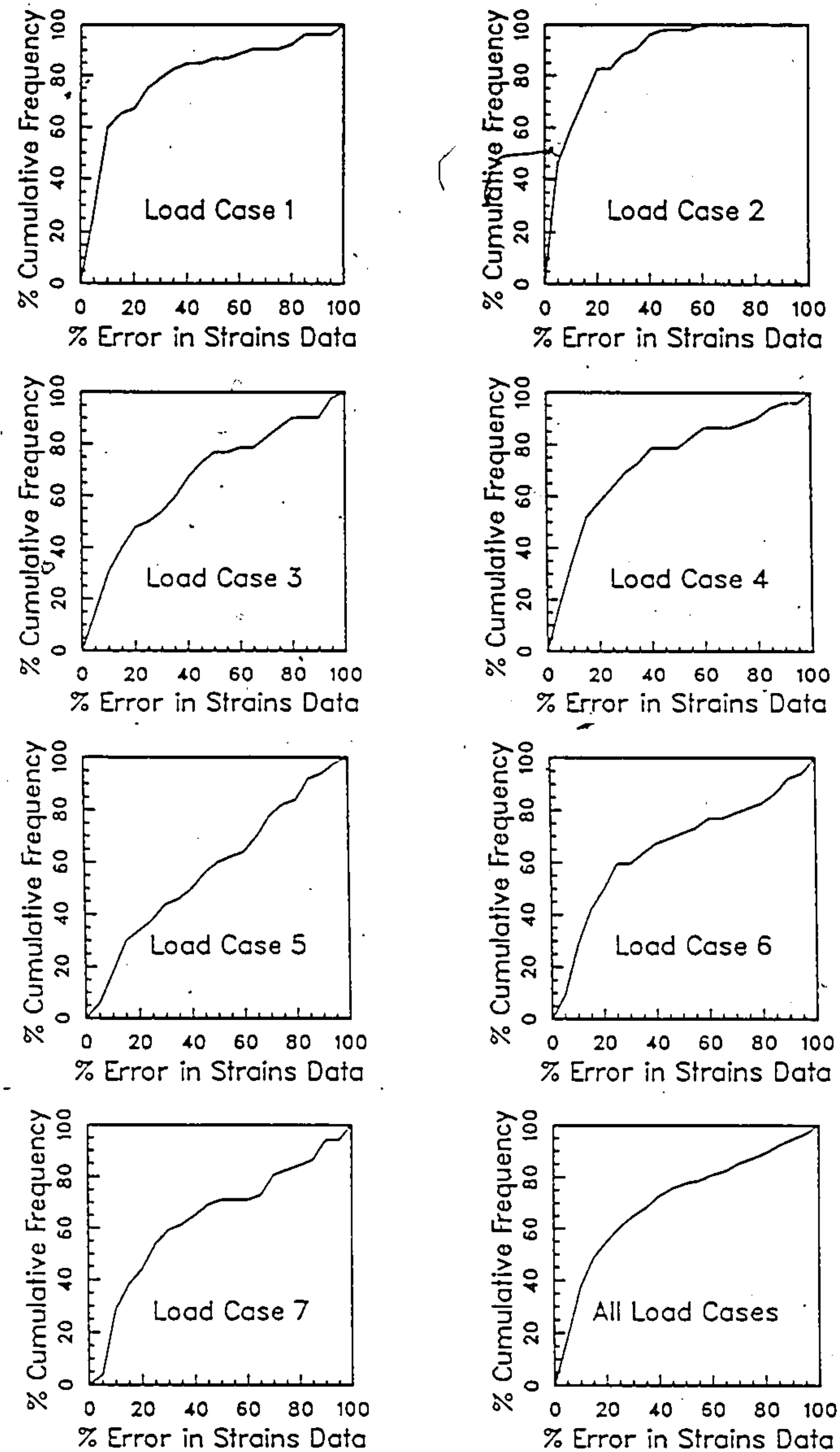

Figure 3.19: Cumulative frequency diagrams for predicted strain data.

3.5.2 Stresses

The reduced experimental strain data at **OHBD** truck load were the basis from which normal stresses (σ) and shear stresses (τ) were computed. Due to the curvilinear nature of the model geometry, it is convenient to adopt the cylindrical coordinate system shown in Figure 3.20.

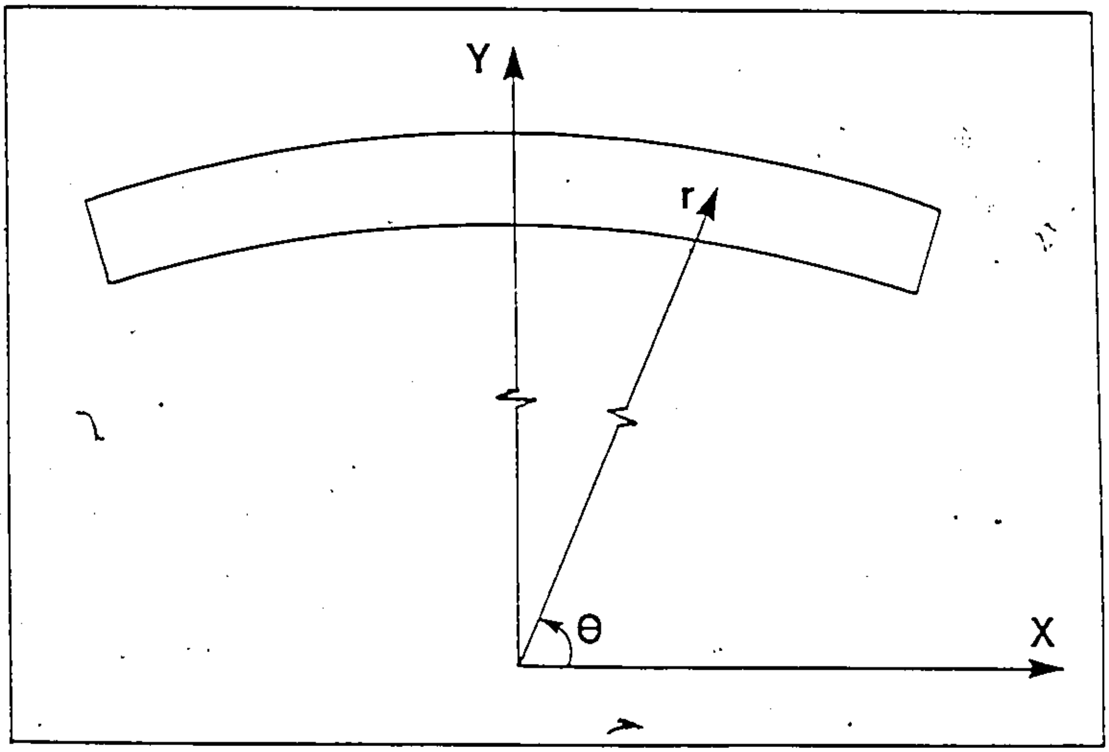

Figure 3.20: Cylindrical coordinate system for the bridge.

From the strain data the following stress components can be identified:

1. Normal stress components.
   - Tangential stress ($\sigma_{\theta\theta}$).
   - Radial stress (σ_{rr}).
2. Shear stress components.
   - Torsional shear stress ($\tau_{\theta r}$).
   - Vertical shear stress ($\tau_{\theta z}$).

Normal shear stresses were computed using the classical Hook's Law relations namely;

$$\sigma = E\,\epsilon_L \tag{3.20}$$

$$\tau = G\,\gamma \tag{3.21}$$

where E, G denote Young's modulus and Shear modulus respectively. γ denote shear strain computed from the rosette gage readings as follows:

$$\gamma = 2\,\epsilon_D - \epsilon_L - \epsilon_T \tag{3.22}$$

where ϵ_L , ϵ_T , ϵ_D denote Longitudinal, Transverse, and Diagonal strain components in the rosette plane.

The average material properties listed in Table 3.3 were used for the micro concrete. On the other hand the appropriate values listed for the webs and bottom plate from Table 3.4 were employed in stress calculations. A summary of the stress results are given in Table 3.8.

Table 3.8: Stress data set (a) at OHBD trucks load

Stress(MPa)		Load Case						
ID		1	2	3	4	5	6	7
	C_{12}^{L}	-1.63	-1.38	-0.72	-0.53	-2.22	0.31	-.69
	A_{12}^{L}	-3.17	0	-1.44	0.36	-3.24	0.65	-0.72
	A_{22}^{L}	2.95	1.08	1.22	1.08	8.28	-0.65	0.65
	A_{32}^{L}	5.13	4.36	3.09	2.53	10.54	-0.56	2.18
$\sigma_{\theta\theta}$	A_{42}^{L}	2.45	1.94	2.16	1.30	-14.26	11.45	-4.39
	A_{52}^{L}	-4.61	-4.10	-4.03	-1.30	-14.26	11.45	-4.39
	A_{62}^{L}	-3.38	-2.16	-2.30	-1.08	8.64	1.08	-1.01
	A_{82}^{L}	-3.60	-2.09	-2.30	-0.94	8.78	0.86	-1.01
	C_{25}^{L}	-1.88	-2.44	-2.03	-1.31	-3.38	0.75	-1.13
	C_{35}^{L}	-1.06	-1.38	-1.47	-0.63	-2.72	-0.66	-0.66
	A_{15}^{L}	-8.06	-9.72	-9.29	-4.97	-11.09	3.67	-5.76
	A_{25}^{L}	6.48	9.58	10.73	5.98	16.70	-2.38	6.19
	A_{35}^{L}	-7.42	-9.00	-10.87	-4.97	-	3.46	-6.19
$\sigma_{\theta\theta}$	A_{45}^{L}	9.70	15.53	16.37	8.36	21.86	-3.65	8.71
	A_{55}^{L}	8.08	12.65	13.91	7.59	19.47	-3.23	6.11
	A_{65}^{L}	2.74	8.86	7.13	3.74	10.73	-	4.90
	A_{75}^{L}	-6.48	-8.21	-10.01	-4.68	-14.62	3.60	-5.54
	A_{95}^{L}	-6.19	-8.71	-10.58	-4.39	-10.22	3.31	-5.40
	A_{15}^{RL}	-3.77	-8.90	-8.48	-5.42	29.32	1.13	-7.79
	A_{25}^{RL}	10.29	16.28	19.57	8.46	26.70	-6.71	9.18
	A_{35}^{RL}	-3.87	-3.75	-4.94	-6.41	-4.69	-0.13	-4.14
	C_{18}^{L}	1.66	1.03	0.66	1.06	0.72	1.31	0.88
$\sigma_{\theta\theta}$	C_{28}^{L}	3.51	4.88	0.53	2.16	0.59	3.04	4.04
	C_{38}^{L}	0.41	-1.66	0	-0.56	-0.31	0.41	-0.31

Table 3.8: Stress data set (b) at OHBD trucks load

Stress(MPa)		Load Case						
ID		1	2	3	4	5	6	7
$\sigma_{\theta\theta}$	A^L_{18}	9.43	11.30	2.38	5.47	1.15	7.06	3.02
	A^L_{28}	-5.90	-5.62	1.08	-36.07	2.38	-2.45	-3.60
	A^L_{38}	8.64	10.66	2.45	5.40	9.65	5.62	5.4
	A^L_{48}	-10.89	-11.46	-1.83	-4.92	-1.97	-7.03	-5.69
	A^L_{68}	-6.05	-7.63	-1.01	-2.74	-2.02	-3.96	-3.10
	A^L_{78}	6.48	9.72	0.79	3.89	1.94	5.04	6.77
	A^L_{98}	8.14	9.14	2.16	4.10	8.78	5.90	4.10
	A^{RL}_{18}	6.12	6.83	4.58	4.29	6.73	5.48	-8.99
	A^{RL}_{28}	-15.57	-15.35	57.48	1.98	-2.39	-0.60	-6.19
	A^{RL}_{38}	0.06	2.80	0.02	0.65	5.65	1.05	1.92
$\sigma_{\theta\theta}$	C^L_{19}	0.41	-1.19	-0.66	-0.31	-0.72	-0.53	-0.44
	C^L_{29}	1.66	-8.23	0.44	0.53	-0.28	0.56	3.82
	A^L_{19}	19.89	39.99	11.46	18.48	14.34	11.74	16.23
	A^L_{29}	20.24	39.85	11.31	17.15	15.53	12.23	14.90
	A^L_{59}	16.52	29.52	8.36	12.93	12.09	9.56	10.82
	A^L_{69}	16.59	29.87	8.85	12.30	13.35	9.14	11.38
σ_{rr}	A^{RT}_{25}	0.45	2.88	4.23	0.81	6.78	-3.19	0.51
	A^{RT}_{28}	-5.48	-2.55	97.94	13.60	-	12.19	0.08
$\tau_{\theta r}$	A^R_{25}	-0.69	-3.75	-1.10	-1.94	-1.10	-0.79	2.14
	A^R_{28}	-1.12	-2.52	-18.40	-4.33	-	-4.61	-1.91
$\tau_{\theta z}$	A^R_{15}	6.84	-2.14	-1.57	-0.65	-0.78	-1.17	0.52
	A^R_{35}	1.41	2.35	1.67	2.22	1.98	0.84	1.51
	A^R_{18}	1.04	3.99	2.35	1.93	2.19	-0.52	3.65
	A^R_{38}	1.07	3.39	0.99	1.46	0.84	0.34	1.33

Chapter 4

Finite Element Analysis using ADINA

4.1 Introduction

In this chapter, the application of ADINA program to curved box girder bridges is investigated through a case study. A twin box curved girder bridge is selected for the case study. This bridge was analyzed by many investigators using different methods of analysis. An exact solution for the static structural response have been reported in the literature by Chu & Pinjarkar [17] in 1971 and therefore can be used as the reference solution for comparing ADINA's results.

Prior to analyzing the subject bridge, a brief description about the commercially available ADINA program is presented along with some modelling requirements which are specific to curved box girder bridges. The assumptions inherent in the shell element formulations as well as the advantages and disadvantages for the element are then summarized. Next, the case study for the twin-box curved girder bridge structure is presented along with various ADINA models predictions. In this way, modelling technique and the applicability of ADINA elements for such a structure is verified.

4.2 ADINA Program

The Automatic Dynamic Incremental Nonlinear Analysis program is a general purpose Finite Element computer program employed for displacement and stress analysis. The versatility of ADINA system have been demonstrated by many researches in the fields of Solid mechanics, Fracture mechanics, Soil mechanics and fluid mechanics. The capability of the program in analyzing linear, nonlinear, static, or transient problems have been shown in ADINA System Verification Product [45] and many other references given in ADINA Theory and Modelling Guide [44]. This program, however, has ~~not~~ been used, at least not to the author's best knowledge, in analyzing the complex problem of curved box girder bridge structures.

The use of ADINA program in this research is justified on the following grounds:

- ADINA is the only finite element program which is available at the University of Ottawa capable of analyzing the particular bridge problem at hand.
- The use of ADINA for curved box girder bridges would open the opportunity for future modifications in the program to make it more specific and consequently more cost effective to bridge analysis.
- One major cumbersome and error prone process in any finite element analysis is the massive input data preparation. ADINA system is equipped with an excellent pre processor called ADINA-IN which makes this procedure simple and error free.

4.3 Modelling Requirements

In idealizing curved box girder structures, top and/or bottom flange elements are annular in shape while web elements could be conical or cylindrical. The elements should represent both in-plane and bending deformations. Since the bending action of the diaphragm is usually very small relative to the in-plane action, diaphragms could be adequately idealized using in-plane elements only. Due to the very nature of a bridge structure with a given aspect ratio, it is desirable to have spatially unisotropic element behavior. In this way long bridge structures can be idealized using a limited number of elements.

ADINA provides a family of isoparametric shell elements. They may be classified into three categories:

1. Thin plate/shell elements.
2. Thick shell elements.
3. Shell to solid transition elements.

It is this shell element category that is required in modelling curved box girder bridge structural components. In this group the shell element can have 4, 9, or 16 mid-surface nodes. As such and depending on the application, the appropriate number of nodes for the element is employed. For the current application, the quadratic 9-node thin shell element is selected for its effective representation of curved surfaces. A 4-node element model would require too many elements whereas the 16-node element model would be unnecessarily expensive particularly in the transverse (or radial) direction of the bridge . Details on the selected shell element are given in the next section.

4.4 The Thin Shell Isoparametric Element

The current state of ADINA system (version 1984) limits the use of this shell element to the following analysis conditions:

- Linear (static or dynamic) analysis where deformations and strains are infinitesimally small. Material behavior can be linear elastic, orthotropic, or linear-isotropic thermo-elastic.
- Materially-Nonlinear analysis for which deformation and strains are infinitesimally small, but the material behavior is nonlinear. Material models are limited to plastic, plastic multilinear with isotropic hardening, and /or nonlinear-isotropic thermo-elastic material models.
- Geometrically Non-linear analysis in which deformations are large but strains are small. Material behavior is limited to linear elastic model or nonlinear

elasto-plastic model with isotropic hardening.

The basic equations used in formulating the general shell element are given in [25].

The two Fundamental assumptions used in the formulation of the shell element are:

1. Material particles that originally lie on a straight line normal to the mid-surface of the structure remain on that straight line during the deformations.
2. The normal stress in the direction normal to the mid-surface of the structure is zero.

In the first assumption, the straight line which is originally normal to the shell mid-surface may or may not be normal to the shell mid-surface during deformations. This implies that shear deformations are included in the analysis. The transverse shear deformations are assumed to be constant across the shell thickness. The second assumption on the stress situation enters the finite element solution by imposing zero stress in the t-direction which is the direction of the normal vector to shell mid-surface.

In the calculations of the shell element matrices the following coordinate systems are used:

- The element natural coordinate system r, s, t. This system is established in accordance to element nodal numbering scheme as shown in Figure 4.1.
- The cartesian shell-aligned coordinate system $\hat{r}, \hat{s}, \hat{t}$. Unlike the previous system, the axes for this one are orthogonal. This system is established at any integration point once the shell midsurface normal is defined. Unit vectors along $\hat{r}$ and $\hat{s}$ are given as follows:

$$e_{\hat{r}} = \frac{e_s \times e_t}{|e_s \times e_t|} \tag{4.1}$$

$$e_{\hat{s}} = e_t \times e_{\hat{r}} \tag{4.2}$$

  where e_s, e_t are unit vectors along s and t directions. The unit vector e_t at the integration point is defined by interpolating between shell midsurface normal vectors at nodal points.

- The structure or global cartesian coordinate system X, Y, Z.

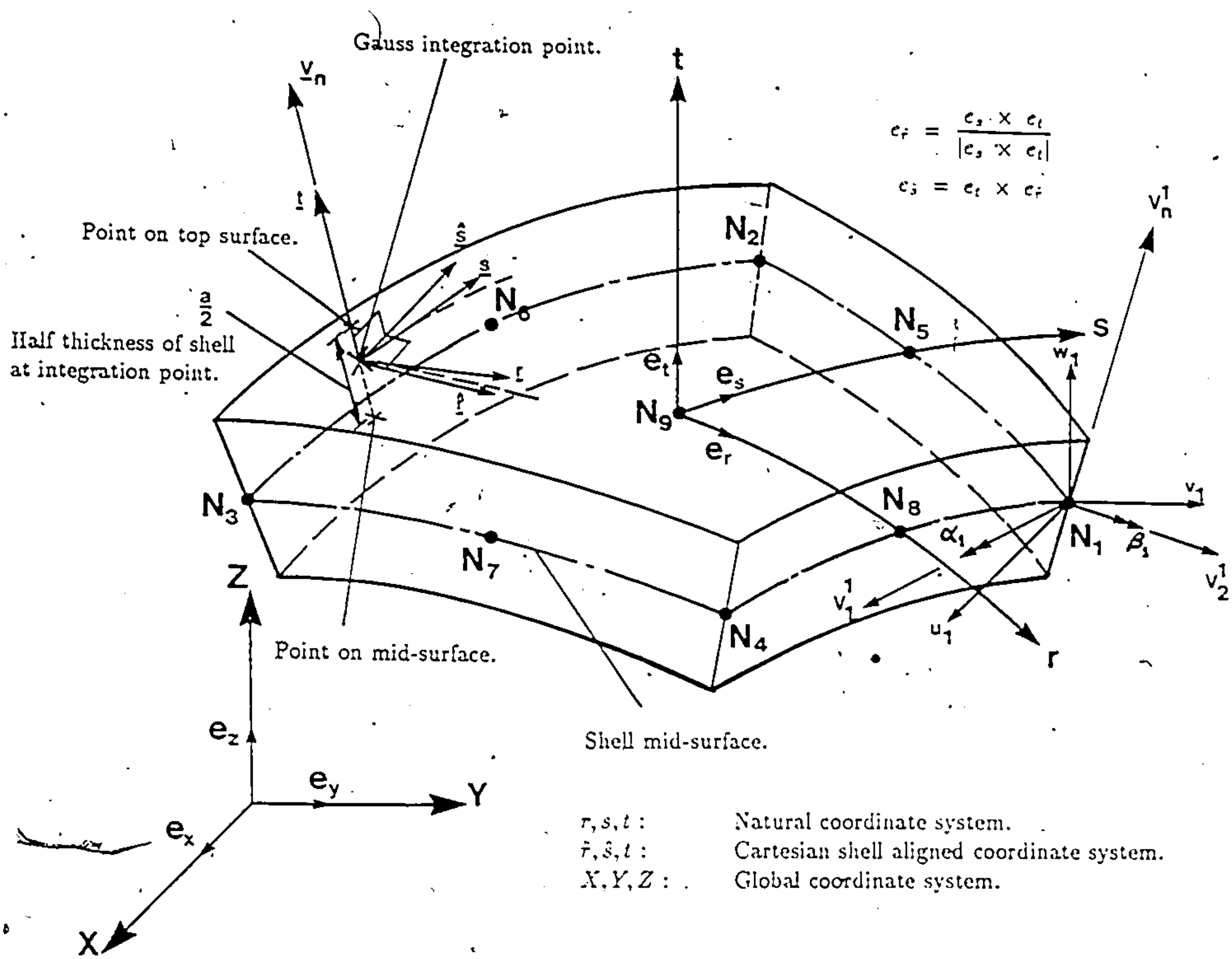

u_k, v_k, w_k = 3 translational D.O.F. along global X,Y,Z axses respectively.
α_k, β_k = 2 rotational D.O.F. about vectors V_1^k & V_2^k respectively.

$$V_1^k = \frac{e_y \times V_n^k}{|e_y \times V_n^k|}$$

$$V_2^k = V_n^k \times V_1^k$$

when $V_n^k = \pm Y$ then: $V_1^k = \pm Z$, $V_2^k = \mp X$

Figure 4.1: ADINA's 9-node thin shell element.

A typical node on the shell mid-surface can have a maximum of 5 degrees of freedom; 3 translations and 2 rotations. The translational D.O.F, u_k, v_k, w_k, are referred to the global cartesian coordinate system. The two rotations α_k and β_k are referenced with respect to the orthogonal vectors V_1^k and V_2^k at node k respectively. These vectors are defined from the normal vector at node k as follows:

$$V_1^k = \frac{e_y \times V_n^k}{|e_y \times V_n^k|} \tag{4.3}$$

$$V_2^k = V_n^k \times V_1^k \tag{4.4}$$

For the special case when the normal vector V_n^k at node k is aligned with the global Y-axis, then the following rule is employed:

$$\text{when } V_n^k = \pm Y \text{ then:} \qquad \begin{aligned} V_1^k &= \pm Z \\ V_2^k &= +X \end{aligned}$$

In this way a unique set of orthogonal vectors V_1^k and V_2^k at node k is defined for a unique normal vector V_n^k at node k. A problem arises when shell elements intersect at common boundaries and hence a unique normal vector at intersection nodes can no longer be defined. This is the case in modelling box girder structures where top and bottom flange elements intersect with the web elements and sometimes with diaphragm elements at one or more common nodes. This problem was a major drawback in ADINA 82 system. In that version the only way to circumvent this problem was by defining as many nodes as there are intersecting shell elements and proper constraint equations are then written to tie up the five degrees of freedom at each node. This procedure results in tremendous increase in the number of nodes particularly in box girder structure. A much more efficient method was provided by the 1984 ADINA system. In this version the program automatically generates as many normal vectors at the common node k as there are shell elements attached to the node. Hence for each individual intersecting shell element a unique normal vector is defined at node k. The components of the shell element matrices corresponding to the rotational degrees of freedom at this node are first formulated in the local mid-surface system defined by the normal vector and then rotated to the global cartesian system [44].

4.5 Case study: Twin Cell Curved Box Girder Bridge

4.5.1 Introduction

The versatility and general nature of the ADINA system along with the fact that this program has not been used in analyzing the complex problems such as curved box girder bridge structures would render the direct use of this system for the current bridge model susceptible to hesitation about the proper use of this program and the interpretation of its results. It is therefore worthwhile to apply this program first to a similar structure for which reliable solutions are available. In this way any doubts about the proper use, modelling technique, and program output interpretation are eliminated.

4.5.2 Previous Work

The twin box girder bridge shown in Figure 4.2 is used to verify the proper use of ADINA system. The bridge is a simply supported composite construction concrete-steel structure having mean radius of curvature of 300 feet (91.44 m) and spanning 80 feet (24.38 m) along the mean circumferential direction between supports centerlines. The horizontally curved structure is subjected to three load cases each of which consisting of a single concentrated load of 100 Kips (445 KN) applied at the mid-span section of the bridge. The radial locations of the point loads are 292 ft (89.00 m), 300 ft (91.40 m), and 308 ft (93.88 m) for load cases 1, 2 and 3 respectively.

This particular bridge problem was analyzed by four distinct methods of analysis. Chu and Pinjarkar in 1971 [17] presented a solution for the bridge using the stiffness (or displacement) approach by applying the folded plate theory to simply supported curved box girder bridges. In their method of analysis they assumed an isotropic material, no intermediate diaphragms and no interaction between membrane forces and bending action of the plates. They compared their solution to that obtained using Tung's method [16] which neglects the interaction between the deformation of

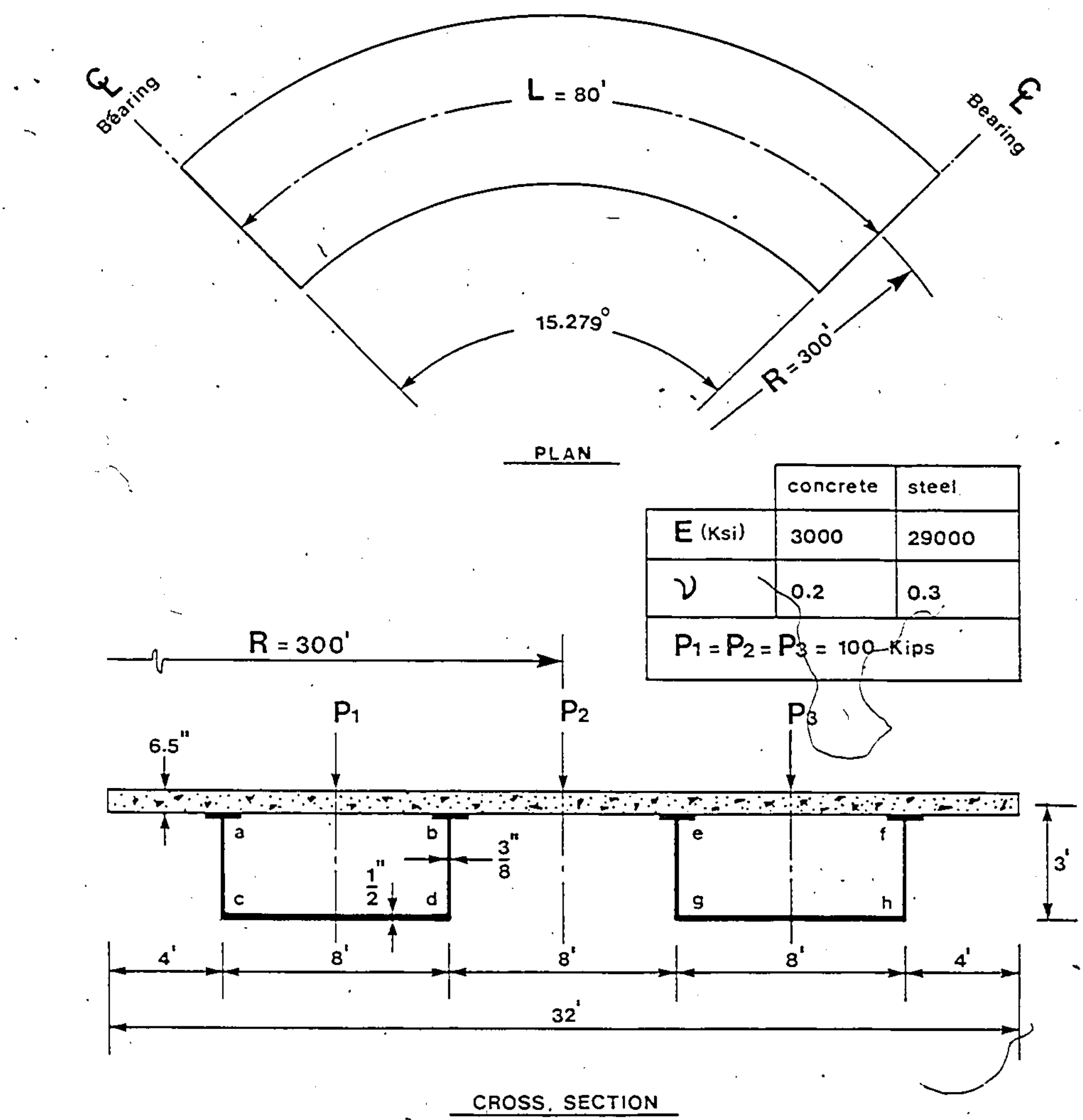

	concrete	steel
E (Ksi)	3000	29000
ν	0.2	0.3
$P_1 = P_2 = P_3 =$ 100 Kips		

Figure 4.2: Geometry of the curved twin box girder bridge.

the annular plates and cylindrical shell elements. Meyer and Scordelis [19] presented two sets of results for the twin box girder bridge problem using the curved finite strip method. They idealized the bridge using 19 nodal lines and 20 strips by employing 15 and 59 term harmonics for the two sets of solution.

The problem was also solved by Fam and Turkstra [18] using their special purpose finite element program CBRIDG. In this program, Adel Fam used annular plate elements and cylindrical shell elements which were developed specifically for curved or straight box girder structures. The accuracy of these elements and the program was established by comparing CBRIDG results with Pinjarkar solution for the twin box girder bridge. Furthermore, they tested their program by comparing with experimental results obtained from a small scale plexiglas single box girder bridge model [35].

For comparison purposes the different researchers presented their results in terms of longitudinal normal stresses and membrane shear stresses at mid-span section and end support sections of the curved bridge respectively. The radial location of normal stress points are shown in Figure 4.2 (points a,b,c,d,e,f,g,h). In comparing the results, the various methods of analysis showed good agreement with the exception of Tung's method. There was a general consensus among the researchers that the poor agreement of Tung's solution is due to its simplifying assumptions which neglect the fact that a curved box girder structure is made of plates and shells that interact together in resisting the applied loads. Chu and Pinjarkar were commended for their successful application of the curved Folded Plate Theory and their solution was considered as an exact solution for this particular problem by Scordelis et al. and Fam et al.

4.5.3 Description of F.E.M. ADINA Models

In applying ADINA to the twin-box girder curved bridge, several models having different element topography were considered. The nine-node thin shell element was the basic element employed in modelling the annular plates and cylindrical webs. Common features of the various models consistent with those used by the previous researchers are listed below:

- The complete simply supported structure was discretized using the geometry shown in Figure 4.2.
- The 32 feet (9.75 m) wide bridge deck was idealized using 6.5" (165 mm) thick annular shell elements. Linear, elastic and isotropic material behavior was assumed with modulus of elasticity of 3000 ksi (20670 Mpa) and Poisson's ratio of 1/5.
- The steel portion of the box was idealized using 3/8" (9.525 mm) thick cylindrical shell elements for the webs and 1/2" (12,70 mm) annular elements for the bottom flange. The top flange plates were neglected and the web elements are assumed to extend to the mid-surface of the concrete slab with a total web depth of 3 feet (0.914 m). Linear, elastic and isotropic material was assumed for the steel with modulus of elasticity of 29,000 ksi (199,810 Mpa) and Poisson's ratio of 0.3.
- The in-plane infinitely stiff internal diaphragm action at bridge end sections was assumed by imposing the proper constraint equations which prohibits any radial translation at end supports.
- Identical boundary conditions were employed at both supports. At these sections, bottom flange nodes were fixed in vertical and radial translation and set free to move longitudinally. In order to avoid any rigid body movement in the circumferential direction, mid-span section nodes had restraints in that direction.
- The bridge in all models was subjected to the three load cases described earlier and labeled P_1, P_2, P_3 respectively.

Of the various models analyzed, element topology for models A,B,C,D,E, and H are shown in Figure 4.3. Model A is the basic coarsest mesh consisting of one element for each side of the box section, two overhang elements, and one element connecting the two boxes through the deck. A total of 11 elements per transverse section were used in model A. Longitudinally, the bridge was discretized using eight element zones. Model B has the same transverse idealization as model A; however, 16 element zones were used to idealize the structure longitudinally. In model C, two transverse elements were employed for the boxes annular plates while one element was kept through the web depth as in model A. In this way 16 elements were employed in

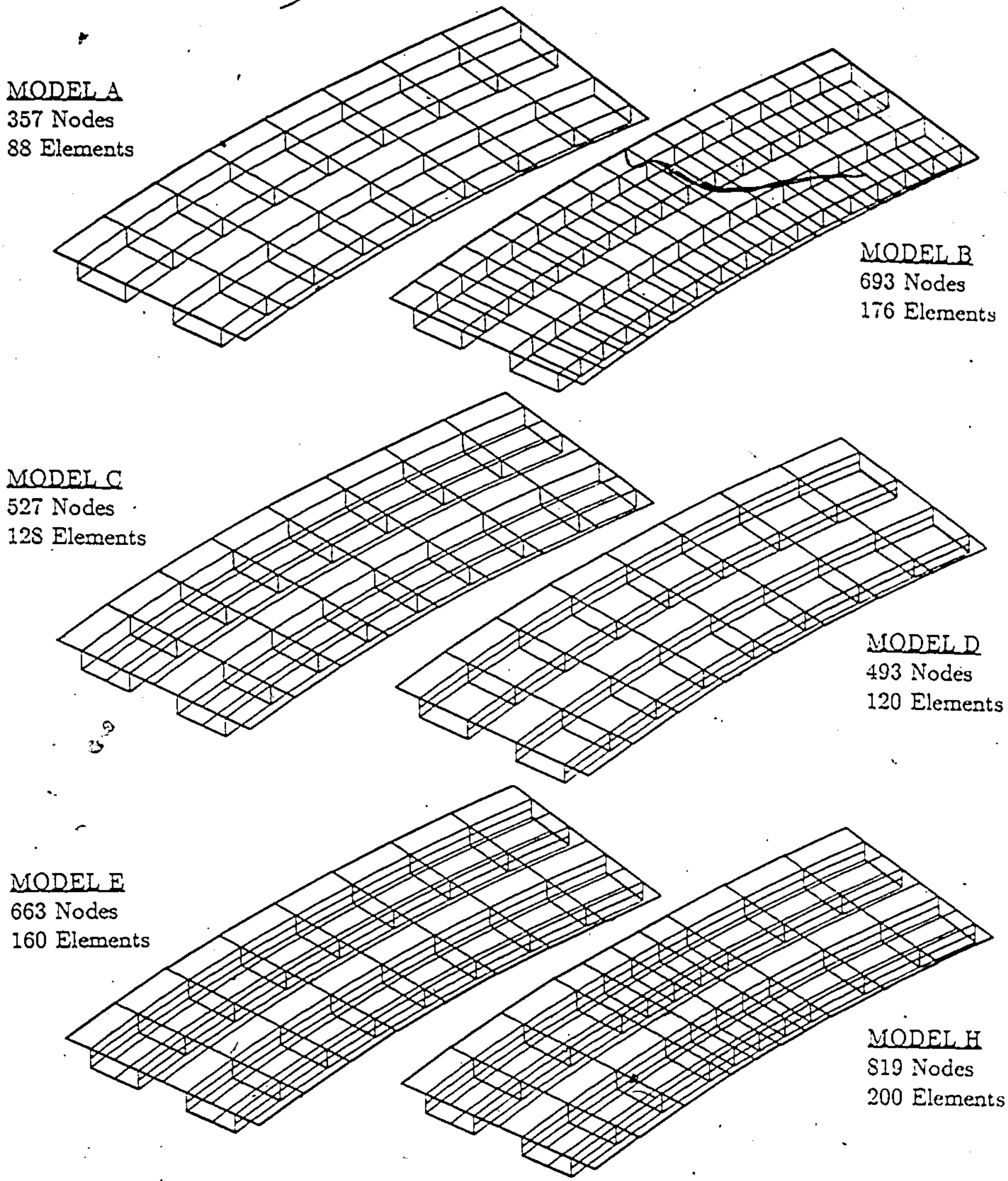

Figure 4.3: Finite element discretizations of the twin-box girder bridge.

idealizing the structure transversely. Moreover, longitudinal discretization was kept at 8 element zones as in model A. Model D is somewhat similar to model C except that element fineness is increased in the vertical direction rather than in the radial direction. As such two elements were used through the web depth and one element was employed in the top or bottom annular plates of the boxes. A total of 15 elements per section and 8 element zones were used in model D.

Model E combines features of models C and D by employing two elements per box flange or web and hence consists of 20 elements per bridge section. In this way the individual and the combined effect of mesh fineness in both transverse (or radial) and vertical direction can be examined in models C, D, E, while longitudinal convergence can be studied in model B. Element topography used in model H represent the mesh which resulted in converged solutions. Model H have the same transverse idealization as model E; however it differs by the number of element zones used in the circumferential direction of the bridge. Model H consists of 10 element zones with finer element zones located around the mid-span section of the bridge.

4.5.4 Convergence of ADINA Models

Displacements

Since in all load cases the 100 ksi (445 KN) concentrated load was applied at the mid-span section, bridge deck deflection at this section is plotted for models A,B,C,D, and E for the three load cases in Figure 4.4. Unfortunately, previous researchers did not report bridge deflection and therefore comparison between ADINA results and previous work cannot be made. However, it is interesting to note the difference in transverse distribution of vertical deflection between the various ADINA models.

It is evident that model A has sufficient longitudinal elements for deflection convergence. This observation can be seen for all load cases when comparing model A deflections with those obtained in model B. Comparison of deflections from model C with those from model A indicates that transverse idealization of the box annular plates with one element is too coarse and hence structure response is too stiff. The percentage error in inner overhang (R = 284 ft. = 86.56 m) deflection in model A is 54 %, 35 %, and over 100 % at load case 1, 2, and 3 respectively. Similar

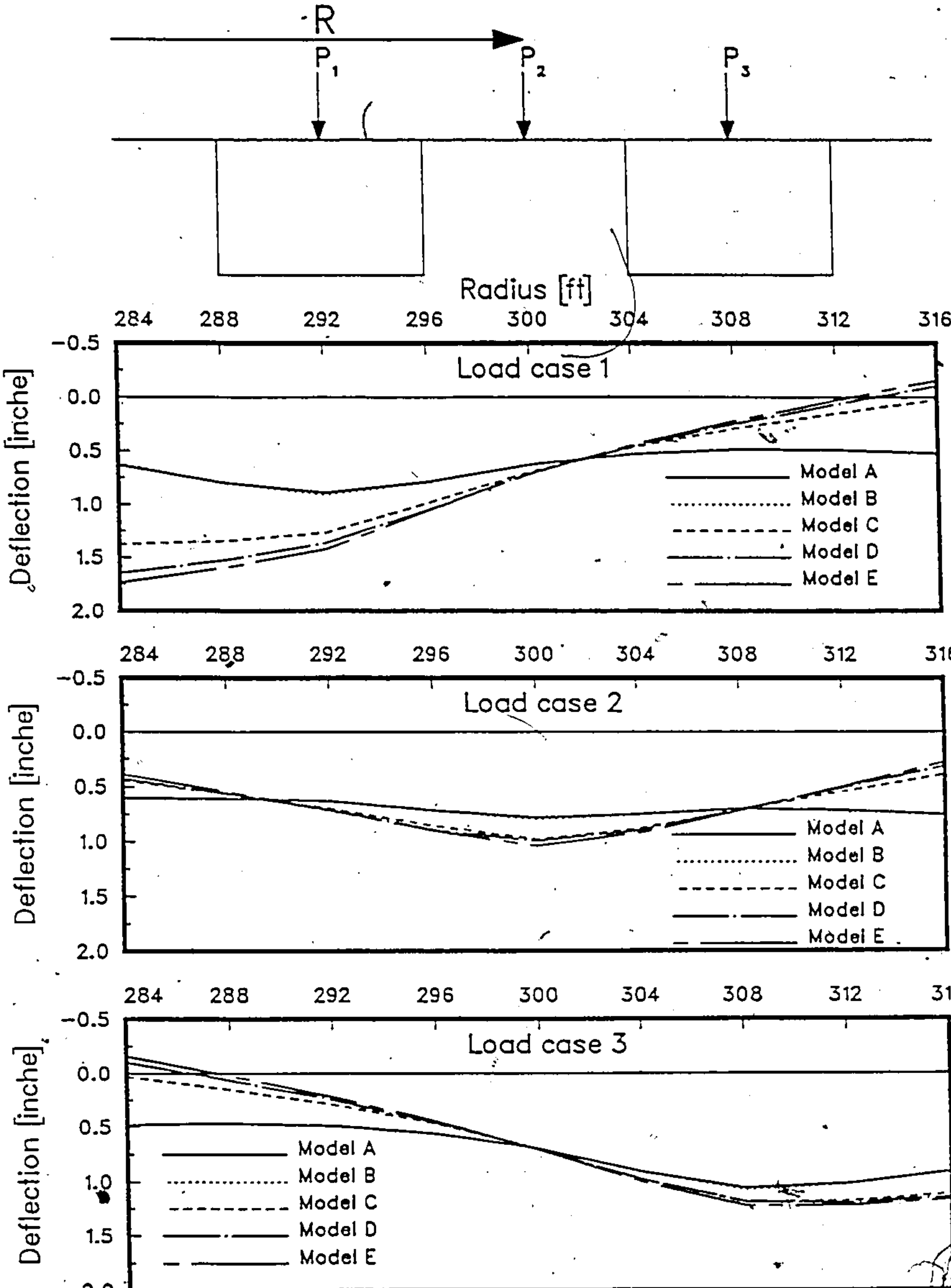

Figure 4.4: ADINA's prediction of bridge deck deflection at mid-span section.

observations can be made when comparing results of model D with those of model A. The percentage error in model A maximum deflection can be as high as 62 % and 42 % for load cases 1 and 2 respectively.

It can be shown that there is no need to idealize the box annular plates or cylindrical webs with more than two elements radially or in the vertical direction. As such, deflections of model E can be considered as a converged solution for the three load cases. In fact, for all practical purposes, deflections of model D are considered accurate enough when compared to those obtained in model E.

Another interesting feature which can be observed in Figure 4.4 is the influence of the type of loading on deflection solution convergence. It is evident that eccentric loading has slower convergence compared to concentric loading. This can be seen when comparing deflection curves of load case 2 to those in either load case 1 or load case 3. Last, deflection curves for both load cases 1 and 3 seem to have higher convergence errors at the inner edge of the bridge deck (R = 284 ft. = 86.56 m) than those computed at the outer edge (R = 316 ft. = 96.32 m)

Stresses

Transverse distribution of longitudinal normal stresses developed at bridge mid-span section is given for load case 1,2,3 in Figures 4.5, 4.6, 4.7 respectively. In these Figures stresses at element mid-surface is plotted for ADINA models A,B,C,D, and E. For a typical section, the magnitude of stress at box corners, representing those computed at top or bottom plate midsurface, are shown. It is these stress points which have been used by previous researchers in comparing their results. From these figures a number of important observations can be established with respect to the application of ADINA 9-node thin-shell element to curved box girder bridges subjected to eccentric type of loading.

Comparing Model A stresses with those of model B in any load case, it can be shown that the maximum error in normal stress computed for the coarse model A is less than 10 %. As for normal stress distribution between the two box girders, both models predict the same distribution. If we would modify model A slightly by doubling the number of element sections longitudinally only arround the mid-

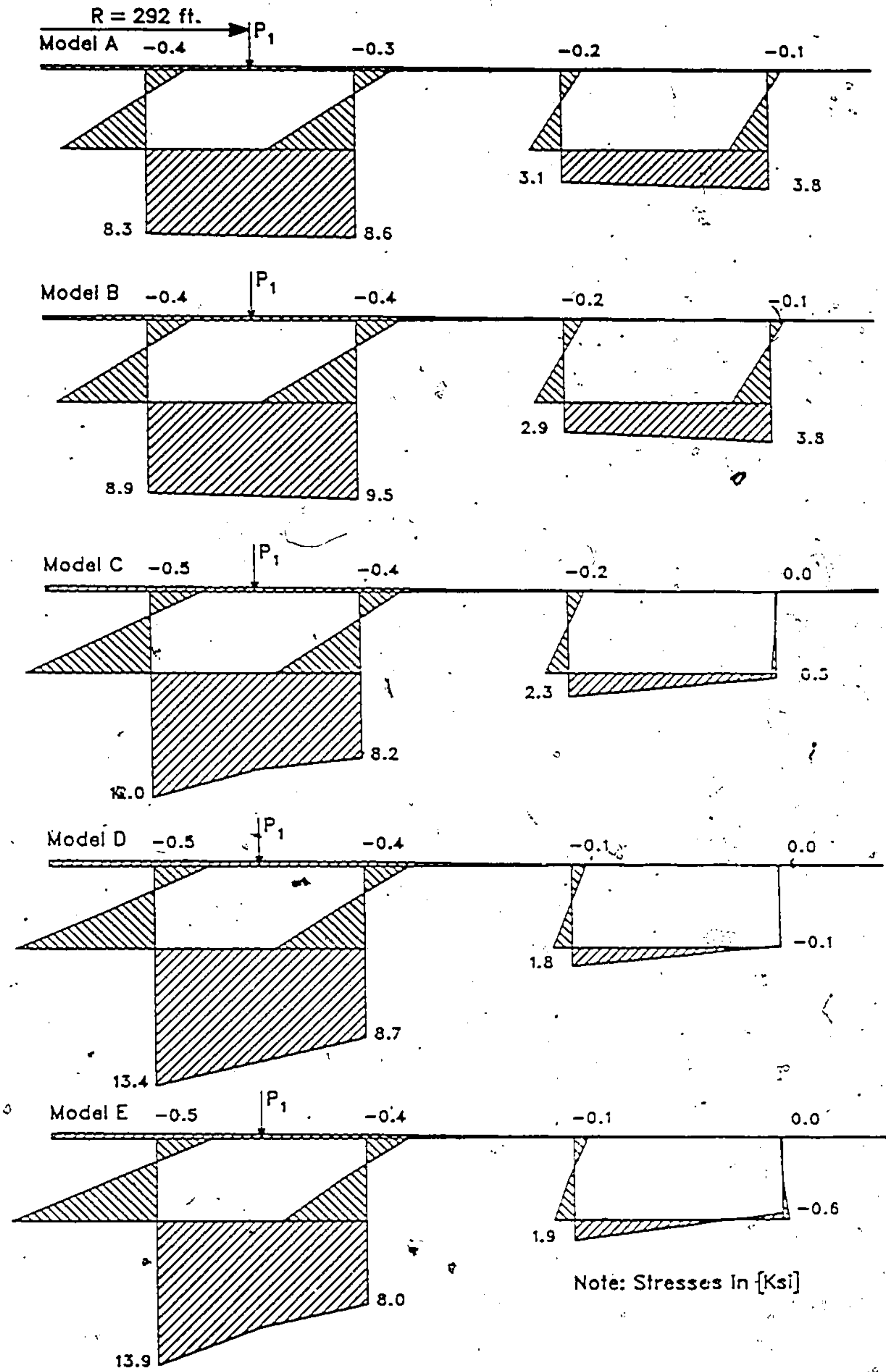

Figure 4.5: ADINA's prediction of longitudinal normal stresses at mid-span section at Load Case 1.

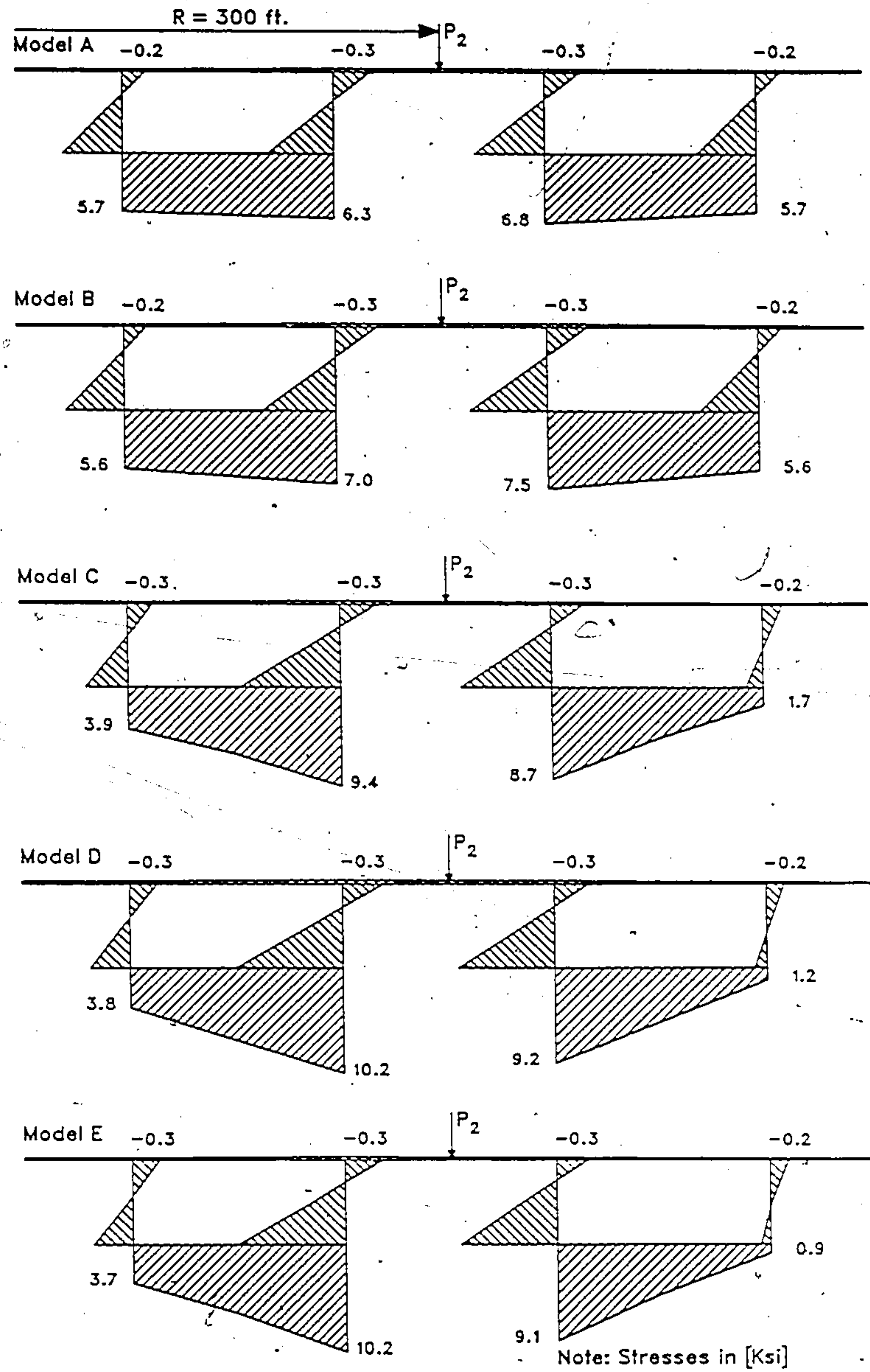

Figure 4.6: ADINA's prediction of longitudinal normal stresses at mid-span section at Load Case 2.

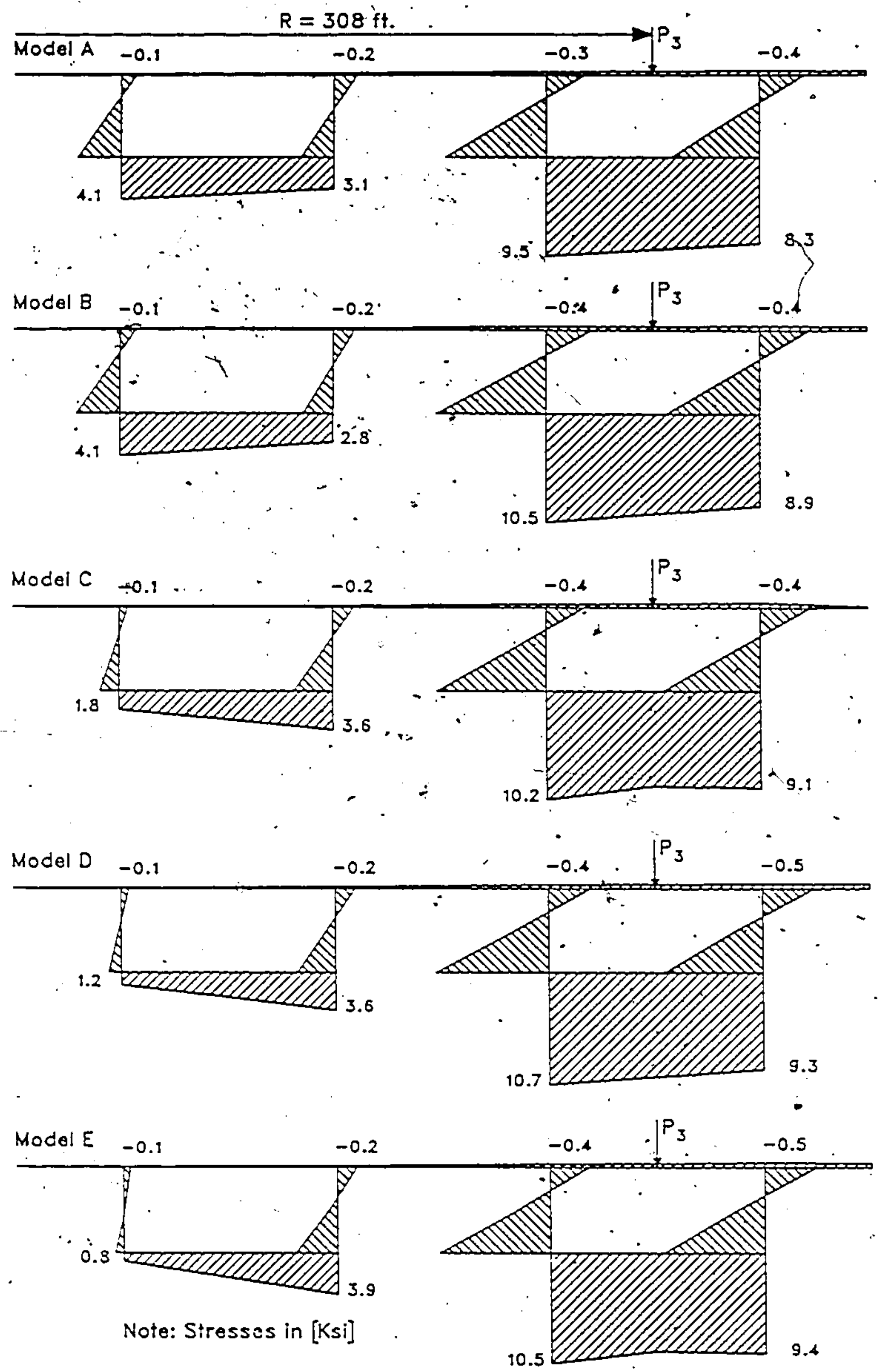

Figure 4.7: ADINA's prediction of longitudinal normal stresses at mid-span section at Load Case 3.

span section then it is reasonable to expect that the 10 % maximum error would be reduced to a much lower level. In this way a much more cost effective model is analyzed with predictions as accurate as those in model B. However, by ignoring the investigation of radial and vertical mesh fineness of the curved box section elements, models A or B would result in erroneous distribution of longitudinal normal stresses.

If we ignore model C and model D stress distribution and compare model A or B stresses to those plotted for model E, the erroneous stresses in model A or B is evident. The errors are highest in load case 1 where the load is applied at the centerline of the inner box and are lowest in load case 2 where the load is applied at the centerline of bridge section. For load case 1, Figure 4.5 shows that model A underestimates the maximum steel or compressive stress by 40 % in the inner girder and overestimates the outer girder stresses by 63 %. Furthermore model A predicts compressive stress of 3.8 ksi (26.2 Mpa) at the intersection of bottom flange with the outer web in the outer box, whereas the more accurate model E predicts tensile stress of 0.6 ksi (4.13 Mpa)at the same location. Recalling that in model E two element per box side were employed in the bridge cross-section compared to one element used in model A, it is clear that a minimum of two 9-node thin shell element are required per box side in modelling curved box girder bridges particularly when subjected to eccentric loading.

Comparison of the results of models C and D shows that element fineness is more effective in the vertical direction, i.e. through the web depth, rather than in the radial direction through the annular plates. This is reflected by the relatively smaller errors incurred in model D compared to those computed for model C.

The inaccuracy of models A and B results cannot be attributed to element formulation. Similar models have been applied for straight box girder bridges subjected to concentric loading and yielded accurate solutions. It is the combined effect of eccentric loading with curved geometry that results in a highly complex deformation patterns resulting in rather inaccurate displacements and stresses in models A and B.

Although not clearly indicated in the figures, it can be shown that any increase in the number of elements employed in transversely idealizing the box girder over those used in model E will not result in any change in normal stresses or their distribution at the mid-span section. Based on the above, Model H was selected to have the same transverse idealization as model E. Model H, however, is finer longitudinally near the bridge mid-span section than model E. In this way errors incurred in model E are reduced in model H. Therefore results of model H shall be used in comparing ADINA prediction to those reported by the previous researchers.

4.5.5 Comparison between ADINA Results and Previous Work

The results of ADINA models discussed previously clearly indicate that that the converged displacement and stress fields can be obtained by analyzing model H. Therefore the results of this model are used in comparing with the results of previous researchers. In model H, the twin box girder is discretized transversely into 20 thin shell elements of which 8 elements were employed in modelling the deck and the remaining 12 elements were used for the steel components of the boxes. Longitudinally, the bridge was divided into 10 element segments as shown in Figure 4.3. Model H input file is listed in Appendix C for future reference. This file represents ADINA-IN input file and should not be confused with ADINA data file which would be prepared by the pre-processor ADINA-IN program.

Previous researchers have reported their results for the twin box girder bridge in terms of longitudinal normal stress and membrane shear stress at bridge mid-span and end support sections respectively. Table 4.1 lists the normal stress values at the eight stress points a,b,c,d,e,f,g,h which are shown in Figure 4.2. The tables include the results computed by M.Y.T. Chan[1] using his finite strip program which was developed for simply supported curved box girder bridges. Chan analyzed the twin box girder structure by using the same idealization used by Meyer and Scordelis [19]. Both researchers analyzed the structure using 15 term harmonics and 59 term harmonics. The stresses given in Table 4.1 are those of the 59 term harmonic solution.

Comparing ADINA predictions for normal stresses with those obtained by other researchers, it is clear that ADINA provide excellent results for the twin box girder bridge. Furthermore, in all methods of analyses used by different researchers there is general agreement with the exception of Tung's simplified method of analysis. The

[1]Structural Engineer at Public Works Canada, A.E.S., R.D.D., OTTAWA.

Table 4.1: Longitudinal normal stress (psi) at mid-section of the bridge.

Load case 1 Point	Tung	Pinjarkar Chu	Meyer Scordelis	Fam Turkstra	M.Y.T. Chan	ADINA Model II
a	-368	-561	-555	-563	-559	-555
b	-368	-427	-420	-431	-413	-428
c	8256	14770	15100	15100	13379	14490
d	8256	8545	8320	8505	8612	8714
e	-143	-137	-137	-134	-129	-139
f	-143	29	30	31	37	22
g	3197	1858	1925	1817	1941	1840
h	3197	-780	-845	-830	-704	-577
Load case 2 Point	**Tung**	**Pinjarkar Chu**	**Meyer Scordelis**	**Fam Turkstra**	**M.Y.T. Chan**	**ADINA Model II**
a	-273	-259	-	-254	-255	-258
b	-273	-370	-	-376	-363	-372
c	6127	3348	-	3100	3075	3352
d	6127	11040	-	11320	11108	11025
e	-251	-320	-	-325	-316	-322
f	-251	-165	-	-160	-163	-167
g	5640	10070	-	10820	9908	10070
h	5640	535	-	532	541	605
Load case 3 Point	**Tung**	**Pinjarkar Chu**	**Meyer Scordelis**	**Fam Turkstra**	**M.Y.T. Chan**	**ADINA Model II**
a	-143	-67	-65	-65	-70	-70
b	-143	-186	-185	-183	-187	-188
c	3185	618	528	515	547	805
d	3185	3860	3930	3840	3829	3761
e	-396	-392	-384	-394	-395	-393
f	-396	-497	-492	-502	-489	-494
g	8895	11150	11080	11300	10896	11195
h	8895	10110	10070	10180	10668	10003

various researchers have used Pinjarkar & Chu [17] solution as an exact solution in verifying the accuracy of their programs. Keeping Pinjarkar & Chu solution as the reference solution we can quantify the effectiveness of ADINA's prediction for stresses by evaluating the percentage error in maximum normal stress developed in each load case. As such, errors of magnitude 1.9 %, 0 %, and 0.4 % are found for load cases 1,2, and 3 respectively.

Comparing these errors with those computed for other solutions given in Table 4.1, ADINA's errors are the lowest ones. The accuracy of ADINA solution is also evident in Figure 4.8. In this Figure, normal stresses obtained using ADINA model H and those reported by Pinjarkar & Chu [17] are plotted at mid-span section of the bridge for the three load cases.

ADINA predictions in terms of membrane shear stresses at end support sections are no less accurate than the normal stress component. Table 4.2 shows solutions of the different investigators for the average membrane shear stresses in each box element and for the three load cases. The table includes the results of Chan's finite strip program as well as ADINA model H solutions. Again, there is good agreement between the various solutions with the exception of Tung's results.

4.5.6 Influence of Boundary Conditions on ADINA Solution

In modelling curved box girder structures, boundary conditions play an important role in the accuracy of both displacement and stress fields. While the thin shell element does have torsional stiffness, failing to restrain the simply supported box girder in the radial translation at end support sections can result in erroneous structural response. To assess these errors, two ADINA models were analyzed for the twin box girder bridge; namely model H and model I. Model I have identical element topography as the previously described model H. The only difference between the two models is the type of boundary conditions imposed upon the structure. In model I, radial translation was not totally constrained at both supports as for the case of model H. Instead, bottom plate nodes were pinned in the three global directions X, Y, Z at one support whereas only vertical translation was fixed at the other support. As such, the basic difference between the two models lies in

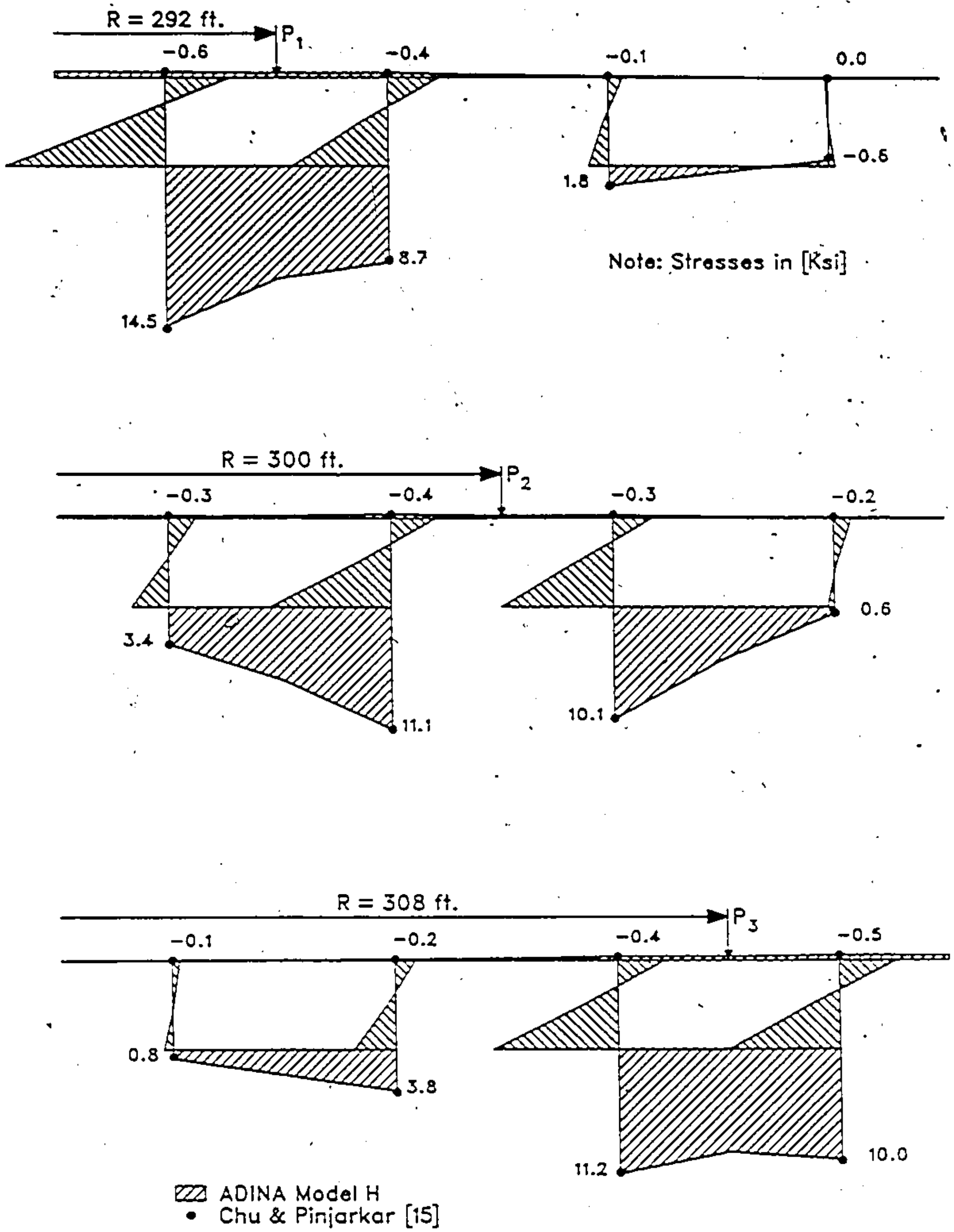

Figure 4.8: Comparison of longitudinal stresses at mid-span section between ADINA and Chu & Pinjarkar solution.

Table 4.2: Membrane shear stress (psi) at end supports of the bridge.

Load case 1 / Element	Tung	Pinjarkar Chu	Meyer Scordelis	Fam Turkstra	M.Y.T. Chan	ADINA Model H
ac	1356	1140	1150	1460	1377	1443
bd	474	2138	2170	2305	1831	2154
ab	-25	42	42	43	31	39
cd	331	-682	-700	-685	-413	-667
eg	1543	369	374	424	449	513
fh	183	-46	-49	-45	-18	-67
ef	-39	1	1	1	4	0
gh	510	43	35	32	67	48
Load case 2 / Element	**Tung**	**Pinjarkar Chu**	**Meyer Scordelis**	**Fam Turkstra**	**M.Y.T. Chan**	**ADINA Model H**
ac	51	459	-	574	535	522
bd	1663	1804	-	1940	1625	1920
ab	46	46	-	48	43	46
cd	-605	-599	-	-582	-479	-625
eg	672	260	-	402	522	424
fh	1170	1048	-	1025	962	1082
ef	-14	21	-	16	30	19
gh	187	-270	-	-262	-146	-246
Load case 3 / Element	**Tung**	**Pinjarkar Chu**	**Meyer Scordelis**	**Fam Turkstra**	**M.Y.T. Chan**	**ADINA Model H**
ac	-301	-35	-36	-11	-46	-88
bd	2080	1141	1150	1140	1035	1269
ab	69	29	29	28	31	31
cd	-893	-314	-313	-290	-276	-334
eg	-337	200	240	355	495	284
fh	2115	2305	2350	2358	2201	2266
ef	71	54	54	51	47	54
gh	-920	-758	-756	-715	-593	-765

the assumption of stiff diaphragm action at support sections, i.e., by employing the diaphragm action in model H and ignoring it in model I.

Figure 4.9 shows the transverse distribution of vertical deflection at the bridge mid-span section for the three load cases and the two models H and I. It is evident that model I results in a softer structure and therefore overestimates the displacement field. The percentage error for maximum deflection developing at the bridge deck outer edge was computed as high as 380 % and 127 % for load case 2 and load case 3 respectively. For load case 1, there was 0.152" (4 mm) of uplift in the bridge deck outer edge in model H whereas model I resulted in 0.510" (13 mm) deflection at the same location.

Similar errors for longitudinal normal stresses can be observed from Figure 4.10.

4.5.7 Conclusions of Case Study

The curved twin box girder bridge case study investigated have resulted in a number of important findings which may prove valuable in modelling such structures using ADINA thin shell elements.

1. In idealizing curved-box girder bridges, mesh convergence should be investigated in the three global axes of the structure. Displacements and stresses convergence in one direction is a necessary step for convergence but not sufficient for accurate structure response.
2. Transverse idealization of curved box structures requires at least 2 thin-shell element per box annular plate and box cylindrical webs.
3. While certain element topography may prove sufficient for curved box girder structures under concentric loads, the same element layout may not result in accurate results under extreme eccentric loading conditions. Structures subjected to the latter type of loads may require finer discretization in reaching accurate solutions.
4. Special attention must be accounted for when modelling the boundary conditions of the curved box girder; particularly in the radial direction (or transverse) of the structure. The assumption of stiff diaphragm action at end sup-

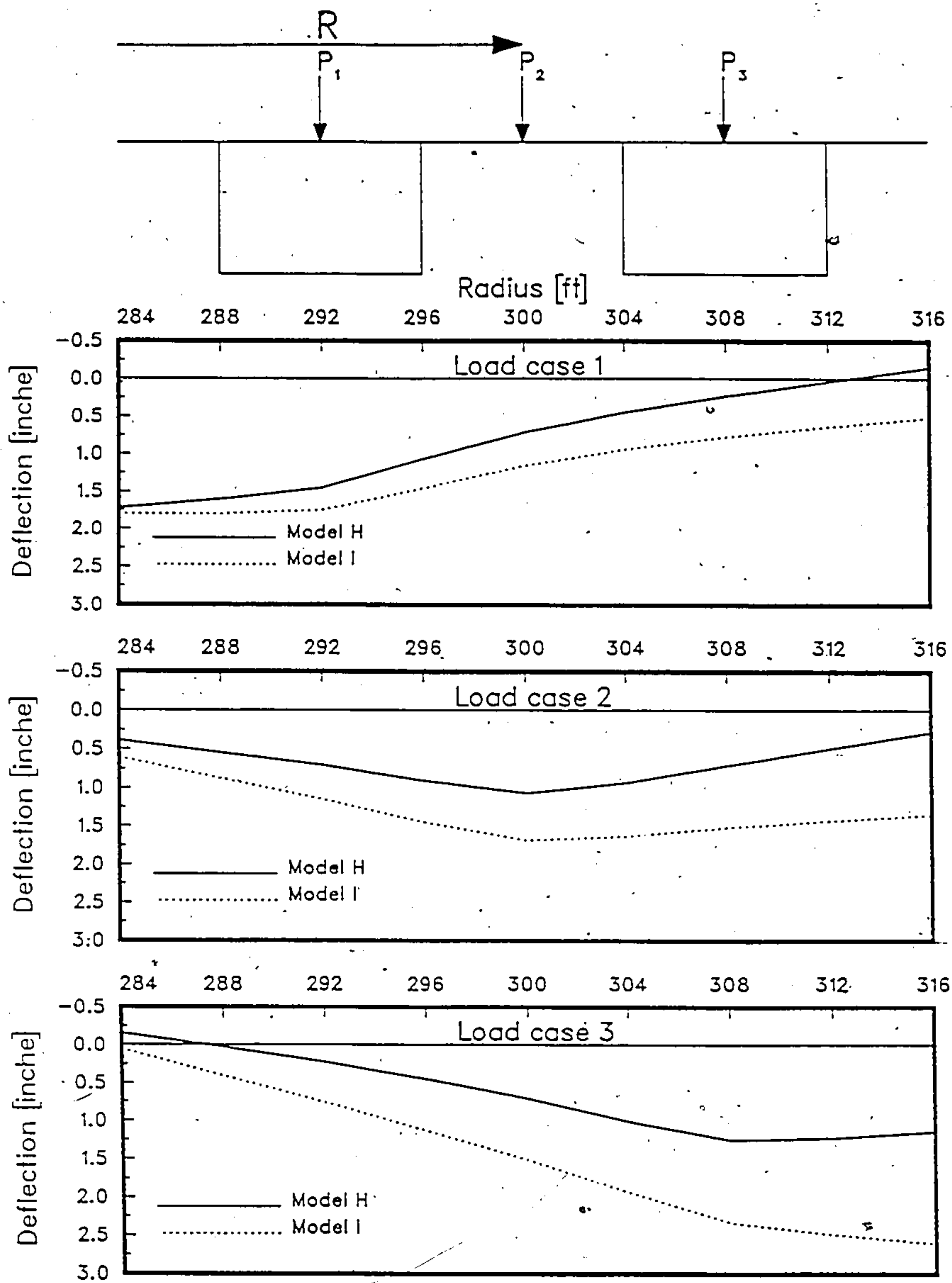

Figure 4.9: Influence of boundary conditions on bridge deck deflection at mid-span section.

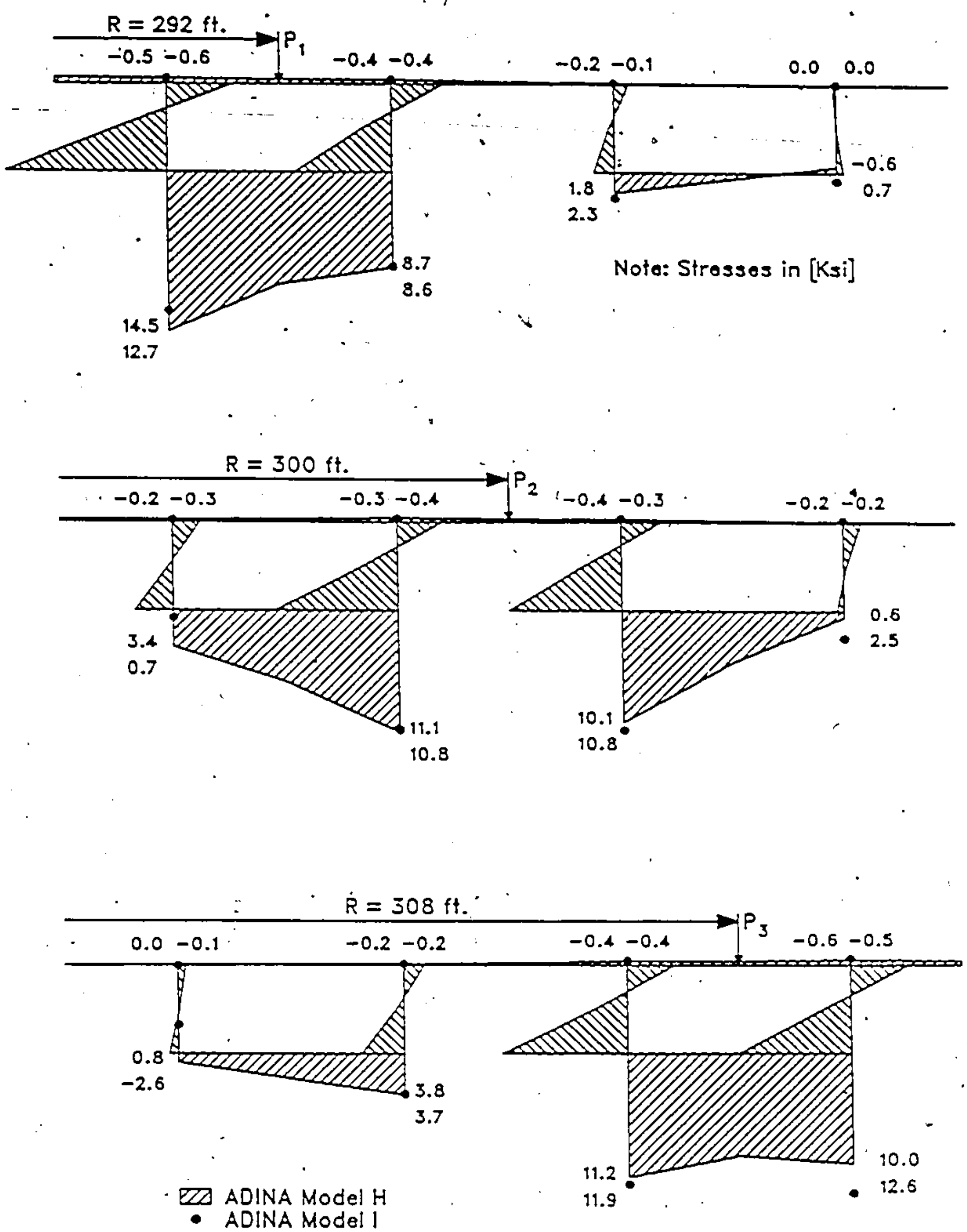

Figure 4.10: Influence of boundary conditions on longitudinal stresses at mid-span section of the bridge.

ports is very important especially when the structure is subjected to eccentric type of loads.

Chapter 5

ADINA Predictions and Experimental Results

5.1 Introduction

Experimental details of the physical bridge model were presented in Chapter 3 along with the experimental results of the static structural response under the seven load cases. The previous chapter described the application of ADINA program to curved box girder bridges through a detailed case study. In this chapter the physical bridge model is analyzed using ADINA in an attempt to predict its static response under conditions which are deemed equivalent to those used in the experimental program. Comparison between the finite element results and the experimental results is presented for the structure response under the full equivalent OHBD trucks load level. Both vertical deflection and normal stress quantities will be used in comparing structure response.

In idealizing the four box curved bridge model, the same modelling techniques used in the case study are employed. The successful application of the 9-node thin shell element in the case study would justify its use in modelling the various structural components in the physical bridge. The importance of mesh fineness in the radial and vertical directions of the bridge as well as the influence of imposed boundary conditions on structural response are kept in mind in light of the findings of Chapter 4. While the twin box girder bridge which was used in the case study has many features that are similar to those of the four box girder bridge, the two structures differ in boundary conditions. The twin box girder is a single span simply supported bridge while the four box girder is a two span continuous structure over the central column support. The continuous nature of the physical bridge introduces the problem of support settlements which was not studied in the case study.

Prior to comparing ADINA's predictions with experimental results a complete description of the finite element model is presented. The computed experimental bridge response which is presented in Table 3.6 and Table 3.7 for displacements and stresses respectively will be used directly in comparing with ADINA's model predictions.

5.2 Description of ADINA's Bridge Model

5.2.1 Finite Element Discretization

The 9-node thin shell element, described in the previous chapter, was used to model the various components of the horizontally curved, two span, four box girder bridge. The structural components include the micro concrete deck, the cylindrical webs, and the bottom flange as well as the three diaphragms. The two end column supports were not modelled whereas the aluminum portion of the central column support was modelled using the 4-node isoparametric beam element.

The basic geometrical features used in preparing the finite element model for the bridge are given below:

- Subtended angle between end supports = 16.80 degrees.
- Circumferential distance between end supports along central web = 4268 mm.
- Radius of curvature of the central web = 14554 mm.
- Width of micro concrete deck = 480 mm.
- Width of aluminum bottom flange = 400 mm.

- Depth of the cylindrical webs which are assumed to extend to the mid-surface of the deck and bottom flange elements = 120 mm.

Equivalent plate diaphragms were used to model the aluminum C channel diaphragms. The depth of the plate diaphragms was also assumed to extend to the mid-surface of the deck and bottom flange plates. However, the thickness was computed such that the plate diaphragm would provide the same transverse bending stiffness as that provided by the C channel diaphragm. As such the box girder bridge was closed at the end sections by 9.2 mm thick plate diaphragms while 8.3 mm thick plate was used in the central section of the bridge model in ADINA.

The aluminum central column shaft was modelled with an equivalent isoparametric beam element. The beam is 300 mm long having a square cross-section of 67.5 mm × 67.5 mm sides.

Several models were considered for the bridge in a preliminary solution conversion analysis. Both displacements and stresses convergence were employed in studying mesh fineness in all three principal directions. It was concluded that two elements per box side would yield sufficiently accurate results in the transverse and vertical directions of the four box girder section. Longitudinally, the full bridge was discretized into 18 element zones which are symmetrical about the mid-section of the bridge. While the bridge is geometrically symmetrical about the longitudinal and transverse centerlines, the truck loading conditions are not. Consequently, the full bridge had to be discretized.

The finite element idealization for the bridge model is shown in Figure 5.1. In this Figure, a typical transverse discretization and a three dimensional view of ADINA bridge model is presented. Using this idealization, it can be shown that this model has sufficient elements in the three principal directions to satisfy solution convergence in terms of deformation and stresses. A finer mesh has been applied near the center column support to provide accurate results in the region of high stresses and steep stress gradients.

The input file for ADINA pre-processor program ADINA-IN for the bridge model is listed in Appendix D.

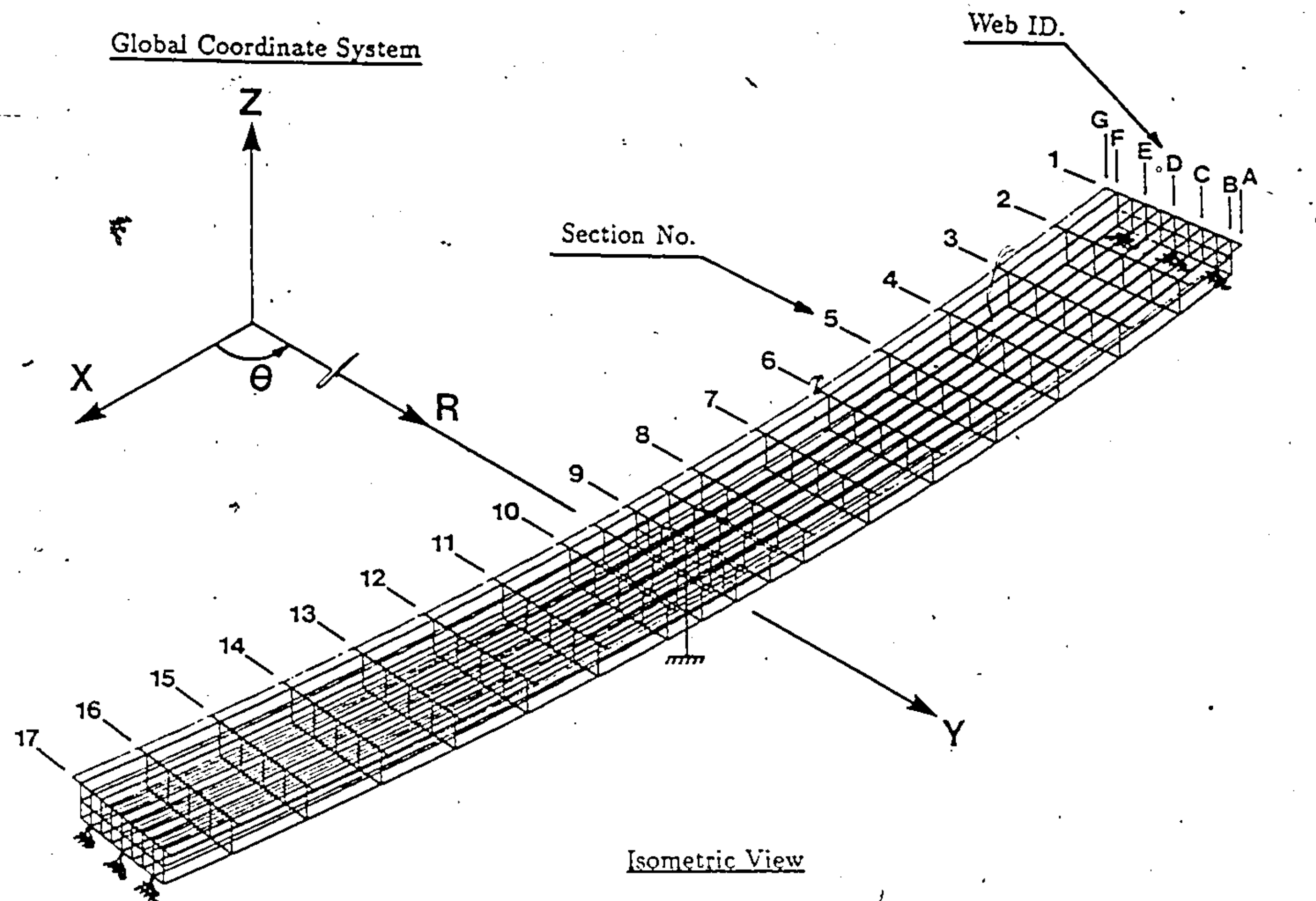

Isometric View

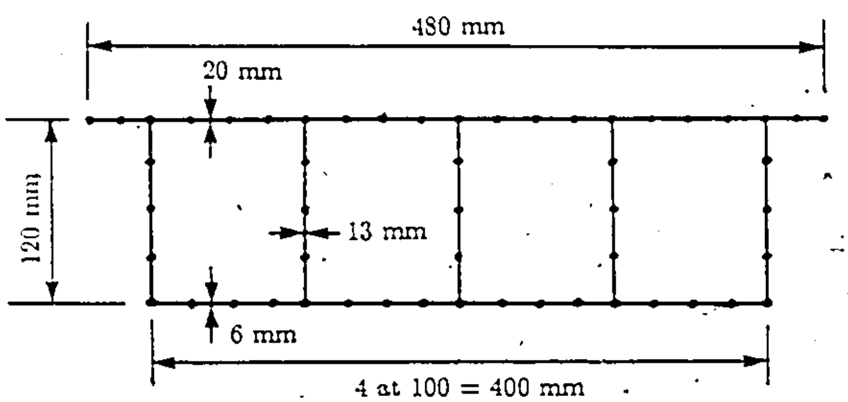

Typical section

Section NO.	θ (degrees)
1	98.40107
2	97.44050
3	96.37757
4	95.31464
5	94.25171
6	93.18879
7	92.12586
8	91.06293
8.5	90.53146
9	90.00000

Web ID.	R (meter)
A	14.794
B	14.754
C	14.654
D	14.554
E	14.454
F	14.354
G	14.314

Figure 5.1: Finite element discretization of ADINA bridge model.

Table 5.1: Elastic material properties assumed in ADINA's bridge model.

Structure Component	Material Type	Young's Modulus E (MPa)	Poisson's Ratio ν (-)	Thickness t (mm)
Top plate	Concrete	31300	0.15	20
Cylindrical webs	Aluminum	72000	0.379	13
Bottom plate	Aluminum	70277	0.379	6.0
Center Diaphragm	Aluminum	72000	0.379	8.3
End Diaphragms	Aluminum	72000	0.379	9.2
Center Column	Aluminum	72000	0.379	-

5.2.2 Material Properties

Homogeneous, isotropic, and elastic material behavior is assumed for the micro concrete deck as well as all aluminum structural components of the ADINA bridge model. The various elastic properties used in the analysis are listed in Table 5.1. The values of Young's moduli and Poisson's ratios follow the experimental data summarized in Table 3.3 and Table 3.4 in Chapter 3.

5.2.3 Boundary Conditions

The boundary conditions imposed on the structure were as follows:

- Totally fixed end at the bottom node of the isoparametric beam element for the central column support while keeping the top node, which connects the bottom plate of the bridge to the central column free.
- Only vertical translation is restrained at the three bottom plate nodes for each end support.

In addition to these conditions one perhaps should include constraint equations for the nodes at end sections to restrain radial translation while keeping tangential or angular translation free. The application of such constraint equations in this bridge would be justified in light of the finding of Chapter 4. However, the use of plate diaphragm elements at the end sections would be sufficient and would simulate end conditions better than the constraint equations, the difference being that diaphragms would result in finite in-plane stiffness while imposing the constraint equations would simulate an infinitely stiff diaphragm action. Therefore, constraint equations were not imposed in the ADINA bridge model for the four box girder bridge.

Recall in the physical bridge model that two MC sections were employed to restrain any uplift at the end sections. In the finite element model there is no need to restrain uplift since the bottom plate nodes fixed in the vertical direction will automatically prevent uplift. Furthermore, restraining bridge deck nodes at the end sections would result in a much stiffer structure response than it should be.

5.2.4 Loading Conditions

The bridge model is subjected to the seven load cases described previously in Chapter 3. The truck load level used in any load case represent the equivalent OHBD truck load of 9590 N given in Table 3.5. Wheel loads are computed using equations 3.14 through 3.17. When wheel loads, which are assumed to be point forces in ADINA model, happen to occur on the element surface rather than element nodal points, equivalent nodal forces were statically derived. This procedure was necessary only in the longitudinal direction of the bridge.

5.3 Comparison of Elastic Structure Response

5.3.1 Load Case 1

The bridge model was loaded with two sets of parallel trucks such that each span is loaded eccentrically with one set. In one set the trucks are situated longitudinally such that the third axle is along section 4 while in the other set the second axle is aligned with section 12 as shown in Figure 3.10.

Bridge bottom flange vertical deflection plots for the six instrumented sections are given in Figure 5.2. Both ADINA model solutions and those predicted experimen-

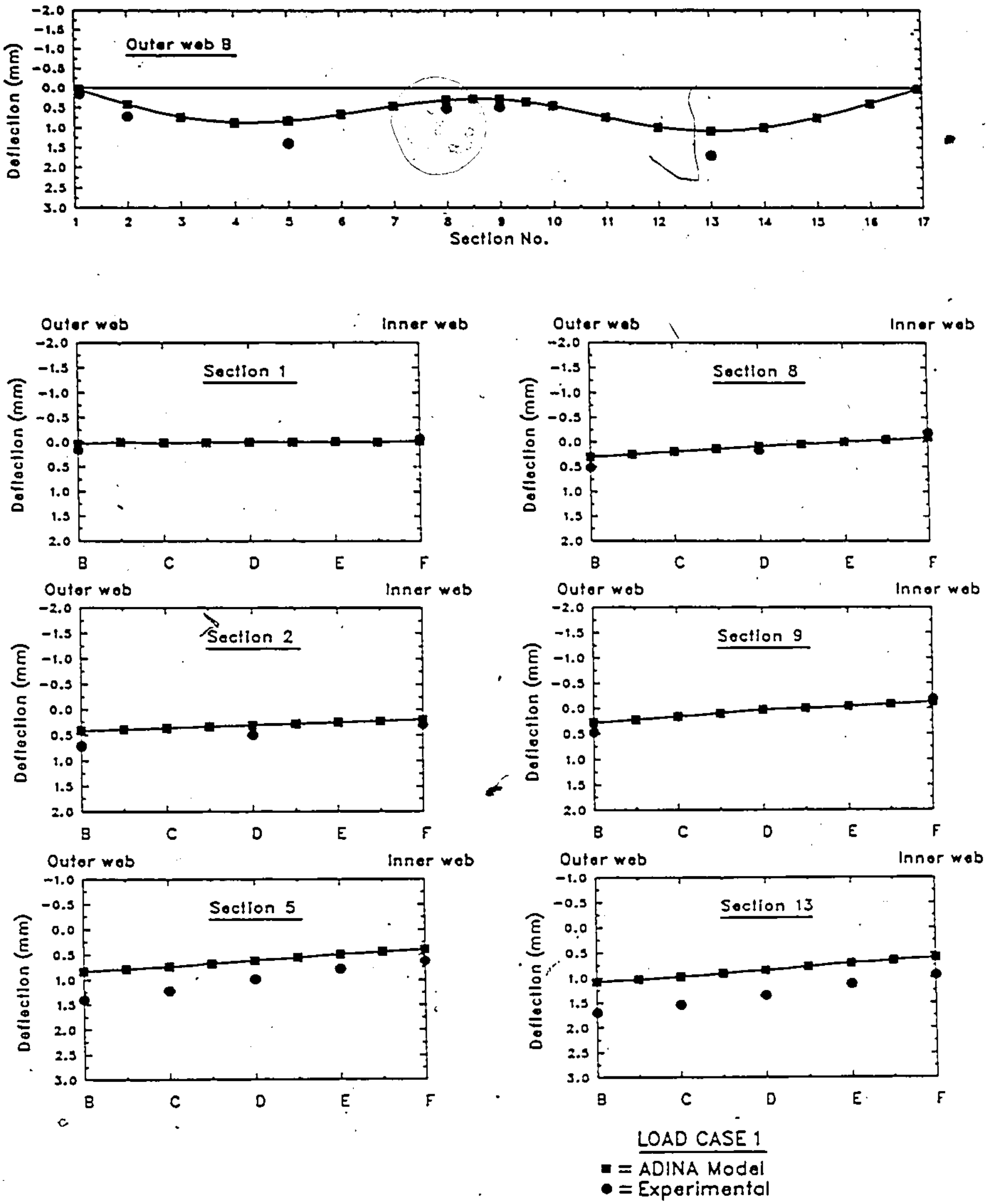

Figure 5.2: Vertical deflection curves of bottom plate at load case 1.

tally are plotted. It is not surprising to find that deflections underneath the outer web, which is designated by the letter B, are highest for any section along the bridge in light of the eccentric nature of the trucks loading. For this reason Figure 5.2 includes longitudinal distribution of vertical deflection under the outer web B. Transverse distributions of vertical deflections predicted by the ADINA model are in good agreement with those obtained experimentally. The highest torsional rotation occurred at section 13. At this section the torsional rotation computed in ADINA model was 1.25×10^{-3} while that computed experimentally was 2.00×10^{-3}. Hence ADINA's model underestimated maximum torsional rotation by 37.5 % .

Maximum vertical deflection values are 1.1 mm and 1.7 mm in ADINA model and the experimental model respectively. Those occurred at section 13 under the outer web B. ADINA model underestimated maximum vertical deflection by 36.4 %

Transverse distribution of circumferential or longitudinal normal stresses are plotted for the three instrumented sections 2,5, and 8 in Figure 5.3. Since the two spans were loaded in this load case, it is natural to expect maximum normal stress to develop at section 9 over the central column support where maximum negative moment exists. At this section, maximum compressive stress of 35.5 MPa was predicted by ADINA model at the bottom plate under the central web D while the highest tensile stress value of 7.0 MPa was developed at the top surface of the bridge deck also over web D. Comparing these values with material strength properties given in Table 3.3 and Table 3.4, it is evident that a maximum of 12 % of aluminum yield strength capacity was used in this load case while concrete tensile strength was exceeded by about 1.8 MPa. It is anticipated that this amount of 1.8 MPa was carried by the WWF reinforcement in the bridge deck.

Positive longitudinal moments at sections 2 and 5 are evident in Figure 5.3 by the development of tensile stresses in the bottom flange and compressive stress field in the bridge deck. Conversely, at section 8, which is close to the central column support, stress fields indicate the influence of the maximum negative moment at section 9. In any section however, transverse distribution of stresses seems to be moderately uniform between the four girders.

Comparing ADINA's predictions with those obtained experimentally, it seems that the percentage error of ADINA stresses are much less for stress points below the neutral plane than those points located above it. Maximum stress within the three

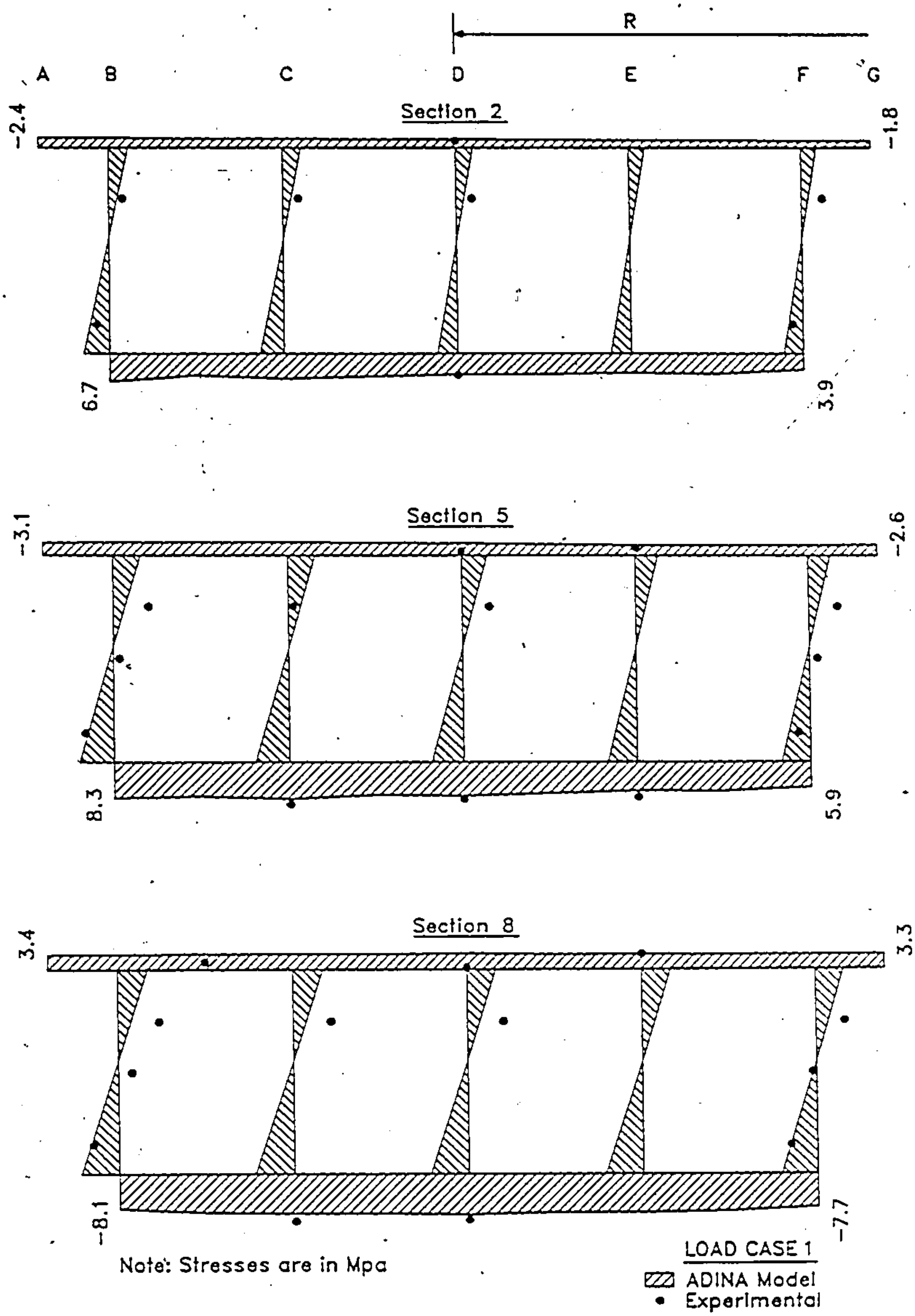

Figure 5.3: Normal stress distributions at load case 1.

sections was developed the bottom plate underneath web D at section 8. At this location ADINA's model predicted compressive stress of 9.4 MPa while the corresponding experimental value was 10.6 MPa. As such, ADINA underestimated the maximum normal stress by 11.3 %. Note that the experimentally predicted stress value is considered to be the reference stress since regression analysis indicated highly reliable strain value at the location of maximum normal stress. The range of maximum strain fluctuation at this location was within only ±2 %.

5.3.2 Load Case 2

Similar to load case 1, the bridge model was loaded with two truck sets. However, in this load case the two truck sets were closer to the central section of the bridge as shown in Figure 3.10. Recall the two distinctive features for this loading condition namely: it was the first load case performed experimentally and unlike the remaining load cases the equivalent OHBD truck load was applied in 5 steps rather than 10 steps. As such, only 5 sampling points instead of 10 points were employed in the regression analysis which was later used in preparing the experimental bridge response.

Deflection plots for this load case are presented in Figure 5.4. Again, ADINA's model seems to be stiffer than the experimental model in terms of deflection as well as rotation. The highest torsional rotation occurring at section 9 was underestimated in ADINA by 60.0 %. Similarly, The maximum vertical deflection point occurring at section 13 under the outer web B was underestimated in ADINA model by 68.0 %. This high percentage of error can be largely attributed to the degree of fixity in the bridge between the bottom plate and the central column support at section 9. It is quite obvious that the degree of fixity provided by the isoparametric beam element and the bottom plate shell element is higher than that actually existed in the physical model. Unfortunately, not knowing the degree of fixity provided in the bridge model makes modelling such junction more difficult. However, one should always keep in mind that finite element models tend to result in a stiffer response than that of the actual structure. Another factor which plays an important role in yielding a stiffer structural response by the ADINA model particularly in terms of torsional rigidity is the modelling of the central diaphragm. The central C channel diaphragm was replaced in ADINA model by an equivalent single

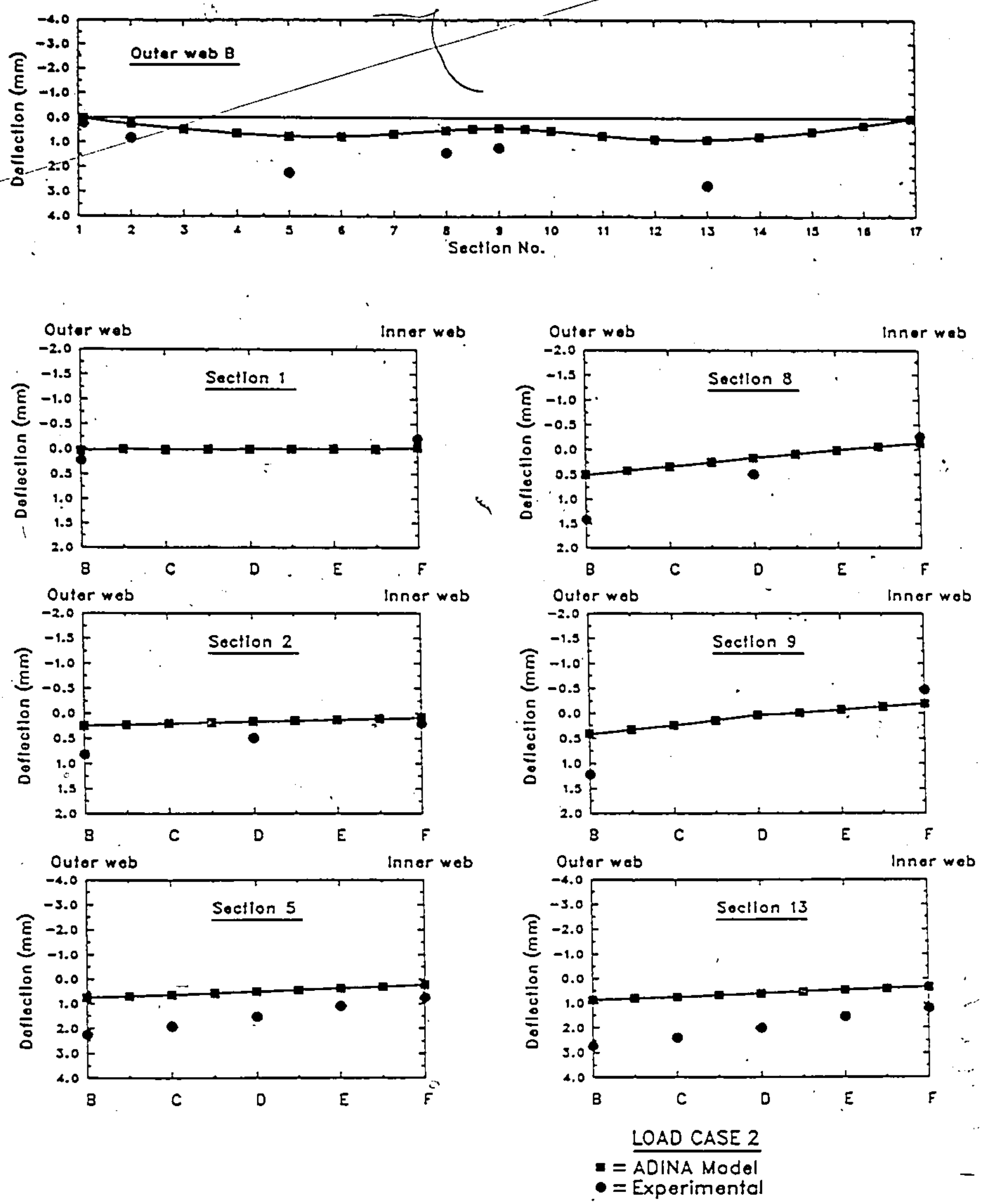

Figure 5.4: Vertical deflection curves of bottom plate at load case 2.

plate diaphragm. The procedure involved several approximations in evaluating the dimensions of the single plate diaphragm.

Normal stress distributions resulted in load case 2 are shown in Figure 5.5. Clearly analytical and experimental stress values do not compare as well as they did in load case 1. However both schemes did agree in predicting the sign of moments developing at the section. Furthermore, for stress fields in the three instrumented sections, both schemes did agree on the location of maximum normal stress sustained by the bridge. The maximum normal stress was developed in section 5 at the bottom flange underneath web C. At this point ADINA predicted compressive normal stress of 6.6 MPa while a value of 15.5 MPa was computed experimentally. The experimental data at this location is actually reliable since the range of strain fluctuation for 99.9 % certainty is very small. Table B.31 in Appendix B indicate maximum error in experimental stress value at strain gage location, A^{L}_{45}, is only ±2 %. The percentage error of ADINA's maximum normal stress is 57.8 %. It is natural to see ADINA's model underestimating maximum normal stress in view of the stiffer structure response which was observed earlier in terms of deformation.

5.3.3 Load Case 3

Unlike the previous load cases, only one span was loaded with the equivalent OHBD trucks load such that the second axle was aligned with section 5 (see Figure 3.10). In this way maximum deflection and stresses are expected to develop near section 5.

Figure 5.6 compares deflection curves obtained by ADINA model and experimentally at the bottom flange of the bridge. Maintaining a stiffer structure response, ADINA's model in this load case seem to result in percentage errors similar to those occurred in the first load case. The maximum deflection was developed underneath the outer web B at section 5. At this point ADINA underestimated the experimental value of 2.0 mm by 32.1 %. Maximum torsional rotation also occurred at section 5 where ADINA model predicted a value of 1.5×10^{-3} while the value computed experimentally was 1.75×10^{-3}. As such ADINA underestimated maximum torsional rotation by only 14.3 % which is quite good.

ADINA and experimental deflection profiles seem to compare very well in this load

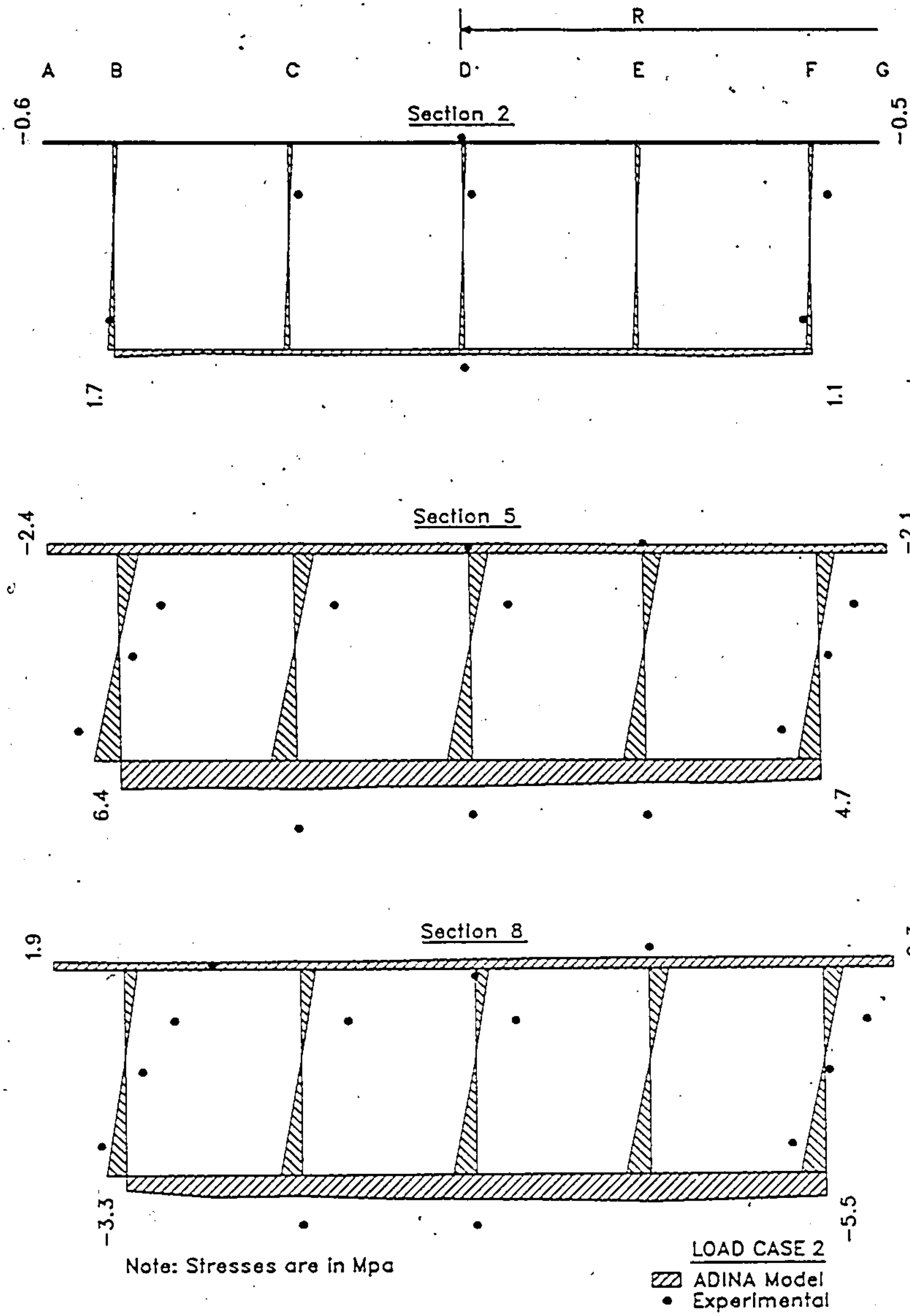

Figure 5.5: Normal stress distributions at load case 2.

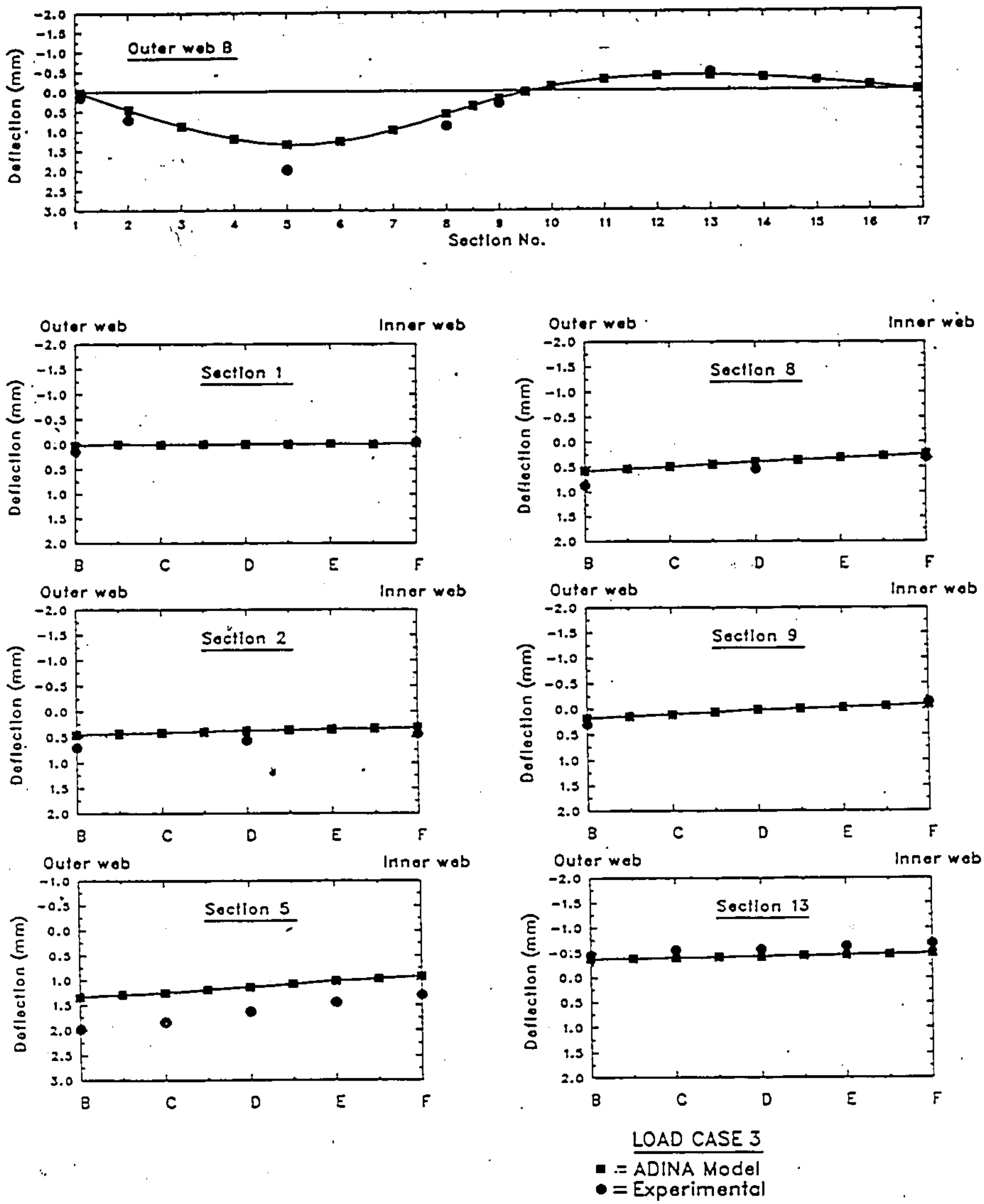

Figure 5.6: Vertical deflection curves of bottom plate at load case 3.

case in terms of longitudinal as well as transverse distribution. In fact the structure response in this load case has resulted in the lowest average percentage errors in terms of deflections and stresses among the seven load cases.

Longitudinal normal stresses for load case 3 are given in Figure 5.7. It is evident that the highest stress level was developed at section 5 which represent the section of maximum positive longitudinal moment. Stress plots clearly show good agreement between ADINA's solution and experimental finding for sections of low stress level such as sections 2 and 8 and sections of high stress level such as section 5. Again stress points located at the aluminum webs and above the neutral plane did not compare very well particularly at section 5.

Maximum tensile stress was developed in the bottom flange under web C at section 5. At this location ADINA's prediction for normal stress was 15.7 MPa while the experimental value was 16.4 MPa. The percentage error in ADINA's prediction for maximum normal stress is as low as 4.2 %. However, maximum compressive stress developed in the bridge deck at section 5 did not compare as well. One should keep in mind that the range of error in the experimental stress value for points on the deck could be as high as 60 % which renders experimental stress value unreliable for comparison purposes.

5.3.4 Load Case 4

In this load case the bridge was loaded by two truck sets, one set per span similar to load case 2. Details on the location of point loads are given in Figure 3.11.

Bottom plate deflection at section 5 were highest particularly under web B as noted from Figure 5.8. At this location ADINA underestimated maximum deflection by 26.3 %. Moreover, ADINA's prediction for deflection at sections 1,2,8, and 9 seems to be in excellent agreement with the experimental values.

ADINA model also predicted maximum torsional rotation at section 5 very well. The percentage error in maximum torsional rotation was 25 % at section 5. It is quite interesting to note the much lower percentage of error for this load case in comparison with the second load case given the similarity between them in terms

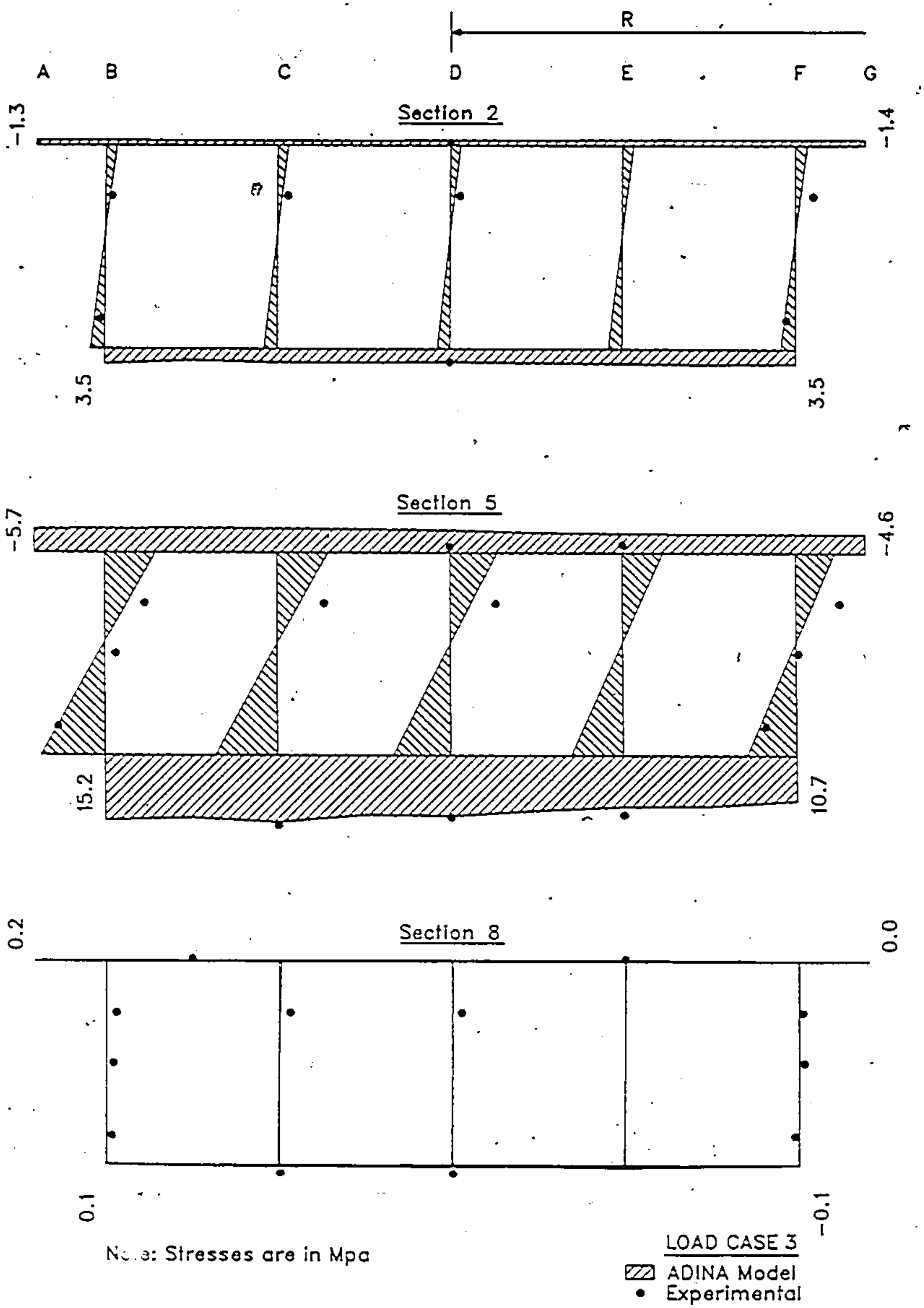

Figure 5.7: Normal stress distributions at load case 3.

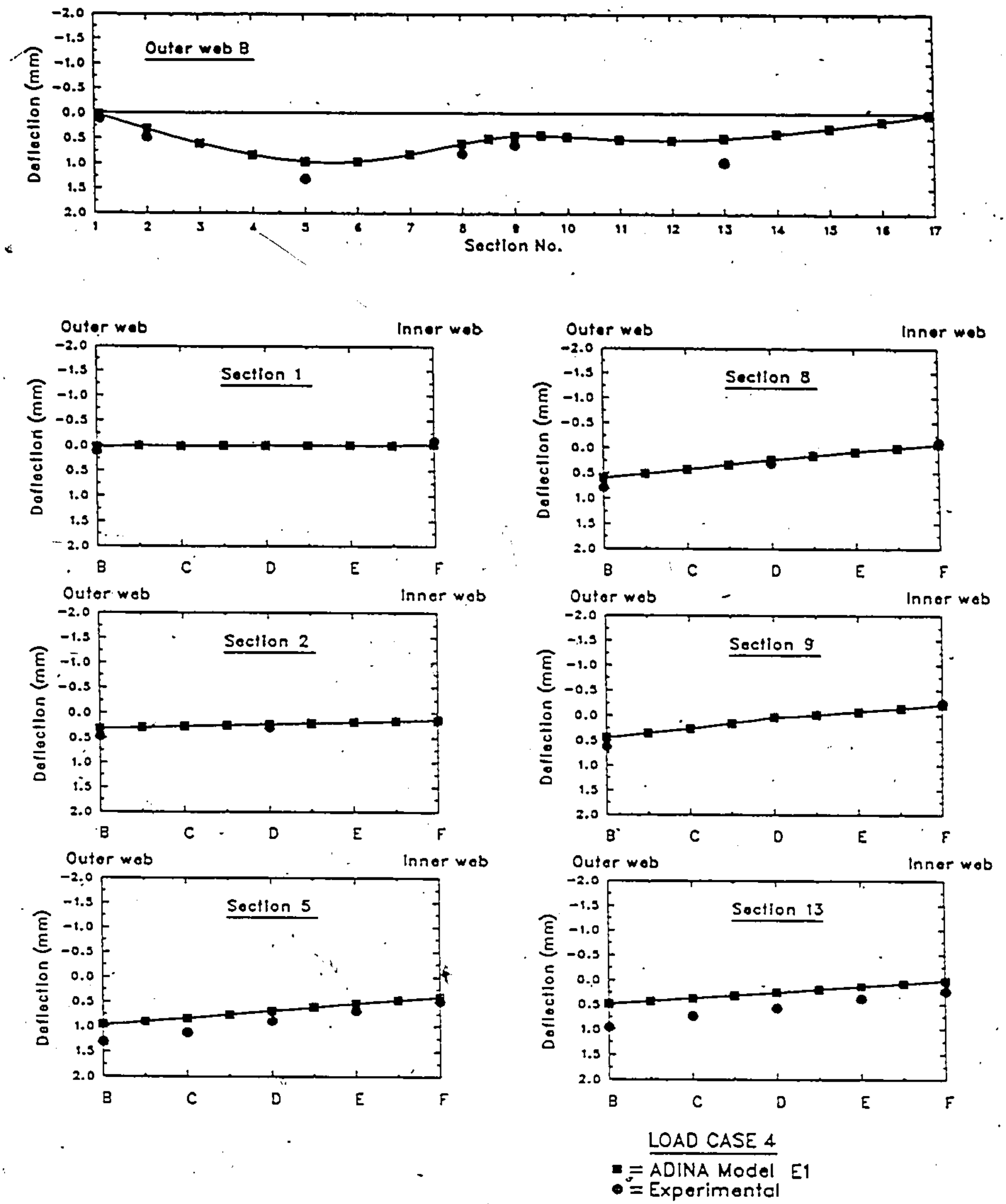

Figure 5.8: Vertical deflection curves of bottom plate at load case 4.

of truck locations.

Stress plots for this load case are given in Figure 5.9. Again both models predicted positive and negative curvatures properly in the instrumented section. Moreover, ADINA's predictions for normal stresses in the low moment section 2 were as good as those in the high moment section 5. The maximum tensile stress was developed at the bottom plate under web C and the values of 9.2 MPa and 8.4 MPa were obtained by ADINA and experimentally respectively. The 10.4 % percentage error in maximum stress computed by ADINA is about twice the percentage error in the experimental stress value[1].This clearly indicates that ADINA's prediction for maximum stress is better than 90 % certainty.

5.3.5 Load Case 5

A particular feature for load case 5 is that only one span of the bridge deck was loaded with two sets of the equivalent OHBD trucks. The instrumented span (sections 1 through 9) was loaded such that the first axle of the first set of trucks was aligned with section ℄ close to the abutment while the second set was 180 mm behind the first set as shown in Figure 3.11. Loading only one span makes this load case somewhat similar to load case 3; however, much higher deformation and stress levels are expected since the loads are doubled in load case 5.

Vertical deflection plots for the box girder bottom flange are given in Figure 5.10. Like all the other load cases, ADINA's model is stiffer than the physical model and deflection curves are linear in the radial direction while nonlinear distributions are observed in the circumferential direction.

As will be noted from Figure 5.10, maximum deflection for the bottom flange occurred under the outer web at section 5. At this location the percentage error in ADINA's prediction was 33.2 % which is similar to that computed in load case 3. Elsewhere within the structure ADINA's deflection seems to correlate very well with experimental values.

In terms of maximum torsional rotation, ADINA did not perform as well as it did in

[1]See error for gage A_{15}^{L} in Table B.35 of Appendix B.

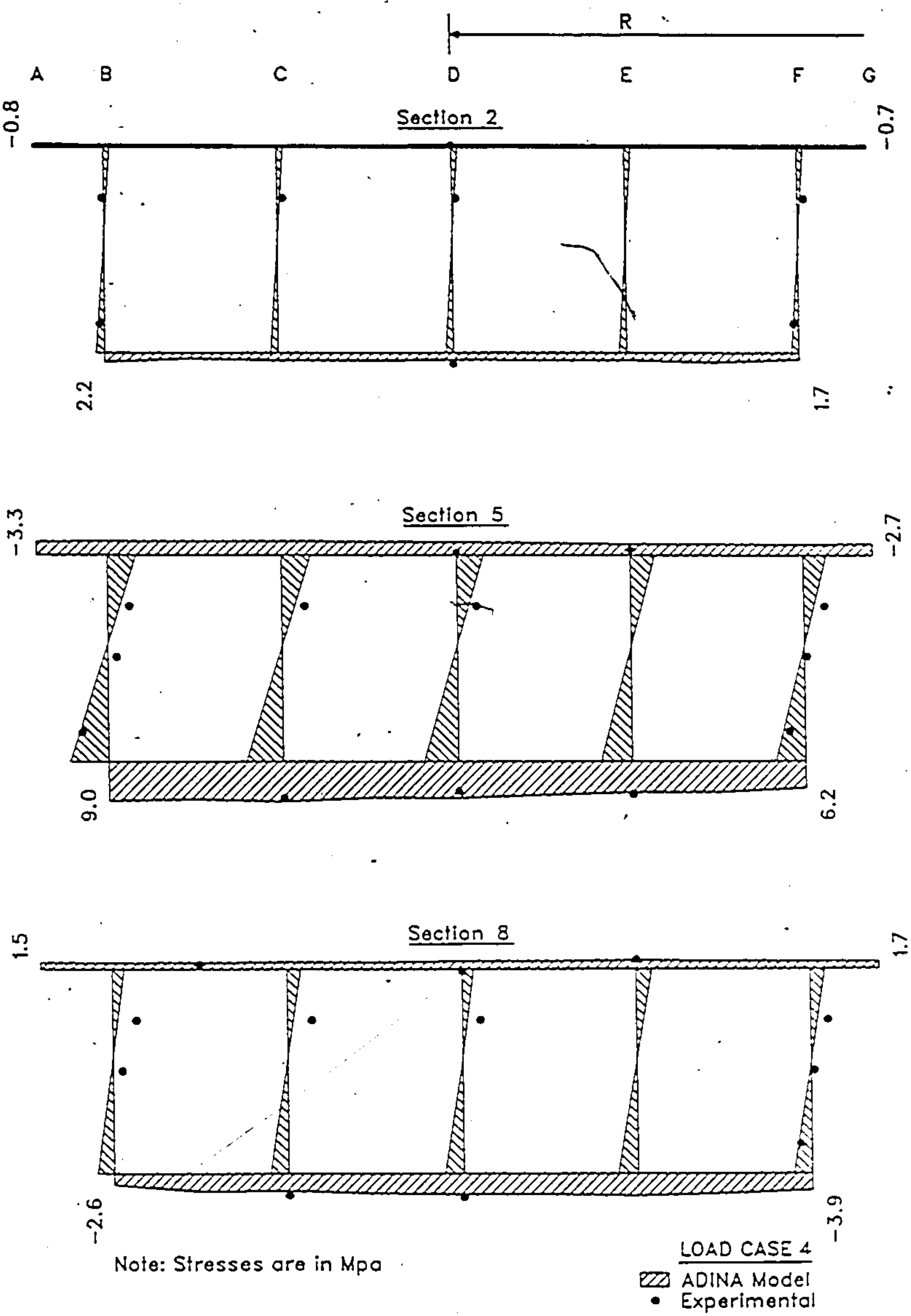

Figure 5.9: Normal stress distributions at load case 4.

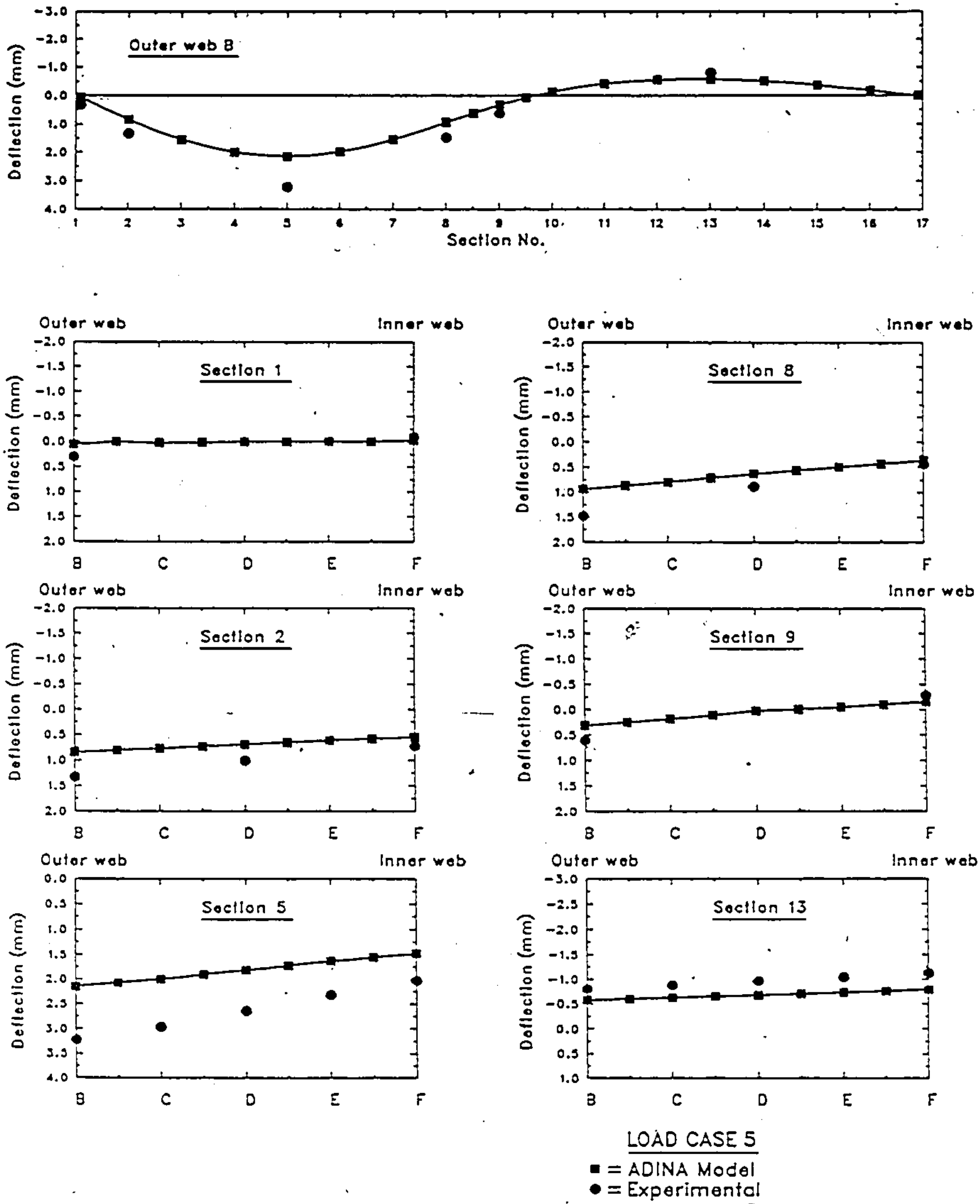

Figure 5.10: Vertical deflection curves of bottom plate at load case 5.

load case 3. In this load case the percentage error in maximum torsional rotation, which occurred at section 5, was 50 % compared to 14.3 % computed in load case 3.

As mentioned earlier this load case resulted in the highest stress level among the seven load cases. The largest normal stress was developed at the bottom plate over the central column support. At this location a compressive stress value of 45.3 MPa was computed by ADINA. This indicates that a maximum of 16 % of the Aluminum yield strength was sustained in this load case[2]. Clearly, structure response was within the elastic range at least for the aluminum components of the curved box girder bridge.

Transverse distribution of normal stresses are compared in Figure 5.11. Moderately linear stress distributions are observed for the bridge deck and bottom flange while steep stress gradients are observed for the webs. This indicates that equal proportions of the longitudinal moment were carried by the four girders. Again maximum stress point was developed in the bottom flange under web C at section 5. At this location, ADINA underestimated the tensile stress by only 7.8 %. Overall, the ADINA model seems to predict experimental stresses fairly well with only a few minor exceptions shown in the figure.

5.3.6 Load Case 6

In this load case the bridge was loaded with a single set of trucks similar to load case 3. However the truck loads were applied such that the third axle is aligned with section 13. As such, the instrumented span would be undergoing negative curvatures while the positive curvature would develop at section 13. Exact trucks location can be found in Figure 3.11.

Deflection response in this load case is similar to that of the other load cases. ADINA's model provides excellent correlation with experimental data at sections of low deformation while it tends to be less accurate at sections with high deformation such as sections 5 and 13. The finite element model underestimates maximum vertical deflection by 34.7 % and maximum torsional rotation is underestimated by

[2]Yield strength of bottom plate aluminum = 285 MPa.

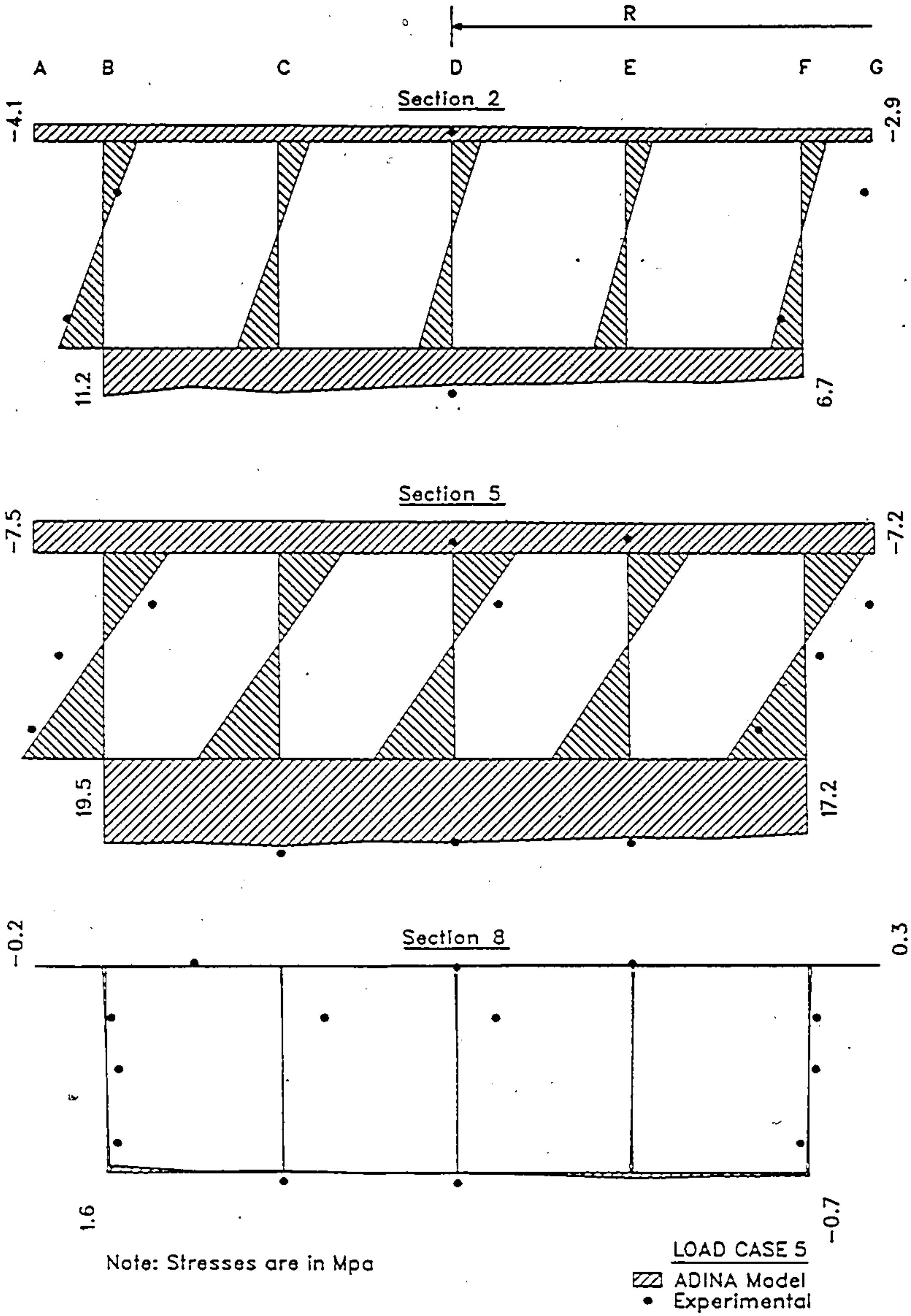

Figure 5.11: Normal stress distributions at load case 5.

42 %. Deflection plots for load case 6 are presented in Figure 5.12.

In terms of normal stresses, ADINA also provides good correlation with experimental findings as depicted in Figure 5.13. Excellent agreement between analytical and experimental stress values is evident for all points in the bottom flange of the structure. Points above the neutral plane and on the cylindrical webs seem to have higher percentage errors. The percentage error in ADINA prediction for maximum normal stress which developed at section 8 under the central web D is as low as 9 %. At section 5, ADINA's prediction for normal stress is even better, the percentage error is only 1.9 %.

Normal stress distributions are almost constant for the deck and the bottom flange while linear variation is observed in the webs. Furthermore, it is evident from Figure 5.13 that the webs are carrying almost equal amounts of longitudinal moment.

5.3.7 Load Case 7

This load case is somewhat similar to load case 4. The bridge deck was loaded with two truck sets, one set per span. However the longitudinal alignment is different as shown in Figure 3.11.

Deflection plots for load case 7 are given in Figure 5.14. From this figure it can be observed that ADINA's predictions for deformation are by far the best among the seven load cases described previously. Maximum deflection of the bottom flange which occurred under web B at section 5 was underestimated by ADINA model by only 15.8 %. Maximum torsional rotation which also occurred at section 5 was underestimated by only 12.5 %.

Longitudinal normal stresses developed in this load case are plotted in Figure 5.15. Surprisingly, ADINA stresses here did not correlate well with the experimental findings. Maximum stress developed in this load case occurred in the bottom flange under web C at section 5. At this location ADINA's model overestimated the normal tensile stress by 47 %. However, lower percentage errors can be observed at sections 2 and 8. It should be noted that the error range for the experimental stress point under web C at section 5 (Gage A^{L}_{45}) is only ±6%. This implies that exper-

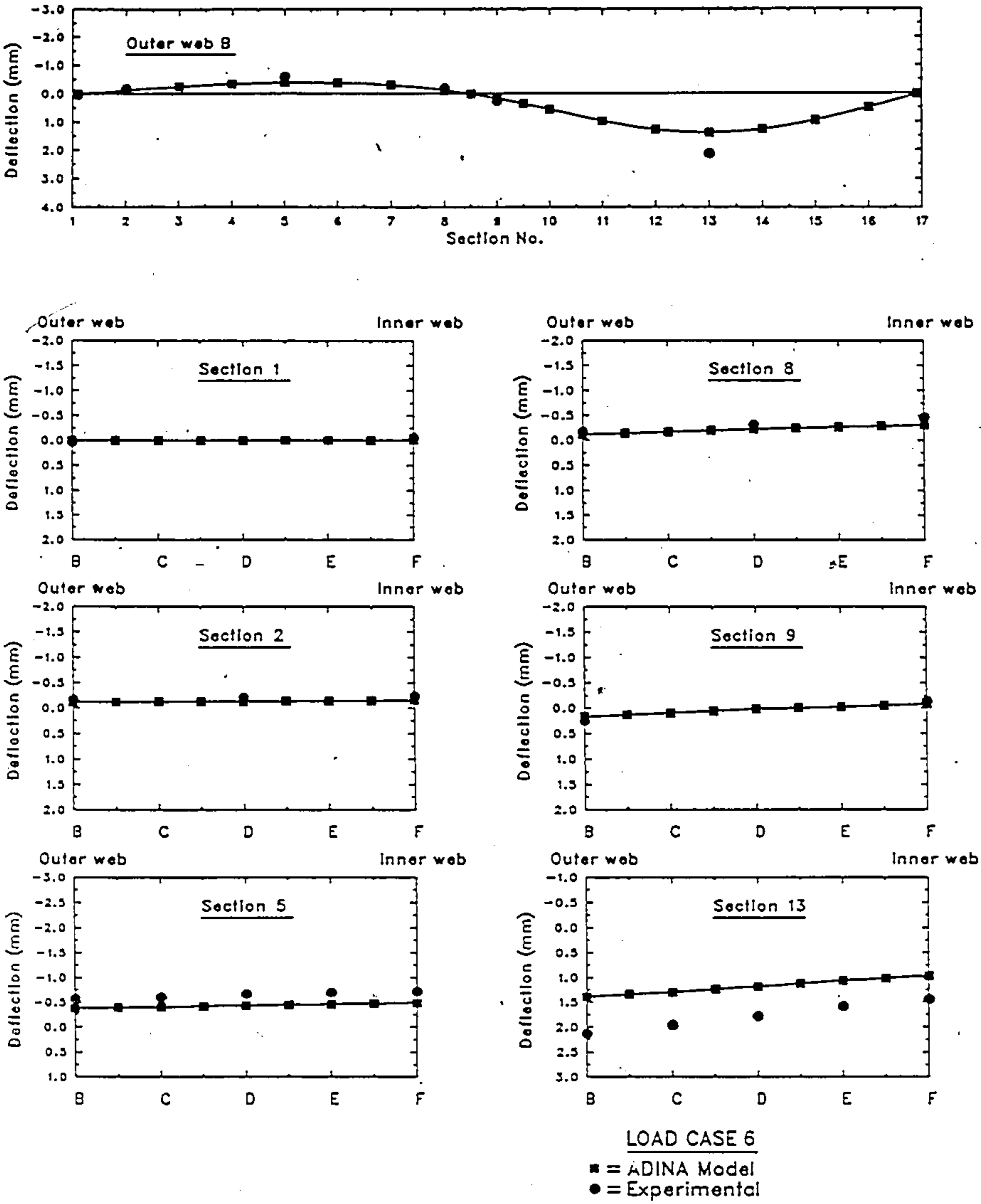

Figure 5.12: Vertical deflection curves of bottom plate at load case 6.

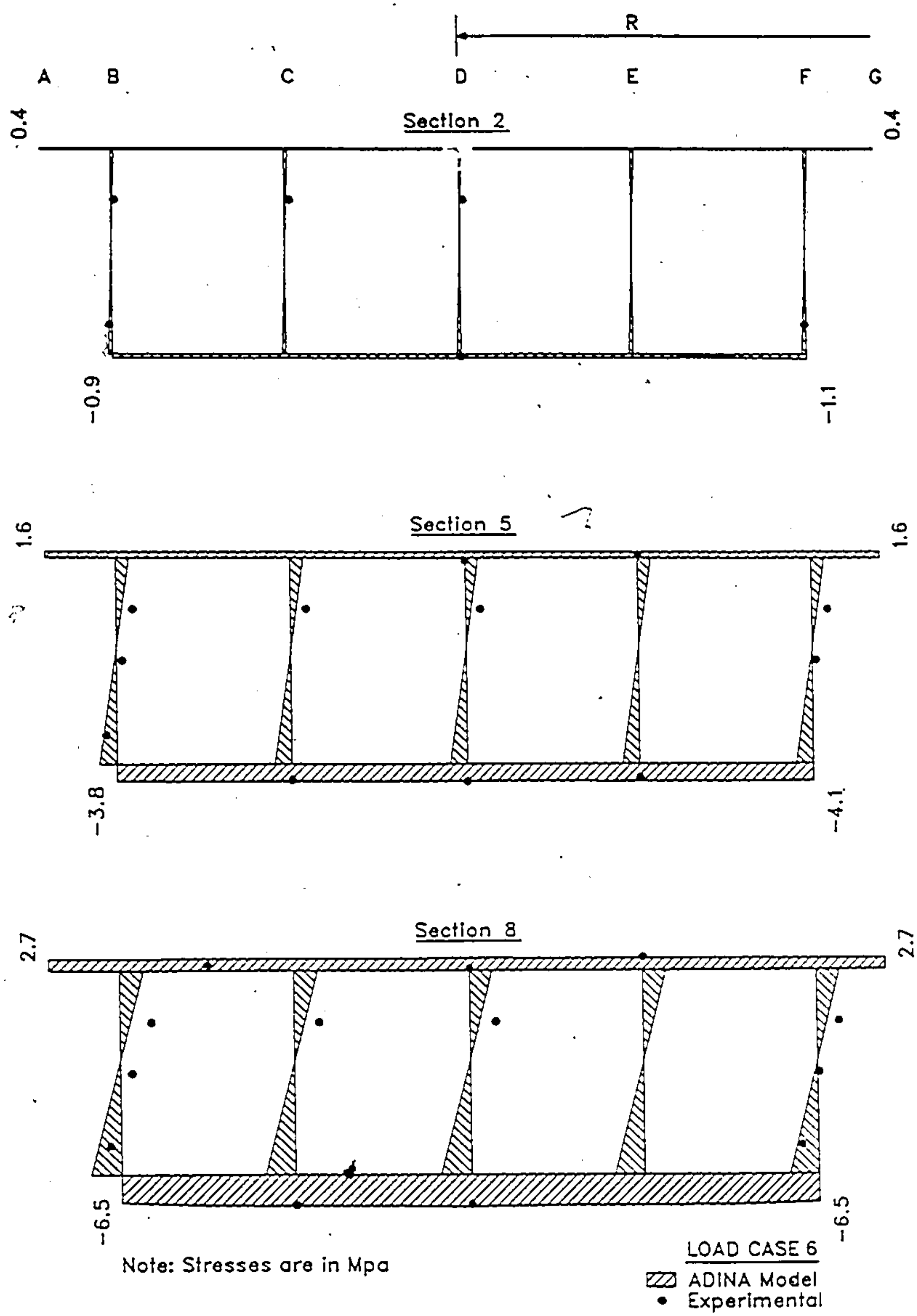

Figure 5.13: Normal stress distributions at load case 6.

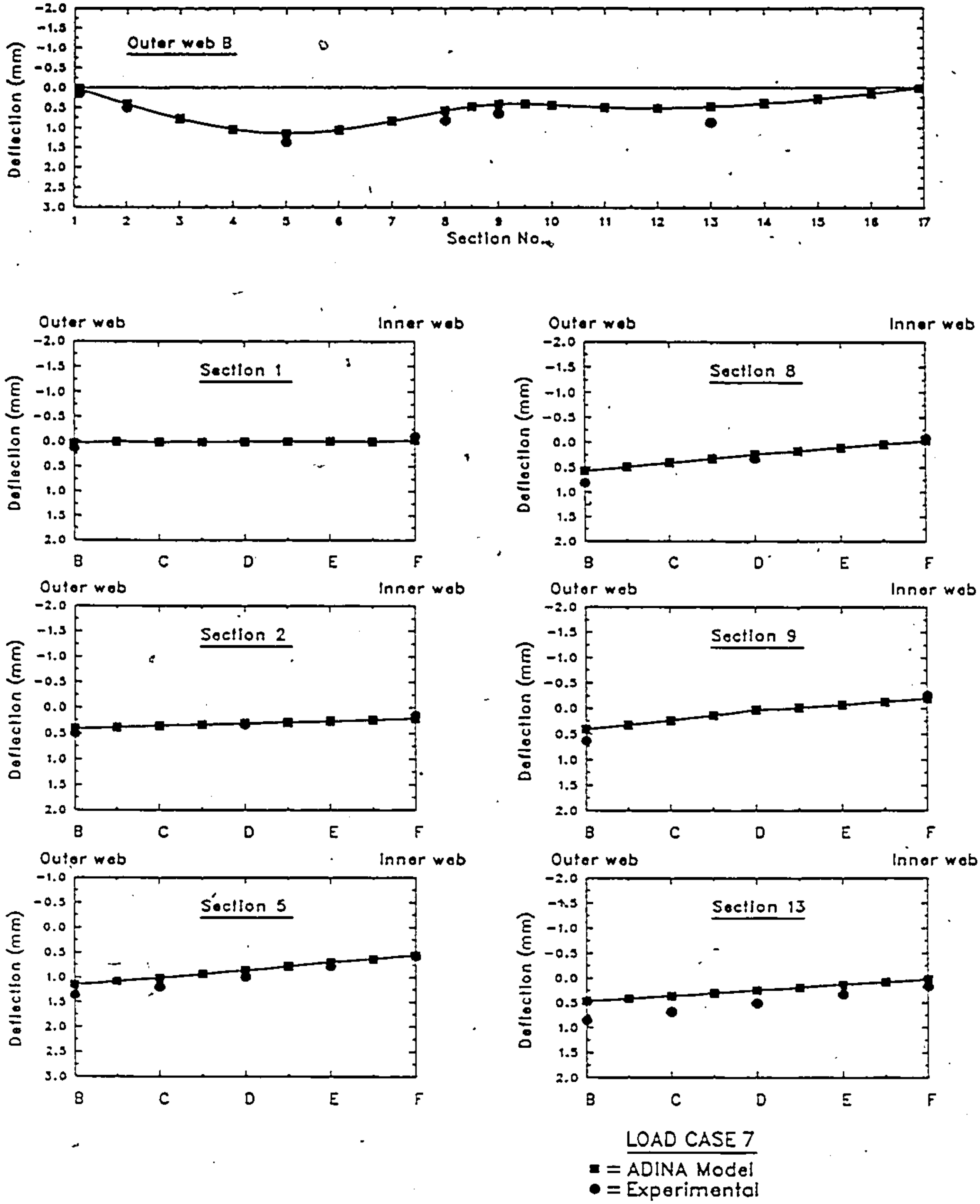

Figure 5.14: Vertical deflection curves of bottom plate at load case 7.

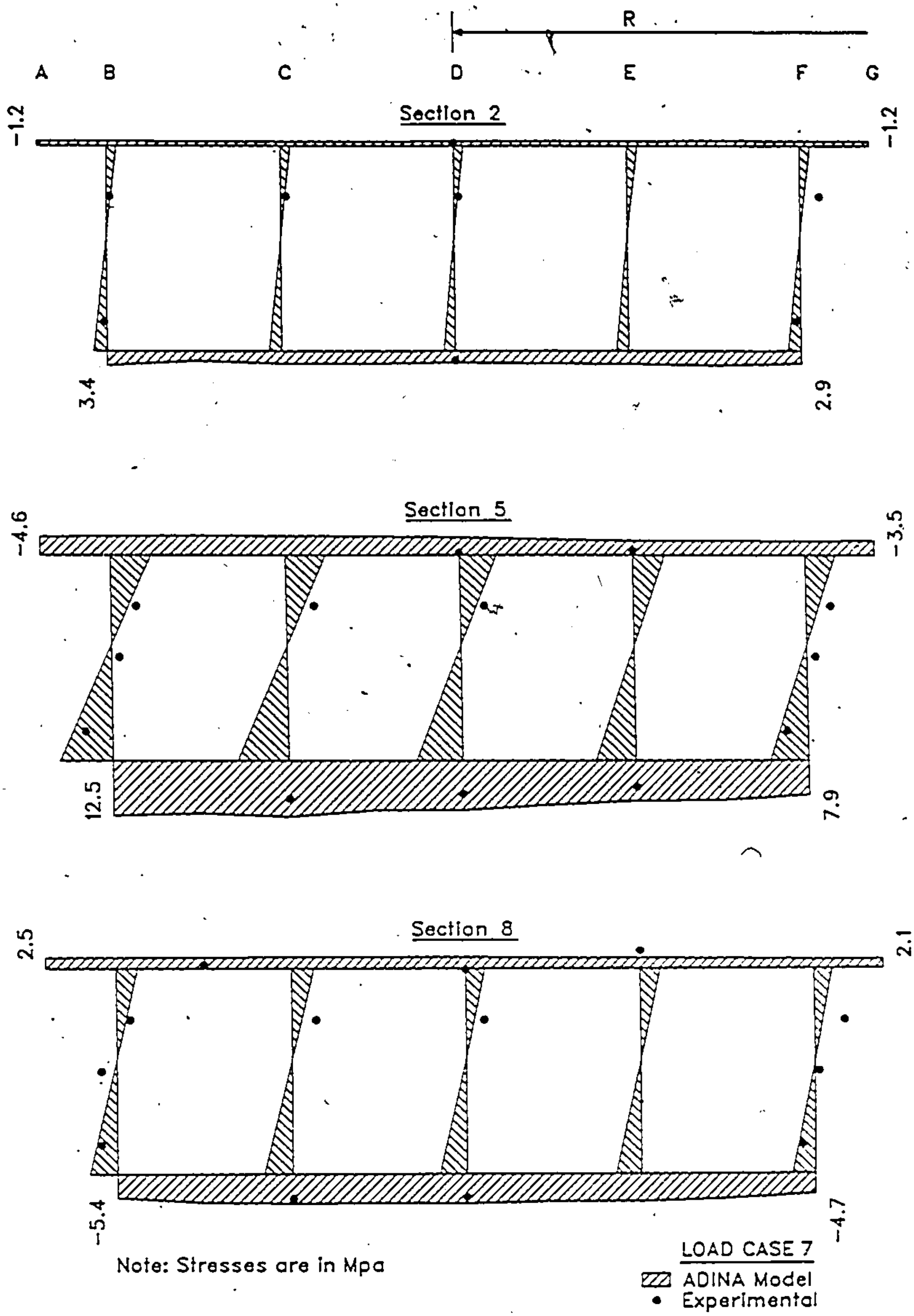

Figure 5.15: Normal stress distributions at load case 7.

imental prediction for maximum stress point is quite reliable. Another surprising observation in this load case is the good correlation between ADINA and experimental findings for stress points located above the neutral plane on the cylindrical webs particularly at section 5. This is quite opposite to earlier findings for previous load cases.

5.4 Summary And Discussion

The elastic structure response for the four box curved girder bridge was examined analytically through the finite element program ADINA and experimentally. Comparison between the two schemes were made in terms of vertical deflection, torsional rotation as well as longitudinal normal stresses. Unfortunately other stress fields such as radial normal stress and shear stress components were not compared due to the limited number of experimental strain data.

Comparing the structure response in the seven distinctive load cases certainly provided sufficient grounds on which one can strongly examine both the accuracy of the experimental response of the structure as well as the reliability of ADINA's model in predicting the real structural response.

The correlation between analytical and experimental solution presented in the previous section for the seven load cases seem to have the following common features.

1. ADINA's model is always stiffer than the experimental bridge model. This is evident for vertical deflection as well as torsional rotation deformation. The higher relative flexibility of the experimental model may be attributed to the fact that spot welds rather than continuous welds were used to connect all interior webs with the bottom flange of the bridge.
2. ADINA's model has always underestimated maximum bridge deflection and rotation by about 35 % of the equivalent experimental value.
3. Both the ADINA bridge model and the experimental model were always in excellent agreement in terms of predicting points of maximum deflection and maximum torsional rotation as well as in predicting the distribution of deflection.

4. Transverse distribution of vertical deflection plots were always constant at end support sections, bilinear at central column support, and linear elsewhere along the bridge while nonlinear distribution were observed in the circumferential direction.

5. The percentage error in ADINA's prediction for deflections was consistent within a transverse section of the bridge and among the various load cases. This clearly reflects the stability as well as the high reliability of the experimental prediction for real structural response. The good predictability of experimental data confirms the same finding obtained through the regression analysis on deflection data which is presented in Chapter 3.

6. While it is evident from stress plots that ADINA's predictions for normal stress are less accurate than those for deformations, it is interesting to note that ADINA's predictions for maximum normal stress points in the seven load cases are much better than its prediction s for maximum deflection. The average percentage error of maximum normal stress in ADINA's model for the seven load cases was 21 % while that for deformation was 35 %.

7. The percentage error in ADINA's prediction for normal stresses were generally lowest for points below the neutral plane particularly on the bottom flange and they were highest for points above the neutral plane particularly on the cylindrical webs.

8. There seems to be some inconsistency in ADINA's prediction for normal stress at various points within a section and within the seven load cases. This is evident for the wide range of errors in maximum normal stress. Percentage errors varied between 4.2 % in load case 3 to 57.8 % in load case 2. Furthermore, percentage errors over 100 % were observed in some sections. In view of the low reliability of strain data that was observed in Chapter 3 and the fact that the same model was examined in ADINA for the seven load cases, it is natural to expect such a wide range of errors in ADINA's predictions for stresses. Perhaps one should have used ADINA's stresses as the real response compared to the experimental stresses. However, it should be noted that at all points of maximum normal stress in each load case the range of the experimental error for 99.9 % certainty was always between 2 % and 5 %. Consequently for those stress points the use of experimental stresses as the real response for comparing ADINA's solution is a valid assumption.

Table 5.2: Summary of maximum elastic structure response.

Load Case No.	Max. Deflection (mm)			Max. Torsional Rotation			Max. Normal Stress (MPa)		
	ADINA	Exp.	% Error	ADINA	Exp.	% Error	ADINA	Exp.	% Error
1	1.1	1.7	-36.4	0.00125	0.00200	-37.5	-9.4	-10.6	-11.3
2	0.9	2.7	-68.0	0.00150	0.00375	-60.0	6.6	15.5	-57.8
3	1.3	2.0	-32.1	0.00150	0.00175	-14.3	15.7	16.4	-4.2
4	1.0	1.3	-26.3	0.00150	0.00200	-25.0	9.2	8.4	10.4
5	2.1	3.2	-33.2	0.00150	0.00300	-50.0	20.2	21.9	-7.8
6	1.4	2.1	-34.7	0.00100	0.00175	-42.8	-7.5	-6.9	9.0
7	1.1	1.4	-15.8	0.00175	0.00200	-12.5	12.8	8.7	47.0
Avg. Error	-	-	35.2	-	-	34.6	-	-	21.1

9. Normal stress distributions were moderately linear in the bridge across the bridge deck as well as at the bottom flange while steep stress gradients dominated the cylindrical webs. This clearly indicates the effectiveness of the box structure in equally distributing the longitudinal moment between the four girders inspite of the eccentric nature of the trucks loading.

10. Both ADINA and the experimental modes were in excellent agreement in terms of predicting the location of positive and negative curvatures. Moreover, maximum normal stress was always developing at the same point within the bridge in the two models.

A summary of maximum deflection, maximum torsional rotation, and maximum normal stress developed in the seven load cases as predicted by the ADINA model and the experimental model is presented in Table 5.2. The table also includes percentage error for ADINA's prediction compared with experimental findings.

Inspite of the different sources of experimental errors and various assumption and approximations inherent in the analytical model, one can reasonably say that ADINA's model prediction for the linear static structure response of the curved box girder bridge model was good.

Chapter 6

Inelastic Response For The Curved Bridge Model

6.1 Introduction

The successful application of the ADINA finite element program in predicting the linear elastic response of curved box girder bridges has been demonstrated through a case study in Chapter 4 and by comparing with experimental findings in Chapter 5. In this Chapter, the application of ADINA is taken one step further to predict the nonlinear structural response of the four-box-girder curved bridge model.

The objective of the analytical study is to determine the ultimate load that can be carried by the bridge model and to present structure response at various load levels before reaching total collapse mechanism. The nonlinear finite element analysis shall be confined to material nonlinearity as opposed to geometric nonlinearity. The displacements and strains are assumed to be infinitesimally small; therefore the usual engineering stress and strain measures are employed in the response description.

Nonlinear experimental data of the curved bridge model is as yet unavailable. However, the analytical findings presented in this chapter can be very valuable in preparing the nonlinear experimental program for the bridge in a future study.

The bridge model response at ultimate limit states is investigated for two loading scenarios. In one loading scenario, the trucks are positioned such that the bridge positive moment capacity is reached while in the other loading scenario the negative moment capacity shall control.

Prior to analyzing the bridge model at overloads, it is worthwhile to examine the inelastic response of a simply supported box girder and compare the results with the beam theory solution. In this way particular modelling requirements for materially-nonlinear analysis can be established before hand.

6.2 Behavior of Simply Supported Box Girder

6.2.1 Description of The Box Girder

The simply supported box girder is a straight beam 6 m long, 60 cm wide and 80 cm deep. The top and bottom flanges of the box are 2.2 cm thick plates while the webs are 1.6 cm thick as shown in Figure 6.1.

The various components of the beam are assumed to be homogeneous and isotropic having elastic-plastic material behavior. Material model is assumed to obey Von-Mises yield criterion and isotropic strain hardening. Figure 6.1 shows stress-strain relation as well as the various material constants used in the analysis.

A uniformly distributed load was applied on the top flange throughout the beam length. The load function was selected such that the beam would undergo elastic and inelastic deformations.

The boundary conditions for the beam consist of a pinned connection at support A and a roller at support B.

6.2.2 Description of ADINA Models

Several finite element models were employed in analyzing the single box girder. A two dimensional discretization for models A, B, C, D and E are shown in Figure 6.2.

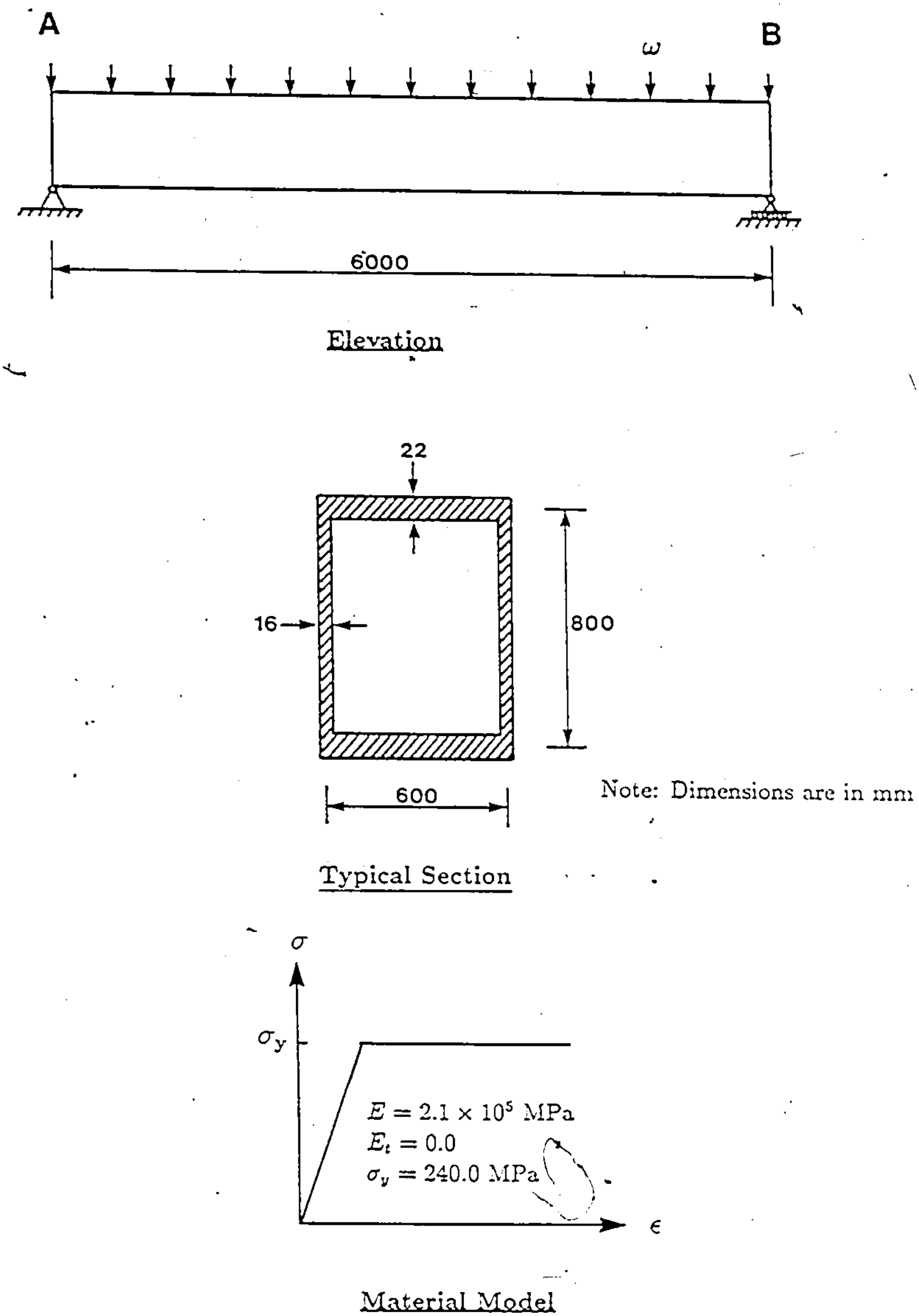

Figure 6.1: Description of the simply supported box girder.

The five models are identical in terms of the following features:

- Flanges and webs were modelled using the isoparametric thin shell 9-node element.
- Transverse discretization of the box features one element in the flange and one element in the web.
- No diaphragm elements anywhere within the box.
- Boundary conditions are imposed by fixing X, Y, and Z translational degrees of freedom at the three nodes of the bottom flange at section A while fixing only the Z translation at the three nodes of the bottom flange at section B.
- Geometry and material behavior are the same as those shown in Figure 6.1.

The distinctive feature for the models stems from the longitudinal discretization of the beam. As will be noted from Figure 6.2, the number of elements employed in subdividing the beam longitudinally is 2, 4, 6, 8 and 10 for models A, B, C, D and E respectively.

6.2.3 Elastic Response of Box Girder

Maximum deflection of the simply supported girder occurs at mid-span and is given by beam theory. If we ignore shear deformation the maximum deflection can be computed as follows:

$$\Delta_{max} = \frac{5\ \omega\ l^4}{384\ E\ I} \tag{6.1}$$

Maximum normal stress would develop also at mid-span at the extreme fibre and is given by:

$$\sigma_{max} = \frac{\omega\ l^2}{8}\ \frac{c}{I} \tag{6.2}$$

When the uniformly distributed load is 0.6 MPa the box girder response is elastic and total plastic strains are still zero. At this load level, the elastic structure response as computed by beam theory and by ADINA models A, B, C, D and E is presented in Table 6.1. It is evident that as the number of elements used in modelling the box girder longitudinally increases from 2 in model A to 10 in model E, the finite element solution converges in terms of maximum deflection and

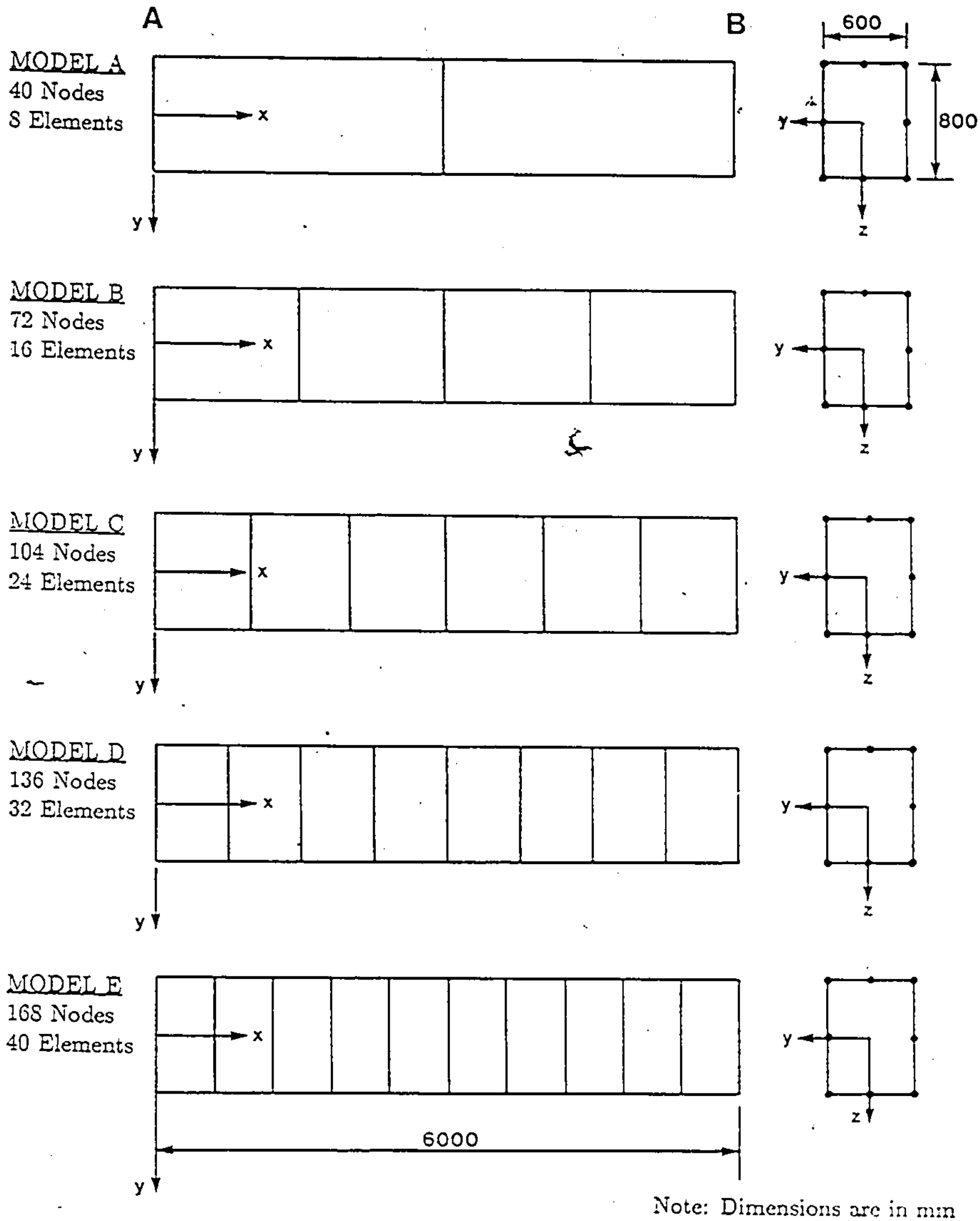

Figure 6.2: Finite element models for the simply supported box girder.

Table 6.1: Elastic response of the box girder at mid-span section.

Method of Analysis	Deflection		Normal Stress	
	Δ_{max} (cm)	Error (%)	σ_{max} (MPa)	Error (%)
Beam theory	0.531	0.0	118.9	0.0
ADINA model A	0.513	-3.4	110.3	-7.2
ADINA model B	0.566	6.6	117.3	-1.3
ADINA model C	0.572	7.7	116.8	-1.8
ADINA model D	0.579	9.4	116.6	-1.9
ADINA model E	0.583	9.8	116.5	-2.0

maximum flexural stress. As such model E seems to provide the converged response for the box girder. The percentage errors given in the table were computed relative to beam theory solution. Model E seems to overestimate maximum deflection by 10 % and underestimate maximum stress by only 2.0 %. In any finite element analysis, stresses should have much higher errors than displacements. It is not surprising in this case to find the opposite since the beam theory neglects shear deformation while ADINA's isoparametric thin shell element includes shear deformation. Perhaps one should consider ADINA's model E displacements as the reference value in computing percentage errors.

At this point the analyst may conclude that element discretization employed in model B would provide sufficiently accurate response for structures similar to the box girder. While the accuracy of model B may not be as high as that for model E, the CPU time needed for model B is less than half the time required for model E. Therefore model B is much more cost effective than model E.

6.2.4 Elastic-Plastic Response of Box Girder

The elastic-plastic response of the box girder can be represented by load-deformation curve. The load represents the uniformly distributed force per unit area ω while the deformation shall be expressed in terms of maximum vertical deflection of beam at mid-span section. The maximum deflection of the simply supported box girder can be expressed as follows:

$$\Delta_{max} = \int_0^{l/2} \Psi(x).x\ dx \tag{6.3}$$

where $\Psi(x)$ denotes beam curvature function.

When the applied bending moment exceeds the yield moment then the beam can be divided into two zones; the elastic zone and the elastic-plastic zone as shown in Figure 6.3. Accordingly, the curvature function can be expressed for the two zones separately as follows :

$$\Psi(x) = \frac{M(x)}{E\ I} \qquad 0 \leq x \leq x_e \tag{6.4}$$

$$\Psi(x) = \frac{\sigma_y}{E\ Y_{ep}} \qquad x_e \leq x \leq l/2 \tag{6.5}$$

where:

σ_y = Yield stress of the material.

$M(x)$ = Bending moment function.

E = Young's modulus.

I = Moment of inertia of section about neutral axis.

Y_{ep} = Vertical distance between neutral axis and elastic-plastic boundary measured in direction perpendicular to original beam axis.

x_e = Distance from support (origin) to edge of elastic zone.

As such maximum deflection at beam mid-span can be expressed in terms of elastic part Δ_e and elastic-plastic part Δ_{ep} as follows :

$$\Delta_{max} = \Delta_e + \Delta_{ep} \tag{6.6}$$

$$\Delta_e = \int_0^{x_e} \frac{M(x).x}{E\ I}.dx \tag{6.7}$$

$$\Delta_{ep} = \int_{x_e}^{l/2} \frac{\sigma_y.x}{E\ Y_{ep}}.dx \tag{6.8}$$

The extent of the elastic zone, x_e, can easily be obtained by solving the following quadratic equation:

$$x_e^2 - l\,x_e + \frac{2\ M_y}{\omega\ b} = 0 \tag{6.9}$$

where:

M_y = Yield moment of the section.

ω = Uniformly distributed load (force/area).

b = Width of the beam.

Once x_e is obtained, the elastic part of deflection, Δ_e, can be easily found by substituting the moment function into equation 6.7:

$$\Delta_e = \frac{\omega.b}{24\ E\ I} x_e^3\ [4l - 3x_e] \tag{6.10}$$

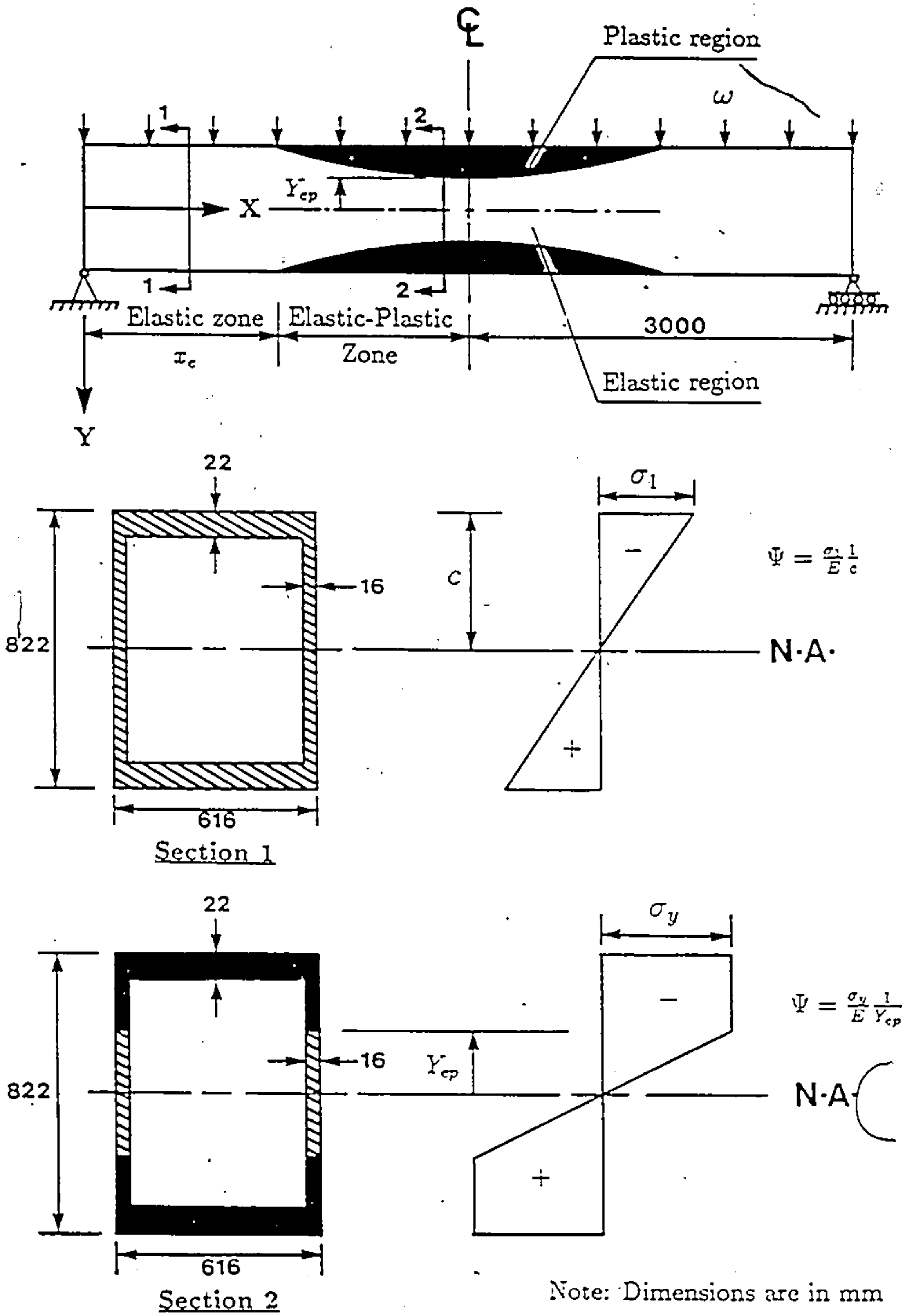

Figure 6.3: Elastic-Plastic behavior of the simply supported box girder.

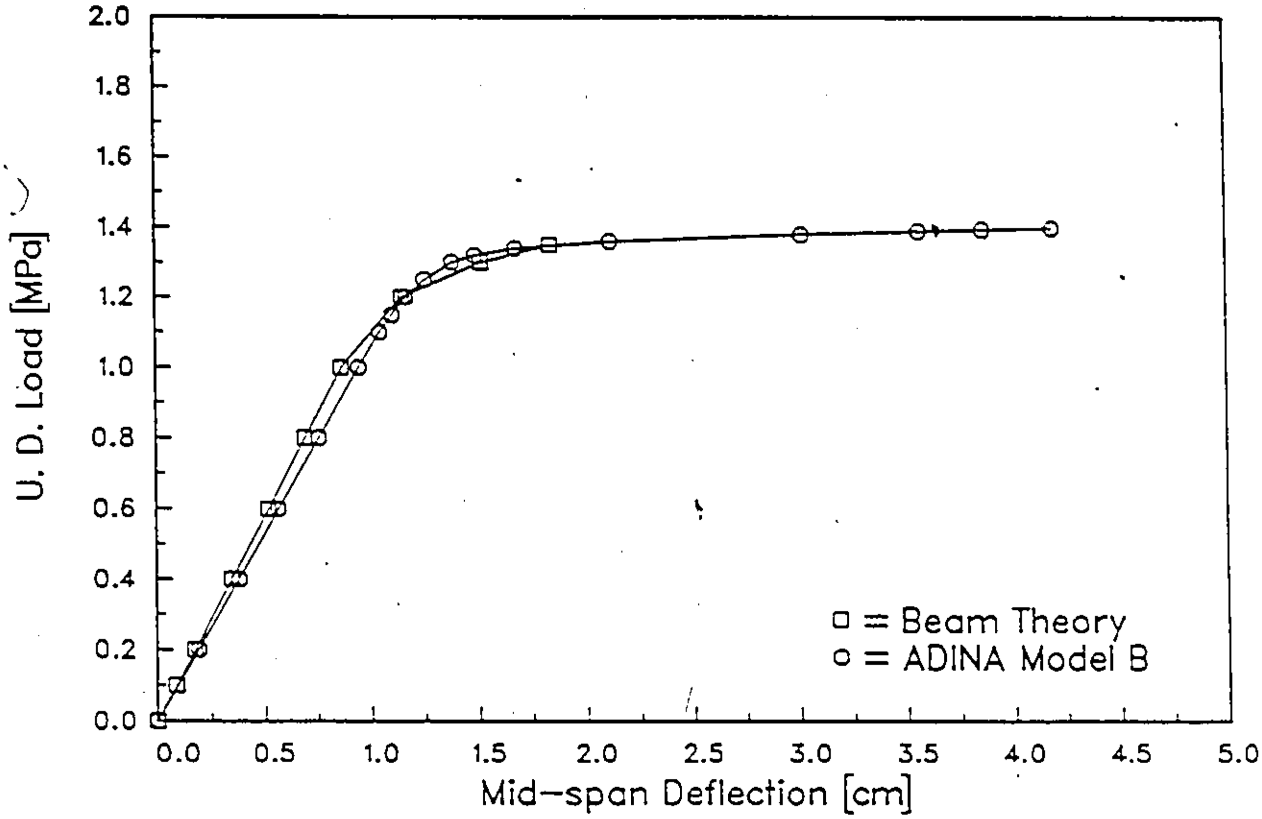

Figure 6.4: Load-deflection diagram – ADINA model B vs. beam theory.

In order to find the elastic-plastic part of deformation one must solve equation 6.8. The integral in this equation however, is rather complex since the function defining the elastic-plastic boundary given by $Y_{ep}(x)$ is very difficult to obtain in one explicit form.

A much more effective procedure would be to establish a moment-curvature relation for the box section, then the curvature function can be evaluated at several points within the elastic-plastic zone by referring to the moment-curvature diagram. Consequently the elastic-plastic part of deflection is computed by numerically integrating the moment of the area under the curvature curve about the beam origin or:

$$\Delta_{ep} = \int_{x_e}^{l/2} \Psi(x).x \; dx \qquad (6.11)$$

Using Equation 6.6, total deflection of the box girder can be computed at any load level. As such the theoretical load-deflection curve was obtained and is plotted in Figure 6.4. It is evident that model B predicts the inelastic response of the simply supported box girder very well.

At this point the analyst may feel quite confident about the successful application

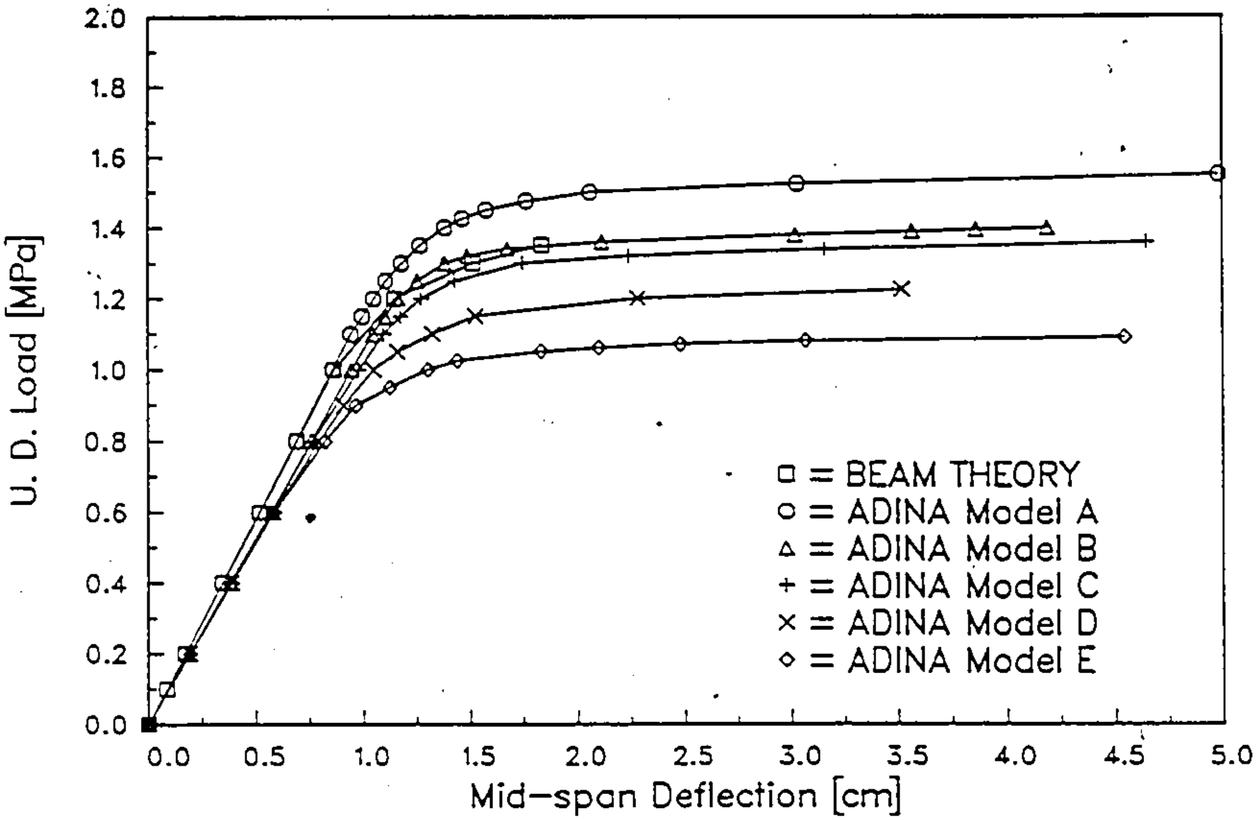

Figure 6.5: Load-deflection diagram – ADINA models A, B, C, D, E.

of ADINA finite element program in terms of modelling technique and various assumptions of boundary conditions and material properties. Perhaps the next step would be to apply the same procedure to analyze a full scale box girder structure.

However, if we go back one step and plot the load-deformation curves for the five models A, B, C, D and E, a very surprising behavior is observed. As will be noted from Figure 6.5 the more elements employed in the longitudinal direction of the beam the softer is the structure and the lower is the ultimate load. Moreover the results of the finer models C, D, E seem to diverge substantially from those of model B. The ultimate load in model E is about 78 % of the ultimate load of model B. While the fine models are diverging in the elastic-plastic load levels, they do converge in the linear elastic load levels.

If we closely examine the development of plastic strains within the box girder by ADINA models another strange behavior is observed. Plastic strains start developing within the webs at support sections and then propagate towards the mid-span of the beam. This behavior is quite opposite to the well established behavior by beam theory. Plastic hinge should develop first at the mid-section and the plastic

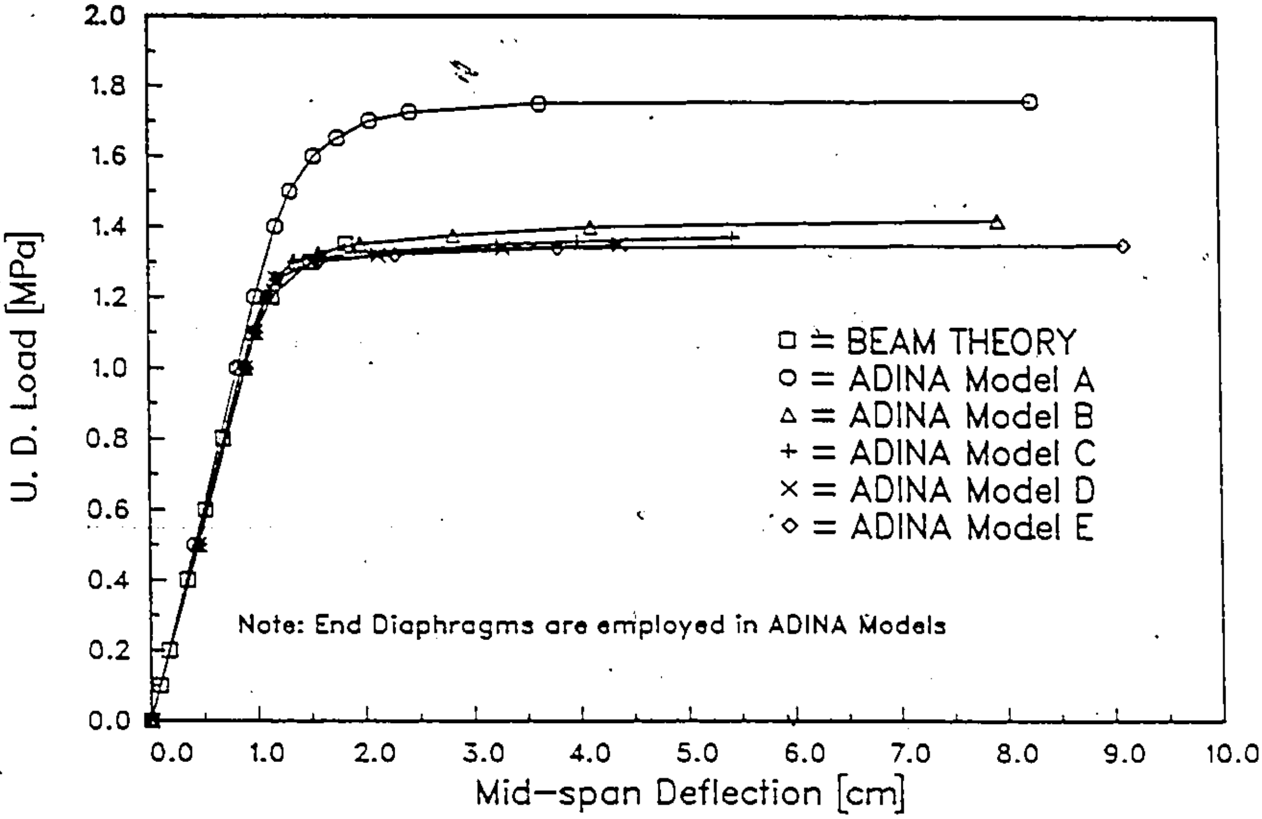

Figure 6.6: Load-deflection diagram - ADINA models including stiff diaphragm action.

flow progress towards the end sections. Moreover the initiation of plastic action starts from the extreme fibre at the top and bottom flanges and then gradually moves towards the neutral plane of the beam.

The only logical explanation for the strange behavior of ADINA models can be attributed to the high vertical shear stress development at the end sections combined with the low in plane stiffness of the box section at end supports. Recall that no diaphragm action was assumed in ADINA models. As such the Von-mises yield criterion is being reached at end sections where maximum shear force exists and the plastic flow seems to follow the shape of the shear force diagram.

In order to verify the above mentioned explanation, a very stiff diaphragm action was assumed at the end sections in all of ADINA models and the load-deformation curves are plotted in Figure 6.6 along with that obtained by beam theory. With the exception of model A, all ADINA models do converge and compare very well with beam theory. Element discretization in model A is evidently too coarse and hence the model is too stiff. As such, the end diaphragm action while not so significant in the linear-elastic finite element analysis, obviously plays a very important role in the materially nonlinear analysis and therefore the analyst should not ignore its influence on the behavior of box girder bridges.

6.3 Description of ADINA Curved Bridge Model

The same finite element discretization which was used for the linear elastic analysis in Chapter 5 shall be employed for the nonlinear analysis. Preliminary application of this discretization for the nonlinear analysis failed however, as the program requirements for computer disk space storage was more than 200 cylinders on the AMDAHL 5860 mainframe. For this reason it was necessary to reduce the total number of nodes employed in the mesh. As such all interior nodes in the transverse or radial direction for the bridge deck and bottom flange elements were eliminated. It should be noted however, by so doing the total number of elements in the mesh did not change and therefore the same finite element discretization shown in Figure 5.1 is employed in the reduced mesh.

A preliminary elastic analysis indicated that by adopting the mesh with reduced number of degrees of freedom does not sacrifice solution accuracy in terms of displacements and stresses. As such solution convergence for the reduced mesh was assured for the elastic analysis and therefore it will be employed for the nonlinear analysis.

The same boundary conditions imposed in the linear elastic analysis is employed in the nonlinear analysis. The only difference between both analyses lies in modelling the constitutive law for the bridge and the loading conditions.

All aluminum components of the bridge was modelled using the isothermal elastic-plastic material model while inelastic concrete model was employed for the bridge deck. Both models are described in detail in the next section.

Details of load scenarios are described separately in section 6.5.

6.4 Material Modelling

Material modelling plays a very important role in any finite element analysis for structures. The constitutive law $[C]$ which relates internal element stresses with strains enters the finite element procedure at two levels in the following order:

1. When developing element stiffness matrix:

$$[K] = \int [B]^T [C][B] \, dV \tag{6.12}$$

   where $[B]$ denotes the strain-displacement matrix and $[K]$ denotes the element stiffness matrix.

2. When computing element stresses:

$$\{\sigma\} = [C]\{\epsilon\} \tag{6.13}$$

   $\{\sigma\}$ denotes the element stress vector and $\{\epsilon\}$ denotes the element strain vector.

In small displacement linear elastic analysis both matrices $[B]$ and $[C]$ are linear and therefore equations 6.12 and 6.13 can easily be solved. If material behavior is further assumed to be homogeneous and isotropic, the only material constants required to define the constitutive matrix $[C]$ would be Young's modulus E and Poisson's ratio ν.

In materially nonlinear analysis, strain-displacement matrix $[B]$ remains linear while the constitutive law is no longer linear and depending on the type of material more constants other than E and ν are required to define the material properly. As such, the problem becomes more complex and time consuming not only due to the iterative nature of the solution procedure but also because of the difficulty in developing the mathematical model which describes the true constitutive relation for the material.

Since in this study, the structural response at ultimate limit state shall be predicted using the ADINA finite element program, modelling the concrete deck and the aluminum plates shall be restricted to those models available in the program library. The following sections will describe the constitutive models employed for each material.

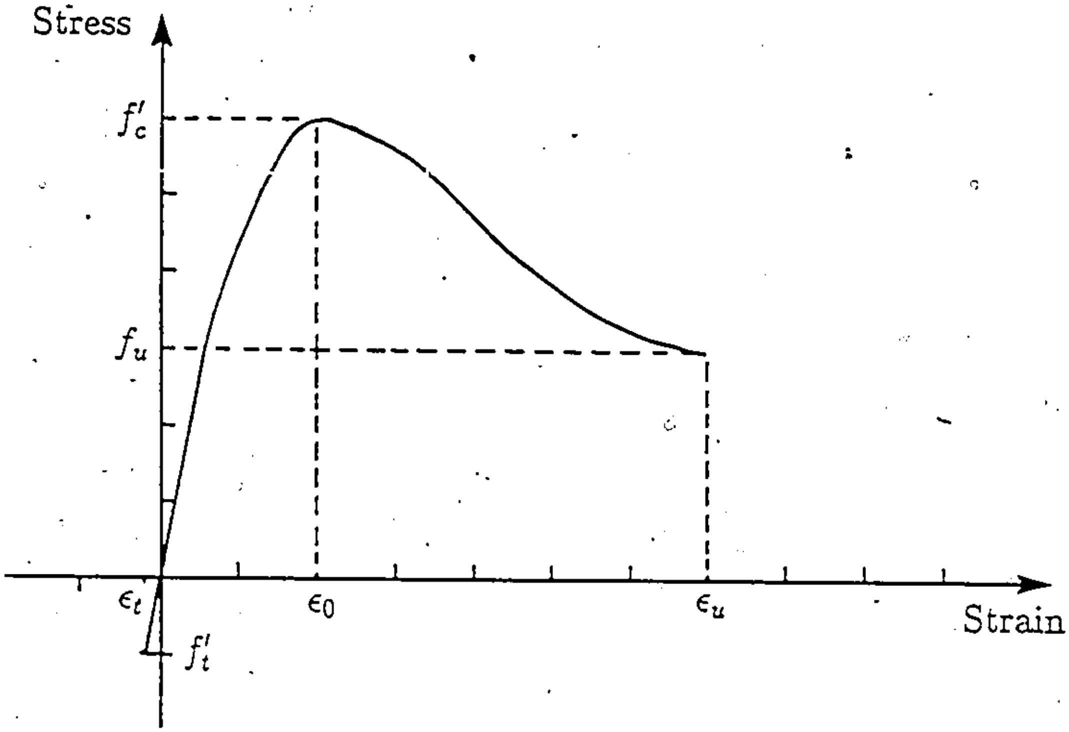

Figure 6.7: Typical uniaxial stress-strain relation for concrete.

6.4.1 Concrete Inelastic Material Model

A typical stress-strain curve for a concrete cylinder subjected to uniaxial stress condition is shown in Figure 6.7. As will be noted from the Figure, the basic constitutive characteristics for the concrete material are:

- Tensile failure at a maximum, relatively small principal tensile stress f'_t.
- Compression crushing failure at high compression f'_c.
- Stress-strain relationship is linear in the tensile stress zone.
- Nonlinear stress-strain distribution is assumed in the compression zone up to f'_c.
- Strain softening from maximum compressive stress f'_c to an ultimate strain, at which the material totally fails.

While the ADINA program provides a concrete material model having the aforementioned basic features, the model cannot be employed with shell elements. The concrete model can only be used with two-dimensional elements under plane-stress, plane-strain and axisymmetric conditions and the three-dimensional solid elements. Unfortunately none of these elements can be used to model the bridge deck. As such bridge deck shell elements are limited to material models that can be employed with the isoparametric shell element. For M.N.O. (materially nonlinear only) analysis the material models which can be used for the shell elements are:

1. Bilinear elastic-plastic model with Von-Mises yield condition.
2. Multilinear elastic-plastic model with Von-Mises yield condition.
3. Nonlinear isotropic thermo-elastic material model.

Furthermore the elastic-plastic material models 1,2 are limited to isotropic hardening only when the isoparametric thin shell elements are employed.

Clearly none of the above material models have the basic constitutive characteristics for concrete and hence would not properly represent the material behavior. Consequently the ADINA program does not provide proper material model for the concrete bridge deck component. However, in light of the fact that bridge deck is not a major component within the section and its contribution to bridge flexural ultimate capacity may not be as significant as the contribution by the aluminum components, it is reasonable to make simplifying assumptions for concrete material behavior. As such, it is worthwhile to examine the feasibility of the following three models to closely represent concrete material behavior:

1. Linear-elastic.
2. Bilinear elastic-plastic.
3. Multilinear elastic-plastic.

The low tensile splitting strength for concrete cannot be represented by any of the three models. This distinct characteristic of concrete is certainly not applicable in the three models since they all assume equal tensile and compressive strengths for the material. This drawback in the models can be avoided if the bridge is loaded to ultimate such that positive moment instead of negative moment controls. In this way only compressive stresses would contribute to section flexural capacity.

The nonlinear stress-strain distribution for concrete in the compression zone and up to f'_c can be best represented by the multilinear elastic-plastic model. As such weakening of the material under increasing compressive stresses is accounted for properly. On the other hand the linear elastic model would overestimate concrete compressive strength particularly at ultimate strain levels.

Strain softening from f'_c to ultimate load unfortunately cannot be represented by any of the three models. However errors introduced by ignoring this constitutive characteristic of the concrete can be reduced by assuming a maximum compressive strength f'_c lower than the actual strength available.

Consequently the use of multilinear elastic-plastic model for concrete deck elements would be the most reasonable material model that can be used within the limited choices available in the program and hence shall be used as the concrete material model for predicting structure ultimate capacity in this study.

The plastic-multilinear material model presented in the ADINA program requires three material constants which are the Young's modulus, Poisson's ratio and the yield stress. Moreover it allows a maximum of 6 stress-strain points to describe the multilinear plastic action beyond the yield stress. It is instructive to note that the model uses Von-Mises yield condition and assumes isotropic hardening.

Recall in Chapter 3, three concrete cylinders were tested under monotonic axial compression for 28 day concrete strength. The stress-strain data are presented in Appendix A, Table A.2. The average strain for the three specimens is plotted against each stress level in Figure 6.8.

The various material constants required by the plastic-multilinear model can be obtained from this figure. The same values of Young's modulus and Poisson's ratio used in the linear elastic analysis are employed in the inelastic analysis. Initial yield is assumed to occur at 65% of f'_c which corresponds to 29.6 MPa. Within this range experimental stress-strain data exhibit perfectly linear relations. Because the elastic plastic model does not account for softening beyond maximum compressive strength f'_c, the ultimate strength is assumed to occur at 85% of f'_c. From this stress level and onward perfectly plastic behavior is assumed. In this way the multilinear elastic-plastic model for concrete can be defined by 4 straight lines giving the following points:

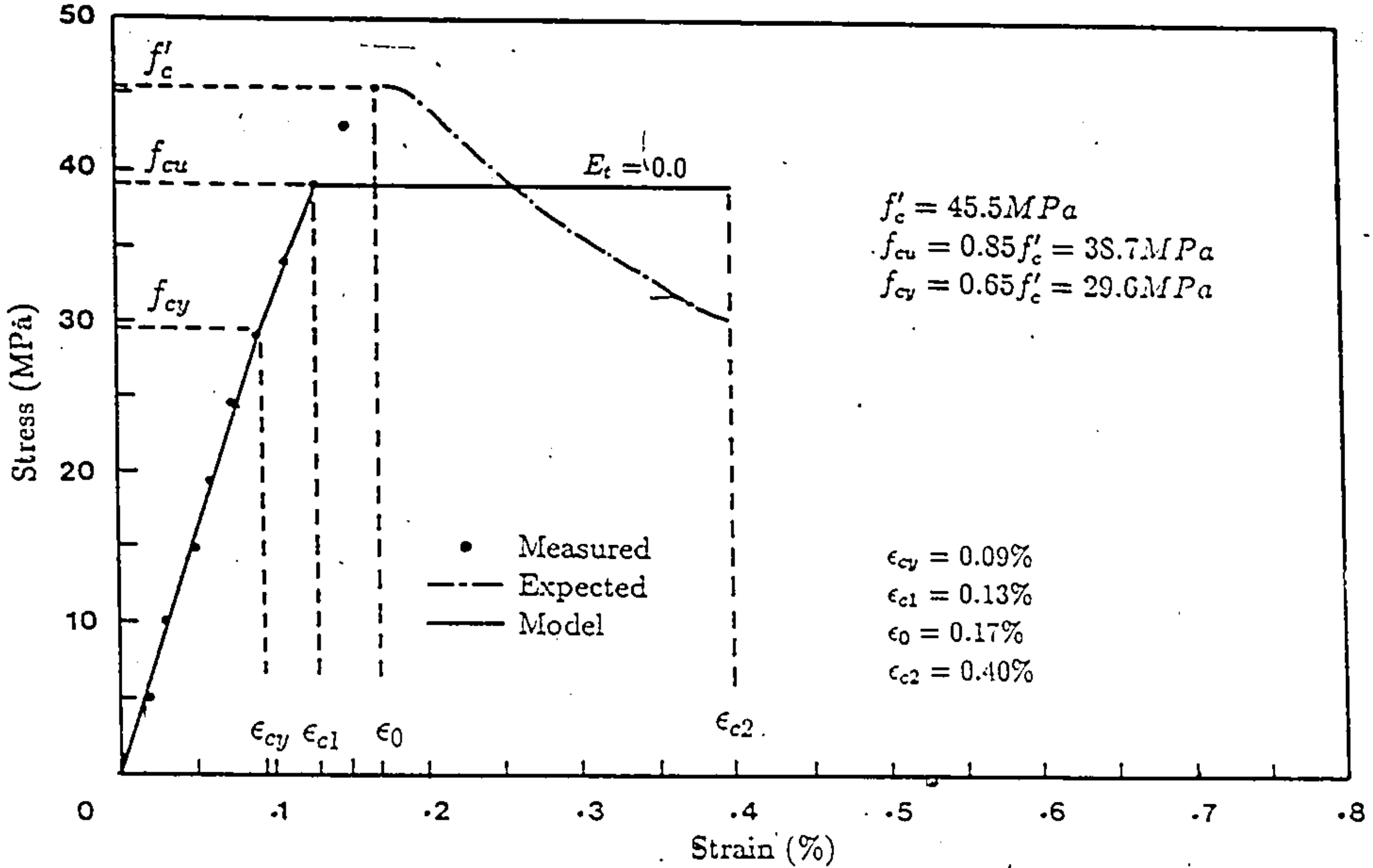

Figure 6.8: Material model employed for concrete in ADINA.

Point (#)	1	2	3	4	5
Stress (MPa)	0.0	29.6	34.2	38.7	38.7
Strain (%)	0.0	0.094	0.108	0.126	0.400

While this model may reasonably represent the behavior of concrete in the bridge deck under compressive stress field it is instructive to note that it does not describe the behavior of concrete in tension. It is therefore not recommended to be applied under such circumstances. If the bridge model is to reach ultimate capacity in a negative moment region, perhaps the most reasonable choice would be to ignore the concrete elements totally within the high tension zone.

6.4.2 Aluminum Elastic-Plastic Material Model

Like any structural steel material, aluminum exhibits elastic-plastic material behavior. Elasto-plastic behavior is characterized by an initial elastic material response on to which a plastic deformation is superimposed after a certain level of stress

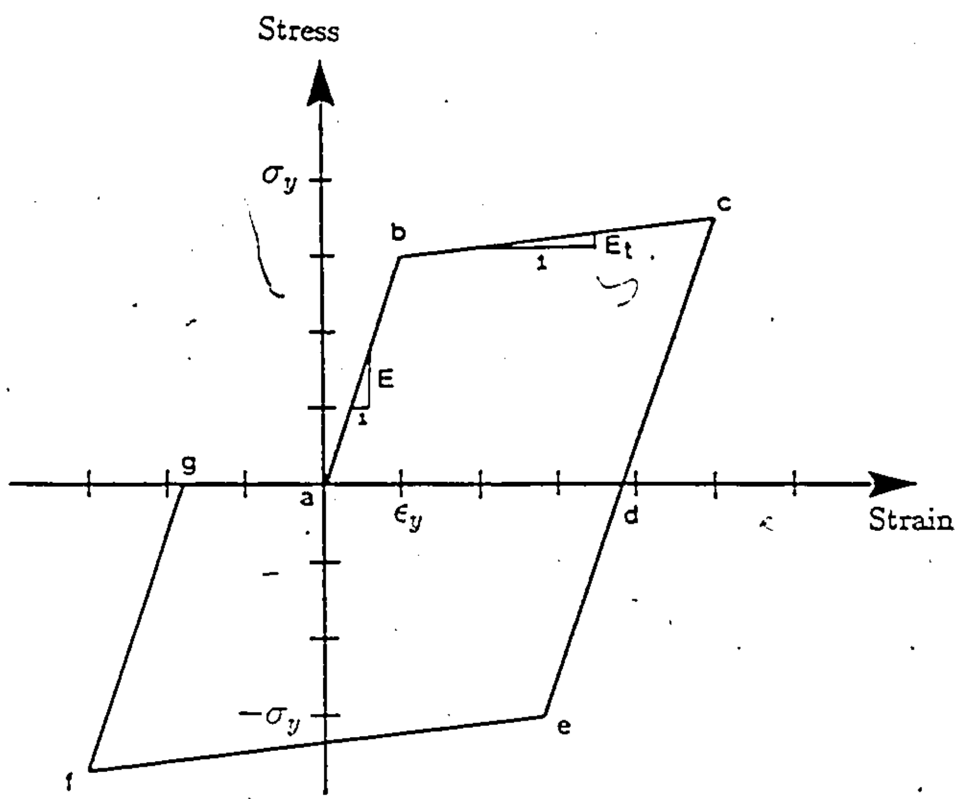

Figure 6.9: Typical elastic-plastic material behavior.

has been reached. Plastic deformation is essentially irrecoverable upon unloading. The onset of plastic deformation (or yielding) is governed by a yield criterion and post-yield deformation generally occurs at a greatly reduced material stiffness.

A typical uniaxial stress-strain relation for a material exhibiting elastic-plastic behavior is given in Figure 6.9. The figure shows a complete stress cycle starting by loading the specimen in tension to and beyond yield, followed by unloading to zero stress and then reloading in compression to and beyond yield and finally to zero stress. The stress path is designated in the figure by the letters a, b, c, d, e, f, g.

While there are many distinct elasto-plastic models in the literature they all have the following basic characteristics in common :

- An explicit relationship between stress and strain which describes material behavior under elastic conditions.
- A yield criterion indicating the multiaxial stress level at which plastic flow commences.
- A flow rule which relates the plastic strain increments to the current stresses

and the stress increments subsequent to yielding.

- A hardening rule specifying the modification of the yield condition during plastic flow.

As mentioned earlier the ADINA program permits the use of isothermal (i.e. temperature independent) elastic-plastic model with the isoparametric thin shell elements. The model has all of the above mentioned basic constitutive characteristics and is further characterized with the following features:

1. Linear elastic behavior before initial yield.
2. Von-Mises yield criterion.
3. Associated flow rule.
4. Isoparametric strain hardening.

Von-Mises suggested that yield occurs when the second deviatoric stress invariant reaches a critical value or:

$$J_2' = \frac{1}{3}\,\sigma_y^2 \tag{6.14}$$

where J_2' denotes the second deviation stress at time t and is defined by :

$$J_2' = \frac{1}{2}[(\sigma_{xx} - \sigma)^2 + (\sigma_{yy} - \sigma)^2 + (\sigma_{zz} - \sigma)^2] + \tau_{xy}^2 + \tau_{xz}^2 + \tau_{yz}^2 \tag{6.15}$$

$$\sigma = [\sigma_{xx} + \sigma_{yy} + \sigma_{zz}]/3 \tag{6.16}$$

The symbol σ_y designates the yield stress at time t which is equal to the radius of the cylinder of Von-Mises yield surface in the principal stress space X, Y and Z as shown in Figure 6.10.

The associated flow rule allows the calculation of plastic strain increments as follows:

$$d\epsilon_{ij}^p = \lambda\frac{\partial F}{\partial \sigma_{ij}} \tag{6.17}$$

$$F = J_2' - \frac{1}{3}\sigma_y^2 \tag{6.18}$$

where $\partial\sigma_{ij}$ and $d\epsilon_{ij}^p$ are differential increments in stresses and plastic strains while λ is a scaler. The isotropic hardening specifies that subsequent yield surfaces are developed by uniform expansion of the original yield curve, without any translation

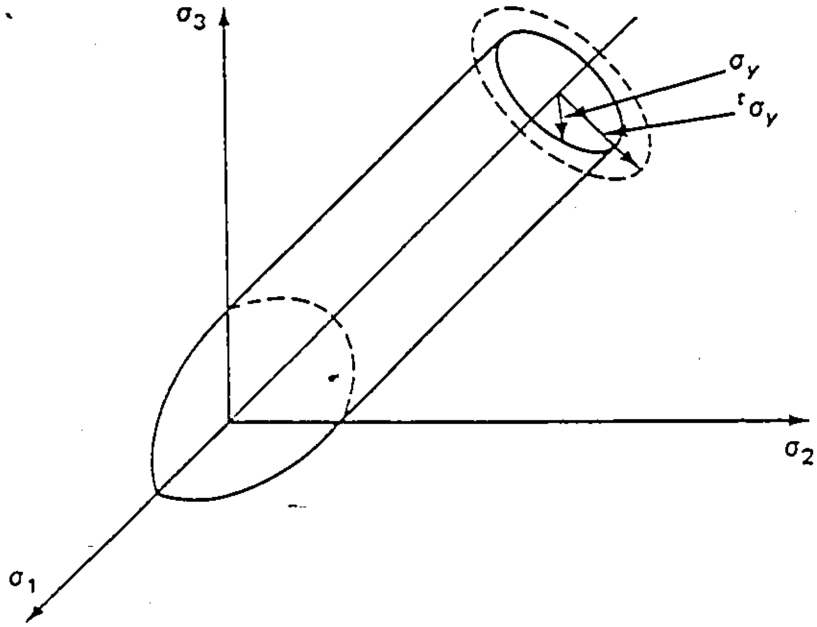

Von Mises yield surface

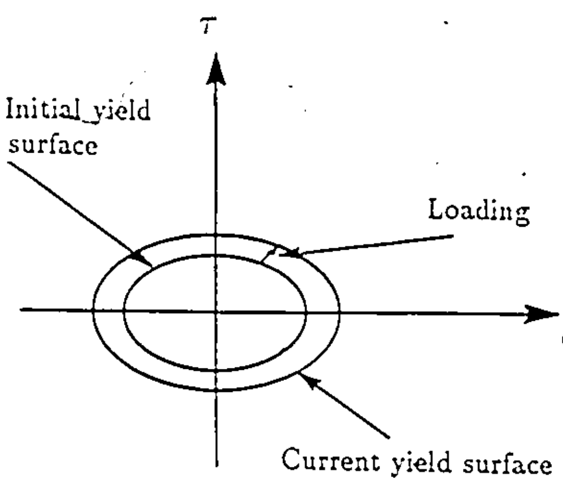

Isotropic Strain-Hardening

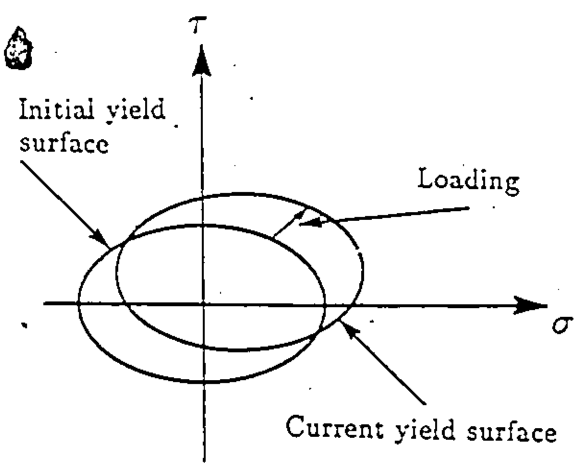

Kinematic Strain-Hardening

Figure 6.10: Von Mises yield surface and types of strain hardening.

as shown in Figure 6.10. On the other hand, if the subsequent yield surfaces preserve their shape and orientation but translate in stress space as a rigid body as shown in Figure 6.10, hardening is described to be kinematic.

Further details on the mathematical formulation for the theory which models the elasto-plastic material behavior is not presented in this study and can be found elsewhere [25,48].

In addition to the linear elastic material constants E and ν, the elastic-plastic model requires the strain hardening modulus E_t which can be determined from a simple tension test. Six aluminum specimens were tested under uniaxial tension up to failure. Testing was performed in accordance with ASTEM-E18-81 standard methods of tension testing of metallic materials. Stress-strain curves for the six aluminum specimens are shown in Figure 6.11. The average stress-strain curve for all specimens is also given in the figure and shall be used for analysis in ADINA program. Hence aluminum material constants used for the nonlinear analysis are :

1. Young's modulus: E = 71100 MPa.
2. Poisson's ratio : $\nu = 0.379$.
3. Strain-Hardening modulus : $E_t = 309$ MPa.
4. Yield stress $F_y = 301$ MPa.

Unlike the concrete model the aluminum elastic-plastic model is equally applicable in tension and compression. In fact material behavior in both regions is identical and therefore there is no restriction on how the bridge section capacity is reached.

6.5 Description of Load Scenarios

The nonlinear structural response of the curved bridge model is examined for two distinct loading scenarios. In the first load scenario, denoted by A, maximum bridge response develops at the critical positive moment section. In load scenario B however, the negative moment at the central support section controls maximum response.

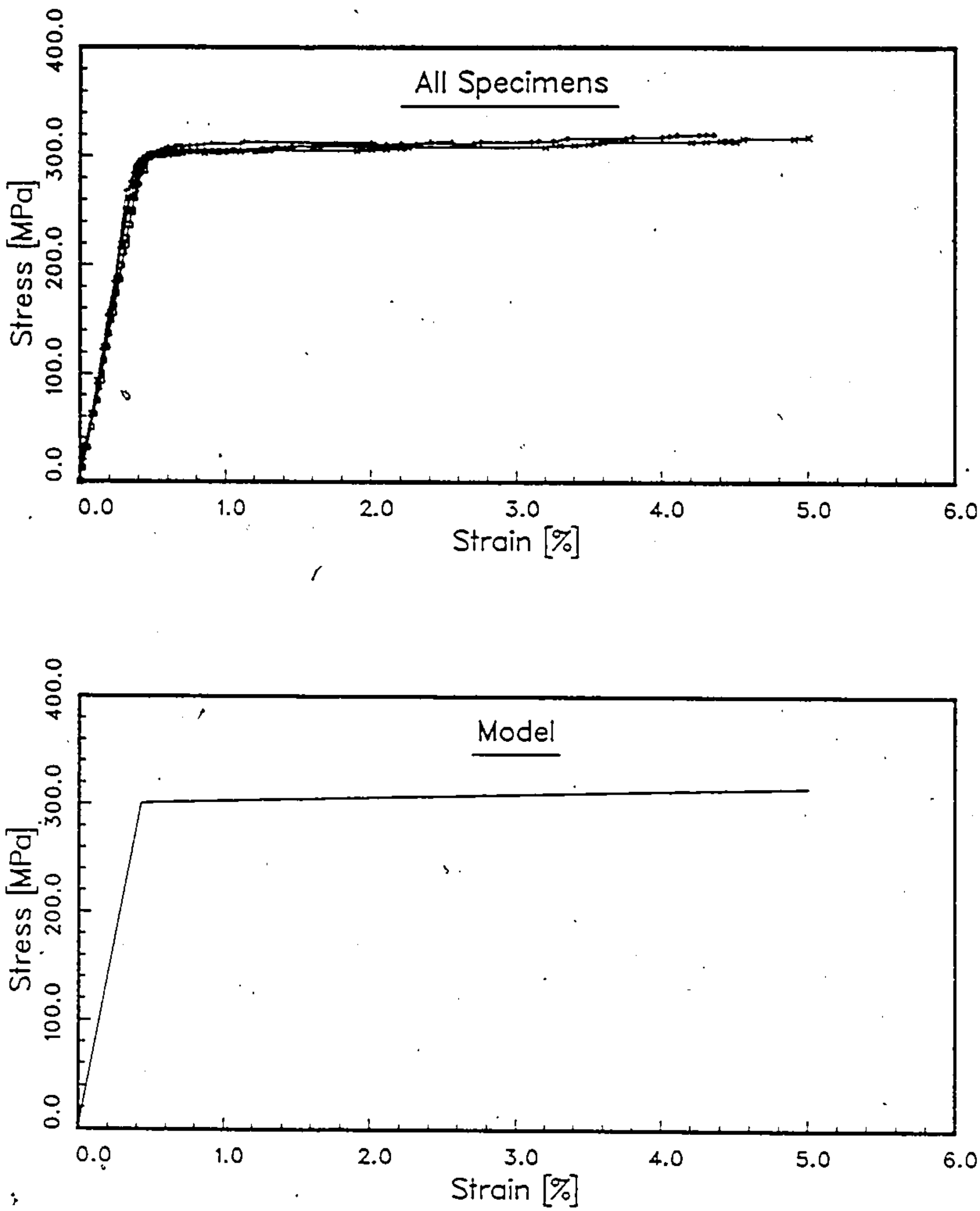

Figure 6.11: Material model employed for aluminum in ADINA.

The same equivalent OHBD parallel trucks model which was described in Figure 3.8 is employed as a unit truck load. The critical position of the unit truck along the bridge deck is established using bending moment influence lines. Hence, the curved bridge was simplified by an equivalent straight two span continuous beam. In order to maximize longitudinal positive moment in load scenario A, only one span needs to be loaded with the unit truck while in load scenario B each span is loaded with a unit truck. Figure 6.12 shows the unit truck positions for both load scenarios.

In order to determine whether one lane eccentric truck loading or two lane truck loading is more critical, the bridge is first analyzed assuming elastic material behaviour for each case. As such, the following four loading cases are considered in the elastic analysis:

- Case A1 : Load scenario A – One lane unit truck loading.
- Case A2 : Load scenario A – Two lane unit truck loading.
- Case B1 : Load scenario B – One lane unit truck loading.
- Case B2 : Load scenario B – Two lane unit truck loading.

It will be noted from Figure 6.12 that in positioning the unit trucks transversely wheel loads are applied directly above the webs so that punching shear in the bridge deck is avoided.

6.6 Elastic Structure Response

6.6.1 Positive Moment Load Scenario A

Longitudinal and transverse deflection profiles for the bridge at this load scenario are presented in Figure 6.13. Deflection profiles for one and two lane unit truck loading is shown in the figure. It is evident that load case A2 results in higher vertical deflection. Maximum deflection in the bottom plate developing at section 5 under Web B was about 1.4 mm and 2.4 mm for one and two lane truck loading respectively. In spite of bridge horizontal curvature and the eccentric nature of truck loads, the torsional rotation at the positive moment section in load case A1

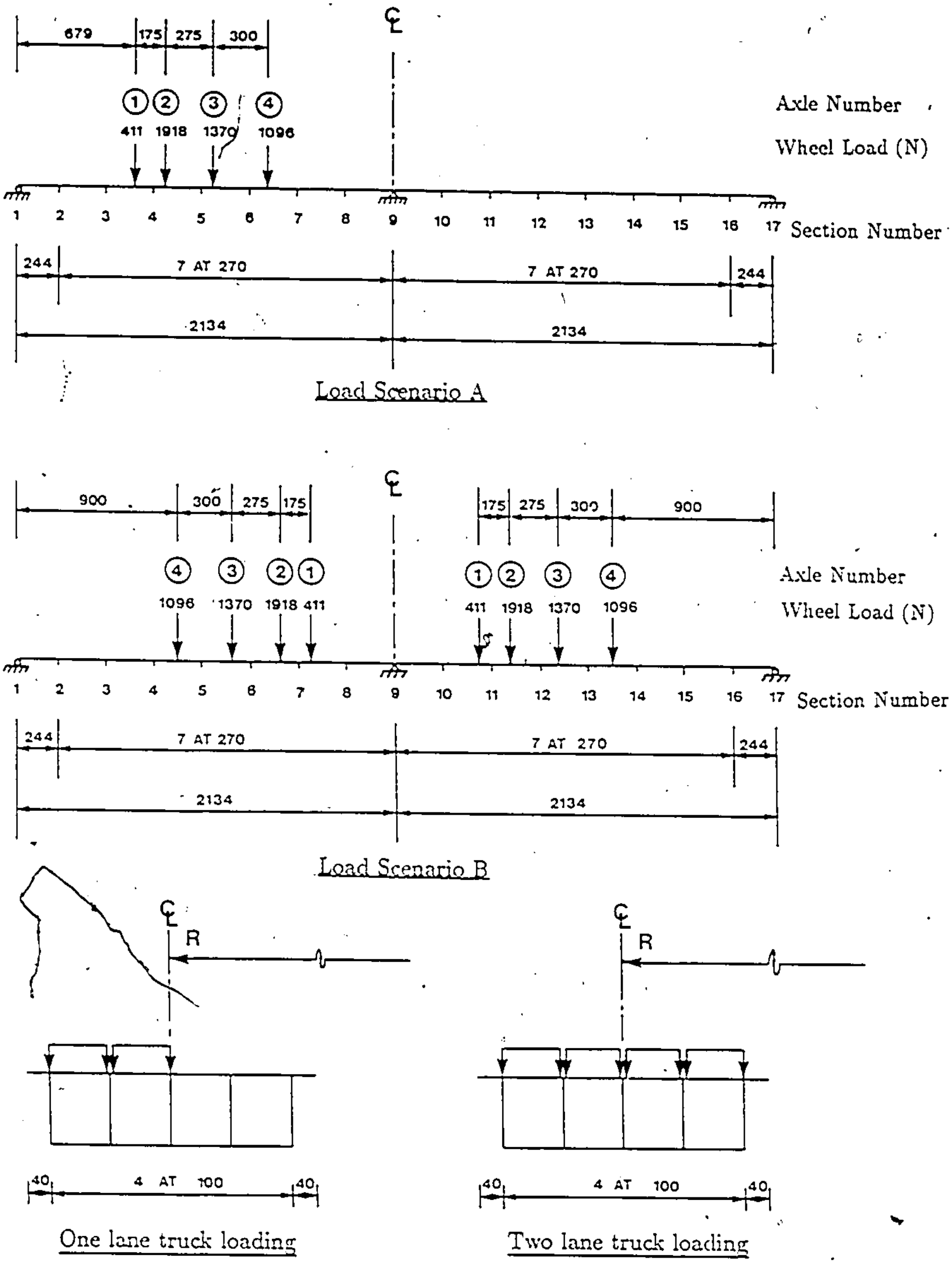

Figure 6.12: Critical truck positions employed in the analysis

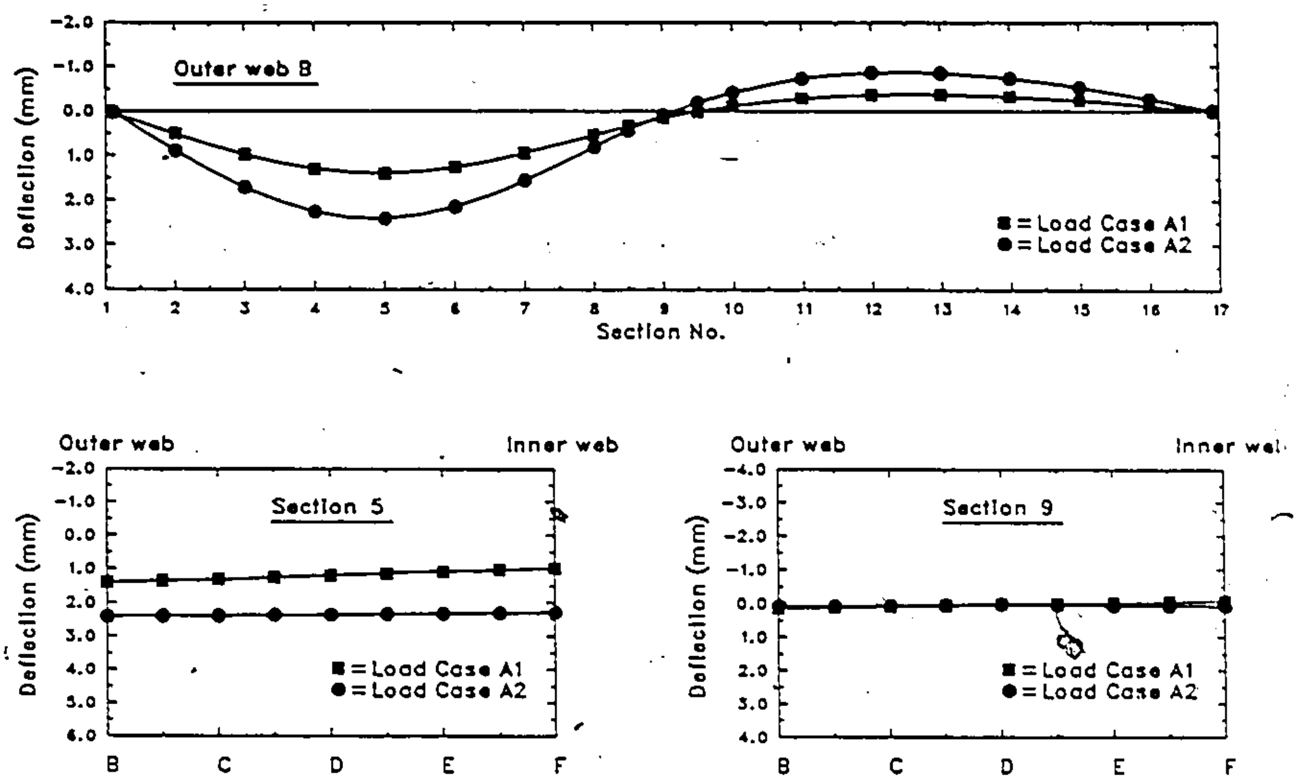

Figure 6.13: Deflection profiles in load scenario A– Elastic Analysis.

is only 5 % higher than that observed in load case A2. This clearly indicates that without interior diaphragms at the positive moment sections the bridge has high torsional stiffness.

Longitudinal normal stresses are also highest at section 5 in load scenario A. Figure 6.14 shows transverse distribution of these stresses at the positive moment section. Maximum stress was developed in the bottom plate in both load cases, A1 and A2. In one lane truck loading maximum stress of 14.7 MPa is observed under the outer web B while in load case A2 a value of 27.3 MPa is observed under web E.

While normal stress component can be used as a response criterion in deciding which load case, A1 or A2, is more critical, it does not reflect the complete state of stress in the bridge section. The second devatoric stress invariant J_2' however, does provide an excellent measure as it includes the two normal stress components, σ_{xx}, σ_{yy} and shear stress components, τ_{xy}, τ_{xz}, τ_{yz}. The highest value of $\sqrt{J_2'}$ in the bridge was 30.7 Mpa and 54.4 Mpa for load case A1 and load case A2 respectively. This clearly shows that the two lane truck loading is more critical than the one lane

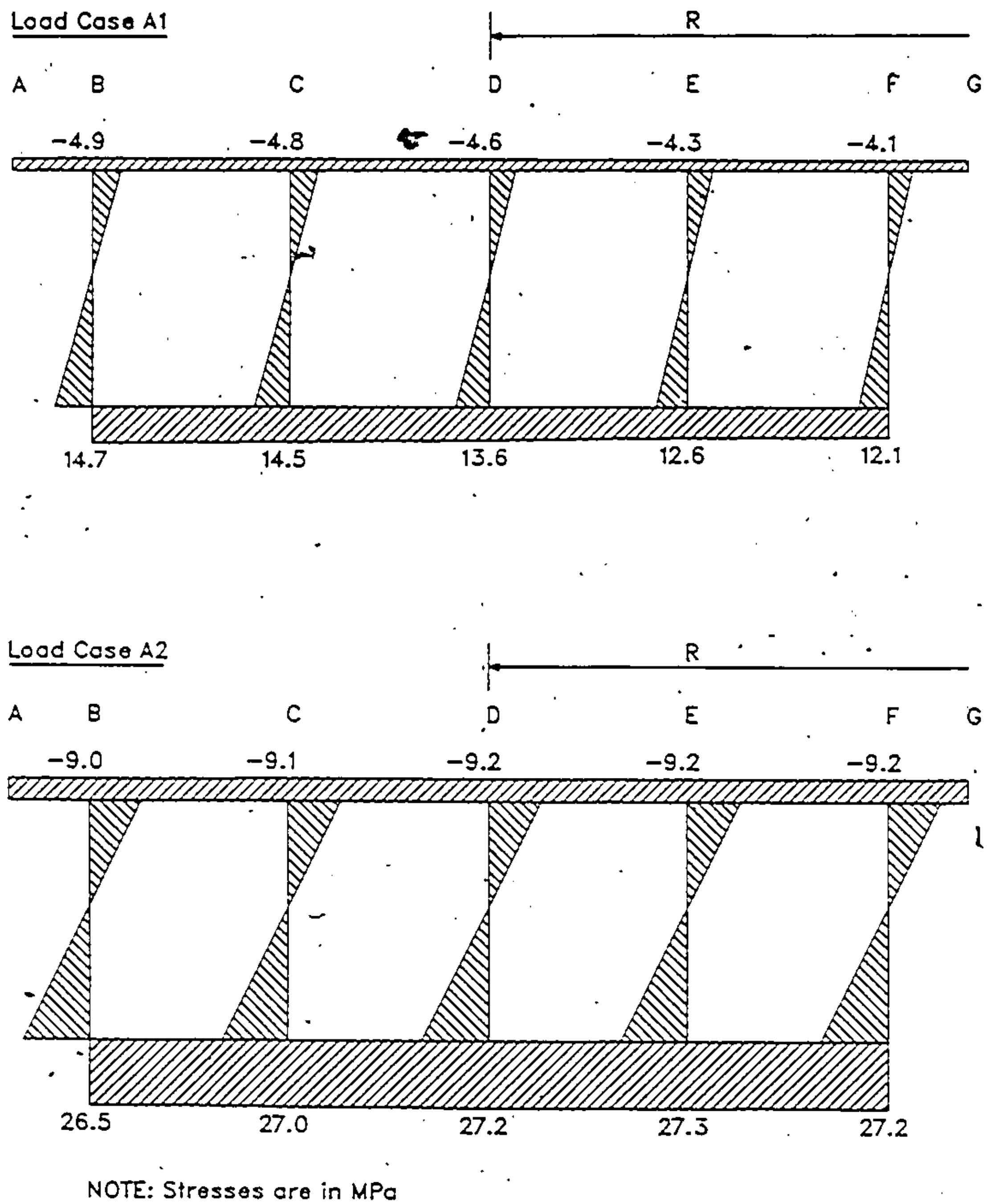

Figure 6.14: Normal stresses at section 5 for load scenario A – Elastic Analysis.

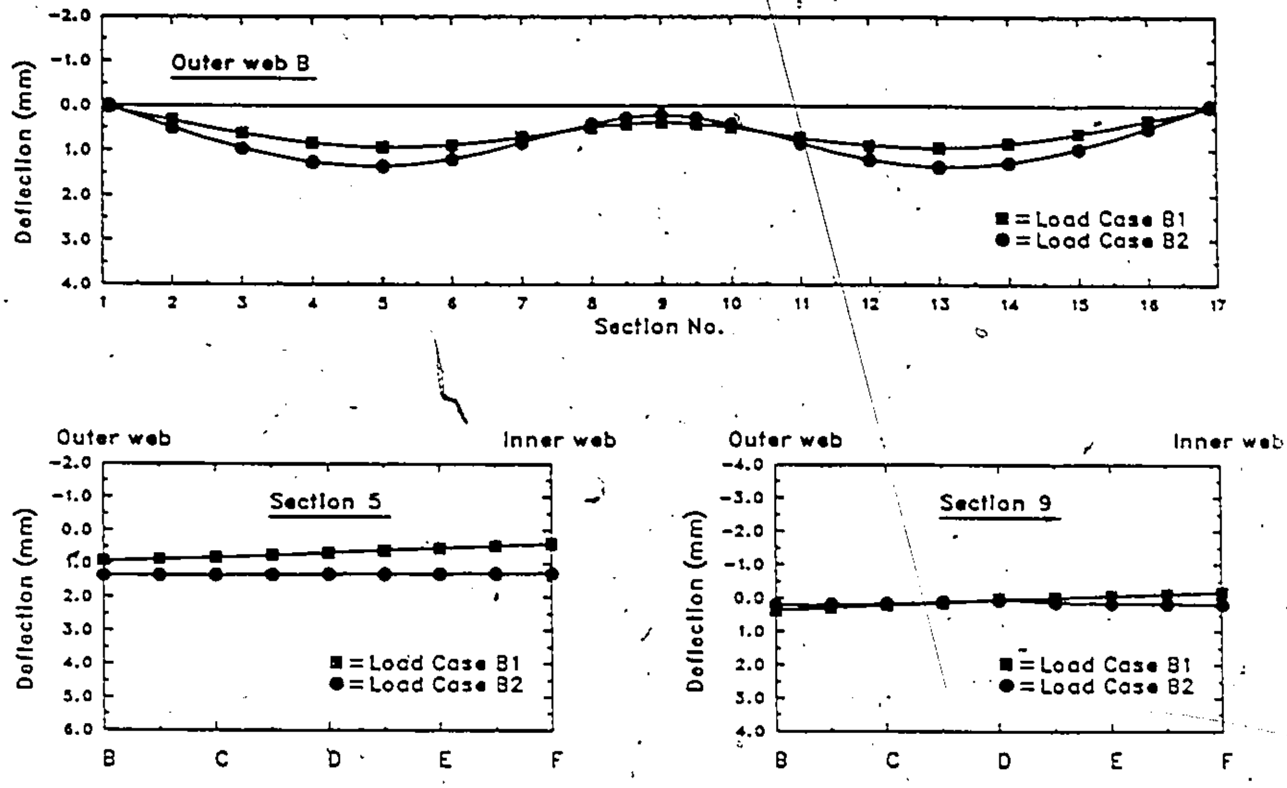

Figure 6.15: Deflection profiles in load scenario B – Elastic Analysis.

truck loading for the positive moment load scenario.

6.6.2 Negative Moment Load Scenario B

Elastic bridge response for this load scenario also indicates that the two lane truck loading is more critical than the one lane truck loading. This is evident from deflection profiles given in Figure 6.15 and normal stresses shown in Figure 3.16.

Maximum normal stress for both load cases, B1 and B2, was developed at the central Web D at the negative moment section 9. Stresses in load case B2 are about twice as high as those in load case B1.

Maximum square root of the second devatoric stress invariant in the bridge is 41.4 MPa and 51.3 MPa for load case B1 and load case B2 respectively.

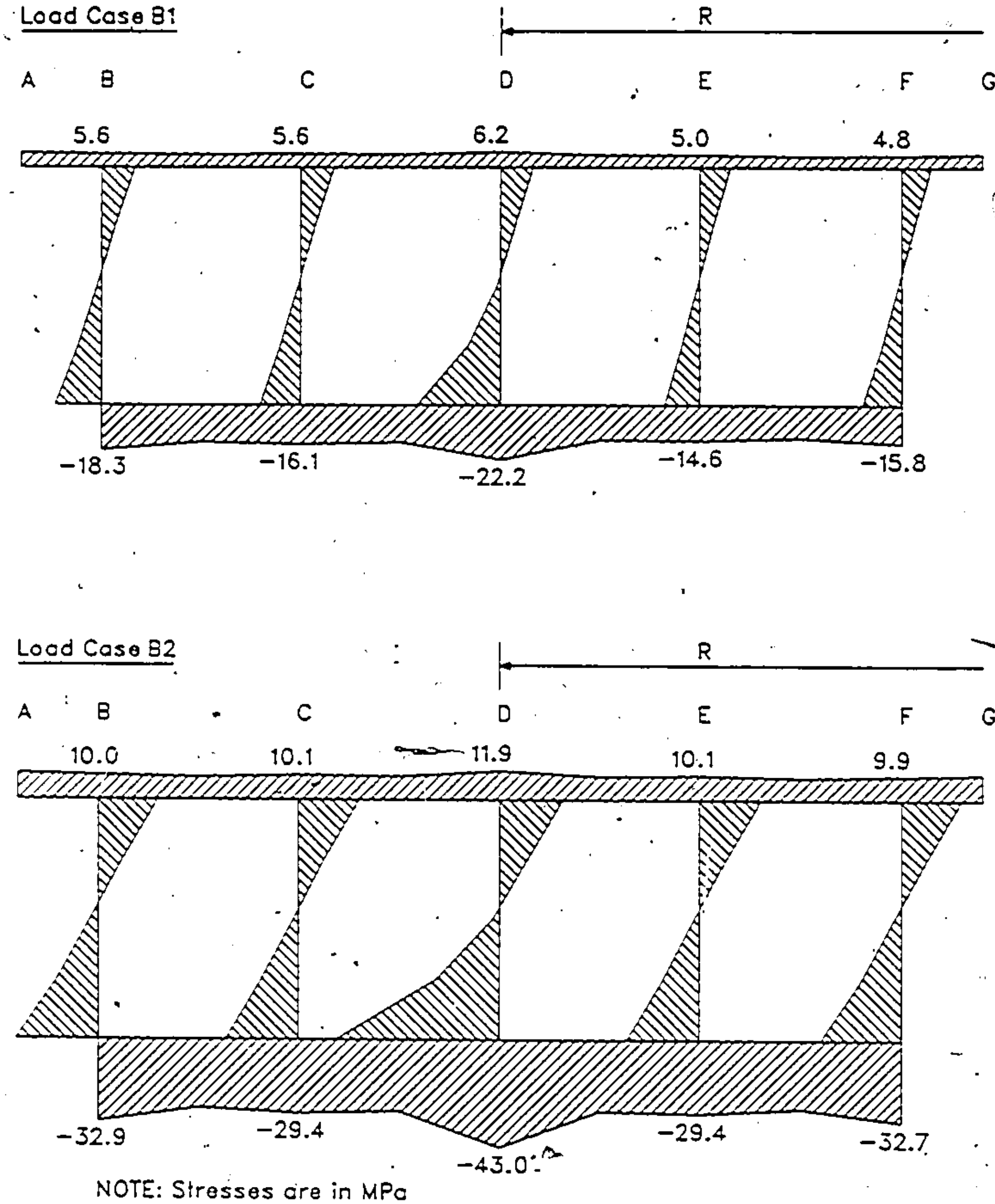

Figure 6.16: Normal stresses at section 9 for load scenario B – Elastic Analysis.

6.7 Nonlinear Solution Strategy

Depending on the number of elements used in idealizing the structure and on elements topology, in a linear analysis the time spent for solving the equilibrium equations can be a large percentage of the total solution time. In nonlinear analysis, the incremental step by step approach and the iterative nature of solution makes this percentage even higher. Therefore it is important to select a solution technique that would be cost-effective. Moreover, the massive output data in nonlinear finite element analysis clearly makes the process of response evaluation or post processing time consuming, laborious and error prone.. Consequently, an effective solution strategy should always be adopted in carrying out nonlinear finite element analysis.

6.7.1 Equilibrium Iteration

The BFGS (Broyden-Fletcher-Goldfarb-Shanno) quasi-Newton method is selected for equilibrium iteration in preference to other methods. The method provides a compromise between the full stiffness reformation performed in the full Newton method and the tangent stiffness formation in the modified Newton method. In the BFGS method, the inverse of the stiffness matrix is updated to provide a secant approximation to the matrix from iteration $(i-1)$ to iteration (i). That is, defining a displacement increment vector:

$$\zeta^{(i)} = U^{(i)} - U^{(i-1)} \tag{6.19}$$

and an increment vector in the out-of-balance loads:

$$\eta^{(i)} = \Delta R^{(i)} - \Delta R^{(i-1)} \tag{6.20}$$

the updated matrix $K^{(i)}$ should satisfy the quasi-Newton equation:

$$K^{(i)}\,\zeta^{(i)} = \eta^{(i)} \tag{6.21}$$

It should be noted that the evaluation of the updated matrix in Equation 6.21 does not involve costly matrix factorization as required in the full Newton method. In this way the method would not be as expensive as the full Newton and convergence rate is much faster than that in the modified Newton method. A step by step procedure for the BFGS iteration method can be found in reference [25].

Table 6.2: Gauss point integration order employed in the analysis.

Bridge Component	Direction		
	Tangential	Radial	vertical
Deck Elements	3	2	2
Web Elements	3	2	3
Bottom plate elements	3	2	2
Diaphragm elements	2	2	2

6.7.2 Convergence Criterion

Among the various convergence criteria available in the ADINA program the internal energy criterion is employed for analysis since it provides some indication as to when both displacements and internal forces are near their equilibrium values. Solution convergence is reached when the ratio of the work done by the out-of-balance loads on the displacement increments at iteration (i) to the initial internal energy increment is less than a preset energy tolerance or:

$$\Delta U^{(i)T}\left({}^{t+\Delta t}R - {}^{t+\Delta t}F^{(i-1)}\right) \leq \epsilon_E\left(\Delta U^{(1)T}\left({}^{t+\Delta t}R - {}^{t}F\right)\right) \tag{6.22}$$

where:

ΔU^T	=	Transpose vector of displacement increments.
R	=	Equivalent External nodal forces vector.
F	=	Equivalent Internal nodal forces vector.
ϵ_E	=	Energy tolerance.
(i), $(i-1)$	=	Superscripts denoting current and previous iteration number.
$t+\Delta t$, t	=	Superscripts denoting current and previous load level.

6.7.3 Numerical Integration Order

In light of the different spatial behaviour of the various bridge structural components, the selective scheme shown in Table 6.2 was employed in choosing Gauss point integration order.

6.7.4 Element Death Option For Concrete

The approximative nature of the concrete plastic-multilinear material model requires that certain deck elements must become inactive when tensile stresses reach concrete tensile strength. The time step or load level at which concrete would crack in tension can be easily predicted from the elastic response by linear extrapolation of stresses.

On the other hand, due to the elastic-plastic action assumed in the compression zone of the concrete model, the load level at which concrete element would fail in compression cannot be extrapolated from stresses and can only be established by monitoring the strain level through a trial and error procedure. In this procedure the elements are permitted to carry loads higher than their nominal crushing load and hence would develop strains higher than the nominal ultimate strain value of 0.4 %. By monitoring element strains at various load levels, the load level at which an element would develop strains higher than the ultimate strain is established. The structure is then reanalyzed by inactivating all elements which should have been failed at the proper time steps or load levels.

In addition to the extra computer effort required for the trial and error process, element deactivation procedure can be real time consuming especially when the failed elements are to be removed from the mesh at various load levels. Luckily ADINA provides the options of element birth or death at a pre specified time step or load level. By employing the element death option at time t the program assumes that the element will no longer contribute to structure stiffness for all load levels following time step t. In this way there was no need to remove concrete elements from the mesh as they fail during the loading history.

6.7.5 Extent of Plastic Flow

In order to detect material behaviour, elastic or plastic. at a particular time step or load level, the ADINA program computes the accumulated effective plastic strain at each integration point in the element using the following equation:

$$ {}^{t}\bar{\epsilon}^{p} = \int_0^t d\bar{\epsilon}^{p} \tag{6.23} $$

$$d\bar{\epsilon}^p = \sqrt{\frac{2}{3} d\epsilon^p_{ij}\, \epsilon^p_{ij}} \qquad (6.24)$$

where:

$^t\bar{\epsilon}^p$ = Accumulated effective plastic strain.

$d\epsilon^p_{ij}$ = Components of the plastic strain increments.

As such when the accumulated effective plastic strain is zero then material behaviour is still elastic at the integration point. On the other hand a positive value for the accumulated effective plastic strain is indicative of the amount of permanent deformation and yielding which have developed from the time of initial yielding till the current time step.

This strain index can be very helpful in detecting critical behavioral changes such as the onset of yielding, the formation of plastic hinges, and the extent of permanent deformation suffered by the structure.

6.8 Inelastic Structure Response

6.8.1 Positive Moment Load Scenario A

In this load scenario the equivalent OHBD trucks are positioned longitudinally[1] such that the resulting maximum positive moment would govern the highest response quantity. The elastic response of the curved bridge model proved that the two lane truck loading is more critical than the one lane or eccentric truck loading. Therefore, in conducting the inelastic analysis, the former loading configuration is employed.

Since each lane is loaded with two parallel equivalent OHBD truck load then at any time throughout the load history, the bridge is subjected to a total of four equivalent OHBD trucks. In defining the load function, the load of four equivalent OHBD trucks shall be referred to as one unit truck force, F_{unit}, and overloads shall be multiples of this unit truck force. Hence:

$$F_{unit} = 4 \times 9.590 = 38.36KN \qquad (6.25)$$

and if we express the load level in terms of the number of unit trucks applied at

[1]Truck location is shown in Figure 6.12

Table 6.3: Load function employed in positive moment load scenario A.

Time	Load level	Total Load	
(#)	(unit truck)	(KN)	(Kips)
0	0.0	0.000	0.000
1	2.0	76.72	17.25
2	4.0	153.4	34.49
3	6.0	230.2	51.74
4	8.0	306.9	68.99
5	10.0	383.6	86.24
6	11.0	422.0	94.86
7	12.0	460.3	103.5
8	13.0	498.7	112.1
9	13.5	517.9	116.4
10	14.0	537.0	120.7
11	14.5	556.2	125.0
12	15.0	575.4	129.4
13	15.5	594.6	133.7

time t then the total load applied to bridge at any time, F^t_{total}, is given as follows:

$$F^t_{total} = \Omega(t)\ F_{unit} \tag{6.26}$$

where $\Omega(t)$ denotes the load level at time t.

The load function employed in the current load scenario is given in Table 6.3. As will be noted the bridge is analyzed for thirteen time steps or load levels. It should be noted however, the total load at the last time step does not necessarily imply the ultimate or failure load for the structure. In conducting the nonlinear analysis using the ADINA program it was not intended to overload the bridge until a preset failure criterion is reached. The objective, however, is to get as much information about post elastic behaviour as possible. Consequently, analysis is carried out until the assumptions of small displacements and small strains are violated.

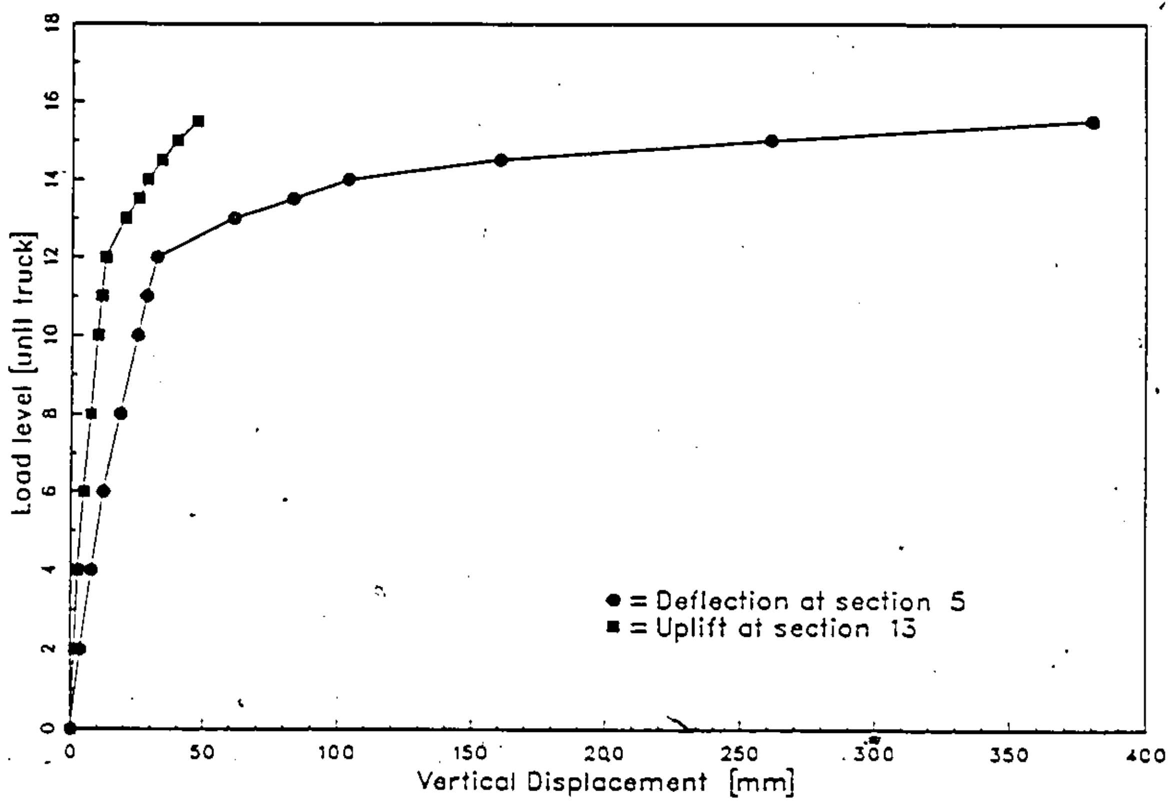

Figure 6.17: Load–Displacement Diagram for load scenario A.

Load–Displacement Diagram

Load–Displacement diagrams are one of the most informative representations of nonlinear behaviour of structures subjected to overloads. From such diagrams one can determine the elastic limit, the onset of material yielding, changes in structure stiffness, and structure ultimate load carrying capacity.

Figure 6.17 shows the load–displacement curves for the bridge when subjected to load scenario A. In this diagram, bottom plate deflection at section 5 under the central web D is plotted for each load level. As will be noted, distinctive structural behaviour is observed at the following four load stages:

1. The behaviour is essentially elastic up to load level 6.0. Although yielding in the bridge deck elements was first observed at the second time step (load level 4.0), the maximum accumulated effective plastic strain was as low as 0.001 % and 0.035 % at load levels 4.0 and 6.0 respectively. As such the purely elastic

material behaviour of the aluminum dominated structure response during this load stage.

2. At this stage, which is confined between load level 6.0 and 12.0, the progression of yielding in the concrete elements at the high compression zone (between section 4 and section 5) is evident from the change in slope of load–deflection curve. About 40 % drop in structure stiffness is observed at section 5. The plastic action continues in the deck while all aluminum components remain elastic until load level 12.0.

3. Significant decline in structure stiffness is observed between load levels 12.0 and 14.0. The slope of load–displacement curve drops over 90 % from the initial slope at load stage 1. At load level 12.0 two critical behavioral changes occurred:

   - Yielding in aluminum elements is observed for the first time since time step 1. This is evident from the development of plastic strains within the elements in the maximum positive moment region. Maximum accumulated effective plastic strain of the order 0.013 % and 0.027 % was observed in the bottom plate and web elements respectively.

   - Failure by compression crushing occurred for all concrete elements located between sections 4 and 5 as the elements incurred total strain above the ultimate strain (0.4 %). Therefore this zone of deck elements were forced to become inactive at all subsequent load levels.

   During this stage, the plastic action in the deck continued to spread on both sides of the inactive zone as the load is increased to load level 14.0 when neighboring concrete zone between sections 5 and 6 crushes in compression.

   At load level 13.0, initial yielding in the central web (D) at the negative moment section (9) was observed while the bottom plate at this section remained elastic until load level 14.0

4. The small slope of load–deflection curve between load level 14.0 and load level 15.5 dictates the progression of plastic flow within the aluminum material at sections 5 and 9. Early in this stage yielding in the aluminum central diaphragm elements was observed for the first time since initial loading.

   This stage is perhaps the most critical in the loading history of the bridge as it confines the ultimate load which can be carried by the structure. The response of the bridge during this stage constitutes the basis for establishing a failure criterion for the nonlinear experimental program. Failure due to progressive development of several plastic hinges cannot be detected from load-deflection curve; However, failure due to excessive deformation can be detected. It we consider the smallest dimension of bridge length, width, depth as the lower limit of excessive deformation then failure is likely to occur just above load level 14.0 when the maximum vertical displacement of 103 mm is observed (see Figure 6.17). Moreover, ADINA predicted a maximum values of 12 mm and 3 mm for longitudinal and transverse displacements respectively at this load level.

Figure 6.17 also shows the load–displacement diagram for the uplift developing at section 13. Unlike section 5, the slope of the load–displacement curve is constant until first yielding at load level 12.0. During this stage concrete elements at section 13 were forced to be inactive after load level 4.0 as they would fail in tension. Therefore the elastic behaviour of the aluminum components dominated structure response.

The drop in bridge stiffness at section 13 beyond load level 12 reflects the initiation of yielding in the aluminum elements. However, this drop in stiffness is not as pronounced as that observed at section 5.

Deflection Profiles

Longitudinal distributions of vertical displacement in the bottom plate along the central web D are given in Figure 6.18. In this figure, deflection profiles are shown at various load levels within each of the previously mentioned load stages. It is evident that maximum deflection was always developing at section 5 up to load level 12.0. As the bridge deforms beyond the initial yielding, the maximum deflection point shifts from section 5 to a point between sections 4 and 5. However, the difference in maximum deflection points is very small. This indicates that the location of the first plastic hinge would be somewhere between sections 4 and 5 but closer to section 5. Moreover, these displacement profiles clearly show that bottom plate rotation at the section remains the same on both sides of the center column until the end of stage 3 at load level 14.0. As the first plastic hinge is developed in the positive moment region, longitudinal redistribution of moments between section 5

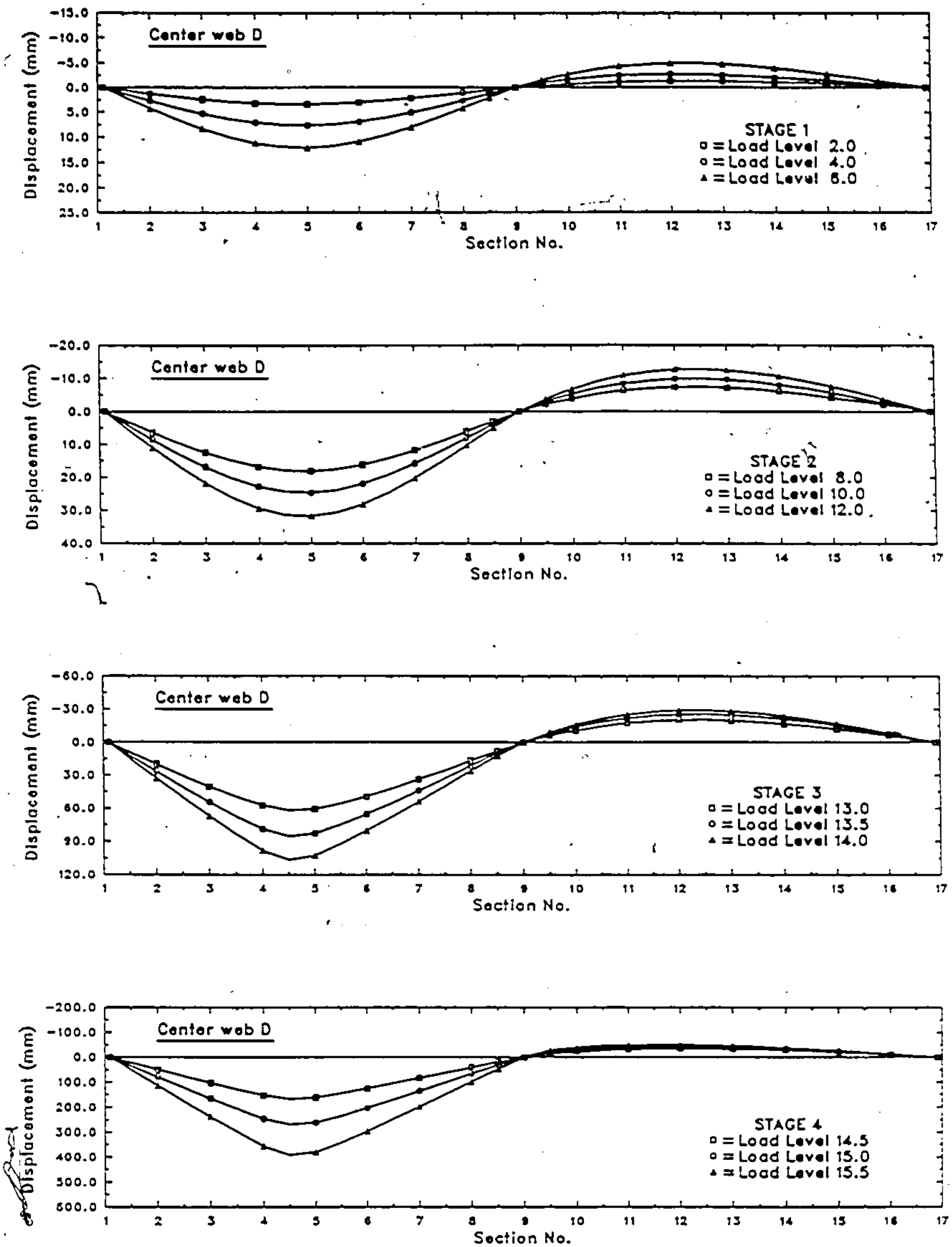

Figure 6.18: Longitudinal distribution of deflections for load scenario A.

and section 9 takes place. The unequal rotations on both sides of the center column at load stage 4 are perhaps indicative of the formation of the second plastic hinge as a result of longitudinal moment redistribution.

Transverse distributions of bottom plate deflections at the positive and hogging moment sections 5 and 9 respectively are given in Figure 6.19. The uniform transverse distribution of deflections throughout the loading history at section 5 indicates one way longitudinal bending action dominated structure response. Moreover, it is unlikely that failure would occur as a result of consecutive local failures in the webs since in resisting the applied moment, the four boxes seem to work together as one structural unit. Unlike section 5 which is dominated by one way bending action, restraining rigid body translations for the central node of the bottom plate section 9 forces the bridge to resist high transverse bending moment in addition to longitudinal negative moment. This perhaps would explain why the plastic action in the aluminum material starts in the central region of section 9 diaphragm elements, where transverse moment is highest, and continues to flow outward.

Formation of Plastic Hinges

While load–displacement diagrams and deflection profiles are evident for different behavioral changes in the structure, the formation of plastic hinges within the bridge cannot be clearly detected. Formation of plastic hinges is perhaps one of the most critical stages in the nonlinear response of the bridge prior to failure.

From a strictly theoretical point of view a plastic hinge is developed at a section in the bridge when the whole section has yielded or characterized by infinite curvature. Obviously this constitutes a singularity point since it is impossible to achieve infinite curvature at a section in the bridge. A rather practical approach would be to define the formation of plastic hinge when plastic action has dominated the section or the section undergoes a drastic increase in curvature during the loading history. By adopting this approach the load level at which the plastic hinge formation occurs can be detected reasonably from the load–curvature diagram.

Load–curvature diagram for the bridge model under load scenario A is given in Figure 6.20. Bridge curvature at maximum positive moment section 5 and maximum negative moment section 9 are plotted at various load levels. It should be noted

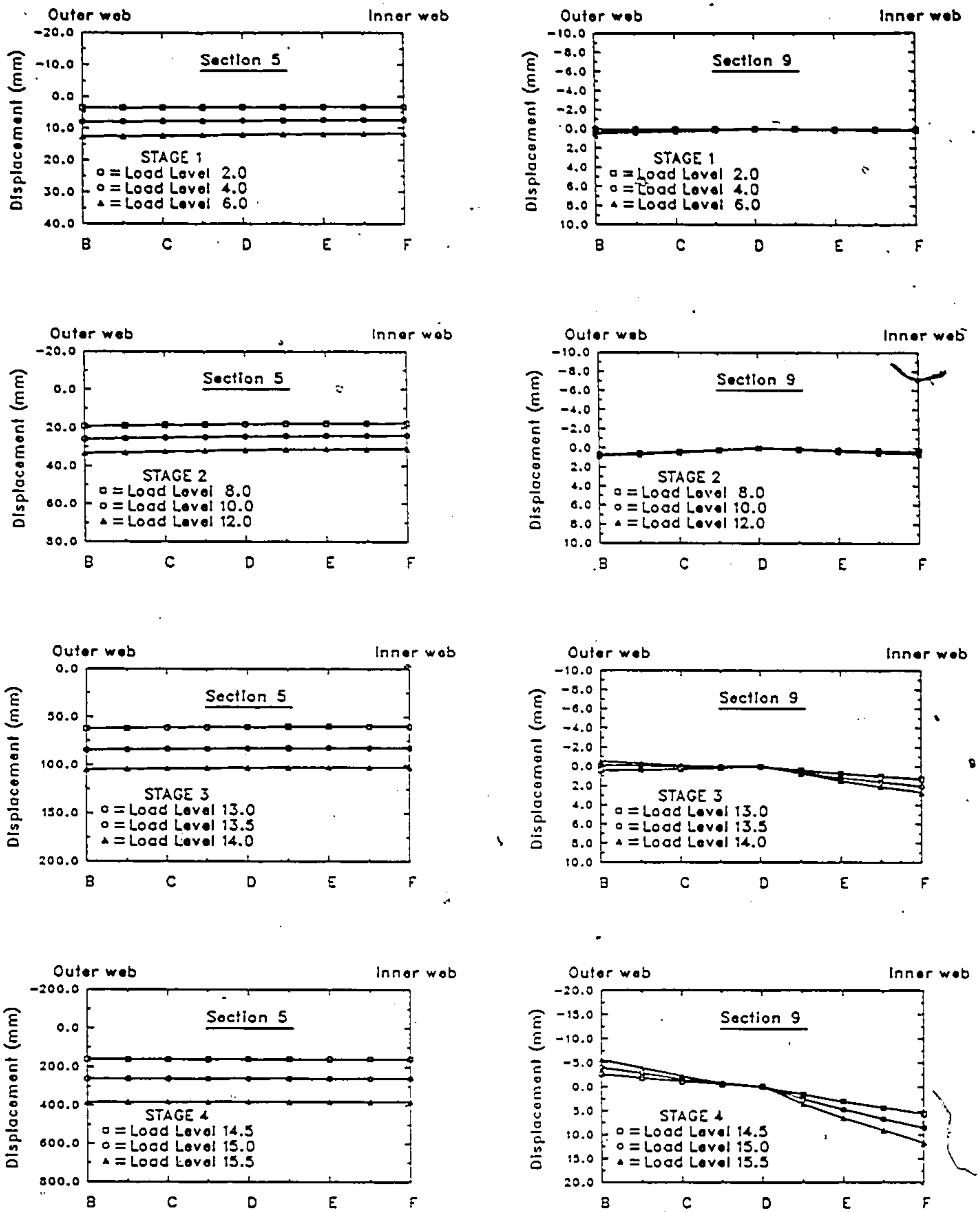

Figure 6.19: Transverse distribution of deflections for load scenario A.

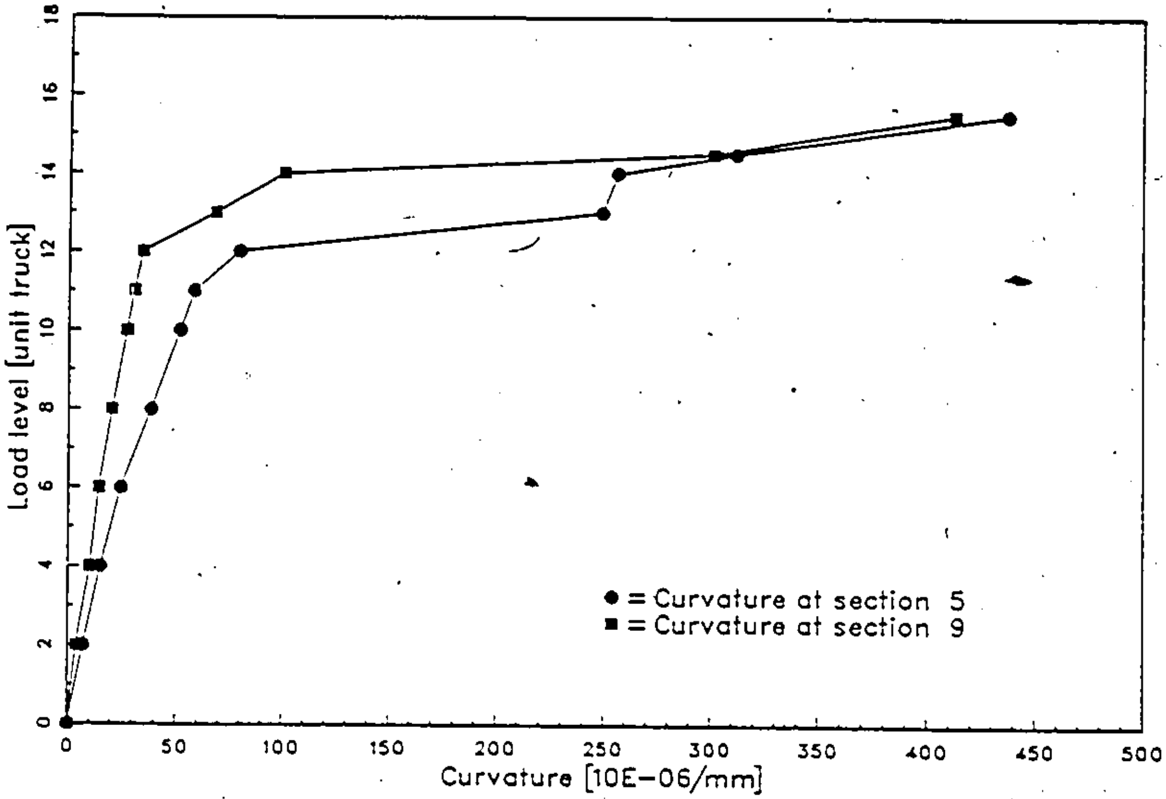

Figure 6.20: Load–curvature diagram for load scenario A.

that section curvature is evaluated by averaging the individual curvatures of the five cylindrical webs. This approach is reasonable in light of the fact that the webs were resisting the applied moment by equal proportions.

The shape of the load–curvature diagram shows a number of important behavioral changes in the bridge model:

- The kink in the curve for section 5 at load level 6.0 reflects the inability of the deck in carrying more compressive loads as the concrete behaviour changes from elastic to elastic-plastic. Curvature at section 9 increased linearly as the load is increased up to load level 12.0. This clearly shows the purely elastic behaviour of aluminum components at the negative moment section. Since concrete elements became inactive due to tension cracking at a very early stage in the loading program, the load–curvature diagram for section 9 does not have the kink observed for section 5.
- The formation of the first plastic hinge occurs in the maximum positive moment region at load level 13.0 This is evident in view of the drastic increase in section 5 curvature from a value of $79 \times 10^{-6}/mm$ at load level 12.0 to a

value of $249 \times 10^{-6}/mm$ at load level 13.0.

- Longitudinal moment redistribution between the maximum positive at section 5 and the maximum negative at section 9 is evident at the third stage ie. from load level 12.0 to load level 14.0.
- Over the hogging moment section and as a result of moment redistribution the bridge undergoes another drastic increase in curvature at load level 14.5 indicating the formation of the second plastic hinge at section 9.

It is instructive to note that ADINA's predictions for the bridge response is perhaps no longer valid for any load level above 14.5 as the two basic assumptions of small displacements and small strains are being violated. Maximum total strain in the aluminum is predicted to be above 10 % and maximum vertical displacement of the order 260 mm is expected at load level 15.0. In light of the above, load level 14.5 is considered to be the ultimate load level for the bridge when subjected to load scenario A.

Longitudinal Normal Stresses

Transverse distribution of longitudinal normal stresses for the two most critical sections 5 and 9 are given in Figure 6.21 to Figure 6.26. The stresses are plotted for load levels at which important behavioral changes were observed. It should be noted these stresses are representative for points in the midsurface of the elements. The numbers shown within the plots indicate the value of normal stress at each corner of the four boxes.

Normal stress plots confirm earlier findings such as:

- The webs carry equal proportions of the applied moments at any time in the loading program.
- The initial yielding in the aluminum at load level 12.0 is marked by the progression of the plastic action in the webs to a distance of 30 mm from the deck (see Figure 6.23).
- The formation of the first plastic hinge at section 5 at load level 13.0 when the section becomes essentially plastic. (see Figure 6.24).

- Longitudinal moment redistribution and the initiation of plastic action at section 9 is evident in Figures 6.24 and 6.25.
- The formation of the second plastic hinge at the hogging moment section at load level 14.5 is evident form Figure 6.26.

6.8.2 Negative Moment Load Scenario B

In contrast to the previous load scenario where the positive moment developed at section 5 was the most critical moment, the bridge in the current load scenario is loaded symmetrically with two sets of unit trucks as shown in Figure 6.12 so that the negative moment developed at the center column support (section 9) is the maximum moment along the bridge. The elastic analysis showed that the two lane truck loading is more critical than the one lane eccentric truck loading; therefore, the former is employed for the inelastic analysis.

The same unit truck load which was described in load scenario A (Equation 6.25) is used in the negative moment load scenario. However, in computing the total load applied to the bridge at any load level using Equation 6.26, the product should be doubled since the two spans are loaded with unit trucks. The load function employed in the current scenario is listed in Table 6.4.

Concrete element zone located between section 7 and section 11 was forced to become inactive for all levels beyond load level 1.0 as it was evident from the elastic analysis that stresses higher than the tensile strength are expected to develop in this region.

Load–Deformation Diagrams

In examining behavioral changes at the most critical section, over the center column support, rotational deformation would perhaps provide better insights as opposed to translational deformation for the negative moment load scenario. Therefore rotations in the bottom plate at section 9 shall be used in representing the deformation axis of the load-deformation diagram.

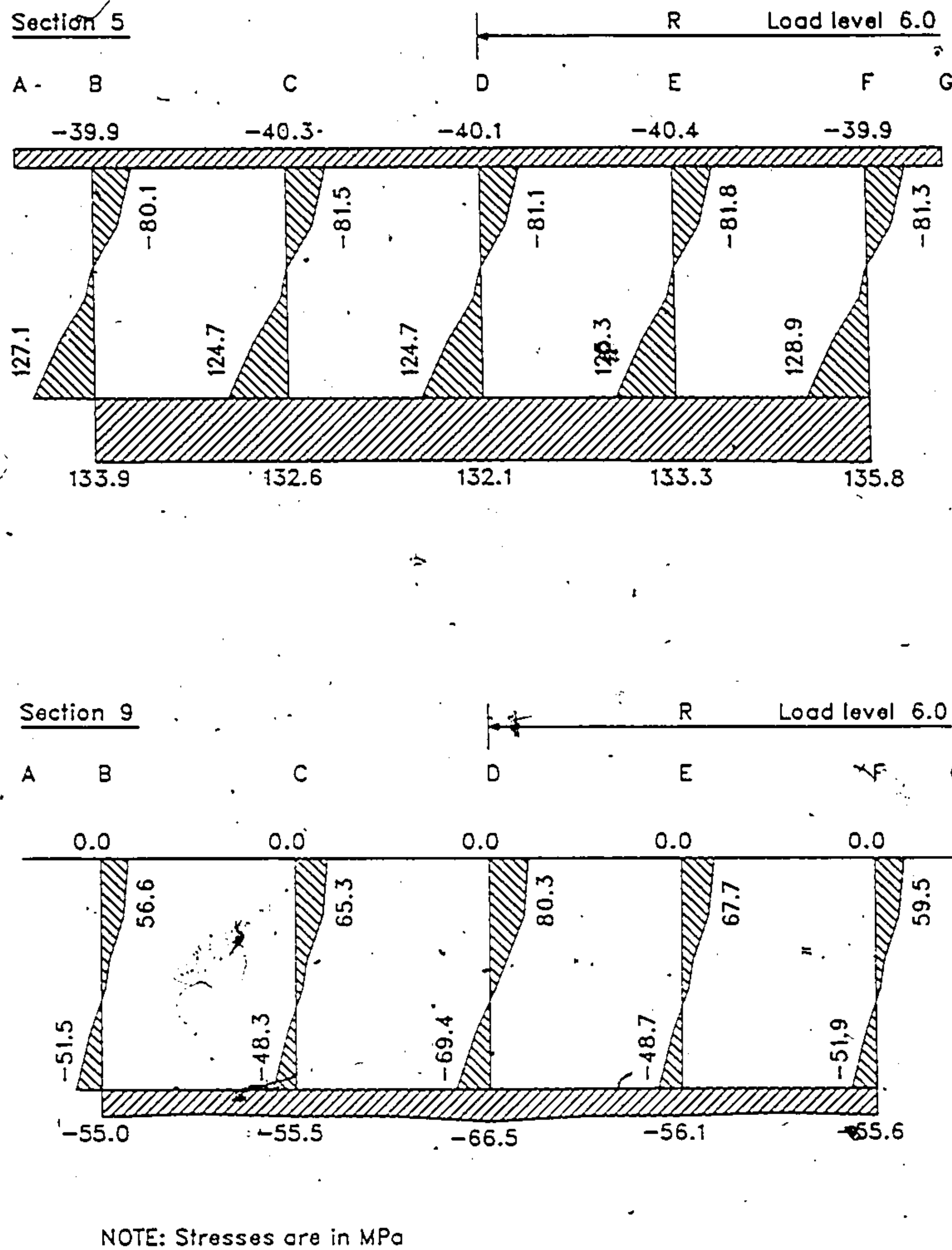

Figure 6.21: Normal stresses for load scenario A at load level 6.0.

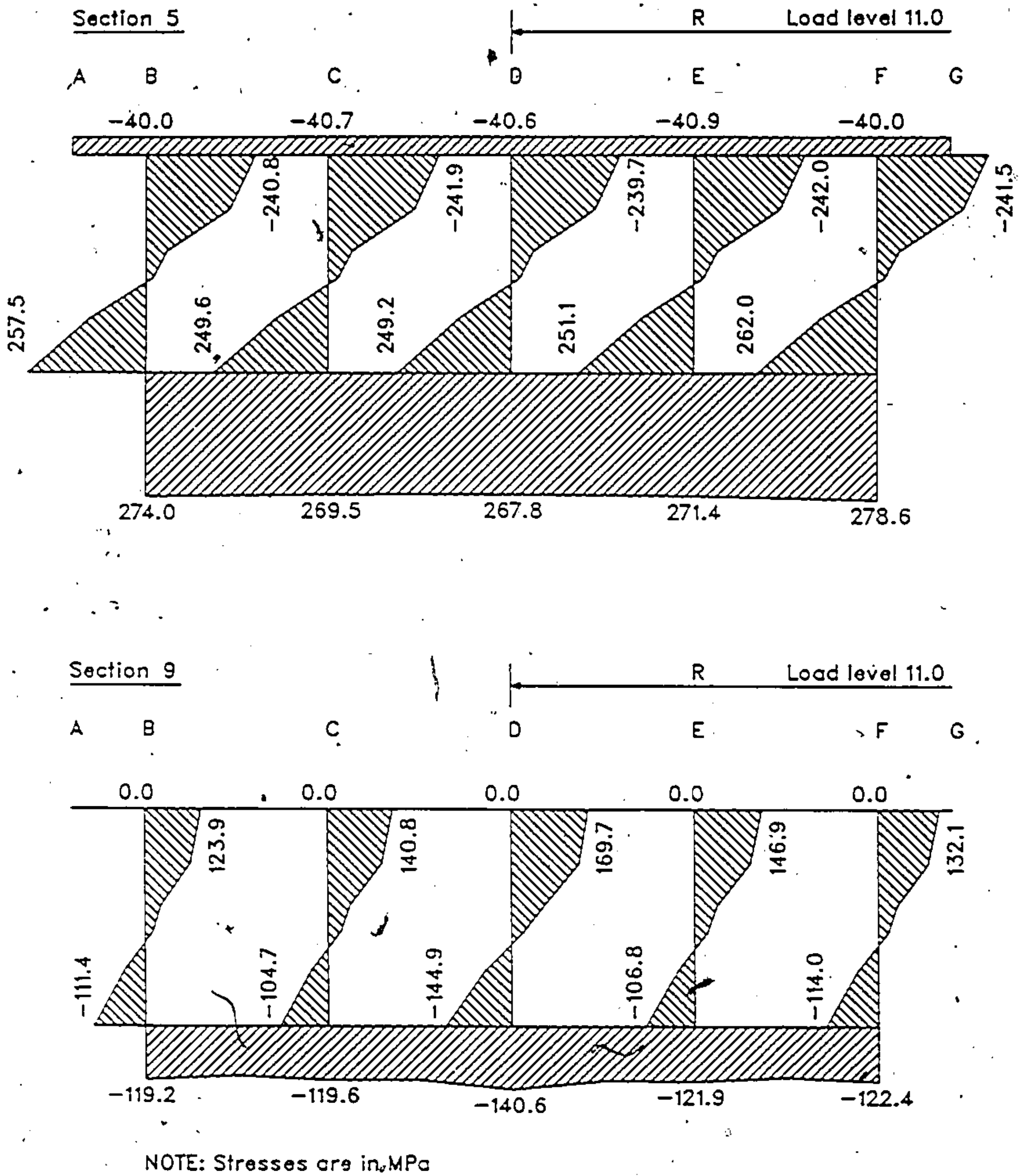

Figure 6.22: Normal stresses for load scenario A at load level 11.0.

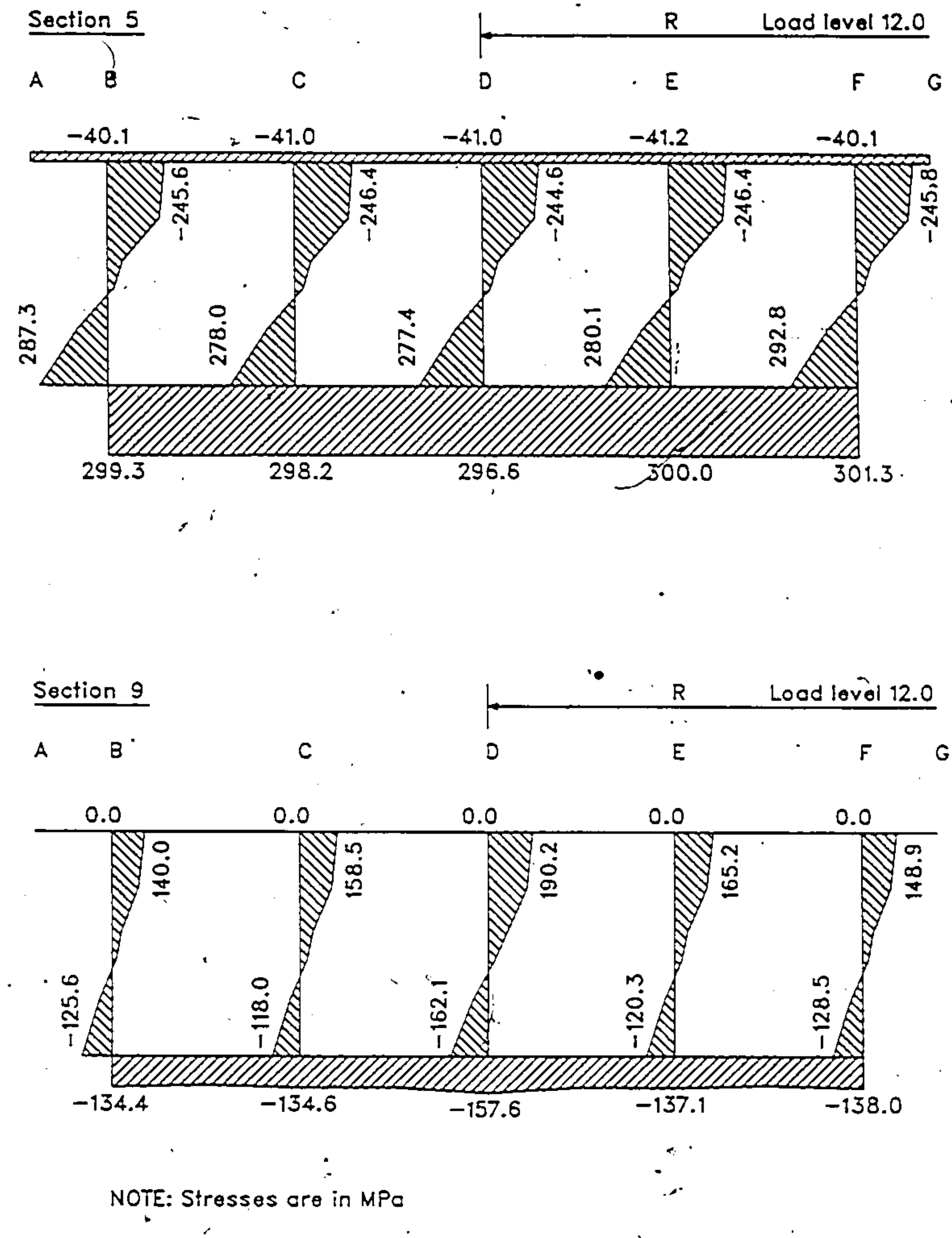

Figure 6.23: Normal stresses for load scenario A at load level 12.0.

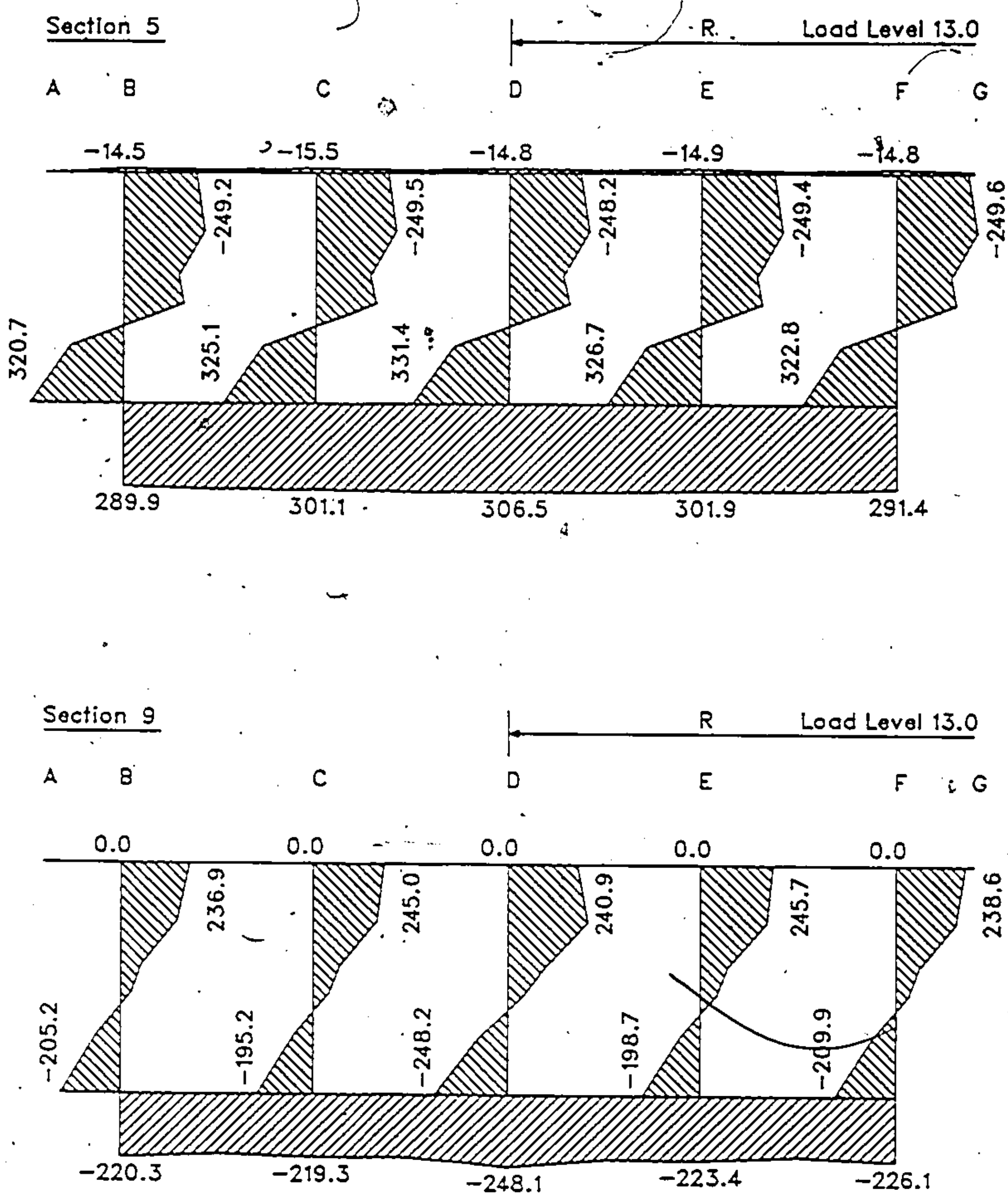

NOTE: Stresses are in MPa

Figure 6.24: Normal stresses for load scenario A at load level 13.0.

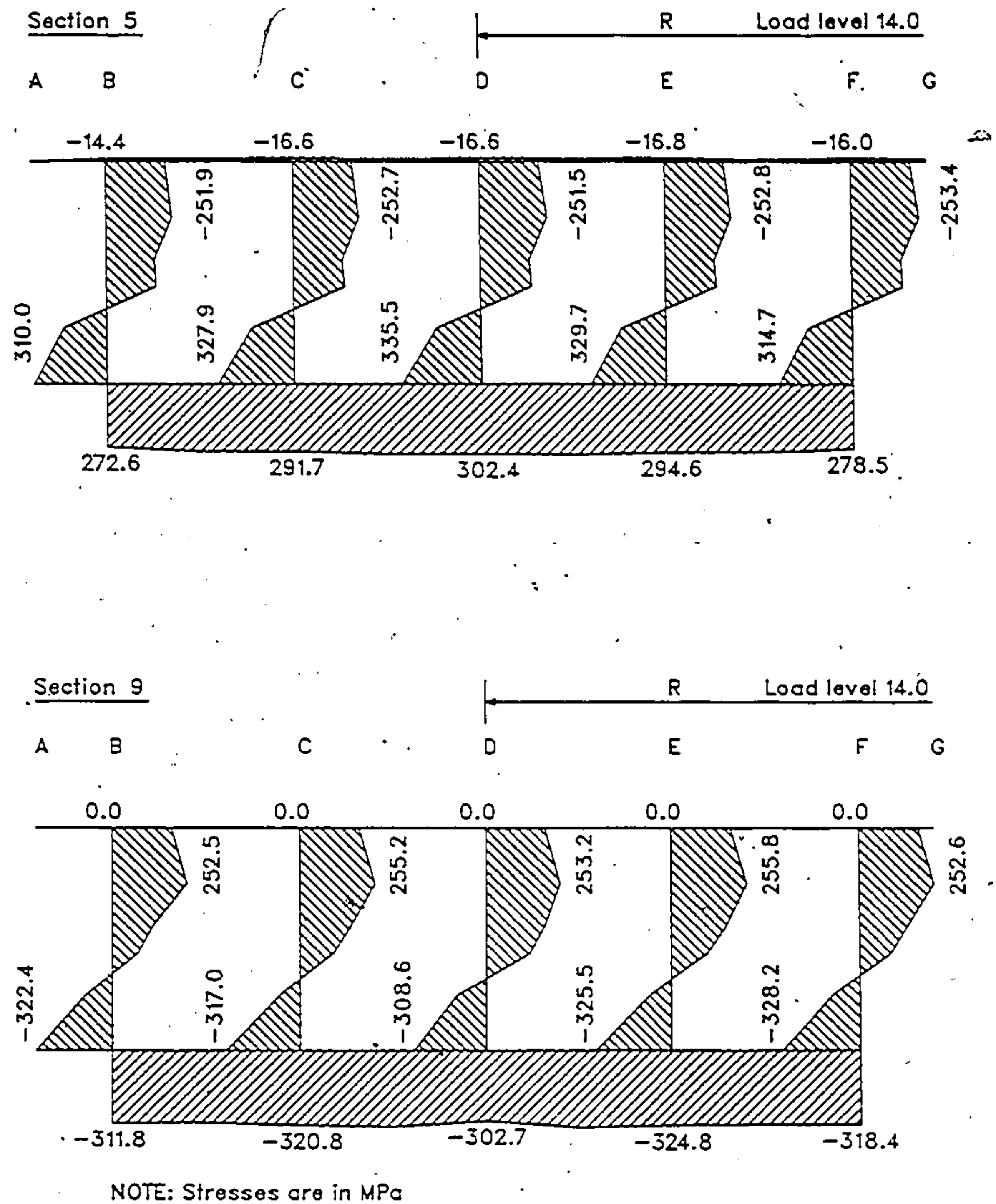

Figure 6.25: Normal stresses for load scenario A at load level 14.0.

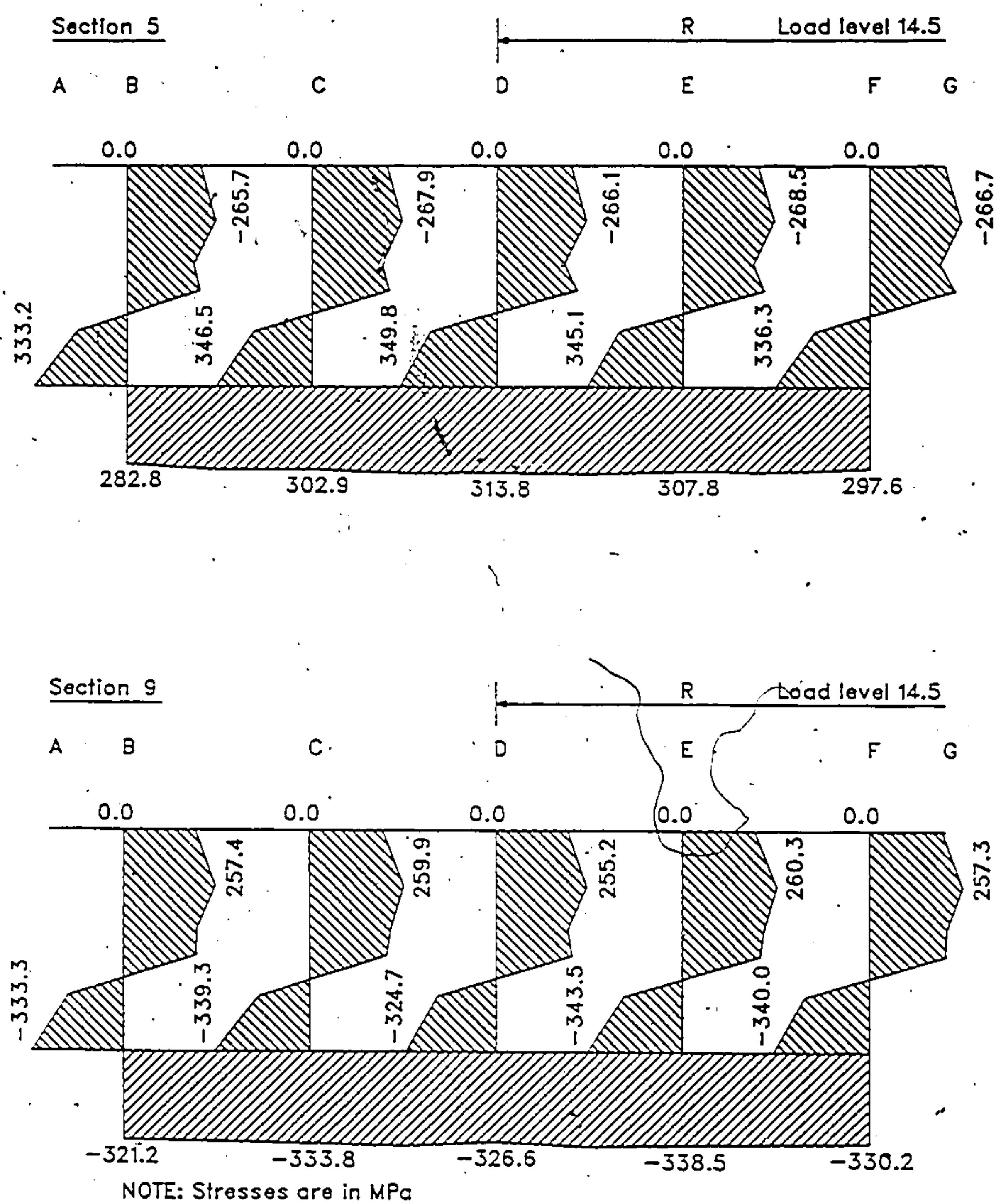

Figure 6.26: Normal stresses for load scenario A at load level 14.5.

Table 6.4: Load function employed in negative moment load scenario B.

Time (#)	Load level (unit truck)	Total Load (KN)	Total Load (Kips)
0	0.0	0.000	0.000
1	1.0	76.72	17.25
2	3.0	230.2	51.74
3	5.0	383.6	86.24
4	6.0	460.3	103.5
5	7.0	537.0	120.7
6	8.0	613.8	138.0
7	9.0	690.5	155.2
8	10.0	767.2	172.5
9	11.0	843.9	189.7
10	12.0	920.6	207.0
11	12.5	959.0	215.6
12	13.0	997.4	224.2

The two rotational degrees of freedom possessed by each nodal point in the bottom plate of the bridge are identified as follows:

1. Rotation about global X-axis. This rotation shall be referred to by the term Torsional rotation.
2. Rotation about global Y-axis. This rotation shall be referred to by the term Flexural rotation.

It should be noted however, associating the terms torsional and flexural to distinguish between the two types of rotation does not necessarily imply that these rotations are resulting from only torsional or only flexural loads. For instance bottom plate rotation about the X-axis can result from combined transverse bending and torsional loads. Figure 6.27 shows the two rotational degrees of freedom along with the sign convention employed in presenting them.

The load–rotation diagram shown in Figure 6.28 is given for the pinned nodal point in the bottom plate at section 9 and web D. This point essentially represents the connection point between the center column and the bottom flange in the physical

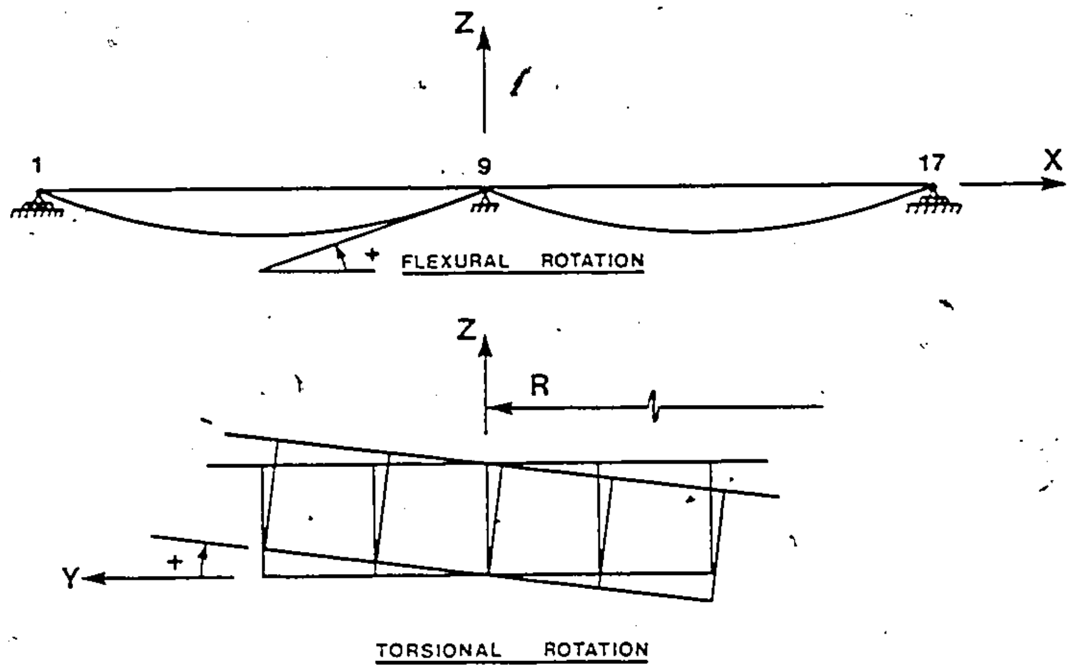

Figure 6.27: Positive direction for bottom plate rotations.

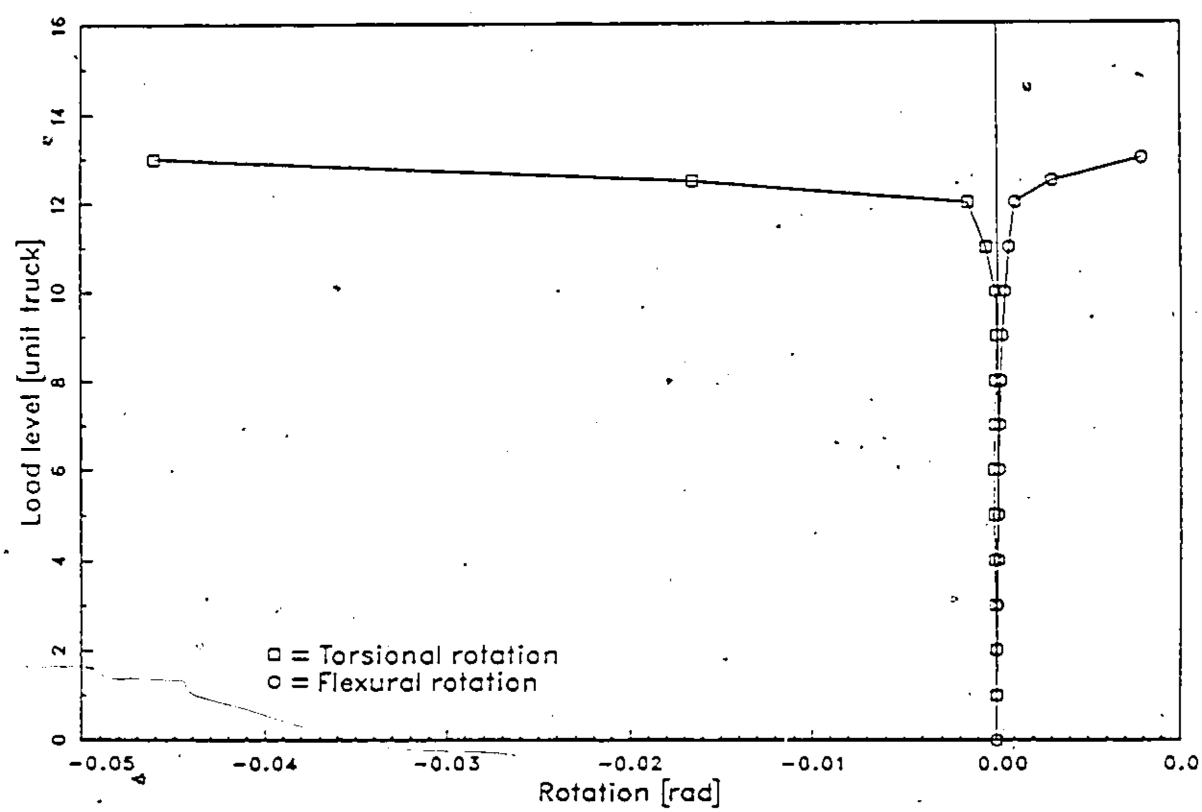

Figure 6.28: Load–rotation diagram at section 9 for load scenario B.

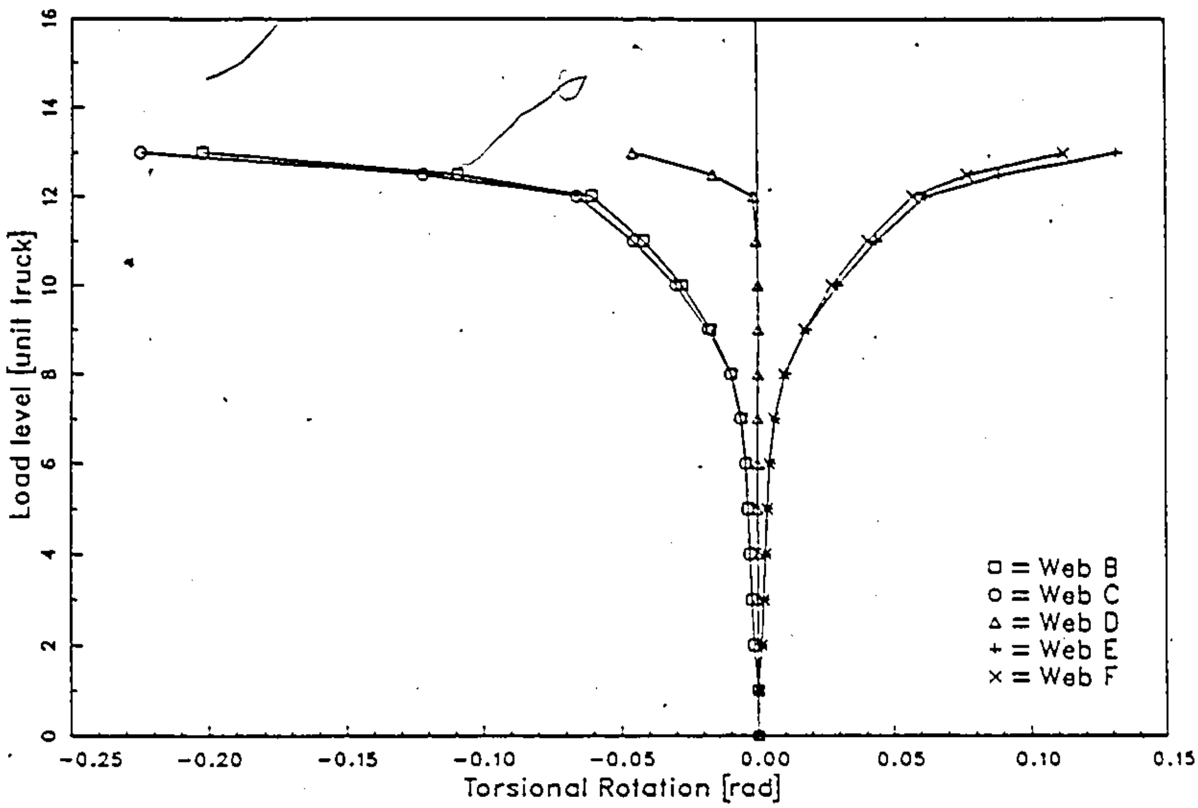

Figure 6.29: Load–torsional rotation diagram at section 9 for load scenario B.

bridge model. The diagram clearly shows a drastic increase in both rotations as the load level increases above 12.0 unit trucks. Moreover this increase is much more pronounced in the torsional rotation compared to the flexural rotation. The ratio of torsional rotation at load level 12.5 to that at load level 12.0 is equal to 10.2 while the ratio for flexural rotation is only 3.1. This indicates that in approaching the ultimate capacity of the bridge at section 9, the behaviour is not dominated by the one way longitudinal bending action as the case in load scenario A. The high torsional rotation observed in Figure 6.28 is indicative to the high transverse forces being resisted at the critical section. It is not clear however, if these forces are dominated by torsional shear or by transverse bending. Moreover, the elastic limit and the onset of yielding cannot be detected clearly from this diagram.

Figure 6.29 shows the load–torsional rotation curves for points corresponding to the five webs in the bottom plate at section 9. The fact that torsional rotation for the inner points (under webs E and F) are opposite in sign to the rotation for the outer points (under webs B and C) indicates that flexural forces rather than shear forces dominated the behaviour in the transverse direction of the bridge.

It is evident from Figure 6.29 that the bridge behaviour at section 9 remains essentially elastic until load level 6.0. At this load level, analysis indicated that yielding in the aluminum components did occur for the first time within the vicinity of the central support. However, the extent of yielding in terms of maximum accumulated effective plastic strain was as low as 0.10 %. Therefore for all practical purposes one can say that the onset of yielding for section 9 occurs at load level 6.0. After yielding, the nonlinear increase in torsional rotation at the outer and inner points reflects the progression of the plastic action and hence the gradual degradation of structure stiffness in resisting transverse bending moment. This behaviour continues until load level 12.0 which perhaps marks the formation of the first plastic hinge at section 9 over the center column support.

It is instructive to note that from the time at which yielding commenced the progression of plastic flow was always more pronounced in the central diaphragm elements than in the neighboring web and bottom plate elements. This confirms earlier finding that the critical section was resisting high transverse bending forces in addition to the longitudinal flexural action.

While load–rotation curves in Figure 6.29 may show that torsional rotation for points under the outer webs B and C are equal in magnitude to rotation for points under the inner webs F and E, the former rotations are actually higher by a minimum factor of 1.04. This observation indicate that section 9 was resisting combined bending and torsion in the transverse direction. Nevertheless the transverse bending action was the dominant response mode. As loading increases above load level 12.0, the action of torsional loads becomes more pronounced as the ratio of outer webs rotation to inner webs rotation increases to 1.4 at load level 12.5.

In the current load scenario, behavioral changes in the bridge model at the positive moment sections 5 and 13 are not as critical as those observed over the hogging moment section. However, one must keep in mind that once the first plastic hinge is formed at the hogging moment section, the formation of other plastic hinges is expected to develop within the positive moment region at sections 5 and 13. Figure 6.30 shows the load–deformation diagram for the vertical displacement in the bottom plate at section 5 and web D. It is evident that the behaviour remains essentially elastic untill load level 7.0. The gradual decrease in stiffness as the load rises to level 12.0 reflects the elastic-plastic action in the deck elements. The drastic

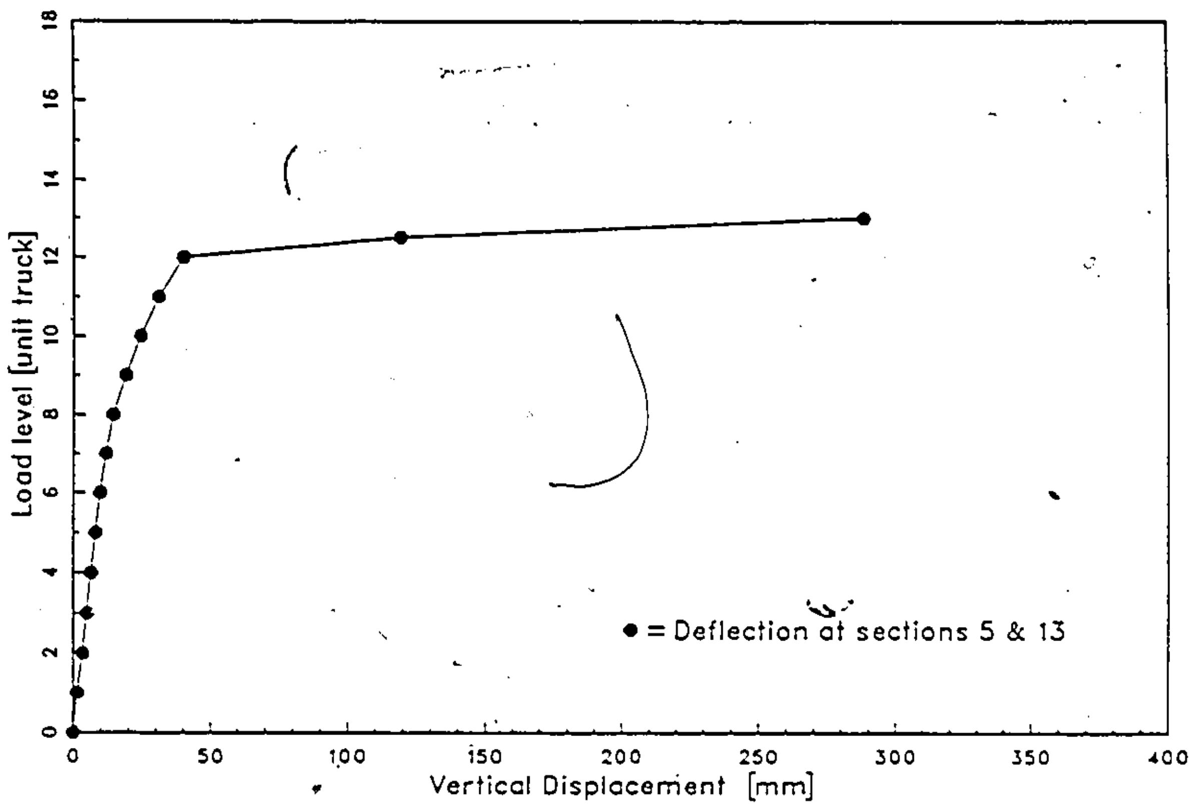

Figure 6.30: Load–displacement diagram for load scenario B.

drop in stiffness at load levels above 12.0 occurs as the concrete elements on both sides of section 5 and similarly at section 13 became inactive due to compression crushing failure and as yielding commences in the aluminum elements.

Analysis indicated that initial elastic-plastic behaviour at the maximum positive moment regions is expected at load levels just below 5.0 and 12.0 in bridge deck elements and aluminum components respectively. It is not surprising to note the high load level at which yielding commences in the aluminum at sections 5 and 13 in comparison with the load level at which section 9 yielded. Positive moment sections not only have lower moment than that applied at section 9, the structure response at section 5 and 13 is dominated by one way longitudinal bending action as opposed to the two way bending action at the hogging moment section.

Deflection Profiles

Longitudinal vertical displacement profiles for nodal points in the bottom plate under the central web D are given in Figure 6.31. The shape of these curves is

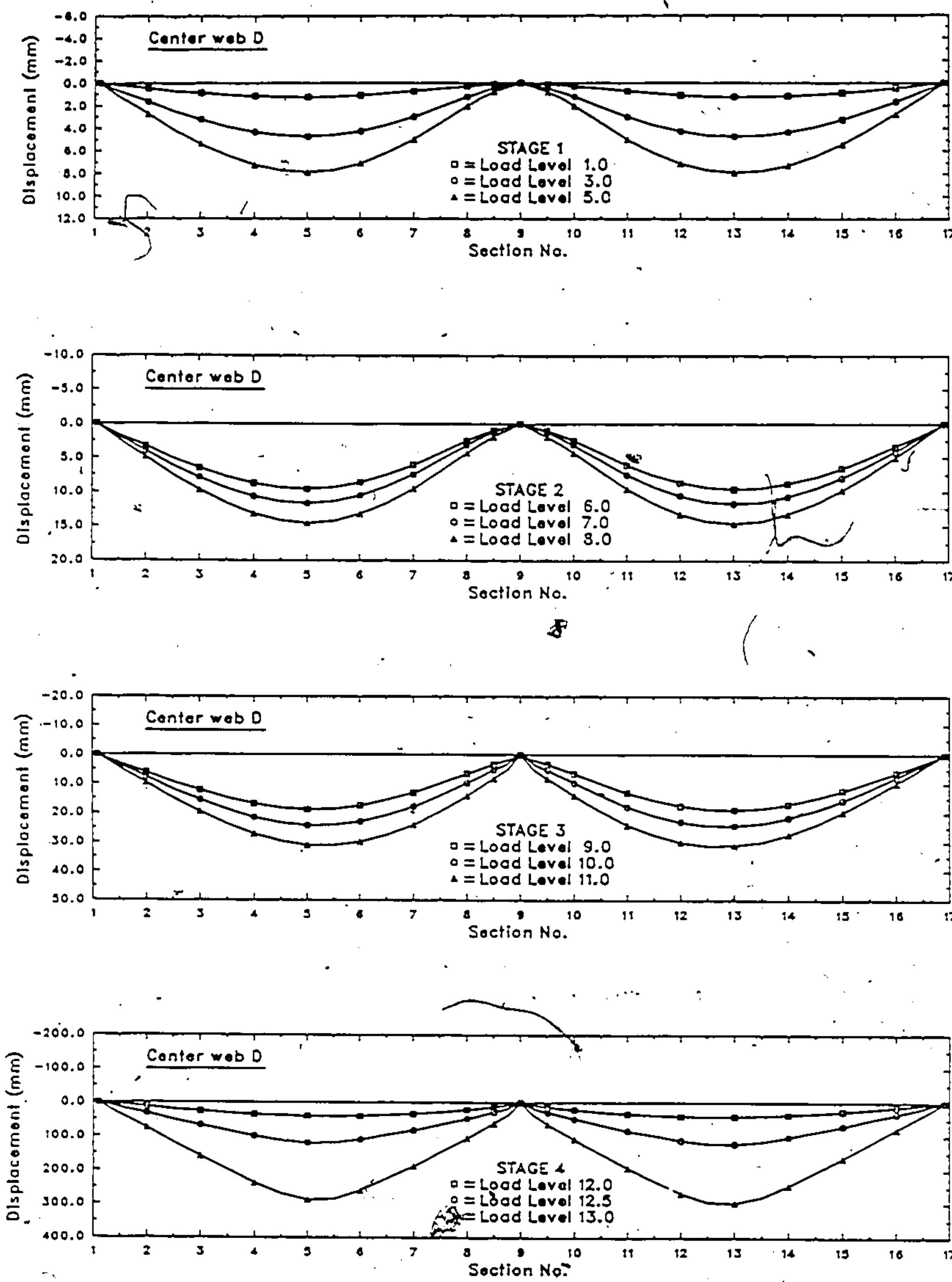

Figure 6.31: Longitudinal deflection profiles for load scenario B.

indicative of the symmetrical truck loading employed in the current load scenario. It is evident that the structure remains quite stable in terms of excessive displacements until load level 12.0. At this time, maximum translational displacements in the vertical, longitudinal and transverse directions were in the order of 43 mm at sections 5 and 13, 8 mm at section 9, and 5 mm at sections 8.5 and 9.5. As load level is increased to 12.5, the structure is expected to suffer excessive deformation at the critical sections particularly in terms of vertical and transverse displacements. The deformation level of the order 126 mm, 14 mm, and 12 mm was observed in the vertical, transverse and longitudinal directions at load level 12.5. ADINA shows that if the structure is overloaded to load level 13.0 then maximum deformation level at the critical section would increase at least by a factor of 2.0 relative to the maximum deformations at load level 12.5.

Transverse distribution of vertical displacements at the positive and negative moment sections 5 and 9 respectively are shown in Figure 6.32. As will be noted deflection profiles are given at various load levels. The shape of displacement curves throughout the loading history dictates that the positive moment section does not suffer the severe transverse bending observed at the hogging moment section. Moreover, it is evident that the central region of the diaphragm elements at section 9 are subjected to very high transverse bending action relative to the external regions around webs B and F.

Formation of Plastic Hinges

The complex deformation patterns observed at the hogging moment section over the center support reflects the highly complex stress field in this region of the bridge. Curvature cannot be easily evaluated at this section; therefore, in detecting the formation of plastic hinges in the critical sections the extent of the plastic flow expressed in terms of the accumulated effective plastic strain at various points within the section is employed as a measure of yielding rather than the drastic changes in curvatures.

Table 6.5 lists the accumulated effective plastic strains developed within the five webs at section 9 for various load levels. The six values listed for each web represent the strain values developed at the six integration points along the web depth.

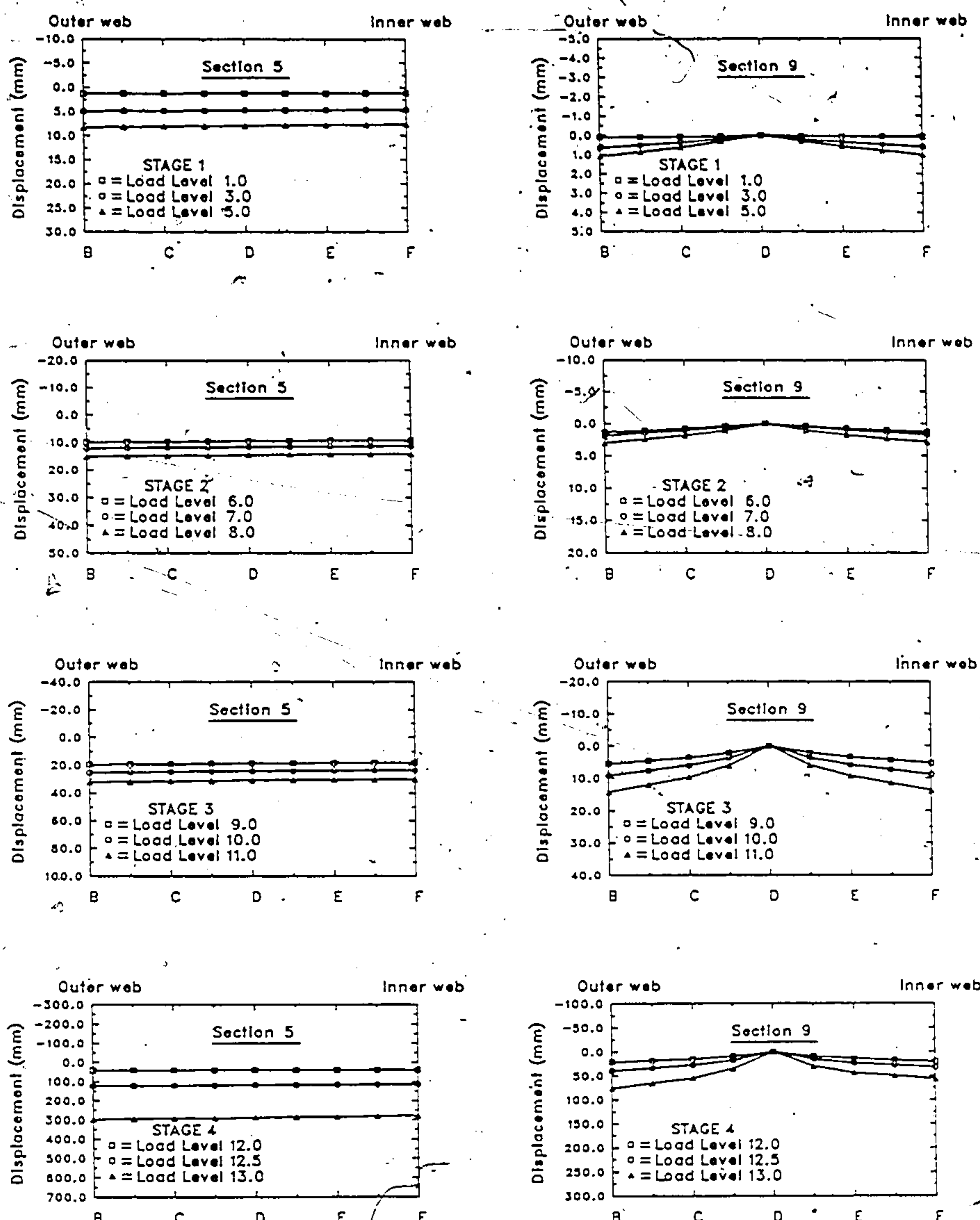

Figure 6.32: Transverse deflection profiles for load scenario B.

Table 6.5: Accumulated effective plastic strains (%) at section 9.

Web ID	Integration Point	d (mm)	Load Level(unit truck)									
			5.0	6.0	7.0	8.0	9.0	10.0	11.0	12.0	12.5	13.0
B	1	6.780	0	0.10	0	0.07	0.20	0.38	0.60	0.91	6.5	17.1
B	2	30.00	0	0	0	0	0	0.08	0.22	0.41	4.1	11.4
B	3	53.22	0	0	0	0	0	0	0	0	2.0	6.0
B	4	66.78	0	0	0	0	0	0	0	0	0.95	3.6
B	5	90.00	0	0	0	0	0	0	0	0	0.70	1.7
B	6	113.2	0	0	0	0	0	0.08	0.23	0.43	3.1	7.6
C	1	6.780	0	0	0	0.07	0.53	0.96	1.5	2.25	9.3	23.9
C	2	30.00	0	0	0	0	0.20	0.47	0.84	1.36	6.3	16.4
C	3	53.22	0	0	0	0	0	0.05	0.24	0.53	3.4	9.2
C	4	66.78	0	0	0	0	0	0	0	0.14	2.1	6.1
C	5	90.00	0	0	0	0	0	0	0	0	0.50	1.8
C	6	113.2	0	0	0.10	0	0	0.20	0.45	0.75	3.53	9.4
D	1	6.780	0	0	0	0.32	1.7	2.8	4.2	6.1	15.3	35.7
D	2	30.00	0	0	0	0.12	1.2	2.1	3.2	4.7	11.8	27.1
D	3	53.22	0	0	0	0	0.85	1.6	2.6	4.0	9.5	21.4
D	4	66.78	0	0	0	0	0.76	1.7	3.3	6.0	11.7	24.6
D	5	90.00	0	0	0	0	1.0	2.3	4.3	7.6	15.0	31.9
D	6	113.2	0	0	0	0.15	1.7	3.3	5.9	9.9	20.2	43.5
E	1	6.780	0	0	0	0.05	0.45	0.79	1.2	1.85	8.7	22.9
E	2	30.00	0	0	0	0	0.16	0.38	0.68	1.1	5.8	15.7
E	3	53.22	0	0	0	0	0	0.02	0.19	0.42	3.1	8.7
E	4	66.78	0	0	0	0	0	0	0	0.04	1.8	5.6
E	5	90.00	0	0	0	0	0	0	0	0	0.67	2.0
E	6	113.2	0	0	0	0	0	0.17	0.42	0.73	3.6	9.5
F	1	6.780	0	0	0	0	0.09	0.18	0.30	0.53	5.4	15.2
F	2	30.00	0	0	0	0	0	0	0.02	0.17	3.4	10.0
F	3	53.22	0	0	0	0	0	0	0	0	1.6	5.2
F	4	66.78	0	0	0	0	0	0	0	0	0.66	3.0
F	5	90.00	0	0	0	0	0	0	0	0	0.86	2.0
F	6	113.2	0	0	0	0	0	0.02	0.16	0.37	3.1	7.6

Clearly a zero value of accumulated effective plastic strain at a certain integration point indicates that the material behaviour is still elastic whereas a value higher than zero is indicative of the amount of effective plastic strain accumulated since initial yielding of the material. The Table shows that the formation of the first plastic hinge at the hogging moment section occurred as a result of consecutive local yielding in the section as opposed to simultaneous yielding among the five webs. It is evident from the table that the webs yielded in the following order:

1. Central web D at load level 7.0 to 8.0.
2. Intermediate webs C and E at load levels 11.0 to 12.0.
3. External webs B and F at load levels 12.0 to 12.5.

As the majority of webs (C,D,E) have essentially yielded at load level 12.0 and since most integration points at section 9 did suffer permanent deformation then one can say that the first plastic hinge is formed at this load level.

Soon after the formation of the first plastic hinge, analysis indicates that the formation of the second and third plastic hinges at the positive moment section 5 and 13 respectively occurs at load level 12.5. This can be seen clearly in the following normal stress plots.

Normal stress distributions

Longitudinal normal stress plots at the positive and negative moment section 5 are given in Figures 6.33 to 6.38 for load levels 6,8,10,11,12,12.5 respectively. It is evident that stresses at the positive moment sections 5 or 13 remain elastic at least till load level 11.0. While Figure 6.37 does indicate some yielding in section 5 at load level 12.0, it is not until load level 12.5 (see Figure 6.38) when the positive moment plastic hinges are formed at sections 5 and 13. This is evident from the drastic change in curvature at section 5 from a value of $83 \times 10^{-6}/mm$ at load level 12.0 to a value of $357 \times 10^{-6}/mm$ at load level 12.5.

Unlike section 5, normal stress distributions at the negative moment section show that in resisting the applied loads the webs were not carrying equal proportions of the longitudinal moment. During the elastic behaviour, the central web (D) was carrying a higher percentage of the longitudinal moments than that carried by the neighboring webs C and E. Similarly the percentage of the longitudinal moments carried by the intermediate webs C and E was higher than that carried by the external webs B and F. This observation from Figure 6.33 explains why the central web D was the first to yield followed by the yielding of the intermediate webs C and E and finally the external webs B and F. As the central web became fully plastic and unable to carry more loads at load level 8.0, transverse redistribution of stresses takes place between the central web D and the intermediate webs as shown in Figure 6.33. As a result of this transverse redistribution, the percentage of longitudinal negative moment carried by the intermediate webs become the highest in the section at load level 10.0 (see Figure 6.35). The progression of plastic flow and stress redistribution among the five webs continues until the first plastic hinge forms at load level 12.0 (see Figure 6.37). At load level 12.5 the distribution of normal stresses at positive and negative moment sections in Figure 6.38 are indicative of the full development of three plastic hinges in the bridge at sections 5, 9, and 13.

In light of the development of the three plastic hinges in the bridge and the high maximum deformation of 126 mm, load level 12.5 is considered as the ultimate load level which can be carried by the bridge for the negative moment load scenario. ADINA prediction for the bridge response beyond load level 12.5 should perhaps be ignored as both displacements and strains can no longer be assumed small.

6.9 Summary

The four-box horizontally curved bridge model was analyzed using the finite element program ADINA under two distinct load scenarios. Only material nonlinearity was incorporated in the analysis and therefore the basic assumptions of small displacements and small strains were adopted.

Experimental evidence confirmed the elasto-plastic material behavior for the aluminum components of the bridge. Von Mises yield criterion and isotropic strain hardening was assumed in the constitutive relation for the aluminum material model.

In view of the limitations imposed by the ADINA program, an elastic multilinear-plastic material model was considered the most reasonable substitution for a real concrete material behavior and therefore was adopted in the analysis. It should be noted; however, this concrete model is limited to elements subjected to compressive type of forces. In the negative moment region where the bridge deck is expected to develop tensile stresses, concrete contribution to strength and stiffness was ignored once tensile strength is reached.

Elastic analysis indicated that for positive moment and for negative moment load scenarios the two lane truck loading is more critical than the eccentric outer lane truck loading. As such the two lane truck loading was employed in carrying out the nonlinear analysis.

6.9.1 Positive Moment Load Scenario A

Inelastic response of the curved bridge model under the positive moment load scenario indicated that one way longitudinal bending action dominated the critical section at maximum positive moment. It was evident that in resisting the applied loads, the box section was working as one structural unit and the webs were carrying equal proportions of the applied moment throughout the loading history. Consequently, the formation of the first plastic hinge in the bridge was characterized by simultaneous plastic flow within the five webs at the critical section.

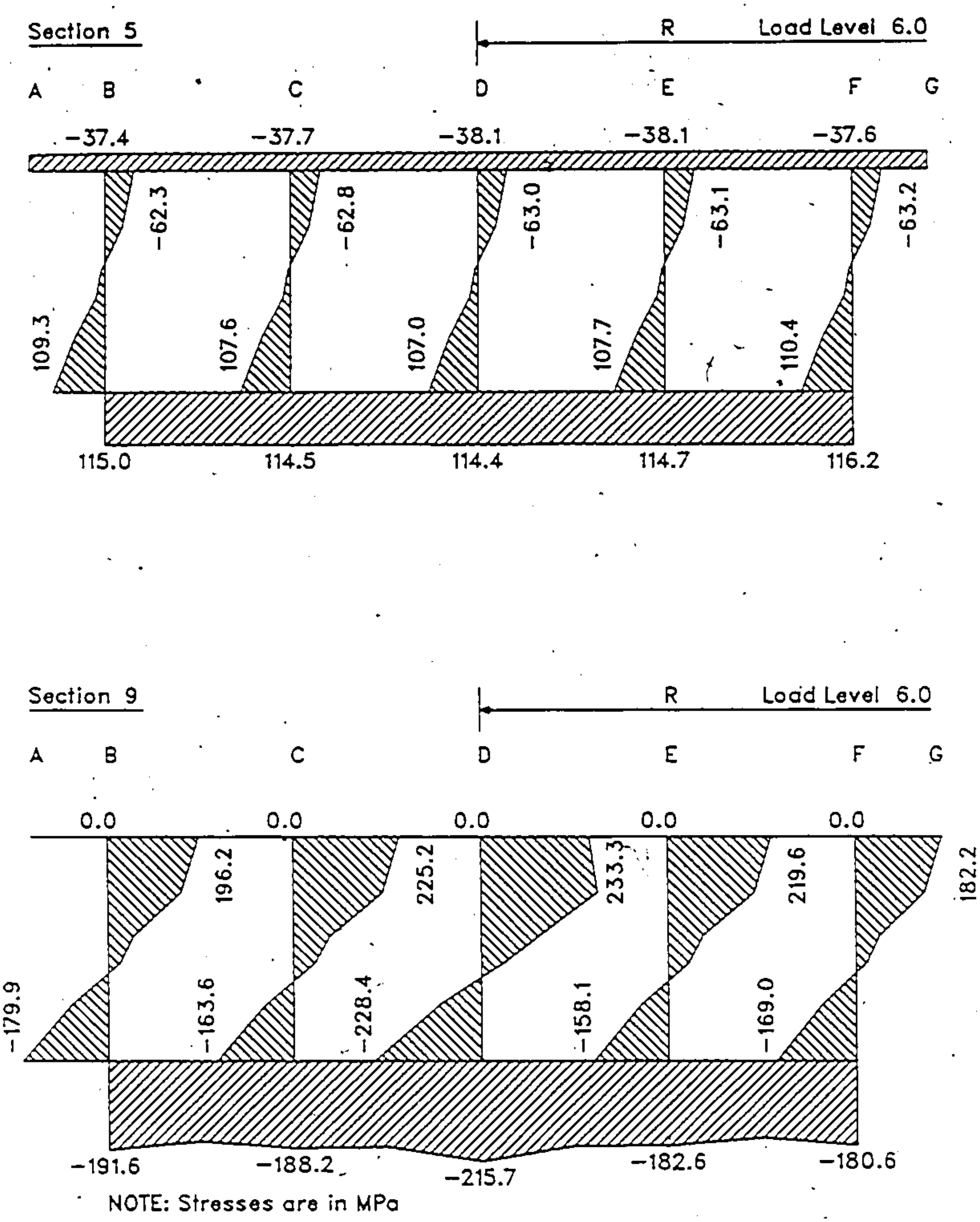

Figure 6.33: Normal stresses for load scenario A at load level 6.0.

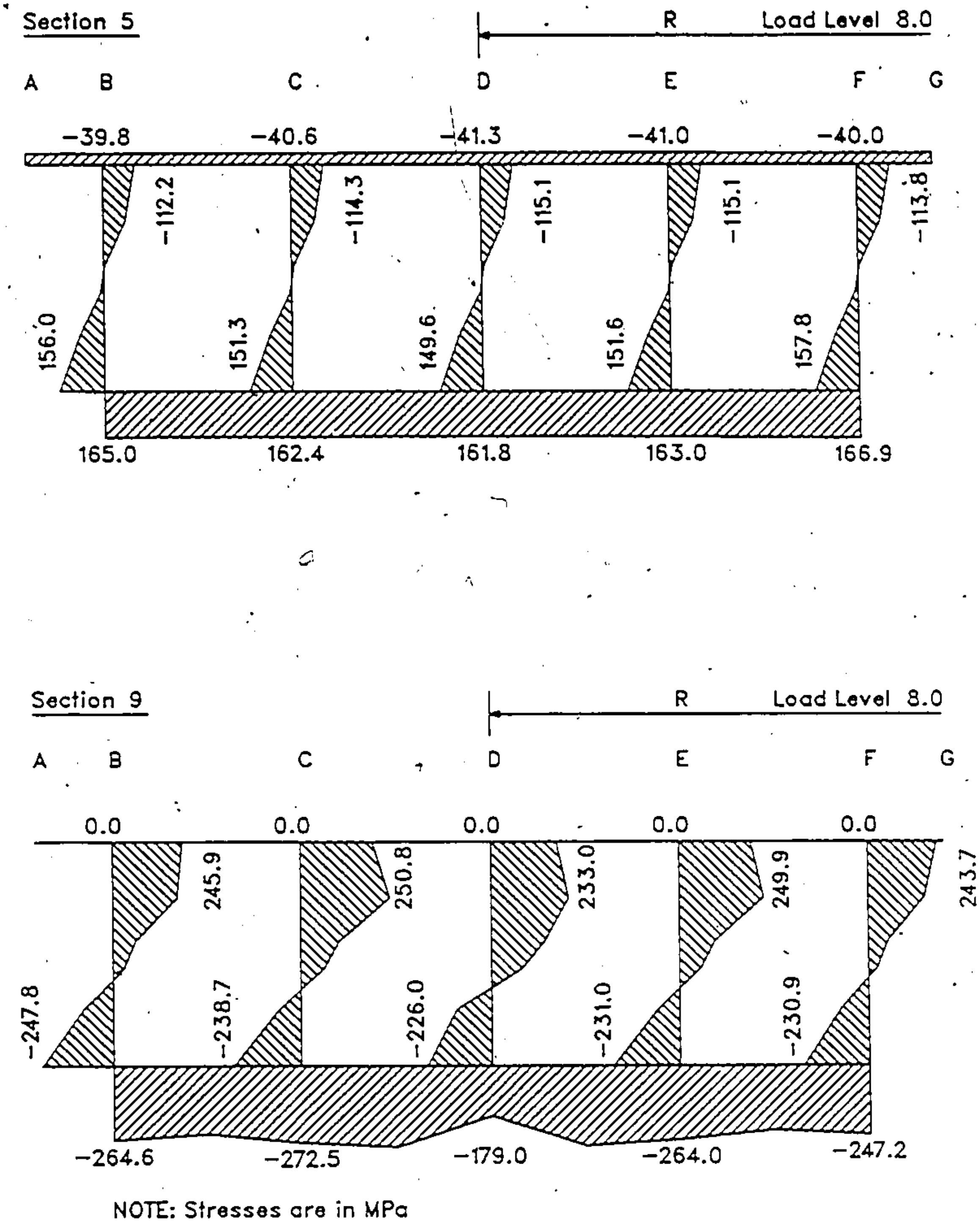

Figure 6.34: Normal stresses for load scenario A at load level 8.0.

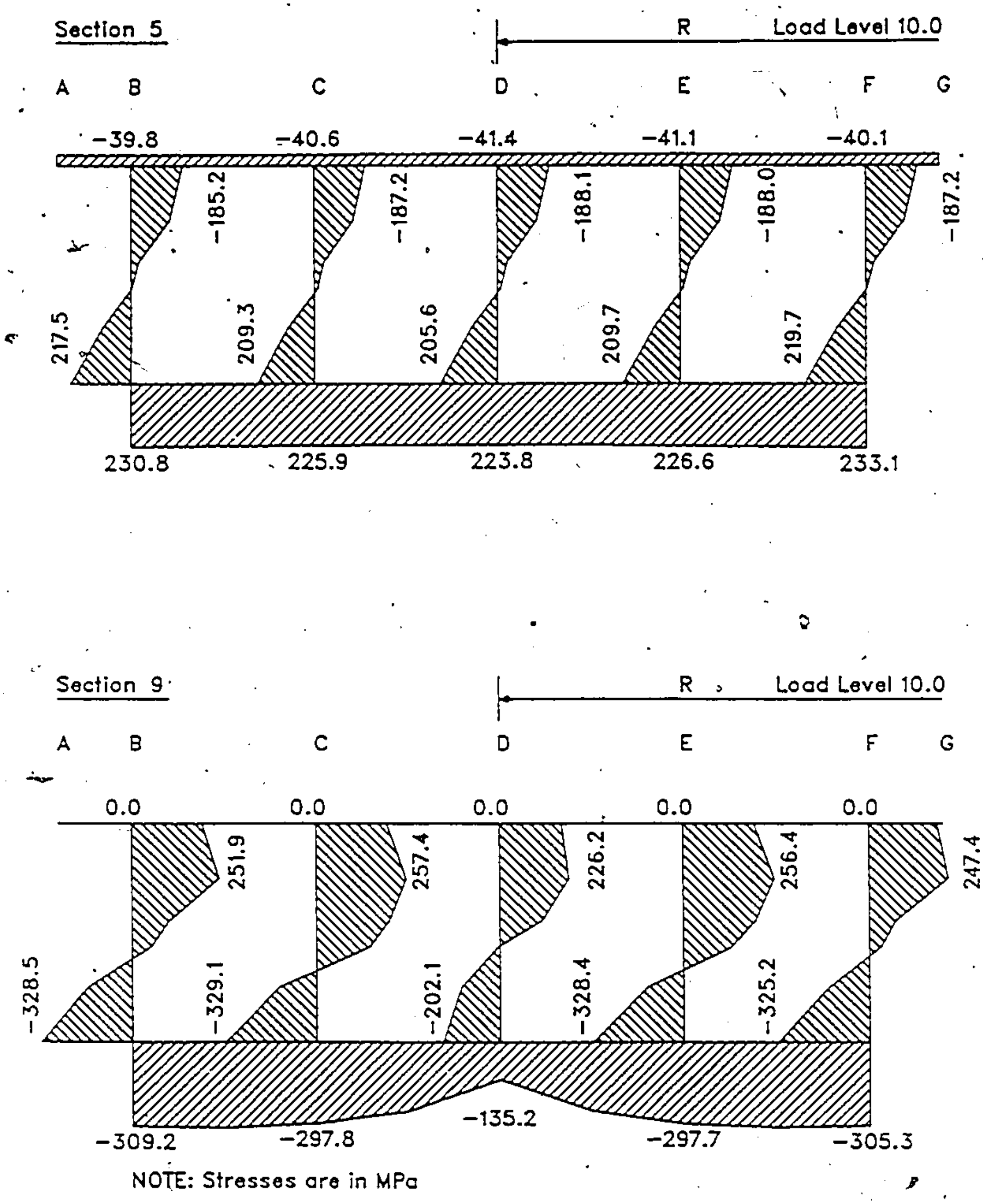

Figure 6.35: Normal stresses for load scenario A at load level 10.0.

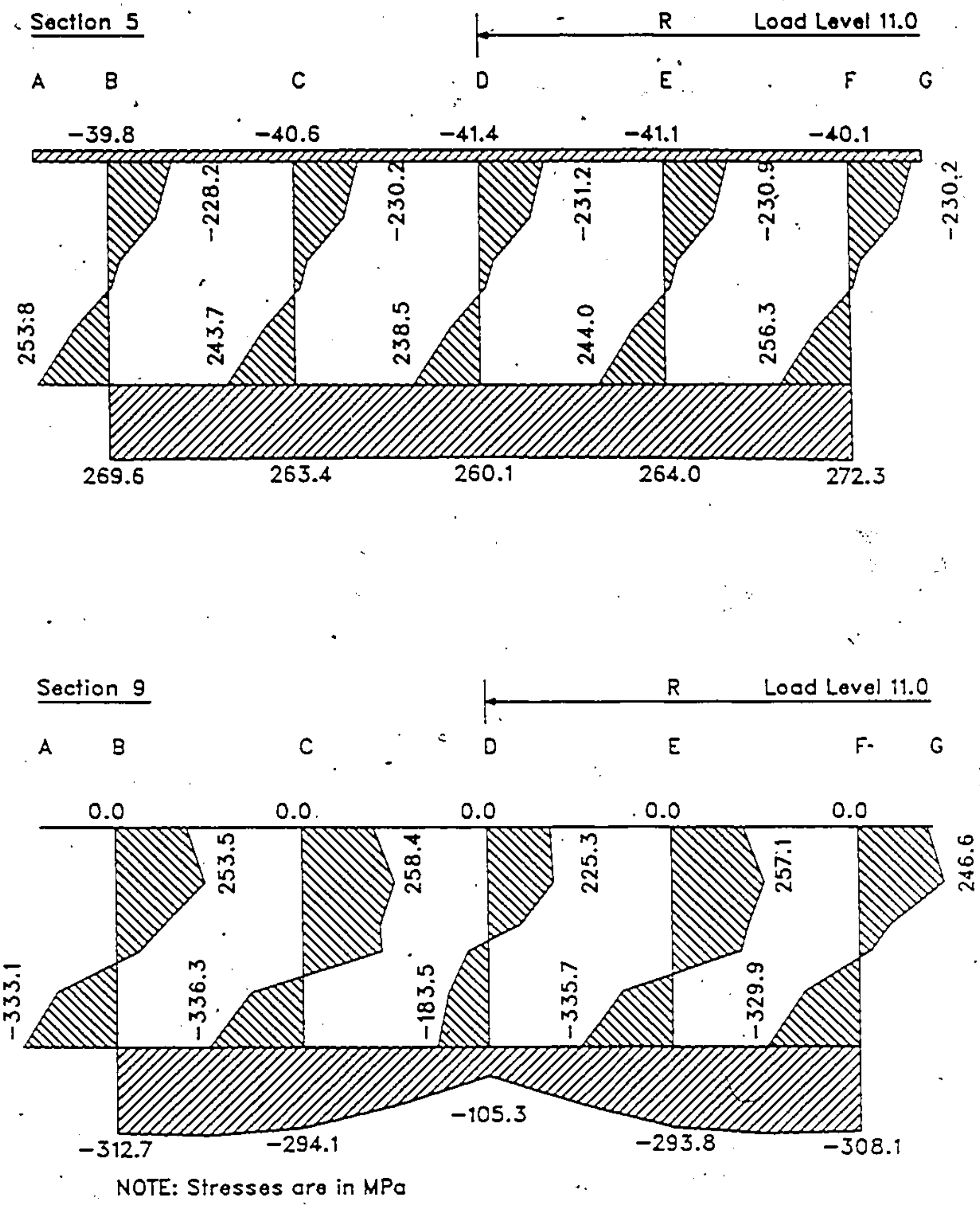

Figure 6.36: Normal stresses for load scenario A at load level 11.0.

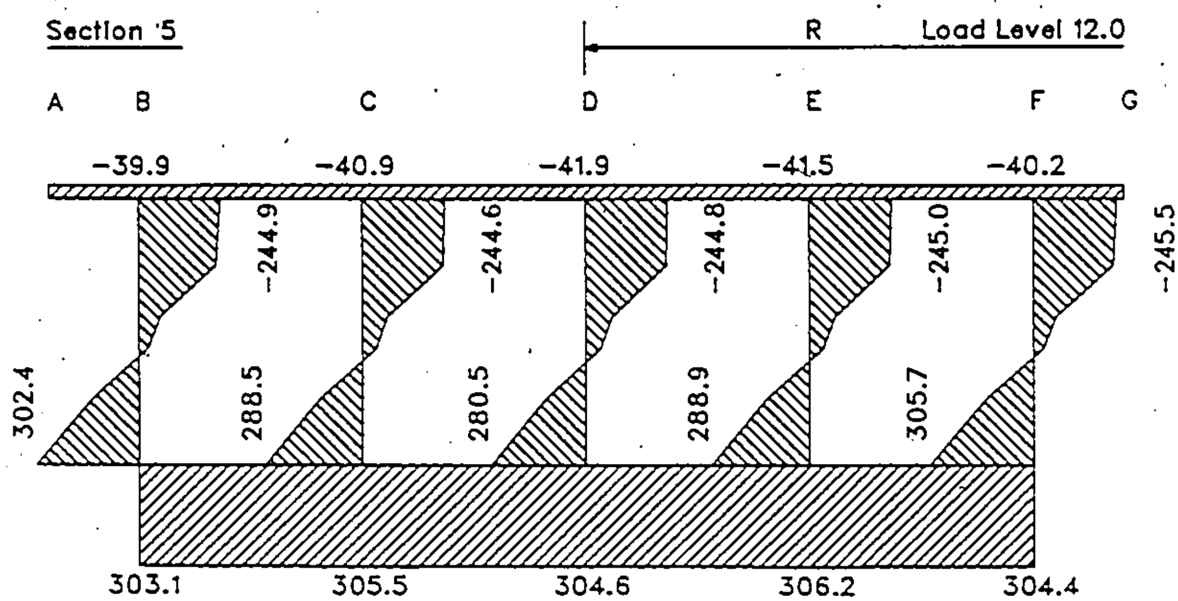

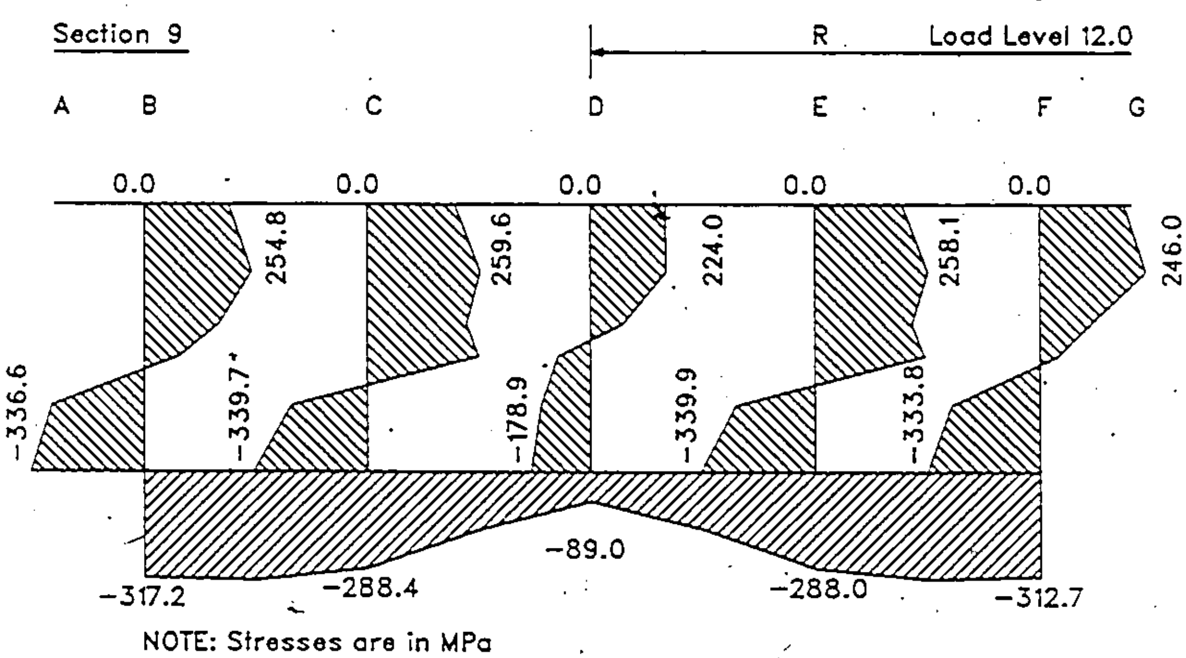

Figure 6.37: Normal stresses for load scenario A at load level 12.0.

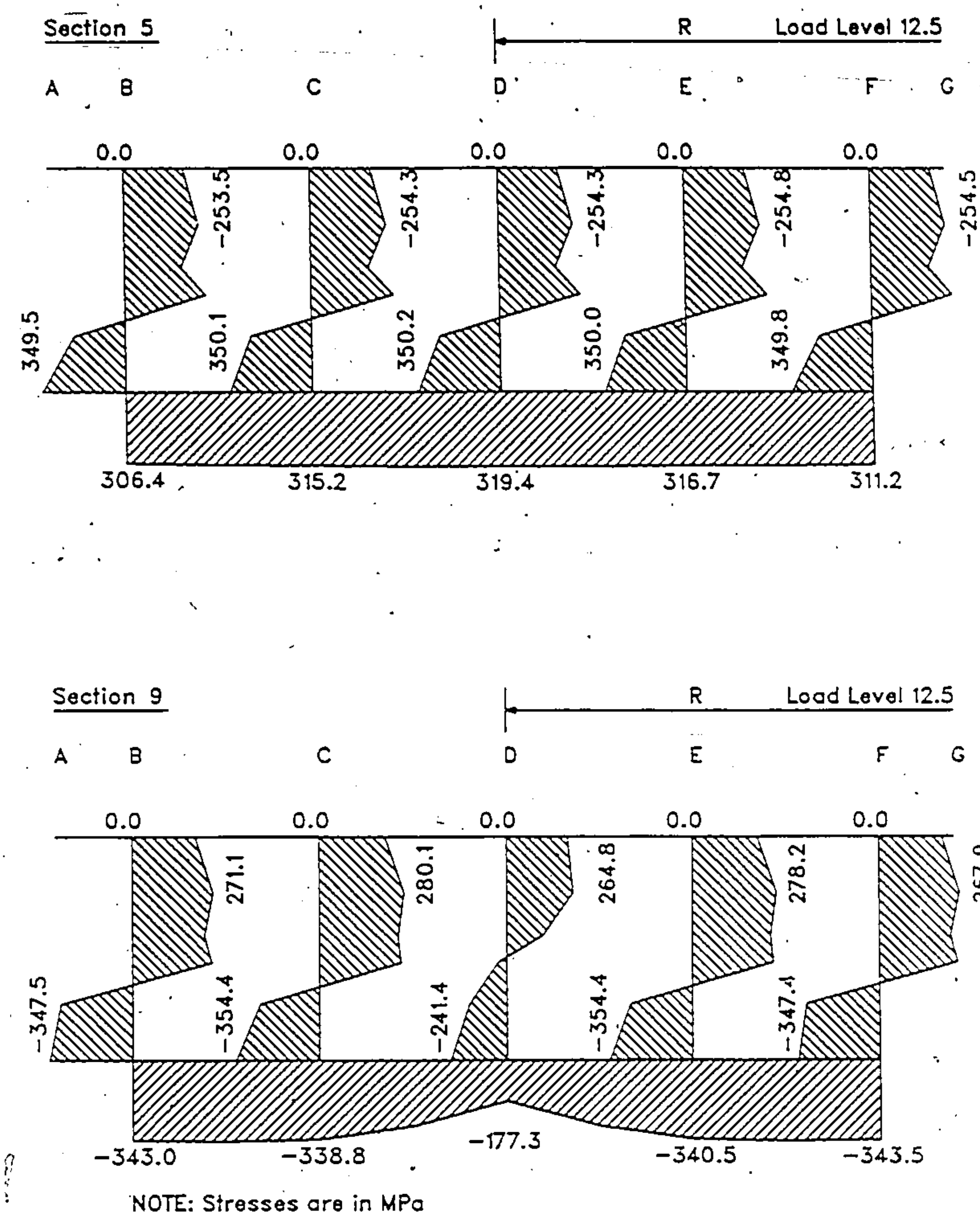

Figure 6.38: Normal stresses for load scenario A at load level 12.5.

Load level 12.0 marked the initiation of yielding in the aluminum webs and bottom plates and the compression failure of the concrete deck zone between sections 4 and 5. The formation of the first plastic hinge occurs at load level 13.0. At this load level, a 90 % drop in initial structure stiffness was observed at the critical section accompanied with a drastic increase in section curvature. The ratio of section curvature at load level 13.0 to that computed at load level 12.0 was as high as 3.15. Maximum vertical deflection at the critical section in the order of 60 mm is expected at load level 13.0. Moreover, this load level marked the initiation of yielding at the maximum negative moment section over the center column support.

Analysis indicated longitudinal redistribution between load levels 12.0 and 13.0 is more pronounced than between load levels 13.0 and 14.0. At load level 14.0 ADINA predicted maximum vertical displacement in the order of 103 mm at the critical section. If we consider this order of deformation excessive then perhaps load level 14.0 would be the ultimate load level which can be carried by the bridge under load scenario A. On the other hand, analysis indicated the formation of the second plastic hinge at the hogging moment section is expected soon at load level 14.5. At this load level the bridge has two plastic hinges and ADINA predicted maximum deflection level in the order of 160 mm at the positive moment section. Therefore the structure has failed due to excessive deformation and perhaps load level 14.5 (556 KN) can be considered a less conservative ultimate load level for the bridge under load scenario A.

6.9.2 Negative Moment Load Scenario B

Inelastic response of the curved bridge model under the negative moment load scenario indicated that two way bending action dominated the critical section at maximum negative moment.

Since the concrete material model is limited to compressive type of loads, concrete contribution to strength and stiffness in the high tension zone (between section 7 and 11) were ignored above load level 1.0 as concrete elements reached their tensile strength.

First yielding in the aluminum material was observed at load level 6.0. Load–

deformation curves showed that the progression of plastic action and hence stiffness degradation at section 9 was more gradual than that observed in the positive moment load scenario.

In resisting the applied loads, the central region above the center column was subjected to higher percentage of both longitudinal and transverse moments than that observed in the external region near webs B and F. As such the formation of the first plastic hinge at section 9 occurred as a result of consecutive local failures of the interior webs and central region of diaphragm elements. It was evident that the central web D was the first to yield at load level 7.0 while the intermediate webs C and E were observed to yield late at load level 11 followed by the yielding of the external webs B and F at load 12.0.

Load level 12.0 marked two distinct behavioral changes in the bridge. Analysis indicated that the formation of the first plastic hinge at the hogging moment section takes place at this load level and first yielding in the aluminum components at maximum positive moment sections was observed. Also, at this load level, analysis indicated compression failure is expected to occur for concrete elements near maximum positive moment sections. It should be noted that concrete in the high compression zones around sections 5 and 13 was incurring plastic deformation since load level 5.0.

Soon after the formation of the first plastic hinge at section 9, the formation of the second and third plastic hinges at maximum positive moment section 5 and 13 was observed to occur simultaneously at load level 12.5. This was evident from the drastic increase in section curvatures. The ratio of section curvature at load level 12.5 to the previous load level 12.0 was as high as 4.30.

In terms of maximum deformation level, ADINA predicted maximum deflection under the positive moment sections in the order of 40 mm and 120 mm at load levels 12.0 and 12.5 respectively. Clearly, in approaching the ultimate load the level of maximum deformation for the negative moment load scenario is not as severe as that observed in the positive moment load scenario.

The development of three plastic hinges in the bridge is sufficient for a collapse mechanism and therefore the bridge would essentially fail upon their formation. As such the ultimate load level for the bridge model under the negative moment load scenario is 12.5 (959 KN).

Chapter 7

Conclusions and Recommendations

7.1 Conclusions

The experimental and analytical model studies on the horizontally curved box girder bridge have led to a number of important findings. The following are conclusions drawn from this investigation.

1. The isoparametric thin shell element employed by the ADINA program does not only provide accurate representation of the various structural components of a curved box girder bridge, the element is also quite versatile in its application.

2. In idealizing a curved box girder bridge using finite elements, solution convergence for mesh fineness in the longitudinal direction is a necessary step but not sufficient for accurate structure response. Depending on bridge curvature and the extent of eccentricity of the applied truck loads, proper transverse idealization of the curved box girder may require more than two thin shell elements per box annular plate and box cylindrical web.

3. Special attention must be given when modelling the boundary conditions of the curved box girder particularly in the box radial direction. The assumption

of stiff diaphragm action being very important when the bridge is subjected to eccentric types of loads. Ignoring the end diaphragms would result in a softer structure and yield erroneous results.

4. When modelling straight box girder structures using thin isoparametric shell elements, ignoring the end diaphragm action may result in unstable and erroneous inelastic behavior particularly when the beam structure is subjected to uniformly distributed types of loads.

5. Linear regression analysis on the experimentally measured bridge response data indicated that displacements were much more reliable than strains in representing the real response of the model.

6. The ADINA four box composite bridge model predicted the elastic experimentally obtained response fairly well. Despite various sources of experimental errors and various assumptions and approximations inherent in the analytical model, the average percentage error for maximum response obtained by ADINA was 35 % and 21 % for displacements and normal stresses respectively. Moreover, both the ADINA and the experimental bridge models were always in excellent agreement in terms of predicting points of maximum response as well as response for spatial distributions.

7. Inelastic analytical analysis proved that one way longitudinal bending action would dominate the curved bridge model behavior in the maximum positive curvature regions while two way bending combined with transverse torsion is expected at the section above the center column support in the region of maximum negative moment.

8. The ADINA model predicted bridge failure due to excessive deformation along with the formation of at least one positive and one negative plastic hinges at a total load of 556 KN (125 Kips) for the positive moment load scenario. For the negative moment load scenario the bridge model is expected to reduce to a collapse mechanism at a total load of 959 KN (216 Kips) as a result of the formation of three plastic hinges at the two critical positive moment sections and at the hogging moment section over the central column support.

9. The ADINA Finite Element program can be successfully applied in predicting accurate elastic response of composite curved box girder bridges. At the

present time, the predictability of the ADINA software for the inelastic response of such structures is not quantitatively verified. Engineering judgment should be exercised in modelling materially nonlinear behavior of the concrete components of the bridge.

10. Despite its current limitations, the finite element method of analysis for curved box girder bridges remains to be an extremely powerful and flexible numerical tool. Unlike other existing methods, its scope of application covers a much wider range of such structures as it incorporates fewer restricting assumptions.

7.2 Recommendations

Having analyzed the inelastic bridge model response using the ADINA finite element model for two distinct load scenarios it is strongly recommended to conduct a further study on the existing physical bridge model to obtain experimentally its materially nonlinear response under either positive or negative moment loadings. Consequently, one can compare and evaluate the accuracy of the ADINA bridge model described in this study. In conducting the materially nonlinear testing program on the existing curved bridge model special considerations should be paid to the following aspects:

- Under the positive moment load scenario, the end supports should allow free longitudinal translational movement. In light of the analytical findings, longitudinal displacement in the order of 25 mm (1 in) are possible at failure.
- Irrespective of the type of load scenario to be adopted experimentally, the connection mechanism for the center column support should be redesigned by taking into consideration the severe combined transverse bending and torsional moments expected in this region.
- In measuring experimental strain data perhaps a data acquisition system would provide a much more reliable strain gage readings than those obtained from conventional strain indicator units. It is also recommended to use long stroke LVDT for displacement measurement in the region of maximum positive moment.

For linear dynamic testing of the model to determine its dynamic properties it is instructive to note that inertial forces in the model bridge will not be representative for those in the prototype bridge. It was evident that the mass of the model is much lower than that required for inertial similitude.

As for future analytical research it is recommended to develop the mathematical formulations in modifying the stiffness matrix for the isoparametric thin shell element so that it would be applicable to represent nonlinear concrete material model.

In light of the successful application of the ADINA program for analyzing curved box girder bridges, perhaps a parametric study may be desirable to evaluate the influence of horizontal curvature and intermediate diaphragms on the elastic response of the bridge.

Bibliography

[1] P. F. Mcmanus, A. N. Ghulam and C. G. Culver. *Horizontally Curved Girders—State of The Art.* ASCE, JSD, proceeding paper 6546, vol. 95, No. ST5, May 1969, pp. 853–870.

[2] C. P. Tan, S. Shore and K. Ketchek. Discussion of *Horizontally Curved Girders—State of The Art.* by P. F. Mcmanus, A. N. Ghulam and C. G. Culver. ASCE, JSD, vol. 95, No. ST12, Dec. 1969, pp. 2997–3001.

[3] ONTARIO HIGHWAY BRIDGE DESIGN CODE. *design and analysis of superstructure.* Chapter 3, Table 3-9.

[4] Edmund C. Hambly. *Bridge Deck Behaviour.* 1972 John Wiley & Sons Inc. NewYork. pp. 55–70.

[5] M. E. Mohsin. *Additional Contribution.* International Conference on Developments in Bridge Design and Construction. University College of South wales and Monmouthshire. Proceeding 1971.

[6] K. Hasebe, S. Usuki, Y. Horie. *Shear Lag Analysis and effective width of curved girder bridge.* ASCE, JEM, proceeding paper 19390, vol. 111, No. 1, January 1985.

[7] T. Kano, S. Usuki, K. Hasebe. *Theory of Thin walled Curved Members With shear deformation.* Ingenieur-Archiv, 51, 1982.

[8] H. R. Evans and N. E. Shanmugam. *An Approximate Grillage Approach to the Analysis of Cellular Structures.* Institute of Civil Engineers proceeding, part 2, vol. 67, March 1979, pp. 133–154.

[9] H. R. Evans and N. E. Shanmugam. *Simplified Analysis for Cellular Structures.* ASCE, JSD, proceeding paper 18671, vol. 110, No. 3, March 1984, PP. 531–543.

[10] F. Sawko. *Computer Analysis of Grillage Curved in Plan.* International Association Of Bridge AND Structural Engineering (IABSE) Publications, vol. 27, 1967, pp. 151-170.

[11] M. S. Troitsky *Orthotropic Bridges Theory and Design.* 1967, The James F. Lincoln Arc Welding Foundation.

[12] Y. K. Cheung. *The Analysis of Cylindrical Orthotropic Curved Bridge Decks.* IABSE publications, vol. 29, part II, 1969, pp. 41–52.

[13] F. Sawko and P. A. Merriman. *An Annular Segment Finite Element for Plate Bending.* International Journal for Numerical Methods in Engineering. vol. 3, 1971, pp. 119–129.

[14] A. Coull and P. C. Das. *Analysis of Curved Bridge Decks.* Proc. Inst. Civ. Engrs., vol. 37, 1967, pp. 75–85.

[15] L. C. Bell and C. P. Heins. *Analysis of Curved Girder Bridges.* ASCE, JSD, proceeding paper 7462, vol. 96, No.ST8, Aug. 1970, pp. 1657–1673.

[16] D. H. H. Tung. *Analysis of Curved Twin Box Girder Bridges.* presented in may 8–12, 1967, ASCE national meeting in Structural Engineering. Held at Seatle, Washington.

[17] K. Chu and S.G. Pinjarkar. *Analysis of Horizontally Curved Box Girder Bridges.* ASCE, JSD, proceeding paper 8453, vol. 97, No. ST10, Oct. 1971, pp. 2481–2501.

[18] A. Fam and C. J. Turkstra. Discussion of *Analysis of Horizontally Curved Box Girder Bridges.* by Kaung-Hun Chu and Suresh G. Pinjarkar, ASCE, JSD, vol. 98, No. ST5, May 1972, pp. 1212–1214.

[19] A. C. Scordelis, C. Meyer and A. Seni. Discussion of *Analysis of Horizontally Curved Box Girder Bridges.* by Kaung-Hun Chu and Suresh G. Pinjarkar, ASCE, JSD, vol. 98, No. ST8, Aug. 1972, pp. 1878–1880.

[20] S. G. Pinjarkar. *Analysis of Curved Box Girder Bridges* Ph.D. Thesis,Illinois Institute of Technology, Chicago, Ill. June 1969.

[21] H. R. Evans. *Simplified Methods for the Analysis and Design of Bridges of Cellular Cross-Section.* Proceedings of the NATO Advanced Study Institue on Analysis and Design of Bridges, Cesme, Izmir, Turkey, June 28–July 9, 1982, pp. 105–111. Martinus Nijhoff Publishers, The Hague, 1984.

[22] Y. K. Cheung *Folded Plate Structures by Finite Strip Method.* ASCE, JSD, proceeding paper 6985, vol. 95, No.ST 12, Dec. 1969, pp. 2963–2979.

[23] C. Meyer and A. C. Scordelis. *Analysis of Curved Folded Plate Structures.* ASCE, JSD, proceeding paper 8434, vol. 97, No. ST10, Oct. 1971, pp. 2459–2480.

[24] Yew Chaye Loo and Anthony R. Cusens. *The Finite—Strip Method in Bridge Engineering.* 1978, Viewpoint Publications.

[25] Bathe Klaus-Jurgen. *Finite Element Procedures in Engineering Analysis.* 1982, Prentice-hall Inc., Englewood Cliffs, New Jersy.

[26] O. C. Zienjiewicz. *The Finite Element Method.* 1983, McGraw-Hill book Company (UK) Ltd.

[27] Robert D. Cook. *Concepts and Applications of Finite Element Analysis.* 1981, 2nd ed., John Wiley and Sons Inc., Toronto, Canada.

[28] G. Dhatt and G. Touzot. *The Finite Element Method Displayed.* 1984, John Wiley and Sons Inc., NewYork.

[29] Iph K. Anija and Roll Frederic. *Model Analysis of Curved Box-Beam Highway Bridge.* ASCE, JSD, proceeding paper 8603, vol. 97, No. ST12, Dec. 1971, PP. 2861–2878.

[30] K. J. Willam and A. C. Scordelis. *Cellular Structures of Arbitrary Plan Geometry.* ASCE, JSD, proceeding paper 9013, vol. 98, No. ST7, July 1972, PP. 1377–1394.

[31] Z. P. Bazant and M. El Nimeiri. *Stiffness Method for Curved Box Girders at Initial Stress.* ASCE, JSD, proceeding paper 10877, vol. 100, No. ST10, Oct. 1974, PP. 2071–2090.

[32] A. Fam and C. J. Turkstra. Discussion of *Model Analysis of Curved Box-Beam Highway Bridges.* by Iph K. Anija and Roll Frederic. ASCE, JSD, vol. 98, No. ST10, Oct. 1972, PP. 2320–2323.

[33] A. Fam and C. J. Turkstra. *A Finite-Element Scheme for Box Bridge Analysis.* Computers and Structures, vol. 5, 1975, PP. 179–186

[34] M. Aslam and W. G. Godden. *Model Studies of Multi-Cell Curved Box Girder Bridges.* ASCE, JEMD, proceeding paper 11366, vol. 101, No. EM3, June 1975, PP. 207–222.

[35] A. R. Fam and C. J. Turkstra. *Model Study of Horizontally Curved Box Girder.* ASCE, JSD, proceeding paper 12151, vol. 102, No. ST5, May 1976, PP. 1097–1108.

[36] A. C. Scordelis and P. K. Larsen. *Structural Response of Curved RC Box-Girder Bridge.* ASCE, JSD, proceeding paper 13112, vol. 103, No. ST8, Aug. 1977, PP. 1507–1524.

[37] A. C. Scordelis,P. K. Larsen and L. G. Elfgren. *Ultimate Strength of Curved RC Box Girder Bridge.* ASCE, JSD, proceeding paper 13113, vol. 103, No. ST8, Aug. 1977, PP. 1525–1542.

[38] D. R. Schelling, C. P. Heins and G. H. Sikes. *State of The Art Curved Girder Bridge Programs.* Computers and Structures, vol. 9, 1978, PP. 27–37.

[39] C. P. Heins, B. Bonakdarpour, and L. C. Bell. *Multicell Curved Girder Model Studiest.* ASCE, JSD, proceeding paper 8835, vol. 98, No. ST4, April 1972, pp. 831–843.

[40] S. F. Ng, M. S. Cheung, and R. S. Shao. *Model Testing of A Curved Continuous Box Girder Bridge.* Report on Design and Manufacture of Model. University of Ottawa, Jan. 1987.

[41] Vishy Educational Products. *How to Make Precision Strain Gage Instalation.* 1970 by Vishay Research and Education.

[42] *ADINA - A Finite Element Program for Automatic Dynamic Incremental Nonlinear Analysis*, Users manual, Report ARD 84-1, ADINA Engineering, December 1984.

[43] *ADINA-IN - A Program for Generation of Input Data to ADINA*, Users manual, Report ARD 84-6, ADINA Engineering 1984.

[44] *ADINA - Theory and Modelling Guide*, Report AE 84-4, ADINA Engineering, December 1984.

[45] *ADINA - Verification Manual*, Report AE 84-5, ADINA Engineering, December1984.

[46] *ADINA-PLOT - A Program for Display and Post-Processing of ADINA Results*, Users manual, Report AE 84-3, ADINA Engineering, December 1984.

[47] *ADINAT - A Finite Element Program for Automatic Dynamic Incremental Analysis of Temperatures*, Users manual, Report AE 84-2, ADINA Engineering, December 1984.

[48] D.R.J. Owen and E. Hinton. *Finite Elements in Plasticity: Theory and Practice.* 1980, Pineridge Press Limited, Swansea, U.K.

Appendix A

Material Data

Table A.1: Trial mix concrete compressive strength

Trial Mix ID	Specimens ID	$f'_c\,(MPa)$			
		6 days	18 days	28 days	46 days
A	1	42.0	38.5	45.9	46.3
	2	41.0	39.0	42.9	46.8
	3	-	41.5	41.0	45.4
	Average	41.5	39.7	43.2	46.2
B	1	25.4	35.1	39.0	39.0
	2	26.8	33.2	39.0	37.6
	3	28.3	-	38.6	37.1
	Average	26.8	34.1	38.9	37.9

Table A.2: Stress-Strain data for 28 day cylinders

Load (Kips)	Stress (MPa)	Specimen Strain (10^{-6})		
		1	2	3
0	0	-1	0	0.9
5	4.88	-114	-229	-203
10	9.76	-240	-362	-349
15	14.64	-466	-495	-492
20	19.52	-583	-625	-638
25	24.39	-730	-750	-821
30	29.27	-855	-903	-986
35	34.15	-1023	-1041	-1185
40	39.03	-1204	-1158	-1450
45	43.91	-1420	-1341	-1717

Appendix B

Experimental Model Response Data

Table B.1: Displacement Data (10^{-2} mm) for Load Case (1)

Load Case 1		Cell Load at each Load Step (Kips)										
		0	1	2	3	4	5	6	7	8	9	10
Cross Sec. #	Dial Gage ID	$C_1 = 2$	2.00	2.00	2.00	2.00	2.00	2.00	2.00	2.00	2.00	2.00
		$C_2 = 0$	0.44	0.88	1.32	1.76	2.20	2.64	3.08	3.52	3.96	4.40
		$C_3 = 0$	0.44	0.88	1.32	1.76	2.20	2.64	3.08	3.52	3.96	4.40
1	ϕ_{B1}	-3	-4	-3	-1	0	2	3	5	7	8	10
	ϕ_{F1}	0	0	-1	-1	-2	-3	-4	-4	-5	-5	-6
2	ϕ_{B2}	1	6	13	20	27	34	42	48	56	64	72
	ϕ_{D2}	1	5	10	15	20	25	30	35	40	45	50
	ϕ_{F2}	0	3	6	9	12	15	18	21	24	27	30
5	ϕ_{B5}	2	15	29	44	56	71	85	100	114	128	144
	ϕ_{C5}	2	13	25	37	49	62	75	88	100	112	125
	ϕ_{D5}	1	11	20	30	40	51	62	71	81	90	101
	ϕ_{E5}	1	10	18	26	34	42	50	58	66	73	82
	ϕ_{F5}	0	8	14	21	27	34	40	46	53	59	65
	ψ_{T5}	-1	-2	1	3	6	8	11	14	17	20	22
	ψ_{B5}	-3	-5	-6	-7	-8	-8	-9	-10	-11	-11	-12
8	ϕ_{B8}	0	3	9	14	19	25	30	35	40	45	51
	ϕ_{D8}	1	2	4	6	7	9	10	12	14	16	17
	ϕ_{F8}	1	2	1	1	1	1	1	1	-8	-9	-10
9	ϕ_{B9}	1	4	8	13	18	22	27	32	37	42	47
	ϕ_{F9}	2	2	1	-1	-3	-4	-6	-8	-10	-12	-14
	ψ_{T9}	-5	-9	-6	-4	-1	2	5	8	11	14	17
	ψ_{B9}	-5	-9	-9	-8	-7	-6	-5	-4	-3	-2	-1
13	ϕ_{B13}	3	18	35	53	72	88	105	121	139	158	174
	ϕ_{C13}	2	19	33	49	66	82	92	114	129	143	160
	ϕ_{D13}	2	17	30	44	59	72	87	100	113	126	141
	ϕ_{E13}	1	15	26	37	49	61	73	84	95	105	118
	ψ_{F13}	1	13	22	32	42	52	62	71	80	89	99

Table B.2: Displacement Data (10^{-2} mm) for Load Case (2)

Load Case		Cell Load at each Load Step (Kips)										
2		0	1	2	3	4	5	6	7	8	9	10
Cross	Dial	$C_1 = 2$	2.00	2.00	2.00	2.00	2.00	2.00	2.00	2.00	2.00	2.00
Sec.	Gage	$C_2 = 0$	0.44	0.88	1.32	1.76	2.20	2.64	3.08	3.52	3.96	4.40
#	ID	$C_3 = 0$	0.44	0.88	1.32	1.76	2.20	2.64	3.08	3.52	3.96	4.40
1	ϕ_{B1}	2		5		8		10		12		14
	ϕ_{F1}	-1		-2		-4		-6		-8		-10
2	ϕ_{B2}	1		9		18		26		34		43
	ϕ_{D2}	0		5		10		15		20		25
	ϕ_{F2}	-1		2		4		6		8		10
5	ϕ_{B5}	0		23		46		69		91		115
	ϕ_{C5}	0		20		39		59		78		98
	ϕ_{D5}	0		15		31		47		62		77
	ϕ_{E5}	0		13		25		36		46		58
	ϕ_{F5}	0		9		18		25		33		40
	ψ_{T5}	1		2		7		12		17		23
	ψ_{B5}	-1		-3		-4		-5		-6		-7
8	ϕ_{B8}	1		16		30		45		59		74
	ϕ_{D8}	0		6		11		16		21		26
	ϕ_{F8}	-1		-2		-4		-7		-11		-11
9	ϕ_{B9}	1		13		25		38		50		63
	ϕ_{F9}	-1		-4		-8		-13		-18		-23
	ψ_{T9}	0		-5		2		8		15		23
	ψ_{B9}	0		-10		-8		-6		-4		-2
13	ϕ_{B13}	3		29		61		88		114		142
	ϕ_{C13}	2		27		51		76		100		125
	ϕ_{D13}	1		22		43		64		84		104
	ϕ_{E13}	1		18		34		50		66		81
	ψ_{F13}	1		14		26		39		51		63

Table B.3: Displacement Data (10^{-2} mm) for Load Case (3)

Load Case 3		Cell Load at each Load Step (Kips)										
		0	1	2	3	4	5	6	7	8	9	10
Cross Sec. #	Dial Gage ID	$C_1 = 2$	2.00	2.00	2.00	2.00	2.00	2.00	2.00	2.00	2.00	2.00
		$C_2 = 0$	0.44	0.88	1.32	1.76	2.20	2.64	3.08	3.52	3.96	4.40
		$C_3 = 0$	0	0	0	0	0	0	0	0	0	0
1	ϕ_{B1}	-3	4	-3	-2	0	1	2	3	4	5	6
	ϕ_{F1}	0	-1	-1	-1	-2	-2	-2	-3	-3	-4	-4
2	ϕ_{B2}	0	8	15	22	29	36	44	51	58	65	72
	ϕ_{D2}	0	6	12	18	24	29	35	41	46	52	57
	ϕ_{F2}	0	5	9	14	18	23	28	32	36	40	46
5	ϕ_{B5}	2	23	43	63	85	105	125	145	165	185	204
	ϕ_{C5}	1	20	39	58	79	94	115	134	153	170	188
	ϕ_{D5}	1	18	35	53	70	85	102	120	136	152	168
	ϕ_{E5}	1	17	32	47	61	77	92	107	121	136	149
	ϕ_{F5}	1	15	28	41	55	68	82	95	108	121	133
	ψ_{T5}	0	1	3	6	8	10	12	15	18	19	22
	ψ_{B5}	0	-3	-4	-5	-7	-8	-9	-11	-12	-13	-15
8	ϕ_{B8}	1	10	19	28	37	46	55	64	72	81	90
	ϕ_{D8}	0	7	12	18	24	29	35	40	45	50	56
	ϕ_{F8}	0	5	8	11	15	18	21	25	27	30	34
9	ϕ_{B9}	0	4	6	10	13	16	19	22	25	28	31
	ϕ_{F9}	-1	-1	-3	-5	-6	-7	-8	-10	-11	-12	-14
	ψ_{T9}	0	1	3	5	7	9	11	13	15	17	19
	ψ_{B9}	0	0	1	2	3	4	4	5	5	5	6
13	ϕ_{B13}	-2	-6	-12	-14	-19	-23	-27	-32	-38	-43	-48
	ϕ_{C13}	-3	-4	-11	-17	-22	-27	-32	-37	-44	-50	-56
	ϕ_{D13}	-1	-6	-12	-23	-26	-29	-35	-41	-47	-53	-60
	ϕ_{E13}	-3	-6	-13	-19	-25	-32	-38	-44	-51	-58	-64
	ψ_{F13}	-5	-8	-15	-21	-28	-35	-42	-49	-56	-63	-70

Table B.4: Displacement Data (10^{-2} mm) for Load Case (4)

Load Case		Cell Load at each Load Step (Kips)										
4		0	1	2	3	4	5	6	7	8	9	10
Cross	Dial	$C_1 = 2$	2.00	2.00	2.00	2.00	2.00	2.00	2.00	2.00	2.00	2.00
Sec.	Gage	$C_2 = 0$	0.44	0.88	1.32	1.76	2.20	2.64	3.08	3.52	3.96	4.40
#	ID	$C_3 = 0$	0.44	0.88	1.32	1.76	2.20	2.64	3.08	3.52	3.96	4.40
1	ϕ_{B1}	1	2	3	4	5	7	8	9	10	11	12
	ϕ_{F1}	0	-1	-2	-2	-3	-4	-5	-6	-7	-8	-9
	ϕ_{B2}	1	6	11	15	20	25	30	34	39	44	49
2	ϕ_{D2}	1	4	8	10	12	15	19	22	25	28	30
	ϕ_{F2}	0	2	4	5	6	8	10	11	12	14	15
	ϕ_{B5}	2	12	24	41	54	67	80	93	106	119	132
	ϕ_{C5}	1	10	21	35	46	57	68	80	91	102	113
	ϕ_{D5}	1	9	18	28	37	47	57	65	74	82	90
5	ϕ_{E5}	0	8	16	23	30	37	43	50	57	64	71
	ϕ_{F5}	0	7	13	16	22	27	32	37	42	47	52
	ψ_{T5}	2	0	7	10	12	15	18	20	24	26	29
	ψ_{B5}	1	-2	-1	-1	-2	-3	-3	-4	-4	-5	-5
	ϕ_{B8}	1	10	18	27	35	43	51	59	67	75	83
8	ϕ_{D8}	0	4	7	11	14	17	20	23	26	29	32
	ϕ_{F8}	-1	-1	-2	-2	-2	-2	-5	-5	-7	-9	-10
	ϕ_{B9}	2	8	15	20	27	33	40	46	52	59	65
9	ϕ_{F9}	-2	-4	-7	-8	-10	-13	-15	-18	-21	-24	-26
	ψ_{T9}	9	17	20	24	27	30	34	38	41	45	49
	ψ_{B9}	8	15	15	16	17	18	19	20	21	23	24
	ϕ_{B13}	1	11	20	29	39	59	62	71	80	89	95
	ϕ_{C13}	1	10	18	25	32	40	47	54	63	70	77
13	ϕ_{D13}	0	7	13	19	25	31	37	42	48	54	60
	ϕ_{E13}	-1	5	9	13	17	21	25	28	32	36	40
	ψ_{F13}	0	3	6	8	11	13	16	18	20	23	24

Table B.5: Displacement Data (10^{-2} mm) for Load Case (5)

Load Case 5		Cell Load at each Load Step (Kips)										
		0	1	2	3	4	5	6	7	8	9	10
Cross Sec. #	Dial Gage ID	$C_1 = 2$	2.00	2.00	2.00	2.00	2.00	2.00	2.00	2.00	2.00	2.00
		$C_2 = 0$	0.44	0.88	1.32	1.76	2.20	2.64	3.08	3.52	3.96	4.40
		$C_3 = 0$	0.44	0.88	1.32	1.76	2.20	2.64	3.08	3.52	3.96	4.40
1	ϕ_{B1}	5	3	5	7	10	14	16	19	22	26	30
	ϕ_{F1}	-1	-1	-2	-3	-4	-5	-6	-7	-7	-8	-9
2	ϕ_{B2}	6	15	29	42	55	70	82	96	109	124	138
	ϕ_{D2}	3	12	23	34	44	54	64	75	85	95	105
	ϕ_{F2}	1	10	17	25	32	40	47	55	62	69	76
5	ϕ_{B5}	10	41	75	109	140	172	206	240	271	305	337
	ϕ_{C5}	8	37	69	101	129	160	189	221	249	280	310
	ϕ_{D5}	6	32	62	88	115	143	169	197	222	250	275
	ϕ_{E5}	4	30	55	80	103	128	149	175	197	221	243
	ϕ_{F5}	2	27	50	71	91	113	132	154	174	195	213
	ψ_{T5}	4	3	6	10	15	20	25	29	33	38	42
	ψ_{B5}	2	-5	-8	-10	-12	-13	-14	-17	-19	-21	-24
8	ϕ_{B8}	8	19	33	49	64	79	93	108	124	140	155
	ϕ_{D8}	3	12	21	30	40	48	56	66	75	84	93
	ϕ_{F8}	-1	8	13	18	23	27	31	35	40	44	48
9	ϕ_{B9}	5	7	12	19	25	30	37	43	49	56	63
	ϕ_{F9}	-2	0	-3	-5	-7	-10	-14	-17	-19	-22	-26
	ψ_{T9}	11	18	21	24	28	31	36	39	43	47	51
	ψ_{B9}	8	12	13	14	15	17	19	19	20	21	22
13	ϕ_{B13}	-3	-5	-12	-19	-25	-34	-41	-50	-62	-68	-76
	ϕ_{C13}	-4	-10	-18	-27	-34	-43	-52	-62	-71	-80	-89
	ϕ_{D13}	-4	-10	-20	-29	-38	-48	-57	-68	-78	-88	-98
	ϕ_{E13}	-5	-11	-22	-32	-42	-51	-61	-73	-84	-96	-108
	ψ_{F13}	-5	-11	-23	-35	-45	-55	-62	-79	-91	-102	-115

Table B.6: Displacement Data (10^{-2} mm) for Load Case (6)

Load Case		Cell Load at each Load Step (Kips)										
6		0	1	2	3	4	5	6	7	8	9	10
Cross Sec. #	Dial Gage ID	$C_1 = 2$	2.00	2.00	2.00	2.00	2.00	2.00	2.00	2.00	2.00	2.00
		$C_2 = 0$	0.44	0.88	1.32	1.76	2.20	2.64	3.08	3.52	3.96	4.40
		$C_3 = 0$	0	0	0	0	0	0	0	0	0	0
1	ϕ_{B1}	-1	0	0	0	0	1	1	1	1	2	2
	ϕ_{F1}	0	-1	-1	-2	-2	-3	-3	-4	-4	-5	-5
2	ϕ_{B2}	-2	-2	-3	-5	-7	-8	-10	-11	-13	-15	-17
	ϕ_{D2}	-1	-2	-4	-6	-8	-10	-12	-14	-16	-18	-20
	ϕ_{F2}	-1	-3	-5	-7	-9	-12	-15	-17	-19	-21	-24
5	ϕ_{B5}	-1	-6	-12	-17	-22	-29	-35	-40	-46	-52	-58
	ϕ_{C5}	-1	-7	-12	-18	-24	-30	-36	-42	-49	-55	-61
	ϕ_{D5}	-1	-6	-12	-19	-26	-32	-39	-45	-51	-62	-65
	ϕ_{E5}	-1	-7	-14	-20	-27	-34	-41	-48	-55	-63	-70
	ϕ_{F5}	-1	-8	-15	-21	-29	-36	-43	-51	-58	-66	-73
	ψ_{T5}	0	1	2	3	3	4	4	5	6	7	7
	ψ_{B5}	1	1	2	2	3	4	5	6	7	8	9
8	ϕ_{B8}	-1	-2	-4	-5	-7	-9	-11	-12	-14	-15	-18
	ϕ_{D8}	-1	-3	-6	-9	-12	-15	-18	-21	-25	-28	-31
	ϕ_{F8}	-1	-5	-9	-13	-18	-23	-28	-32	-37	-42	-47
9	ϕ_{B9}	0	2	5	7	10	13	15	18	20	23	25
	ϕ_{F9}	-1	-1	-2	-3	-4	-6	-7	-8	-10	-11	-12
	ψ_{T9}	1	1	2	4	6	8	10	11	13	15	16
	ψ_{B9}	0	0	0	1	1	2	2	3	4	5	5
13	ϕ_{B13}	1	25	52	73	89	116	139	161	180	199	320
	ϕ_{C13}	1	23	42	63	84	104	124	143	164	183	202
	ϕ_{D13}	1	21	40	57	76	95	113	131	149	166	185
	ϕ_{E13}	1	19	36	52	68	84	101	117	132	148	164
	ψ_{F13}	1	17	32	46	61	76	91	106	120	134	149

Table B.7: Displacement Data (10^{-2} mm) for Load Case (7)

Load Case		Cell Load at each Load Step (Kips)										
7		0	1	2	3	4	5	6	7	8	9	10
Cross Sec. #	Dial Gage ID	$C_1 = 2$ $C_2 = 0$ $C_3 = 0$	2.00 0.44 0.44	2.00 0.88 0.88	2.00 1.32 1.32	2.00 1.76 1.76	2.00 2.20 2.20	2.00 2.64 2.64	2.00 3.08 3.08	2.00 3.52 3.52	2.00 3.96 3.96	2.00 4.40 4.40
1	ϕ_{B1}	0	2	2	4	5	7	8	9	10	12	13
	ϕ_{F1}	-1	-1	-2	-3	-4	-5	-6	-7	-8	-9	-10
2	ϕ_{B2}	1	5	10	15	20	25	30	36	40	45	50
	ϕ_{D2}	0	4	7	10	13	17	20	23	27	30	33
	ϕ_{F2}	-1	1	3	5	8	9	10	12	13	15	16
5	ϕ_{B5}	0	17	31	45	60	74	88	101	114	129	142
	ϕ_{C5}	0	15	27	42	51	64	76	89	100	112	125
	ϕ_{D5}	0	11	22	31	42	53	64	73	81	92	102
	ϕ_{E5}	0	9	17	25	33	41	50	57	63	72	80
	ϕ_{F5}	0	7	13	19	25	31	37	43	48	54	59
	ψ_{T5}	-1	3	6	8	11	14	16	19	22	25	28
	ψ_{B5}	-1	-2	-2	-3	-4	-5	-6	-6	-7	-7	-8
8	ϕ_{B8}	0	11	20	29	37	45	53	62	70	78	86
	ϕ_{D8}	-1	4	8	12	15	18	22	25	28	31	34
	ϕ_{F8}	-1	0	-1	-2	-2	-3	-4	-5	-6	-6	-7
9	ϕ_{B9}	-1	8	15	21	28	34	40	47	53	60	66
	ϕ_{F9}	-1	-2	-5	-7	-10	-12	-15	-17	-20	-23	-25
	ψ_{T9}	1	4	8	11	14	18	21	25	28	32	35
	ψ_{B9}	0	1	2	3	4	5	6	7	7	8	9
13	ϕ_{B13}	0	11	22	33	43	51	60	68	76	85	89
	ϕ_{C13}	-1	10	16	23	30	36	43	51	58	65	71
	ϕ_{D13}	-1	7	12	18	22	28	33	38	43	49	54
	ϕ_{E13}	-1	5	8	12	15	18	21	25	28	32	35
	ψ_{F13}	-1	3	5	7	9	10	12	14	15	17	19

Table B.8: Micro Strain Data for Load Case (1) set (a)

Load Case		Cell Load at each Load Step (Kips)										
1		0	1	2	3	4	5	6	7	8	9	10
Strain		$C_1 = 2$	2.00	2.00	2.00	2.00	2.00	2.00	2.00	2.00	2.00	2.00
Line	Gage	$C_2 = 0$	0.44	0.88	1.32	1.76	2.20	2.64	3.08	3.52	3.96	4.40
#	ID	$C_3 = 0$	0.44	0.88	1.32	1.76	2.20	2.64	3.08	3.52	3.96	4.40
1	C^L_{19}	4	3	2	4	4	6	9	7	12	12	12
2	C^L_{35}	-7	-7	-11	-11	-17	-20	-24	-27	-30	-34	-37
3	C^L_{38}	-3	0	5	6	8	8	9	10	10	9	8
4	C^L_{39}	-	-	-	-	-	-	-	-	-	-	-
5	C^L_{18}	-7	12	22	31	38	42	49	51	56	57	59
6	C^L_{29}	-2	18	22	24	26	26	26	28	24	23	20
7	C^L_{28}	1	27	39	47	60	71	85	93	105	115	132
8	C^L_{25}	-4	-11	-12	-18	-27	-32	-38	-45	-49	-58	-62
9	C^L_{15}	-	-	-	-	-	-	-	-	-	-	-
10	C^L_{12}	-7	-5	-12	-15	-23	-27	-33	-37	-42	-48	-53
11	A^L_{19}	2	30	56	85	114	144	176	203	230	258	289
12	A^L_{29}	5	32	60	88	116	149	182	208	234	265	295
13	A^L_{59}	8	37	59	83	108	131	160	182	203	227	251
14	A^L_{69}	6	33	56	80	104	130	157	180	201	224	249
15	A^{RL}_{18}	8	6	9	13	16	22	29	30	35	39	42
16	A^{RD}_{18}	7	12	14	19	24	28	35	37	42	46	51
17	A^{RT}_{18}	7	7	7	6	9	8	10	10	9	10	10
18	A^L_{18}	6	16	29	41	55	68	84	97	107	123	136
19	A^L_{28}	-14	-37	-46	-48	-66	-72	-86	-97	-96	-95	-105
20	A^L_{55}	6	20	30	44	53	66	80	91	101	113	124
21	A^{RL}_{25}	-6	9	20	33	47	59	72	84	96	107	120
22	A^{RL}_{28}	0	-14	-29	-44	-59	-75	-91	-107	-120	-135	-151
23	A^L_{58}	-	-	-	-	-	-	-	-	-	-	-
24	A^L_{48}	0	-17	-31	-50	-65	-79	-96	-113	-127	-143	-160
25	A^{RD}_{28}	1	-2	-8	-16	-24	-31	-38	-47	-53	-60	-68
26	A^{RD}_{25}	0	7	10	12	12	13	15	15	17	19	18
27	A^{RT}_{28}	7	9	13	22	29	28	40	32	34	39	57
28	A^{RT}_{25}	0	-4	-12	-21	-30	-37	-44	-49	-57	-63	-70
29	A^L_{45}	-4	16	32	42	67	78	85	101	110	129	146
30	A^L_{65}	18	22	28	33	32	41	39	39	49	52	59

Table B.9: Micro Strain Data for Load Case (1) set (b)

Load Case 1		Cell Load at each Load Step (Kips)										
		0	1	2	3	4	5	6	7	8	9	10
Strain		$C_1 = 2$	2.00	2.00	2.00	2.00	2.00	2.00	2.00	2.00	2.00	2.00
Line	Gage	$C_2 = 0$	0.44	0.88	1.32	1.76	2.20	2.64	3.08	3.52	3.96	4.40
#	ID	$C_3 = 0$	0.44	0.88	1.32	1.76	2.20	2.64	3.08	3.52	3.96	4.40
31	A^{L}_{68}	-2	-4	-14	-24	-32	-41	-50	-58	-66	-74	-81
32	A^{L}_{75}	-2	-4	-15	-25	-33	-42	-52	-61	-70	-79	-88
33	A^{RL}_{35}	2	4	-1	-4	-6	-10	-10	-14	-16	-15	-19
34	A^{L}_{78}	1	17	23	31	41	50	58	67	77	88	99
35	A^{RT}_{38}	0	2	0	0	0	0	0	0	0	0	0
36	A^{RD}_{38}	2	8	8	9	12	14	15	17	19	21	24
37	A^{RL}_{38}	0	7	5	5	5	6	5	6	6	7	10
38	A^{RD}_{35}	1	7	7	7	9	9	11	11	13	15	16
39	A^{RT}_{35}	2	3	0	0	-1	-2	-3	-3	-4	-5	-4
40	A^{L}_{42}	1	11	13	16	20	23	27	29	34	38	42
41	A^{L}_{22}	3	11	14	16	21	25	29	33	37	42	49
42	A^{L}_{72}	-	-	-	-	-	-	-	-	-	-	-
43	A^{L}_{55}	-	-	-	-	-	-	-	-	-	-	-
44	A^{L}_{12}	-2	-3	-8	-15	-19	-23	-28	-32	-37	-40	-43
45	A^{L}_{32}	0	13	19	25	33	41	50	56	63	71	80
46	A^{L}_{52}	-6	-8	-17	-29	-35	-40	-47	-53	-59	-63	-66
47	A^{L}_{25}	0	17	25	35	43	52	62	70	79	89	101
48	A^{L}_{39}	-	-	-	-	-	-	-	-	-	-	-
49	A^{L}_{49}	-	-	-	-	-	-	-	-	-	-	-
50	A^{L}_{88}	-	-	-	-	-	-	-	-	-	-	-
51	A^{RL}_{15}	5	8	5	1	4	-4	-5	-1	-4	-3	-9
52	A^{RD}_{15}	8	13	13	11	12	7	8	13	11	15	12
53	A^{RT}_{15}	3	8	7	4	6	0	1	4	1	5	1
54	A^{L}_{38}	8	22	32	42	56	63	77	93	104	119	129
55	A^{L}_{98}	6	21	30	39	52	59	71	87	97	112	123
56	A^{L}_{35}	-3	-2	-9	-21	-25	-37	-53	-60	-72	-83	-94
57	A^{L}_{95}	2	-1	-9	-20	-27	-40	-48	-53	-63	-69	-81
58	A^{L}_{15}	2	-6	-19	-33	-42	-56	-68	-76	-88	-97	-111
59	A^{L}_{62}	3	3	-2	-8	-13	-21	-25	-27	-31	-34	-40
60	A^{L}_{82}	1	0	-5	-11	-16	-24	-28	-30	-36	-40	-47

Table B.10: Micro Strain Data for Load Case (2) set (a)

Load Case		Cell Load at each Load Step (Kips)										
2		0	1	2	3	4	5	6	7	8	9	10
Strain		$C_1 = 2$	2.00	2.00	2.00	2.00	2.00	2.00	2.00	2.00	2.00	2.00
Line	Gage	$C_2 = 0$	0.44	0.88	1.32	1.76	2.20	2.64	3.08	3.52	3.96	4.40
#	ID	$C_3 = 0$	0.44	0.88	1.32	1.76	2.20	2.64	3.08	3.52	3.96	4.40
1	C^L_{19}	-3		11		13		9		6		-1
2	C^L_{35}	-3		-10		-11		-16		-20		-27
3	C^L_{38}	-4		-5		-10		-16		-20		-27
4	C^L_{39}	-		-		-		-		-		-
5	C^L_{18}	-3		3		4		10		12		15
6	C^L_{29}	-5		17		22		22		21		17
7	C^L_{28}	-6		11		25		39		58		74
8	C^L_{25}	-3		-13		-21		-29		-37		-45
9	C^L_{15}	-		-		-		-		-		-
10	C^L_{12}	-4		-8		-12		-15		-22		-25
11	A^L_{19}	4		63		120		179		237		295
12	A^L_{29}	3		62		121		178		236		294
13	A^L_{59}	3		47		88		131		173		219
14	A^L_{69}	3		47		91		132		177		221
15	A^{RL}_{18}	7		12		18		20		28		34
16	A^{RD}_{18}	3		17		28		37		49		58
17	A^{RT}_{18}	7		9		8		8		8		7
18	A^L_{18}	7		25		41		57		73		89
19	A^L_{28}	3		-3		-11		-24		-21		-34
20	A^L_{55}	7		26		46		63		82		100
21	A^{RL}_{25}	4		27		45		65		83		98
22	A^{RL}_{28}	2		-17		-33		-48		-66		-86
23	A^L_{56}	-		-		-		-		-		-
24	A^L_{48}	0		-18		-33		-49		-65		-85
25	A^{RD}_{28}	2		-6		-15		-24		-32		-44
26	A^{RD}_{25}	4		0		-4		-5		-7		-12
27	A^{RT}_{28}	-2		6		9		23		32		35
28	A^{RT}_{25}	4		-6		-16		-24		-32		-42
29	A^L_{45}	4		23		48		71		93		113
30	A^L_{65}	11		12		25		42		55		57

Table B.11: Micro Strain Data for Load Case (2) set (b)

Load Case		Cell Load at each Load Step (Kips)										
2		0	1	2	3	4	5	6	7	8	9	10
Strain		$C_1 = 2$	2.00	2.00	2.00	2.00	2.00	2.00	2.00	2.00	2.00	2.00
Line	Gage	$C_2 = 0$	0.44	0.88	1.32	1.76	2.20	2.64	3.08	3.52	3.96	4.40
#	ID	$C_3 = 0$	0.44	0.88	1.32	1.76	2.20	2.64	3.08	3.52	3.96	4.40
31	A^L_{68}	-2		-17		-27		-40		-49		-60
32	A^L_{75}	-2		-16		-27		-40		-51		-62
33	A^{RL}_{35}	4		-6		-7		-12		-14		-16
34	A^L_{78}	0		8		21		33		48		63
35	A^{RT}_{38}	0		-2		-1		-3		0		0
36	A^{RD}_{38}	-1		3		11		17		26		35
37	A^{RL}_{38}	0		-3		-1		-3		0		0
38	A^{RD}_{35}	-1		-1		1		2		6		11
39	A^{RT}_{35}	-2		-5		-4		-6		-6		-4
40	A^L_{42}	-3		-4		-1		-1		3		7
41	A^L_{22}	-5		-8		-7		-6		-5		-2
42	A^L_{72}	-		-		-		-		-		-
43	A^L_{85}	-		-		-		-		-		-
44	A^L_{12}	2		0		0		0		0		0
45	A^L_{32}	-2		0		8		13		19		26
46	A^L_{52}	-7		-9		-17		-25		-29		-30
47	A^L_{25}	-5		10		22		37		50		64
48	A^L_{39}	-		-		-		-		-		-
49	A^L_{49}	-		-		-		-		-		-
50	A^L_{88}	-		-		-		-		-		-
51	A^{RL}_{15}	-8		-31		-25		-34		-37		-36
52	A^{RD}_{15}	-10		-36		-35		-50		-58		-63
53	A^{RT}_{15}	-3		-17		-11		-20		-22		-22
54	A^L_{38}	-2		+3		+26		+36		+49		+66
55	A^L_{98}	-4		-2		+16		+23		+40		+50
56	A^L_{35}	-2		-19		-26		-47		-55		-67
57	A^L_{95}	-4		-20		-26		-43		-56		-66
58	A^L_{15}	-4		-18		-26		-43		-58		-70
59	A^L_{62}	-1		-5		-2		-9		-11		-12
60	A^L_{82}	-2		-6		-3		-10		-12		-12

Table B.12: Micro Strain Data for Load Case (3) set (a)

Load Case		Cell Load at each Load Step (Kips)										
3		0	1	2	3	4	5	6	7	8	9	10
Strain		$C_1 = 2$	2.00	2.00	2.00	2.00	2.00	2.00	2.00	2.00	2.00	2.00
Line	Gage	$C_2 = 0$	0.44	0.88	1.32	1.76	2.20	2.64	3.08	3.52	3.96	4.40
#	ID	$C_3 = 0$	0	0	0	0	0	0	0	0	0	0
1	C^L_{19}	0	3	5	6	3	1	0	0	4	3	3
2	C^L_{35}	2	6	9	12	16	12	8	4	-5	-12	-20
3	C^L_{38}	3	0	0	0	0	-1	-2	0	0	0	0
4	C^L_{39}	-	-	-	-	-	-	-	-	-	-	-
5	C^L_{18}	5	5	8	11	13	14	16	20	23	22	20
6	C^L_{29}	6	5	8	11	13	14	12	14	17	16	16
7	C^L_{28}	-5	-5	-2	-1	0	1	2	10	7	7	8
8	C^L_{25}	2	-8	-12	-16	-20	-28	-34	-40	-47	-57	-67
9	C^L_{15}	-	-	-	-	-	-	-	-	-	-	-
10	C^L_{12}	-2	-7	-11	-11	-13	-17	-22	-24	-21	-24	-27
11	A^L_{19}	6	23	37	53	68	86	104	123	139	154	168
12	A^L_{29}	15	30	44	62	76	92	113	131	146	159	174
13	A^L_{59}	11	20	29	42	53	64	79	93	105	115	125
14	A^L_{69}	13	27	36	47	60	72	86	104	116	125	139
15	A^{RL}_{18}	13	12	10	11	11	13	16	22	24	25	25
16	A^{RD}_{18}	16	20	23	29	35	41	47	58	65	72	76
17	A^{RT}_{18}	15	12	11	13	12	14	15	22	24	24	25
18	A^L_{18}	2	0	1	2	5	9	14	19	22	25	25
19	A^L_{28}	7	5	2	1	1	1	4	9	7	8	9
20	A^L_{55}	15	34	52	70	92	110	132	154	175	194	213
21	A^{RL}_{25}	2	25	45	67	86	109	127	151	174	192	214
22	A^{RL}_{28}	3	-1	-6	-8	-13	-14	-20	-20	-23	-24	-27
23	A^L_{58}	-	-	-	-	-	-	-	-	-	-	-
24	A^L_{48}	5	4	1	-1	-3	-6	-9	-12	-15	-18	-18
25	A^{RD}_{28}	6	6	6	6	8	8	8	8	11	11	12
26	A^{RD}_{25}	8	10	13	16	21	23	25	30	35	37	42
27	A^{RT}_{28}	12	39	36	40	37	38	43	31	61	28	37
28	A^{RT}_{25}	9	-2	-10	-25	-34	-44	-54	-61	-71	-79	-88
29	A^L_{45}	9	38	58	83	108	137	152	177	205	229	247
30	A^L_{65}	8	12	23	33	44	58	67	75	81	93	104

Table B.13: Micro Strain Data for Load Case (3) set (b)

Load Case		Cell Load at each Load Step (Kips)										
3		0	1	2	3	4	5	6	7	8	9	10
Strain		$C_1 = 2$	2.00	2.00	2.00	2.00	2.00	2.00	2.00	2.00	2.00	2.00
Line	Gage	$C_2 = 0$	0.44	0.88	1.32	1.76	2.20	2.64	3.08	3.52	3.96	4.40
#	ID	$C_3 = 0$	0	0	0	0	0	0	0	0	0	0
31	A^{L}_{68}	4	12	5	7	6	6	6	3	0	0	0
32	A^{L}_{75}	7	2	-14	-25	-38	-52	-66	-81	-98	-111	-125
33	A^{RL}_{35}	9	10	5	3	0	-2	-5	-4	-14	-17	-19
34	A^{L}_{78}	11	21	17	20	22	23	25	24	22	23	24
35	A^{RT}_{38}	18	20	17	20	21	22	22	28	28	28	28
36	A^{RD}_{38}	11	21	19	23	26	28	31	32	34	36	39
37	A^{RL}_{38}	12	20	14	17	15	16	16	14	14	14	14
38	A^{RD}_{35}	10	18	15	17	18	18	19	17	17	17	19
39	A^{RT}_{35}	9	19	15	16	17	16	16	14	13	13	15
40	A^{L}_{42}	11	23	22	28	32	35	37	39	42	45	49
41	A^{L}_{22}	10	21	20	26	27	28	28	29	31	33	37
42	A^{L}_{72}	-	-	-	-	-	-	-	-	-	-	-
43	A^{L}_{85}	-	-	-	-	-	-	-	-	-	-	-
44	A^{L}_{12}	9	18	14	18	15	12	8	6	5	4	3
45	A^{L}_{32}	13	27	29	37	41	45	47	51	57	62	68
46	A^{L}_{52}	2	9	0	-2	-10	-12	-19	-29	-33	-36	-42
47	A^{L}_{25}	11	36	50	68	85	97	110	128	143	156	174
48	A^{L}_{39}	-	-	-	-	-	-	-	-	-	-	-
49	A^{L}_{49}	-	-	-	-	-	-	-	-	-	-	-
50	A^{L}_{88}	-	-	-	-	-	-	-	-	-	-	-
51	A^{RL}_{15}	1	7	0	-1	-3	-3	-11	-19	-5	-6	-7
52	A^{RD}_{15}	19	25	18	14	13	14	8	0	17	17	17
53	A^{RT}_{15}	17	25	17	17	16	16	10	3	17	18	16
54	A^{L}_{38}	20	34	29	34	38	42	39	36	52	54	56
55	A^{L}_{98}	15	27	20	23	24	26	23	18	32	33	34
56	A^{L}_{35}	11	3	-15	-17	-37	-54	-77	-96	-98	-116	-131
57	A^{L}_{95}	16	13	-5	-17	-32	-46	-67	-87	-91	-106	-120
58	A^{L}_{15}	15	6	-13	-26	-40	-52	-70	-82	-87	-101	-116
59	A^{L}_{62}	16	21	13	15	13	11	3	-2	-6	3	0
60	A^{L}_{82}	14	22	14	12	10	8	0	-6	0	0	-4

Table B.14: Micro Strain Data for Load Case (4) set (a)

Load Case		Cell Load at each Load Step (Kips)										
4		0	1	2	3	4	5	6	7	8	9	10
Strain		$C_1 = 2$	2.00	2.00	2.00	2.00	2.00	2.00	2.00	2.00	2.00	2.00
Line	Gage	$C_2 = 0$	0.44	0.88	1.32	1.76	2.20	2.64	3.08	3.52	3.96	4.40
#	ID	$C_3 = 0$	0.44	0.88	1.32	1.76	2.20	2.64	3.08	3.52	3.96	4.40
1	C^L_{19}	0	12	10	11	11	10	7	6	5	6	5
2	C^L_{35}	0	-8	-7	-12	-13	-16	-19	-21	-21	-22	-25
3	C^L_{38}	-2	0	0	0	-3	-6	-10	-9	-12	-12	-14
4	C^L_{39}	-	-	-	-	-	-	-	-	-	-	-
5	C^L_{18}	0	0	0	5	4	7	11	14	13	27	27
6	C^L_{29}	9	20	25	28	31	32	32	33	32	34	32
7	C^L_{28}	-13	-7	0	5	11	16	22	33	38	49	56
8	C^L_{25}	10	5	0	-8	-13	-16	-20	-24	-28	-27	-34
9	C^L_{15}	-	-	-	-	-	-	-	-	-	-	-
10	C^L_{12}	-12	-12	-15	-20	-21	-22	-24	-24	-26	-25	-27
11	A^L_{19}	7	32	56	84	111	140	166	193	218	246	272
12	A^L_{29}	-2	19	43	67	95	118	143	170	192	217	243
13	A^L_{59}	8	35	52	71	90	109	128	149	164	184	204
14	A^L_{69}	0	68	33	52	71	92	110	130	148	169	188
15	A^{RL}_{18}	-2	-3	-2	-1	5	7	11	14	15	19	21
16	A^{RD}_{18}	-1	0	6	10	18	25	30	34	39	44	48
17	A^{RT}_{18}	-3	-9	-9	-9	-7	-9	-7	-6	-7	-7	-6
18	A^L_{18}	2	4	10	17	26	35	42	50	57	65	72
19	A^L_{28}	-4	-15	-14	-18	-19	-19	-22	20	-24	-23	-24
20	A^L_{55}	-3	10	19	30	42	54	65	75	85	97	109
21	A^{RL}_{25}	6	23	30	41	50	60	70	81	91	100	110
22	A^{RL}_{28}	4	0	-10	-18	-26	-33	-41	-48	-56	-64	-72
23	A^L_{58}	-	-	-	-	-	-	-	-	-	-	-
24	A^L_{48}	-6	-11	-19	-25	-33	-41	-47	-54	-62	-68	-76
25	A^{RD}_{28}	7	6	0	-4	-9	-14	-19	-22	-28	-33	-39
26	A^{RD}_{25}	4	3	1	0	-3	-4	-5	-6	-9	-10	-12
27	A^{RT}_{28}	2	-5	1	20	38	-13	-6	-2	31	45	32
28	A^{RT}_{25}	3	-2	-9	-13	-18	-25	-30	-34	-40	-48	-50
29	A^L_{45}	4	21	31	44	54	64	78	91	101	117	130
30	A^L_{65}	9	13	22	31	34	35	44	50	51	61	59

Table B.15: Micro Strain Data for Load Case (4) set (b)

Load Case		Cell Load at each Load Step (Kips)										
4		0	1	2	3	4	5	6	7	8	9	10
Strain		$C_1 = 2$	2.00	2.00	2.00	2.00	2.00	2.00	2.00	2.00	2.00	2.00
Line	Gage	$C_2 = 0$	0.44	0.88	1.32	1.76	2.20	2.64	3.08	3.52	3.96	4.40
#	ID	$C_3 = 0$	0.44	0.88	1.32	1.76	2.20	2.64	3.08	3.52	3.96	4.40
31	A^L_{68}	-2	5	0	-2	-7	-12	-16	-18	-22	-27	-30
32	A^L_{75}	15	15	9	4	-2	-11	-18	-23	-31	-37	-43
33	A^{RL}_{35}	2	8	5	5	0	-2	-6	-2	-5	-9	-10
34	A^L_{78}	36	47	52	60	63	67	74	80	86	92	96
35	A^{RT}_{38}	25	31	31	34	33	35	37	36	36	36	36
36	A^{RD}_{38}	34	47	49	55	56	58	62	66	69	72	76
37	A^{RL}_{38}	29	36	35	37	36	34	40	36	36	35	36
38	A^{RD}_{35}	30	40	40	43	43	42	43	44	46	46	49
39	A^{RT}_{35}	29	36	35	37	37	35	41	35	36	35	35
40	A^L_{42}	34	42	43	48	49	50	51	54	55	57	59
41	A^L_{22}	21	28	28	31	32	34	36	36	39	40	41
42	A^L_{72}	-	-	-	-	-	-	-	-	-	-	-
43	A^L_{85}	-	-	-	-	-	-	-	-	-	-	-
44	A^L_{12}	21	30	30	32	31	33	33	33	34	33	33
45	A^L_{32}	34	45	48	53	55	59	63	66	71	74	78
46	A^L_{52}	42	50	48	49	47	45	41	39	39	37	35
47	A^L_{25}	44	62	67	77	84	94	103	111	119	128	137
48	A^L_{39}	-	-	-	-	-	-	-	-	-	-	-
49	A^L_{49}	-	-	-	-	-	-	-	-	-	-	-
50	A^L_{88}	-	-	-	-	-	-	-	-	-	-	-
51	A^{RL}_{15}	2	15	10	20	9	17	15	10	7	11	8
52	A^{RD}_{15}	4	16	7	13	0	6	0	-5	-12	-11	-16
53	A^{RT}_{15}	11	25	20	29	21	28	23	21	18	21	18
54	A^L_{38}	20	40	43	59	62	75	81	86	91	101	106
55	A^L_{98}	20	36	37	50	52	62	66	70	73	82	86
56	A^L_{35}	8	15	2	3	3	0	-8	-18	-34	-34	-47
57	A^L_{95}	19	25	17	16	4	5	-2	-11	-20	-23	-30
58	A^L_{15}	20	29	20	17	5	5	-3	-11	-22	-28	-34
59	A^L_{62}	23	35	31	35	30	36	33	31	28	30	30
60	A^L_{82}	21	33	30	34	29	34	32	30	27	28	27

Table B.16: Micro Strain Data for Load Case (5) set (a)

Load Case		Cell Load at each Load Step (Kips)										
5		0	1	2	3	4	5	6	7	8	9	10
Strain		$C_1 = 2$	2.00	2.00	2.00	2.00	2.00	2.00	2.00	2.00	2.00	2.00
Line	Gage	$C_2 = 0$	0.44	0.88	1.32	1.76	2.20	2.64	3.08	3.52	3.96	4.40
#	ID	$C_3 = 0$	0.44	0.88	1.32	1.76	2.20	2.64	3.08	3.52	3.96	4.40
1	C^L_{19}	-2	0	0	-4	-9	-10	-9	-14	-14	-5	-13
2	C^L_{35}	-4	-13	-7	-20	-27	-30	-40	-48	-60	-73	-87
3	C^L_{38}	-3	0	0	0	-1	-2	-5	-5	-5	-8	-7
4	C^L_{39}	-	-	-	-	-	-	-	-	-	-	-
5	C^L_{18}	-1	1	7	14	12	14	17	20	20	18	17
6	C^L_{29}	-2	8	10	12	8	10	7	7	7	6	7
7	C^L_{28}	-7	0	0	0	3	4	9	11	13	11	12
8	C^L_{25}	0	-17	-27	-34	-45	-54	-65	-78	-90	-104	-115
9	C^L_{15}	-	-	-	-	-	-	-	-	-	-	-
10	C^L_{12}	-9	-14	-16	-20	-26	-34	-37	-45	-59	-67	-75
11	A^L_{19}	10	38	66	91	111	123	154	171	190	210	227
12	A^L_{29}	13	39	69	95	117	130	160	182	203	224	246
13	A^L_{59}	20	39	60	83	100	108	130	147	164	182	201
14	A^L_{69}	20	40	65	85	104	114	141	160	178	198	217
15	A^{RL}_{18}	13	10	16	15	16	7	14	14	15	15	15
16	A^{RD}_{18}	14	23	36	42	48	47	61	68	76	83	90
17	A^{RT}_{18}	15	15	22	22	23	16	24	23	27	29	31
18	A^L_{18}	15	18	24	26	28	22	28	26	28	29	28
19	A^L_{28}	25	20	28	26	25	16	22	25	26	29	29
20	A^L_{55}	28	60	93	122	150	168	204	232	259	288	318
21	A^{RL}_{25}	4	37	60	91	114	144	173	205	232	257	287
22	A^{RL}_{28}	14	8	-2	-3	-12	-16	-17	-17	-19	-20	-20
23	A^L_{58}	-	-	-	-	-	-	-	-	-	-	-
24	A^L_{48}	13	3	-2	-3	-12	-16	-15	-14	-11	-14	-12
25	A^{RD}_{28}	0	0	-2	2	-6	-4	-2	0	5	5	8
26	A^{RD}_{25}	8	14	16	27	23	30	37	45	53	57	64
27	A^{RT}_{28}	-	-	-	-	-	-	-	-	-	-	-
28	A^{RT}_{25}	10	-4	-18	-28	-47	-62	-68	-77	-88	-102	-110
29	A^L_{45}	6	40	67	100	130	166	197	229	261	290	323
30	A^L_{65}	-7	14	19	48	39	70	84	102	116	131	140

Table B.17: Micro Strain Data for Load Case (5) set (b)

Load Case		Cell Load at each Load Step (Kips)										
5		0	1	2	3	4	5	6	7	8	9	10
Strain		$C_1 = 2$	2.00	2.00	2.00	2.00	2.00	2.00	2.00	2.00	2.00	2.00
Line	Gage	$C_2 = 0$	0.44	0.88	1.32	1.76	2.20	2.64	3.08	3.52	3.96	4.40
#	ID	$C_3 = 0$	0.44	0.88	1.32	1.76	2.20	2.64	3.08	3.52	3.96	4.40
31	A^{L}_{68}	6	0	0	-5	-7	-10	-12	-14	-7	-8	-5
32	A^{L}_{75}	1	-23	-43	-68	-88	-112	-134	-156	-168	-189	-207
33	A^{RL}_{35}	-3	-13	-14	-23	-28	-33	-40	-47	-43	-49	-46
34	A^{L}_{78}	0	0	3	0	4	5	5	5	15	15	19
35	A^{RT}_{38}	5	5	6	3	5	5	5	4	13	13	17
36	A^{RD}_{38}	1	2	7	8	11	14	17	19	31	33	39
37	A^{RL}_{38}	7	4	4	0	0	0	0	-2	6	5	7
38	A^{RD}_{35}	3	2	4	3	4	4	3	6	14	16	19
39	A^{RT}_{35}	5	0	2	0	0	-1	-2	-2	5	5	7
40	A^{L}_{42}	1	8	16	20	27	33	38	44	57	63	71
41	A^{L}_{22}	18	4	14	18	28	31	40	47	81	92	102
42	A^{L}_{72}	-	-	-	-	-	-	-	-	-	-	-
43	A^{L}_{85}	-	-	-	-	-	-	-	-	-	-	-
44	A^{L}_{12}	15	-7	-6	-12	-16	-26	-31	-36	-20	-22	-28
45	A^{L}_{32}	15	13	29	40	53	61	75	88	121	135	147
46	A^{L}_{52}	5	3	7	-20	-103	-114	-93	-83	-91	-98	-101
47	A^{L}_{25}	19	28	53	72	95	109	133	152	195	218	239
48	A^{L}_{39}	-	-	-	-	-	-	-	-	-	-	-
49	A^{L}_{49}	-	-	-	-	-	-	-	-	-	-	-
50	A^{L}_{88}	-	-	-	-	-	-	-	-	-	-	-
51	A^{RL}_{15}	14	-21	-4	-18	-25	-28	-38	-39	17	19	20
52	A^{RD}_{15}	24	-12	5	-5	-11	-9	-15	-19	34	43	45
53	A^{RT}_{15}	31	0	20	7	7	9	7	7	64	69	73
54	A^{L}_{38}	32	3	24	24	25	32	39	40	96	102	109
55	A^{L}_{98}	28	0	14	9	14	23	17	21	77	81	86
56	A^{L}_{35}	-	-	-	-	-	-	-	-	-	-	-
57	A^{L}_{95}	29	-20	-31	-56	-76	-92	-117	-132	-98	-112	-127
58	A^{L}_{15}	44	-26	-21	-49	-72	-94	-119	-137	-105	-121	-138
59	A^{L}_{62}	40	-16	7	0	-5	-6	-22	-23	23	17	15
60	A^{L}_{82}	44	-18	3	-5	-10	-14	-25	-29	22	26	25

Table B.18: Micro Strain Data for Load Case (6) set (a)

bf Load Case		Cell Load at each Load Step (Kips)										
6		0	1	2	3	4	5	6	7	8	9	10
Strain		$C_1 = 2$	2.00	2.00	2.00	2.00	2.00	2.00	2.00	2.00	2.00	2.00
Line	Gage	$C_2 = 0$	0.44	0.88	1.32	1.76	2.20	2.64	3.08	3.52	3.96	4.40
#	ID	$C_3 = 0$	0	0	0	0	0	0	0	0	0	0
1	C^L_{19}	-6	0	5	5	5	6	5	2	0	0	0
2	C^L_{35}	-9	0	1	1	5	3	1	2	0	0	0
3	C^L_{38}	-1	4	4	7	9	10	13	13	13	12	12
4	C^L_{39}	-	-	-	-	-	-	-	-	-	-	-
5	C^L_{18}	-3	11	20	26	31	35	38	43	44	47	50
6	C^L_{29}	0	7	12	15	17	19	20	21	22	23	22
7	C^L_{28}	-4	1	11	21	29	39	47	62	71	80	88
8	C^L_{25}	-2	2	6	18	12	15	16	20	19	18	21
9	C^L_{15}	-	-	-	-	-	-	-	-	-	-	-
10	C^L_{12}	-1	-4	0	1	0	0	0	0	1	0	0
11	A^L_{19}	14	32	49	65	84	104	122	137	151	167	184
12	A^L_{29}	15	34	52	71	93	112	129	146	160	176	194
13	A^L_{59}	-10	7	17	30	47	63	78	89	101	115	129
14	A^L_{69}	12	27	40	54	69	86	100	109	122	134	144
15	A^{RL}_{18}	9	11	14	17	22	28	32	35	37	39	42
16	A^{RD}_{18}	11	8	9	10	13	15	16	16	17	17	17
17	A^{RT}_{18}	11	10	9	8	10	13	12	13	13	12	14
18	A^L_{18}	13	24	30	40	53	65	74	85	92	102	109
19	A^L_{28}	16	6	2	-2	-4	-7	-10	-13	-17	-22	-27
20	A^L_{55}	11	2	0	-6	-9	-12	-16	-21	-27	-32	-41
21	A^{RL}_{25}	3	1	-5	-15	-18	-24	-30	-36	-41	-47	-54
22	A^{RL}_{28}	8	-2	-13	-27	-34	-45	-55	-64	-72	-84	-94
23	A^L_{56}	-	-	-	-	-	-	-	-	-	-	-
24	A^L_{48}	11	-1	-14	-23	-34	-45	-54	-64	-73	-84	-95
25	A^{RD}_{28}	9	0	-6	-12	-18	-26	-32	-38	-44	-52	-57
26	A^{RD}_{25}	12	8	2	3	-3	-7	-13	-16	-20	-24	-27
27	A^{RT}_{28}	4	15	18	-5	-24	-24	0	18	22	19	29
28	A^{RT}_{25}	9	10	14	14	12	14	16	15	16	19	20
29	A^L_{45}	11	8	0	-8	-10	-18	-20	-25	-31	-35	-43
30	A^L_{65}	-	-	-	-	-	-	-	-	-	-	-

Table B.19: Micro Strain Data for Load Case (6) set (b)

Load Case		Cell Load at each Load Step (Kips)										
6		0	1	2	3	4	5	6	7	8	9	10
Strain		$C_1 = 2$	2.00	2.00	2.00	2.00	2.00	2.00	2.00	2.00	2.00	2.00
Line	Gage	$C_2 = 0$	0.44	0.88	1.32	1.76	2.20	2.64	3.08	3.52	3.96	4.40
#	ID	$C_3 = 0$	0	0	0	0	0	0	0	0	0	0
31	A^{L}_{68}	7	2	-1	-8	-14	-19	-26	-31	-36	-41	-47
32	A^{L}_{75}	13	17	23	28	32	37	43	46	52	58	64
33	A^{RL}_{35}	0	0	3	3	0	3	0	3	4	5	6
34	A^{L}_{78}	8	20	26	33	40	48	55	62	69	76	84
35	A^{RT}_{38}	5	7	7	8	8	8	7	8	8	8	8
36	A^{RD}_{38}	9	15	16	17	18	20	20	22	23	24	25
37	A^{RP}_{38}	8	12	12	14	13	14	14	15	15	16	17
38	A^{RD}_{35}	6	9	10	13	12	14	14	16	17	19	20
39	A^{RT}_{35}	7	11	11	11	11	11	10	11	11	11	11
40	A^{L}_{42}	9	11	11	10	9	9	9	7	7	6	6
41	A^{L}_{22}	3	6	5	5	3	0	2	0	0	0	-1
42	A^{L}_{72}	-	-	-	-	-	-	-	-	-	-	-
43	A^{L}_{85}	-	-	-	-	-	-	-	-	-	-	-
44	A^{L}_{12}	4	9	9	11	10	11	13	14	14	16	17
45	A^{L}_{32}	7	9	8	8	7	5	6	5	4	3	2
46	A^{L}_{52}	-1	8	-18	-3	-20	-26	-20	-4	-2	4	2
47	A^{L}_{25}	6	5	0	-3	-6	-12	-11	-15	-18	-23	-26
48	A^{L}_{39}	-	-	-	-	-	-	-	-	-	-	-
49	A^{L}_{49}	-	-	-	-	-	-	-	-	-	-	-
50	A^{L}_{88}	-	-	-	-	-	-	-	-	-	-	-
51	A^{RL}_{15}	11	19	17	20	16	19	26	24	23	24	30
52	A^{RD}_{15}	10	20	15	17	10	15	18	13	11	10	15
53	A^{RT}_{15}	7	18	14	15	10	11	15	11	9	7	11
54	A^{L}_{38}	7	26	30	40	44	53	67	72	77	85	97
55	A^{L}_{98}	10	29	33	44	48	58	72	76	83	91	104
56	A^{L}_{35}	12	20	19	25	30	27	37	42	47	53	62
57	A^{L}_{95}	19	28	28	35	34	39	48	51	55	60	68
58	A^{L}_{15}	8	17	17	24	25	31	40	44	48	53	62
59	A^{L}_{62}	4	14	10	13	9	11	15	14	13	13	16
60	A^{L}_{82}	7	16	14	16	12	14	19	18	17	17	20

Table B.20: Micro Strain Data for Load Case (7) set (a)

Load Case		Cell Load at each Load Step (Kips)										
7		0	1	2	3	4	5	6	7	8	9	10
Strain		$C_1 = 2$	2.00	2.00	2.00	2.00	2.00	2.00	2.00	2.00	2.00	2.00
Line	Gage	$C_2 = 0$	0.44	0.88	1.32	1.76	2.20	2.64	3.08	3.52	3.96	4.40
#	ID	$C_3 = 0$	0.44	0.88	1.32	1.76	2.20	2.64	3.08	3.52	3.96	4.40
1	C^L_{19}	-6	0	-2	-3	-5	-5	-5	-6	-7	-1	-8
2	C^L_{35}	-2	-9	-13	-12	-14	-17	-20	-21	-21	-27	-28
3	C^L_{38}	-1	0	0	0	0	2	0	-1	-5	-5	-4
4	C^L_{39}	-	-	-	-	-	-	-	-	-	-	-
5	C^L_{18}	0	14	26	29	32	35	32	32	37	36	41
6	C^L_{29}	-8	4	10	11	13	13	13	12	11	13	4
7	C^L_{28}	-1	-10	-14	-4	2	10	57	64	68	70	77
8	C^L_{25}	1	-7	-14	-16	-20	-20	-27	-29	-37	-36	-40
9	C^L_{15}	-	-	-	-	-	-	-	-	-	-	-
10	C^L_{12}	-4	-5	-7	-8	-10	-13	-14	-16	-19	-21	-26
11	A^L_{19}	3	46	72	101	127	153	174	192	215	237	261
12	A^L_{29}	3	45	69	95	117	141	160	175	198	219	245
13	A^L_{59}	3	35	55	72	91	107	121	130	148	163	182
14	A^L_{69}	2	33	53	69	92	109	123	134	150	166	186
15	A^{RL}_{18}	0	14	15	18	21	22	19	13	14	14	16
16	A^{RD}_{18}	1	19	24	30	35	39	40	35	40	42	48
17	A^{RT}_{18}	2	12	14	13	13	13	8	-1	-1	-5	-3
18	A^L_{18}	-1	20	24	31	40	44	44	44	50	52	60
19	A^L_{28}	5	11	9	7	4	1	-9	-18	-22	-25	-27
20	A^L_{55}	3	27	38	50	60	71	78	81	90	99	110
21	A^{RL}_{25}	8	28	37	46	57	71	80	91	104	114	126
22	A^{RL}_{28}	1	0	-12	-18	-30	-38	-42	-50	-56	-65	-72
23	A^L_{58}	-	-	-	-	-	-	-	-	-	-	-
24	A^L_{48}	9	3	-3	-10	-22	-32	-39	-47	-54	-62	-68
25	A^{RD}_{28}	15	9	3	0	-10	-15	-19	-24	-28	-33	-38
26	A^{RD}_{25}	6	8	6	5	0	-3	-3	-5	-5	-6	-8
27	A^{RT}_{28}	-16	-54	-46	-41	-63	-47	-43	-44	-31	-29	-30
28	A^{RT}_{25}	1	2	-4	-9	-22	-29	-33	-37	-44	-48	-53
29	A^L_{45}	9	33	49	62	76	86	100	111	126	139	145
30	A^L_{65}	-1	13	12	15	34	43	45	55	56	63	62

Table B.21: Micro Strain Data for Load Case (7) set (b)

Load Case		Cell Load at each Load Step (Kips)										
7		0	1	2	3	4	5	6	7	8	9	10
Strain		$C_1 = 2$	2.00	2.00	2.00	2.00	2.00	2.00	2.00	2.00	2.00	2.00
Line	Gage	$C_2 = 0$	0.44	0.88	1.32	1.76	2.20	2.64	3.08	3.52	3.96	4.40
#	ID	$C_3 = 0$	0.44	0.88	1.32	1.76	2.20	2.64	3.08	3.52	3.96	4.40
31	A^L_{68}	3	12	9	6	2	-4	-7	-11	-17	-22	-27
32	A^L_{75}	5	10	4	-1	-8	-18	-25	-33	-42	-51	-58
33	A^{RL}_{35}	5	15	15	16	13	10	8	4	0	-2	-5
34	A^L_{78}	7	25	32	38	43	48	5	54	59	63	68
35	A^{RT}_{38}	-1	10	12	15	15	13	16	16	14	14	14
36	A^{RD}_{38}	8	21	26	30	35	36	41	45	47	50	53
37	A^{RL}_{38}	6	14	16	18	18	18	18	19	18	19	18
38	A^{RD}_{35}	6	16	20	22	23	23	25	26	26	26	27
39	A^{RT}_{35}	8	18	19	20	20	19	20	20	18	17	17
40	A^L_{42}	4	18	21	24	26	27	30	31	31	32	34
41	A^L_{22}	9	20	23	25	26	25	26	26	27	28	28
42	A^L_{72}	-	-	-	-	-	-	-	-	-	-	-
43	A^L_{85}	-	-	-	-	-	-	-	-	-	-	-
44	A^L_{12}	7	20	22	24	23	22	22	21	22	20	19
45	A^L_{32}	7	22	27	31	33	36	40	42	46	49	51
46	A^L_{52}	-5	4	2	-3	-2	-2	-32	-16	-6	-9	-15
47	A^L_{25}	9	31	39	49	58	66	76	84	93	101	109
48	A^L_{39}	-	-	-	-	-	-	-	-	-	-	-
49	A^L_{49}	-	-	-	-	-	-	-	-	-	-	-
50	A^L_{88}	-	-	-	-	-	-	-	-	-	-	-
51	A^{RL}_{15}	9	17	23	14	12	14	16	18	15	14	13
52	A^{RD}_{15}	2	5	7	-1	-6	-7	-8	-10	-14	-18	-21
53	A^{RT}_{15}	5	12	18	12	10	12	14	16	13	12	12
54	A^L_{38}	-6	12	26	28	34	45	55	62	68	75	79
55	A^L_{98}	0	15	26	26	30	38	46	53	57	63	65
56	A^L_{35}	10	3	10	-3	-9	-18	-26	-33	-45	-59	-66
57	A^L_{95}	2	5	3	-9	-18	-24	-29	-37	-46	-53	-64
58	A^L_{15}	3	6	4	-8	-18	-24	-31	-39	-48	-56	-67
59	A^L_{62}	4	12	16	11	8	10	12	11	9	8	4
60	A^L_{82}	7	16	21	15	12	14	16	15	13	12	9

Table B.22: Regression Results for Dial Gage Data at Load Case (1)

Load Case 1		a	b	r^2	σ_e	ϕ^*	Error
Sec. #	Gage ID	N	$\frac{N}{10^{-2}mm}$	-	$10^{-2}mm$	$10^{-2}mm$	%
1	ϕ_{B1}	7806	1242	0.996	0.3	15	6
	ϕ_{F1}	2196	-2892	0.976	0.3	-7	15
2	ϕ_{B2}	901	269	0.999	0.7	71	3
	ϕ_{D2}	392	392	1.000	0.0	49	0
	ϕ_{F2}	392	653	1.000	0.0	29	0
5	ϕ_{B5}	359	137	1.000	0.8	140	2
	ϕ_{C5}	414	157	1.000	0.5	122	1
	ϕ_{D5}	319	195	1.000	0.7	99	2
	ϕ_{E5}	-132	246	1.000	0.3	78	1
	ϕ_{F5}	-118	307	1.000	0.3	62	2
	ψ_{T5}	3931	723	0.998	0.4	27	4
	ψ_{B5}	-10973	-2544	0.984	0.3	-8	12
8	ϕ_{B8}	1067	372	1.000	0.4	51	2
	ϕ_{D8}	-189	1170	0.996	0.3	16	6
	ϕ_{F8}	9265	-997	0.688	3.5	-19	55
9	ϕ_{B9}	969	408	0.999	0.4	47	2
	ϕ_{F9}	5204	-1083	0.996	0.4	-18	7
	ψ_{T9}	8668	674	0.999	0.3	28	3
	ψ_{B9}	22244	2053	0.991	0.3	9	9
13	ϕ_{B13}	282	113	1.000	0.9	170	2
	ϕ_{C13}	125	124	0.999	1.9	154	4
	ϕ_{D13}	-61	142	1.000	0.7	135	2
	ϕ_{E13}	-186	171	1.000	0.7	112	2
	ψ_{F13}	-327	204	1.000	0.6	94	2

Table B.23: Regression Results for Dial Gage Data at Load Case (2)

Load Case 2		a	b	r^2	σ_c	ϕ^*	Error
Sec. #	Gage ID	N	$\frac{N}{10^{-2}mm}$	-	$10^{-2}mm$	$10^{-2}mm$	%
1	ϕ_{B1}	-2385	883	0.992	0.4	22	5
	ϕ_{F1}	392	-979	1.000	0.0	-20	0
2	ϕ_{B2}	209	233	0.999	0.4	82	1
	ϕ_{D2}	392	392	1.000	0.0	49	0
	ϕ_{F2}	392	979	1.000	0.0	20	0
5	ϕ_{B5}	384	85	1.000	0.5	224	1
	ϕ_{C5}	362	100	1.000	0.3	191	0
	ϕ_{D5}	406	126	1.000	0.5	152	1
	ϕ_{E5}	-9	176	0.999	0.6	109	2
	ϕ_{F5}	-80	254	0.998	0.6	76	2
	ψ_{T5}	1679	376	0.999	0.4	51	2
	ψ_{B5}	-3524	-1958	1.000	0.0	-10	0
8	ϕ_{B8}	217	135	1.000	0.3	142	1
	ϕ_{D8}	0	392	1.000	0.0	49	0
	ϕ_{F8}	1074	-742	0.947	1.1	-26	13
9	ϕ_{B9}	346	157	1.000	0.3	122	1
	ϕ_{F9}	890	-407	0.998	0.4	-47	2
	ψ_{T9}	3831	283	0.998	0.6	68	3
	ψ_{B9}	12139	979	1.000	0.0	20	0
13	ϕ_{B13}	182	70	0.999	1.9	274	2
	ϕ_{C13}	208	80	1.000	0.3	240	0
	ϕ_{D13}	211	95	1.000	0.5	201	1
	ϕ_{E13}	95	124	1.000	0.4	155	1
	ψ_{F13}	122	159	1.000	0.3	121	1

Table B.24: Regression Results for Dial Gage Data at Load Case (3)

Load Case 3		a	b	r^2	σ_e	ϕ^*	Error
Sec. #	Gage ID	N	$\frac{N}{10^{-2}mm}$	-	$10^{-2}mm$	$10^{-2}mm$	%
1	ϕ_{B1}	8370	1395	0.492	3.2	14	70
	ϕ_{F1}	-191	-4935	0.932	0.3	-4	26
2	ϕ_{B2}	211	274	1.000	0.3	70	1
	ϕ_{D2}	120	345	1.000	0.4	56	2
	ϕ_{F2}	260	434	0.999	0.5	44	3
5	ϕ_{B5}	83	97	1.000	0.8	198	1
	ϕ_{C5}	187	105	1.000	1.2	184	2
	ϕ_{D5}	136	117	1.000	0.8	163	2
	ϕ_{E5}	50	132	1.000	0.7	145	2
	ϕ_{F5}	117	148	1.000	0.6	130	1
	ψ_{T5}	1603	838	0.997	0.4	23	6
	ψ_{B5}	-1607	-1467	0.995	0.3	-13	7
8	ϕ_{B8}	84	221	1.000	0.3	87	1
	ϕ_{D8}	-226	360	0.999	0.5	53	3
	ϕ_{F8}	-687	611	0.998	0.4	31	4
9	ϕ_{B9}	-26	643	0.999	0.3	30	3
	ϕ_{F9}	108	-1435	0.991	0.4	-13	9
	ψ_{T9}	1371	979	1.000	0.0	20	0
	ψ_{B9}	931	2923	0.932	0.6	7	26
13	ϕ_{B13}	61	-424	0.994	1.1	-45	8
	ϕ_{C13}	716	-348	0.998	0.8	-55	5
	ϕ_{D13}	115	-336	0.990	1.8	-57	10
	ϕ_{E13}	497	-305	1.000	0.4	-63	2
	ψ_{F13}	186	-284	1.000	0.3	-68	1

Table B.25: Regression Results for Dial Gage Data at Load Case (4)

Load Case 4		a	b	r^2	σ_e	ϕ^*	Error
Sec. #	Gage ID	N	$\frac{N}{10^{-2}mm}$	-	$10^{-2}mm$	$10^{-2}mm$	%
1	ϕ_{B1}	-903	1699	0.994	0.3	11	8
	ϕ_{F1}	1093	-2142	0.988	0.3	-9	11
2	ϕ_{B2}	-70	411	1.000	0.3	47	2
	ϕ_{D2}	-359	666	0.996	0.6	29	7
	ϕ_{F2}	-532	1344	0.994	0.4	14	7
5	ϕ_{B5}	478	147	0.999	1.2	131	3
	ϕ_{C5}	500	171	0.999	0.9	112	2
	ϕ_{D5}	262	215	0.999	1.1	89	4
	ϕ_{E5}	-152	284	1.000	0.5	68	2
	ϕ_{F5}	-408	392	0.999	0.5	49	3
	ψ_{T5}	743	647	0.983	1.3	30	13
	ψ_{B5}	0	-3720	0.875	0.6	-5	35
8	ϕ_{B8}	-155	242	1.000	0.3	79	1
	ϕ_{D8}	-397	632	0.999	0.3	30	3
	ϕ_{F8}	3375	-1730	0.894	1.2	-11	32
9	ϕ_{B9}	-119	309	1.000	0.4	62	2
	ϕ_{F9}	-310	-786	0.992	0.7	-24	9
	ψ_{T9}	-6762	551	0.999	0.4	35	4
	ψ_{B9}	-23398	1838	0.979	0.5	10	14
13	ϕ_{B13}	53	200	0.987	3.6	96	11
	ϕ_{C13}	-287	263	1.000	0.5	73	2
	ϕ_{D13}	-74	334	1.000	0.3	57	1
	ϕ_{E13}	-313	508	0.999	0.3	38	2
	ψ_{F13}	-494	821	0.996	0.5	23	6

Table B.26: Regression Results for Dial Gage Data at Load Case (5)

Load Case 5		a	b	r^2	σ_{e^*}	ϕ^*	Error
Sec. #	Gage ID	N	$\frac{N}{10^{-2}mm}$	-	$10^{-2}mm$	$10^{-2}mm$	%
1	ϕ_{B1}	1301	649	0.992	0.9	30	9
	ϕ_{F1}	-366	-2216	0.988	0.3	-9	11
2	ϕ_{B2}	212	144	1.000	0.7	133	2
	ϕ_{D2}	-75	190	1.000	0.5	101	1
	ϕ_{F2}	-312	265	1.000	0.4	72	2
5	ϕ_{B5}	-144	60	1.000	0.9	322	1
	ϕ_{C5}	-161	65	1.000	1.1	296	1
	ϕ_{D5}	-125	73	1.000	1.2	264	1
	ϕ_{E5}	-273	83	1.000	1.2	232	2
	ϕ_{F5}	-387	95	1.000	1.2	203	2
	ψ_{T5}	1490	438	0.998	0.6	44	4
	ψ_{B5}	-2966	-988	0.988	0.7	-19	11
8	ϕ_{B8}	-29	130	1.000	0.7	148	1
	ϕ_{D8}	-289	218	1.000	0.5	88	2
	ϕ_{F8}	-1573	444	0.998	0.6	43	4
9	ϕ_{B9}	404	315	0.999	0.7	61	3
	ϕ_{F9}	2772	-682	0.994	0.7	-28	7
	ψ_{T9}	-6641	527	0.998	0.6	36	5
	ψ_{B9}	-17507	1667	0.980	0.5	12	14
13	ϕ_{B13}	1669	-242	0.995	1.8	-79	7
	ϕ_{C13}	403	-221	0.999	0.9	-87	3
	ϕ_{D13}	464	-200	0.999	0.7	-96	2
	ϕ_{E13}	497	-184	0.998	1.5	-104	4
	ψ_{F13}	569	-171	0.996	2.2	-112	6

Table B.27: Regression Results for Dial Gage Data at Load Case (6)

Load Case 6		a	b	r^2	σ_e	ϕ^*	Error
Sec. #	Gage ID	N	$\frac{N}{10^{-2}mm}$	-	$10^{-2}mm$	$10^{-2}mm$	%
1	ϕ_{B1}	5566	6992	0.866	0.3	3	36
	ϕ_{F1}	-587	-3916	0.970	0.3	-5	17
2	ϕ_{B2}	442	-1178	0.995	0.4	-16	7
	ϕ_{D2}	392	-979	1.000	0.0	-20	0
	ϕ_{F2}	203	-830	0.997	0.4	-23	5
5	ϕ_{B5}	422	-339	0.999	0.5	-57	3
	ϕ_{C5}	399	-322	0.999	0.5	-60	2
	ϕ_{D5}	757	-291	0.997	1.2	-66	6
	ϕ_{E5}	566	-280	0.999	0.5	-69	2
	ϕ_{F5}	397	-269	0.999	0.5	-71	2
	ψ_{T5}	-869	2864	0.975	0.3	7	15
	ψ_{B5}	1093	2142	0.988	0.3	9	11
8	ϕ_{B8}	151	-1135	0.994	0.4	-17	7
	ϕ_{D8}	652	-625	0.999	0.3	-31	3
	ϕ_{F8}	595	-416	0.999	0.5	-46	3
9	ϕ_{B9}	661	761	0.998	0.3	25	4
	ϕ_{F9}	1371	-1530	0.994	0.3	-13	7
	ψ_{T9}	1554	1117	0.996	0.4	17	6
	ψ_{B9}	4076	3080	0.963	0.4	6	19
13	ϕ_{B13}	2254	66	0.908	29.0	292	30
	ϕ_{C13}	80	98	1.000	0.8	196	1
	ϕ_{D13}	41	108	1.000	0.6	178	1
	ϕ_{E13}	-54	122	1.000	0.5	158	1
	ψ_{F13}	64	133	1.000	0.4	144	1

Table B.28: Regression Results for Dial Gage Data at Load Case (7)

Load Case 7		a	b	r^2	σ_e	ϕ^*	Error
Sec. #	Gage ID	N	$\frac{N}{10^{-2}mm}$	-	$10^{-2}mm$	$10^{-2}mm$	%
1	ϕ_{B1}	301	1508	0.990	0.4	13	10
	ϕ_{F1}	392	-1958	1.000	0.0	-10	0
2	ϕ_{B2}	396	390	1.000	0.3	49	2
	ϕ_{D2}	162	598	0.999	0.3	32	3
	ϕ_{F2}	397	1170	0.985	0.7	16	12
5	ϕ_{B5}	-122	141	1.000	0.7	136	2
	ϕ_{C5}	-150	161	0.999	1.0	119	2
	ϕ_{D5}	79	194	0.999	1.0	99	3
	ϕ_{E5}	18	249	0.999	0.7	77	3
	ϕ_{F5}	-140	336	0.999	0.5	57	2
	ψ_{T5}	362	710	0.998	0.4	27	4
	ψ_{B5}	-2359	-2704	0.971	0.4	-7	17
8	ϕ_{B8}	-423	236	1.000	0.5	81	2
	ϕ_{D8}	-491	591	0.998	0.5	32	5
	ϕ_{F8}	2210	-2486	0.985	0.3	-8	12
9	ϕ_{B9}	-175	305	1.000	0.3	63	1
	ϕ_{F9}	763	-764	0.999	0.3	-25	4
	ψ_{T9}	21	568	0.999	0.3	34	3
	ψ_{B9}	-366	2216	0.988	0.3	9	11
13	ϕ_{B13}	-808	222	0.993	2.4	86	8
	ϕ_{C13}	-283	284	0.999	0.6	68	3
	ϕ_{D13}	-253	375	0.999	0.4	51	2
	ϕ_{E13}	-496	586	0.999	0.3	33	3
	ψ_{F13}	-1383	1130	0.997	0.3	17	5

Table B.29: Regression Results for Strain Gage Data at Load case(1) set(a)

Load Case 1		a	b	r^2	σ_e	ϵ^*	Error
Sec. #	Gage ID	N	$N/10^{-6}$	-	10^{-6}	10^{-6}	%
2	C_{12}^L	200	-372	0.997	0.9	-52	5
	A_{12}^L	390	-434	0.992	1.3	-44	9
	A_{22}^L	-1791	468	0.988	1.4	41	11
	A_{32}^L	-614	261	0.998	1.1	73	4
	A_{42}^L	-2967	558	0.994	0.9	34	8
	A_{52}^L	-1308	-299	0.976	3.2	-64	15
	A_{62}^L	3017	-411	0.983	2.0	-47	13
	A_{72}^L	-	-	-	-	-	-
	A_{82}^L	2107	-382	0.992	1.5	-50	9
5	C_{15}^L	-	-	-	-	-	-
	C_{25}^L	-169	-322	0.992	1.7	-60	9
	C_{35}^L	-1320	-572	0.992	1.0	-34	9
	A_{15}^L	945	-171	0.997	1.9	-112	5
	A_{25}^L	-1039	213	0.998	1.2	90	4
	A_{35}^L	2661	-186	0.994	2.7	-103	8
	A_{45}^L	-77	139	0.992	4.1	138	9
	A_{55}^L	-912	167	0.999	1.2	115	3
	A_{65}^L	-8681	504	0.935	3.2	38	25
	A_{75}^L	1217	-212	0.999	0.7	-90	2
	A_{85}^L	-	-	-	-	-	-
	A_{95}^L	1990	-223	0.995	2.0	-86	7
	A_{15}^{RL}	10369	-988	0.765	3.1	-19	48
	A_{15}^{RD}	9230	168	0.005	37.4	114	98
	A_{15}^{RT}	16033	-1317	0.395	3.7	-15	76
	A_{25}^{RL}	954	158	0.999	0.9	122	2
	A_{25}^{RD}	-10137	1543	0.946	0.9	12	23
	A_{25}^{RT}	748	-269	0.995	1.6	-71	7
	A_{35}^{RL}	3924	-795	0.958	1.6	-24	20
	A_{35}^{RD}	-7102	1739	0.942	0.9	11	24
	A_{35}^{RT}	6765	-2313	0.895	0.9	-8	32

Table B.30: Regression Results for Strain Gage Data at Load case(1) set(b)

Load Case 1		a	b	r^2	σ_e	ϵ^*	Error
Sec. #	Gage ID	N	$N/10^{-6}$	-	10^{-6}	10^{-6}	%
9	C_{19}^L	1002	1431	0.899	1.4	13	31
	C_{29}^L	2608	361	0.035	17.1	53	97
	C_{39}^L	-	-	-	-	-	-
	A_{19}^L	426	68	1.000	1.6	283	2
	A_{29}^L	295	67	0.999	2.2	288	2
	A_{39}^L	-	-	-	-	-	-
	A_{49}^L	-	-	-	-	-	-
	A_{59}^L	-610	82	0.999	1.8	235	2
	A_{69}^L	-311	81	0.999	1.8	236	2
8	C_{18}^L	-3888	361	0.937	4.4	53	25
	C_{28}^L	-2103	171	0.997	1.9	112	5
	C_{38}^L	105	1514	0.595	2.6	13	63
	A_{18}^L	118	146	0.999	1.2	131	3
	A_{28}^L	-6335	-234	0.943	6.4	-82	24
	A_{38}^L	-655	160	0.996	2.5	120	6
	A_{48}^L	289	-123	1.000	1.1	-155	2
	A_{58}^L	-	-	-	-	-	-
	A_{68}^L	1007	-229	0.998	1.2	-84	4
	A_{78}^L	-591	213	0.996	1.8	90	6
	A_{88}^L	-	-	-	-	-	-
	A_{98}^L	-528	169	0.994	2.8	113	7
	A_{18}^{RL}	29	462	0.991	1.3	42	9
	A_{18}^{RD}	-2293	437	0.995	1.0	44	7
	A_{18}^{RT}	-16903	3263	0.687	1.1	6	55
	A_{28}^{RL}	566	-128	1.000	0.8	-149	2
	A_{28}^{RD}	1970	-265	0.999	0.6	-72	3
	A_{28}^{RT}	-769	394	0.847	6.2	49	38
	A_{38}^{RL}	-2328	2175	0.323	2.4	9	81
	A_{38}^{RD}	-4304	1052	0.980	0.8	18	14
	A_{38}^{RT}	12139	-4895	0.273	1.1	-4	84

Table B.31: Regression Results for Strain Gage Data at Load case(2) set(a)

Load Case 2		a	b	r^2	σ_e	ϵ^*	Error
Sec. #	Gage ID	N	$N/10^{-6}$	-	10^{-6}	10^{-6}	%
2	C^L_{12}	-899	-437	0.982	1.1	-44	8
	A^L_{12}	0	0	0.000	0.0	0	0
	A^L_{22}	13506	1293	0.925	0.8	15	15
	A^L_{32}	2183	309	0.995	0.8	62	4
	A^L_{42}	5706	699	0.929	1.4	27	15
	A^L_{52}	-1095	-335	0.923	3.0	-57	16
	A^L_{62}	1304	-636	0.747	2.8	-30	28
	A^L_{72}	-	-	-	-	-	-
	A^L_{82}	670	-651	0.698	3.0	-29	31
5	C^L_{15}	-	-	-	-	-	-
	C^L_{25}	-832	-245	1.000	0.0	-78	0
	C^L_{35}	-995	-432	0.949	1.9	-44	13
	A^L_{15}	136	-143	0.990	2.5	-135	6
	A^L_{25}	1001	144	0.999	0.7	133	2
	A^L_{35}	-278	-153	0.976	3.6	-125	9
	A^L_{45}	219	87	0.998	1.7	221	2
	A^L_{55}	-478	106	1.000	0.7	180	1
	A^L_{65}	325	156	0.953	5.0	123	12
	A^L_{75}	-345	-169	0.999	0.6	-114	2
	A^L_{85}	-	-	-	-	-	-
	A^L_{95}	-398	-158	0.984	2.9	-121	7
	A^{RL}_{15}	-8801	-462	0.519	5.4	-42	39
	A^{RD}_{15}	-5114	-235	0.925	4.2	-82	15
	A^{RT}_{15}	-2614	-483	0.518	5.1	-40	39
	A^{RL}_{25}	-637	109	0.998	1.6	177	3
	A^{RD}_{25}	2431	-685	0.944	1.2	-28	13
	A^{RT}_{25}	937	-222	0.998	0.7	-86	3
	A^{RL}_{35}	-1386	-696	0.959	1.0	-28	11
	A^{RD}_{35}	3889	625	0.926	1.6	31	15
	A^{RT}_{35}	6265	0	0.000	0.0	0	0

Table B.32: Regression Results for Strain Gage Data at Load case(2) set(b)

Load Case 2		a	b	r^2	σ_e	ϵ^*	Error
Sec. #	Gage ID	N	$N/10^{-6}$	-	10^{-6}	10^{-6}	%
	C^L_{19}	10135	-509	0.806	3.1	-38	25
	C^L_{29}	7712	-73	0.004	48.8	-263	56
	C^L_{39}	-	-	-	-	-	-
	A^L_{19}	240	34	1.000	0.5	569	0
9	A^L_{29}	240	34	1.000	0.5	567	0
	A^L_{39}	-	-	-	-	-	-
	A^L_{49}	-	-	-	-	-	-
	A^L_{59}	262	46	1.000	1.5	420	1
	A^L_{69}	239	45	1.000	1.1	425	1
	C^L_{18}	1103	587	0.959	1.2	33	11
	C^L_{28}	1186	123	0.996	1.7	156	3
	C^L_{38}	640	-361	0.995	0.7	-53	4
	A^L_{18}	-710	122	1.000	0.0	157	0
	A^L_{28}	1691	-246	0.904	4.5	-78	17
	A^L_{38}	1614	129	0.983	3.6	148	7
	A^L_{48}	386	-118	0.997	1.7	-163	3
	A^L_{58}	-	-	-	-	-	-
	A^L_{68}	-716	-181	0.998	1.0	-106	3
	A^L_{78}	1332	143	0.998	1.2	135	3
	A^L_{88}	-	-	-	-	-	-
	A^L_{98}	2438	151	0.985	2.9	127	7
8							
	A^{RL}_{18}	-1650	353	0.975	1.6	54	9
	A^{RD}_{18}	-907	190	0.998	0.8	101	2
	A^{RT}_{18}	37591	-3916	0.800	0.4	-5	25
	A^{RL}_{28}	560	-114	0.997	1.8	-168	3
	A^{RD}_{28}	1193	-210	0.996	1.1	-92	4
	A^{RT}_{28}	1439	230	0.951	3.4	83	12
	A^{RL}_{38}	8351	1490	0.533	1.6	13	38
	A^{RD}_{38}	1728	247	0.995	1.0	78	4
	A^{RT}_{38}	7993	1440	0.368	2.0	13	44

Table B.33: Regression Results for Strain Gage Data at Load case(3) set(a)

Load Case 3		a	b	r^2	σ_e	ϵ^*	Error
Sec. #	Gage ID	N	$N/10^{-6}$	-	10^{-6}	10^{-6}	%
2	C_{12}^L	-3577	-833	0.925	2.1	-23	27
	A_{12}^L	21206	-975	0.909	1.9	-20	30
	A_{22}^L	-19999	1113	0.916	1.6	17	28
	A_{32}^L	-9085	436	0.989	1.5	44	10
	A_{42}^L	-11700	649	0.981	1.3	30	14
	A_{52}^L	5188	-343	0.988	2.0	-56	11
	A_{62}^L	15429	-601	0.776	4.9	-32	47
	A_{72}^L	-	-	-	-	-	-
	A_{82}^L	14541	-604	0.837	4.2	-32	40
5	C_{15}^L	-	-	-	-	-	-
	C_{25}^L	1416	-296	0.978	3.1	-65	15
	C_{35}^L	12378	-406	0.636	9.3	-47	59
	A_{15}^L	2544	-148	0.993	3.6	-129	8
	A_{25}^L	-2347	129	0.999	1.7	149	3
	A_{35}^L	3082	-127	0.987	5.7	-151	11
	A_{45}^L	-669	82	0.998	3.1	233	4
	A_{55}^L	-698	97	0.999	1.7	198	3
	A_{65}^L	-265	194	0.995	2.3	99	7
	A_{75}^L	2742	-138	0.999	1.7	-139	4
	A_{85}^L	-	-	-	-	-	-
	A_{95}^L	3881	-130	0.993	3.9	-147	8
	A_{15}^{RL}	8491	-556	0.420	8.6	-34	75
	A_{15}^{RD}	15012	-269	0.091	22.3	-71	94
	A_{15}^{RT}	17376	-401	0.148	14.5	-48	91
	A_{25}^{RL}	112	93	1.000	1.4	207	2
	A_{25}^{RD}	-2764	553	0.992	1.0	35	9
	A_{25}^{RT}	1624	-204	0.995	2.1	-94	7
	A_{35}^{RL}	8579	-600	0.957	2.2	-32	20
	A_{35}^{RD}	-17621	1645	0.107	3.6	12	93
	A_{35}^{RT}	47857	-2383	0.546	1.8	-8	66

Table B.34: Regression Results for Strain Gage Data at Load case(3) set(b)

Load Case 3		a	b	r^2	σ_e	ϵ^*	Error
Sec. #	Gage ID	N	$N/10^{-6}$	-	10^{-6}	10^{-6}	%
9	C_{19}^L	13778	-935	0.098	6.4	-21	93
	C_{29}^L	-6708	1418	0.816	1.9	14	42
	C_{39}^L	-	-	-	-	-	-
	A_{19}^L	-97	118	0.999	1.9	163	4
	A_{29}^L	-1072	119	0.998	2.4	161	4
	A_{39}^L	-	-	-	-	-	-
	A_{49}^L	-	-	-	-	-	-
	A_{59}^L	-542	161	0.998	1.9	119	5
	A_{69}^L	-1154	152	0.996	2.6	126	6
8	C_{18}^L	-2935	927	0.907	2.1	21	30
	C_{28}^L	8200	1096	0.852	2.2	17	38
	C_{38}^L	11088	-239	0.001	0.0	0	0
	A_{18}^L	4101	579	0.967	2.0	33	18
	A_{28}^L	5076	1294	0.541	3.3	15	67
	A_{38}^L	-12002	559	0.786	5.2	34	45
	A_{48}^L	5441	-743	0.991	0.8	-26	9
	A_{58}^L	-	-	-	-	-	-
	A_{68}^L	17377	-1382	0.800	2.0	-14	44
	A_{78}^L	-27331	1742	0.469	2.6	11	72
	A_{88}^L	-	-	-	-	-	-
	A_{98}^L	-5496	641	0.353	7.9	30	79
	A_{18}^{RL}	-3484	867	0.866	2.7	22	36
	A_{18}^{RD}	-2360	290	0.990	2.2	66	10
	A_{18}^{RT}	-5254	954	0.868	2.4	20	36
	A_{28}^{RL}	573	-679	0.971	1.6	-28	17
	A_{28}^{RD}	-9953	2514	0.887	0.8	8	33
	A_{28}^{RT}	10184	25	0.001	251.0	766	98
	A_{38}^{RL}	42714	-2049	0.457	2.3	-9	72
	A_{38}^{RD}	-14287	881	0.973	1.2	22	16
	A_{38}^{RT}	-19210	1298	0.844	1.9	15	39

Table B.35: Regression Results for Strain Gage Data at Load case(4) set(a)

Load Case 4		a	b	r^2	σ_e	ϵ^*	Error
Sec. #	Gage ID	N	$N/10^{-6}$	-	10^{-6}	10^{-6}	%
2	C^L_{12}	-13563	-1145	0.872	2.0	-17	35
	A^L_{12}	-103465	3560	0.705	1.0	5	53
	A^L_{22}	-31794	1245	0.983	0.7	15	13
	A^L_{32}	-21384	532	0.998	0.6	36	5
	A^L_{42}	-41797	1042	0.975	1.0	18	16
	A^L_{52}	57053	-1067	0.958	1.2	-18	20
	A^L_{62}	53022	-1312	0.353	3.9	-15	79
	A^L_{72}	-	-	-	-	-	-
	A^L_{82}	56875	-1504	0.475	3.0	-13	71
5	C^L_{15}	-	-	-	-	-	-
	C^L_{25}	3548	-461	0.967	2.5	-42	18
	C^L_{35}	-4223	-938	0.958	1.4	-20	20
	A^L_{15}	10552	-277	0.988	2.5	-69	11
	A^L_{25}	-11432	230	0.998	1.1	83	4
	A^L_{35}	7888	-277	0.915	6.6	-69	29
	A^L_{45}	-657	162	0.997	2.0	119	5
	A^L_{55}	777	177	0.999	0.9	108	3
	A^L_{65}	-3634	370	0.966	3.1	52	18
	A^L_{75}	7105	-296	0.998	1.0	-65	5
	A^L_{85}	-	-	-	-	-	-
	A^L_{95}	10561	-315	0.982	2.7	-61	13
	A^{RL}_{15}	19814	-709	0.264	7.6	-27	84
	A^{RD}_{15}	11056	-519	0.900	3.8	-37	31
	A^{RT}_{15}	30372	-858	0.308	6.1	-22	82
	A^{RL}_{25}	-1863	199	0.999	0.9	97	3
	A^{RD}_{25}	5777	-1196	0.989	0.6	-16	10
	A^{RT}_{25}	1470	-360	0.996	1.1	-53	6
	A^{RL}_{35}	9679	-926	0.917	2.0	-21	28
	A^{RD}_{35}	-74931	1975	0.868	1.2	10	36
	A^{RT}_{35}	26860	-434	0.019	14.4	-44	97

Table B.36: Regression Results for Strain Gage Data at Load case(4) set(b)

Load Case 4		a	b	r^2	σ_e	ϵ^*	Error
Sec. #	Gage ID	N	$N/10^{-6}$	-	10^{-6}	10^{-6}	%
	C^L_{19}	27744	-1998	0.860	1.2	-10	37
	C^L_{29}	-22581	1128	0.688	3.1	17	55
	C^L_{39}	-	-	-	-	-	-
	A^L_{19}	97	73	1.000	1.1	263	1
9	A^L_{29}	886	79	1.000	1.2	244	1
	A^L_{39}	-	-	-	-	-	-
	A^L_{49}	-	-	-	-	-	-
	A^L_{59}	-1171	104	1.000	1.1	184	2
	A^L_{69}	-478	110	0.919	16.3	175	28
	C^L_{18}	4994	571	0.894	3.6	34	32
	C^L_{28}	4950	278	0.989	2.4	69	10
	C^L_{38}	4285	-1042	0.942	1.5	-18	24
	A^L_{18}	1601	253	0.999	0.8	76	3
	A^L_{28}	10556	-38	0.007	163.8	-501	98
	A^L_{38}	-7942	257	0.984	3.1	75	12
	A^L_{48}	-749	-273	0.999	0.6	-70	2
	A^L_{58}	-	-	-	-	-	-
	A^L_{68}	4689	-502	0.995	0.9	-38	7
	A^L_{78}	-14218	354	0.996	1.1	54	6
	A^L_{88}	-	-	-	-	-	-
	A^L_{98}	-9580	338	0.981	2.6	57	14
8							
	A^{RL}_{18}	5397	670	0.983	1.2	29	13
	A^{RD}_{18}	2068	358	0.993	1.5	54	8
	A^{RT}_{18}	40093	3807	0.660	1.0	5	57
	A^{RL}_{28}	1953	-250	0.999	0.8	-77	3
	A^{RD}_{28}	4632	-403	0.998	0.7	-48	5
	A^{RT}_{28}	9247	127	0.193	44.6	151	88
	A^{RL}_{38}	9617	43	0.000	0.0	0	0
	A^{RD}_{38}	-25968	609	0.991	1.0	32	9
	A^{RT}_{38}	-69102	2326	0.727	1.4	8	51

Table B.37: Regression Results for Strain Gage Data at Load case(5) set(a)

Load Case 5		a	b	r^2	σ_e	ϵ^*	Error
Sec. #	Gage ID	N	$N/10^{-6}$	-	10^{-6}	10^{-6}	%
2	C_{12}^L	596	-269	0.966	4.3	-71	18
	A_{12}^L	2389	-430	0.540	9.9	-45	67
	A_{22}^L	3549	167	0.933	9.8	115	26
	A_{32}^L	1413	128	0.979	7.2	150	14
	A_{42}^L	574	281	0.988	2.4	68	11
	A_{52}^L	4449	-97	0.583	41.9	-198	64
	A_{62}^L	11320	160	0.195	35.3	120	88
	A_{72}^L	-	-	-	-	-	-
	A_{82}^L	11552	157	0.298	33.6	122	82
5	C_{15}^L	-	-	-	-	-	-
	C_{25}^L	10	-177	0.994	2.8	-108	8
	C_{35}^L	2268	-220	0.952	6.3	-87	22
	A_{15}^L	194	-124	0.850	19.6	-154	38
	A_{25}^L	450	83	0.990	7.6	232	10
	A_{35}^L	-	-	-	-	-	-
	A_{45}^L	50	62	1.000	1.9	311	2
	A_{55}^L	-1970	69	0.999	3.3	277	4
	A_{65}^L	1352	129	0.979	7.0	149	14
	A_{75}^L	-73	-95	0.996	4.0	-203	6
	A_{85}^L	-	-	-	-	-	-
	A_{95}^L	-482	-135	0.809	20.3	-142	43
	A_{15}^{RL}	12706	132	0.267	40.7	145	84
	A_{15}^{RD}	10252	162	0.474	28.1	118	71
	A_{15}^{RT}	7003	158	0.628	24.3	121	60
	A_{25}^{RL}	19	70	0.999	2.5	275	3
	A_{25}^{RD}	-1032	333	0.969	3.3	58	17
	A_{25}^{RT}	1192	-165	0.990	3.8	-116	10
	A_{35}^{RL}	-2894	-418	0.914	4.4	-46	29
	A_{35}^{RD}	5043	816	0.750	3.9	24	49
	A_{35}^{RT}	9647	1081	0.341	4.7	18	80

Table B.38: Regression Results for Strain Gage Data at Load case(5) set(b)

Load Case 5		a	b	r^2	σ_e	ϵ^*	Error
Sec. #	Gage ID	N	$N/10^{-6}$	-	10^{-6}	10^{-6}	%
9	C_{19}^L	4707	-827	0.553	5.1	-23	66
	C_{29}^L	28434	-2107	0.443	2.2	-9	73
	C_{39}^L	-	-	-	-	-	-
	A_{19}^L	-1845	94	0.995	4.5	204	7
	A_{29}^L	-1549	87	0.997	3.9	221	5
	A_{39}^L	-	-	-	-	-	-
	A_{49}^L	-	-	-	-	-	-
	A_{59}^L	-2409	112	0.996	3.4	172	6
	A_{69}^L	-2016	101	0.997	3.1	190	5
8	C_{18}^L	-456	830	0.714	4.1	23	53
	C_{28}^L	4645	1034	0.893	2.0	19	32
	C_{38}^L	5052	-1851	0.911	1.0	-10	29
	A_{18}^L	-20260	1223	0.511	3.6	16	69
	A_{28}^L	-3314	588	0.171	9.7	33	90
	A_{38}^L	4063	144	0.850	16.9	134	38
	A_{48}^L	4672	-676	0.552	6.2	-28	66
	A_{58}^L	-	-	-	-	-	-
	A_{68}^L	6455	-692	0.287	7.7	-28	83
	A_{78}^L	5472	801	0.826	3.3	24	41
	A_{88}^L	-	-	-	-	-	-
	A_{98}^L	5768	158	0.780	18.7	122	46
	A_{18}^{RL}	4287	502	0.061	12.1	38	95
	A_{18}^{RD}	-4336	270	0.983	3.1	71	13
	A_{18}^{RT}	-11002	955	0.668	3.8	20	57
	A_{28}^{RL}	4512	-563	0.827	4.6	-34	41
	A_{28}^{RD}	10635	876	0.423	5.5	22	75
	A_{28}^{RT}	-	-	-	-	-	-
	A_{38}^{RL}	9618	642	0.115	9.2	30	92
	A_{38}^{RD}	2717	466	0.949	3.1	41	22
	A_{38}^{RT}	3946	949	0.599	4.2	20	62

Table B.39: Regression Results for Strain Gage Data at Load case(6) set(a)

Load Case 6		a	b	r^2	σ_e	ϵ^*	Error
Sec. #	Gage ID	N	$N/10^{-6}$	-	10^{-6}	10^{-6}	%
	C_{12}^L	11560	2002	0.223	2.8	10	87
	A_{12}^L	-13990	2028	0.942	0.7	9	24
	A_{22}^L	15402	-2121	0.854	1.1	-9	38
	A_{32}^L	25429	-2503	0.953	0.5	-8	21
2	A_{42}^L	37819	-3042	0.951	0.5	-6	22
	A_{52}^L	12114	121	0.059	50.5	159	95
	A_{62}^L	-5509	1302	0.234	4.2	15	86
	A_{72}^L	-	-	-	-	-	-
	A_{82}^L	-13911	1538	0.405	3.2	12	76
	C_{15}^L	-	-	-	-	-	-
	C_{25}^L	-422	788	0.695	4.4	24	54
	C_{35}^L	12374	-934	0.067	6.5	-21	95
	A_{15}^L	-2376	375	0.978	2.5	51	14
	A_{25}^L	4752	-588	0.984	1.3	-33	12
	A_{35}^L	-3197	397	0.948	3.6	48	22
	A_{45}^L	4450	-369	0.988	1.8	-52	11
	A_{55}^L	4392	-418	0.978	2.3	-46	15
	A_{65}^L	-	-	-	-	-	-
	A_{75}^L	-4252	385	0.997	0.9	50	5
	A_{85}^L	392	1958	1.000	0.0	10	0
	A_{95}^L	-7591	420	0.968	2.7	46	18
5							
	A_{15}^{RL}	-12967	1107	0.665	3.3	17	57
	A_{15}^{RD}	24393	-919	0.279	5.8	-21	84
	A_{15}^{RT}	27329	-1336	0.558	3.1	-14	65
	A_{25}^{RL}	2322	-329	0.996	1.3	-58	6
	A_{25}^{RD}	6448	-486	0.988	1.4	-39	11
	A_{25}^{RT}	-15639	1787	0.807	1.5	11	43
	A_{35}^{RL}	5953	1929	0.472	2.4	10	71
	A_{35}^{RD}	-11938	1604	0.963	0.8	12	19
	A_{35}^{RT}	23016	-1088	0.003	5.8	-18	98

Table B.40: Regression Results for Strain Gage Data at Load case(6) set(b)

Load Case 6		a	b	r^2	σ_e	ϵ^*	Error
Sec. #	Gage ID	N	$N/10^{-6}$	-	10^{-6}	10^{-6}	%
9	C_{19}^L	14275	-1112	0.241	4.9	-17	86
	C_{29}^L	-7908	1071	0.862	2.2	18	37
	C_{39}^L	-	-	-	-	-	-
	A_{19}^L	-1446	115	0.998	2.3	167	4
	A_{29}^L	-1673	110	0.997	3.1	174	5
	A_{39}^L	-	-	-	-	-	-
	A_{49}^L	-	-	-	-	-	-
	A_{59}^L	1605	141	0.998	2.2	136	5
	A_{69}^L	-1862	147	0.995	2.9	130	7
8	C_{18}^L	-4768	462	0.956	2.9	42	21
	C_{28}^L	2246	199	0.997	1.6	97	5
	C_{38}^L	-2990	1459	0.781	2.0	13	46
	A_{18}^L	-2097	197	0.995	2.3	98	7
	A_{28}^L	5896	-560	0.988	1.2	-34	11
	A_{38}^L	-3301	245	0.990	2.6	78	10
	A_{48}^L	1832	-192	0.999	1.0	-100	3
	A_{58}^L	-	-	-	-	-	-
	A_{68}^L	3408	-351	0.998	0.8	-55	5
	A_{78}^L	-2890	274	1.000	0.5	70	2
	A_{88}^L	-	-	-	-	-	-
	A_{98}^L	-3698	233	0.991	2.6	82	10
	A_{18}^{RL}	-3502	529	0.978	1.8	36	15
	A_{18}^{RD}	-10484	1568	0.884	1.4	12	34
	A_{18}^{RT}	-16433	2420	0.674	1.5	8	56
	A_{28}^{RL}	1590	-195	0.998	1.6	-98	5
	A_{28}^{RD}	2491	-304	0.999	0.6	-63	3
	A_{28}^{RT}	10310	125	0.162	46.1	153	90
	A_{38}^{RL}	-38318	3484	0.906	0.6	6	30
	A_{38}^{RD}	-22922	1704	0.992	0.3	11	9
	A_{38}^{RT}	-42682	6992	0.325	0.7	3	81

Table B.41: Regression Results for Strain Gage Data at Load case(7) set(a)

Load Case 7		a	b	r^2	σ_e	ϵ^*	Error
Sec. #	Gage ID	N	$N/10^{-6}$	-	10^{-6}	10^{-6}	%
2	C^L_{12}	-972	-873	0.975	1.1	-22	15
	A^L_{12}	51201	-1862	0.225	3.0	-10	87
	A^L_{22}	-44834	2204	0.805	1.3	9	43
	A^L_{32}	-12060	616	0.993	0.8	31	8
	A^L_{42}	-19412	1116	0.946	1.3	17	23
	A^L_{52}	8657	-317	0.329	16.3	-61	81
	A^L_{62}	24974	-1368	0.538	3.1	-14	67
	A^L_{72}	-	-	-	-	-	-
	A^L_{82}	30160	-1329	0.514	3.3	-14	69
5	C^L_{15}	-	-	-	-	-	-
	C^L_{25}	-1943	-533	0.973	1.9	-36	16
	C^L_{35}	-5494	-915	0.957	1.4	-21	20
	A^L_{15}	4461	-238	0.994	2.0	-80	8
	A^L_{25}	-4625	224	0.999	0.7	86	2
	A^L_{35}	5655	-224	0.966	5.2	-86	18
	A^L_{45}	-3210	155	0.997	2.3	124	6
	A^L_{55}	-4393	221	0.988	3.2	87	11
	A^L_{65}	-81	282	0.934	5.7	68	25
	A^L_{75}	5601	-250	0.995	1.7	-77	7
	A^L_{85}	-	-	-	-	-	-
	A^L_{95}	4239	-254	0.992	2.1	-75	9
	A^{RL}_{15}	23661	-801	0.184	7.1	-24	89
	A^{RD}_{15}	6533	-634	0.956	2.1	-30	21
	A^{RT}_{15}	15618	-340	0.018	18.3	-56	97
	A^{RL}_{25}	-2187	177	0.998	1.4	108	4
	A^{RD}_{25}	10037	-1021	0.926	1.7	-19	27
	A^{RT}_{25}	2618	-308	0.980	2.9	-62	14
	A^{RL}_{35}	16670	-745	0.940	2.1	-26	24
	A^{RD}_{35}	-26580	1613	0.859	1.5	12	37
	A^{RT}_{35}	54464	-2303	0.228	2.4	-8	86

Table B.42: Regression Results for Strain Gage Data at Load case(7) set(b)

Load Case 7		a	b	r^2	σ_e	ϵ^*	Error
Sec. #	Gage ID	N	$N/10^{-6}$	-	10^{-6}	10^{-6}	%
9	C^L_{19}	5286	-1398	0.381	3.5	-14	77
	C^L_{29}	9530	157	0.009	39.9	122	98
	C^L_{39}	-	-	-	-	-	-
	A^L_{19}	-1946	83	0.996	4.5	231	6
	A^L_{29}	-2096	91	0.997	3.6	212	5
	A^L_{39}	-	-	-	-	-	-
	A^L_{49}	-	-	-	-	-	-
	A^L_{59}	-2548	124	0.995	3.4	154	7
	A^L_{69}	-2049	118	0.995	3.8	162	7
8	C^L_{18}	-10513	690	0.748	4.6	28	49
	C^L_{28}	6418	148	0.901	13.4	129	31
	C^L_{38}	8784	-1828	0.571	2.3	-10	64
	A^L_{18}	-7522	457	0.937	3.4	42	25
	A^L_{28}	8501	-385	0.955	3.4	-50	21
	A^L_{38}	-1292	257	0.987	2.7	75	11
	A^L_{48}	3232	-237	0.995	1.9	-81	7
	A^L_{58}	-	-	-	-	-	-
	A^L_{68}	8551	-442	0.992	1.2	-43	9
	A^L_{78}	2244	205	0.443	22.9	94	73
	A^L_{88}	-	-	-	-	-	-
	A^L_{98}	-2963	337	0.982	2.5	57	13
	A^{RL}_{18}	17491	-381	0.043	16.1	-50	96
	A^{RD}_{18}	-10854	625	0.848	3.9	31	38
	A^{RT}_{18}	15476	-685	0.817	3.9	-28	42
	A^{RL}_{28}	1522	-252	0.992	2.3	-76	9
	A^{RD}_{28}	5396	-372	0.991	1.6	-52	9
	A^{RT}_{28}	28796	412	0.569	10.0	47	65
	A^{RL}_{38}	-39515	2879	0.535	1.5	7	67
	A^{RD}_{38}	-10143	555	0.989	1.2	35	10
	A^{RT}_{38}	-11299	1616	0.255	3.4	12	85

Appendix C

Twin Box Girder Bridge ADINA-IN Input File

```
'PLOTSIZE'  30.0  27.5
HEAD STRING='TUNGS BRIDGE MODEL H'
MASTER ID=000000
PRINTOUT MIN
PRINTNODES 1 819 1
COORDINATES
ENTRIES NODE X Y Z
   1    453.0542   3377.7516   0.0000 /   2    456.2448   3401.5386   0.0000
   3    459.4353   3425.3256   0.0000 /   4    462.6258   3449.1125   0.0000
   5    465.8163   3472.8995   0.0000 /   6    469.0069   3496.6865   0.0000
   7    472.1974   3520.4735   0.0000 /   8    475.3879   3544.2605   0.0000
   9    478.5784   3568.0475   0.0000 /  10    481.7690   3591.8344   0.0000
  11    484.9595   3615.6214   0.0000 /  12    488.1500   3639.4084   0.0000
  13    491.3405   3663.1954   0.0000 /  14    494.5310   3686.9824   0.0000
  15    497.7216   3710.7694   0.0000 /  16    500.9121   3734.5563   0.0000
  17    504.1026   3758.3433   0.0000 /  18    459.4353   3425.3256   9.0000
  19    472.1974   3520.4735   9.0000 /  20    484.9595   3615.6214   9.0000
  21    497.7216   3710.7694   9.0000 /  22    459.4353   3425.3256  18.0000
  23    472.1974   3520.4735  18.0000 /  24    484.9595   3615.6214  18.0000
  25    497.7216   3710.7694  18.0000 /  26    459.4353   3425.3256  27.0000
  27    472.1974   3520.4735  27.0000 /  28    484.9595   3615.6214  27.0000
  29    497.7216   3710.7694  27.0000 /  30    459.4353   3425.3256  36.0000
  31    462.6258   3449.1125  36.0000 /  32    465.8163   3472.8995  36.0000
  33    469.0069   3496.6865  36.0000 /  34    472.1974   3520.4735  36.0000
  35    484.9595   3615.6214  36.0000 /  36    488.1500   3639.4084  36.0000
  37    491.3405   3663.1954  36.0000 /  38    494.5310   3686.9824  36.0000
  39    497.7216   3710.7694  36.0000 /  40    396.6981   3384.8330   0.0000
  41    399.4917   3408.6699   0.0000 /  42    402.2854   3432.5067   0.0000
  43    405.0790   3456.3436   0.0000 /  44    407.8727   3480.1804   0.0000
  45    410.6663   3504.0173   0.0000 /  46    413.4600   3527.8541   0.0000
  47    416.2536   3551.6910   0.0000 /  48    419.0473   3575.5278   0.0000
  49    421.8409   3599.3647   0.0000 /  50    424.6346   3623.2016   0.0000
  51    427.4282   3647.0384   0.0000 /  52    430.2219   3670.8753   0.0000
  53    433.0155   3694.7121   0.0000 /  54    435.8092   3718.5490   0.0000
```

55	438.6028	3742.3858	0.0000	/	56	441.3965	3766.2227	0.0000
57	402.2854	3432.5067	9.0000	/	58	413.4600	3527.8541	9.0000
59	424.6346	3623.2016	9.0000	/	60	435.8092	3718.5490	9.0000
61	402.2854	3432.5067	18.0000	/	62	413.4600	3527.8541	18.0000
63	424.6346	3623.2016	18.0000	/	64	435.8092	3718.5490	18.0000
65	402.2854	3432.5067	27.0000	/	66	413.4600	3527.8541	27.0000
67	424.6346	3623.2016	27.0000	/	68	435.8092	3718.5490	27.0000
69	402.2854	3432.5067	36.0000	/	70	405.0790	3456.3436	36.0000
71	407.8727	3480.1804	36.0000	/	72	410.6663	3504.0173	36.0000
73	413.4600	3527.8541	36.0000	/	74	424.6346	3623.2016	36.0000
75	427.4282	3647.0384	36.0000	/	76	430.2219	3670.8753	36.0000
77	433.0155	3694.7121	36.0000	/	78	435.8092	3718.5490	36.0000
79	340.2317	3390.9743	0.0000	/	80	342.6277	3414.8544	0.0000
81	345.0237	3438.7345	0.0000	/	82	347.4197	3462.6146	0.0000
83	349.8157	3486.4947	0.0000	/	84	352.2117	3510.3748	0.0000
85	354.6077	3534.2549	0.0000	/	86	357.0037	3558.1350	0.0000
87	359.3997	3582.0151	0.0000	/	88	361.7957	3605.8952	0.0000
89	364.1917	3629.7753	0.0000	/	90	366.5877	3653.6554	0.0000
91	368.9837	3677.5355	0.0000	/	92	371.3797	3701.4156	0.0000
93	373.7757	3725.2957	0.0000	/	94	376.1717	3749.1758	0.0000
95	378.5677	3773.0559	0.0000	/	96	345.0237	3438.7345	9.0000
97	354.6077	3534.2549	9.0000	/	98	364.1917	3629.7753	9.0000
99	373.7757	3725.2957	9.0000	/	100	345.0237	3438.7345	18.0000
101	354.6077	3534.2549	18.0000	/	102	364.1917	3629.7753	18.0000
103	373.7757	3725.2957	18.0000	/	104	345.0237	3438.7345	27.0000
105	354.6077	3534.2549	27.0000	/	106	364.1917	3629.7753	27.0000
107	373.7757	3725.2957	27.0000	/	108	345.0237	3438.7345	36.0000
109	347.4197	3462.6146	36.0000	/	110	349.8157	3486.4947	36.0000
111	352.2117	3510.3748	36.0000	/	112	354.6077	3534.2549	36.0000
113	364.1917	3629.7753	36.0000	/	114	366.5877	3653.6554	36.0000
115	368.9837	3677.5355	36.0000	/	116	371.3797	3701.4156	36.0000
117	373.7757	3725.2957	36.0000	/	118	283.6708	3396.1736	0.0000
119	285.6685	3420.0903	0.0000	/	120	287.6662	3444.0070	0.0000
121	289.6639	3467.9237	0.0000	/	122	291.6616	3491.8404	0.0000
123	293.6593	3515.7571	0.0000	/	124	295.6569	3539.6739	0.0000
125	297.6546	3563.5906	0.0000	/	126	299.6523	3587.5073	0.0000
127	301.6500	3611.4240	0.0000	/	128	303.6477	3635.3407	0.0000
129	305.6453	3659.2574	0.0000	/	130	307.6430	3683.1741	0.0000
131	309.6407	3707.0909	0.0000	/	132	311.6384	3731.0076	0.0000
133	313.6361	3754.9243	0.0000	/	134	315.6338	3778.8410	0.0000
135	287.6662	3444.0070	9.0000	/	136	295.6569	3539.6739	9.0000
137	303.6477	3635.3407	9.0000	/	138	311.6384	3731.0076	9.0000
139	287.6662	3444.0070	18.0000	/	140	295.6569	3539.6739	18.0000
141	303.6477	3635.3407	18.0000	/	142	311.6384	3731.0076	18.0000
143	287.6662	3444.0070	27.0000	/	144	295.6569	3539.6739	27.0000
145	303.6477	3635.3407	27.0000	/	146	311.6384	3731.0076	27.0000
147	287.6662	3444.0070	36.0000	/	148	289.6639	3467.9237	36.0000
149	291.6616	3491.8404	36.0000	/	150	293.6593	3515.7571	36.0000
151	295.6569	3539.6739	36.0000	/	152	303.6477	3635.3407	36.0000
153	305.6453	3659.2574	36.0000	/	154	307.6430	3683.1741	36.0000
155	309.6407	3707.0909	36.0000	/	156	311.6384	3731.0076	36.0000
157	227.0312	3400.4295	0.0000	/	158	228.6300	3424.3762	0.0000
159	230.2288	3448.3229	0.0000	/	160	231.8276	3472.2696	0.0000
161	233.4264	3496.2163	0.0000	/	162	235.0252	3520.1629	0.0000
163	236.6240	3544.1096	0.0000	/	164	238.2229	3568.0563	0.0000
165	239.8217	3592.0030	0.0000	/	166	241.4205	3615.9497	0.0000
167	243.0193	3639.8964	0.0000	/	168	244.6181	3663.8431	0.0000
169	246.2169	3687.7897	0.0000	/	170	247.8157	3711.7364	0.0000
171	249.4145	3735.6831	0.0000	/	172	251.0133	3759.6298	0.0000
173	252.6122	3783.5765	0.0000	/	174	230.2288	3448.3229	9.0000
175	236.6240	3544.1096	9.0000	/	176	243.0193	3639.8964	9.0000
177	249.4145	3735.6831	9.0000	/	178	230.2288	3448.3229	18.0000
179	236.6240	3544.1096	18.0000	/	180	243.0193	3639.8964	18.0000
181	249.4145	3735.6831	18.0000	/	182	230.2288	3448.3229	27.0000

183	236.6240	3544.1096	27.0000	/	184	243.0193	3639.8964	27.0000
185	249.4145	3735.6831	27.0000	/	186	230.2288	3448.3229	36.0000
187	231.8276	3472.2696	36.0000	/	188	233.4264	3496.2163	36.0000
189	235.0252	3520.1629	36.0000	/	190	236.6240	3544.1096	36.0000
191	243.0193	3639.8964	36.0000	/	192	244.6181	3663.8431	36.0000
193	246.2169	3687.7897	36.0000	/	194	247.8157	3711.7364	36.0000
195	249.4145	3735.6831	36.0000	/	196	170.3284	3403.7409	0.0000
197	171.5279	3427.7109	0.0000	/	198	172.7274	3451.6809	0.0000
199	173.9269	3475.6509	0.0000	/	200	175.1264	3499.6209	0.0000
201	176.3259	3523.5909	0.0000	/	202	177.5254	3547.5610	0.0000
203	178.7249	3571.5310	0.0000	/	204	179.9244	3595.5010	0.0000
205	181.1239	3619.4710	0.0000	/	206	182.3234	3643.4410	0.0000
207	183.5229	3667.4110	0.0000	/	208	184.7224	3691.3810	0.0000
209	185.9219	3715.3510	0.0000	/	210	187.1214	3739.3210	0.0000
211	188.3209	3763.2910	0.0000	/	212	189.5204	3787.2610	0.0000
213	172.7274	3451.6809	9.0000	/	214	177.5254	3547.5610	9.0000
215	182.3234	3643.4410	9.0000	/	216	187.1214	3739.3210	9.0000
217	172.7274	3451.6809	18.0000	/	218	177.5254	3547.5610	18.0000
219	182.3234	3643.4410	18.0000	/	220	187.1214	3739.3210	18.0000
221	172.7274	3451.6809	27.0000	/	222	177.5254	3547.5610	27.0000
223	182.3234	3643.4410	27.0000	/	224	187.1214	3739.3210	27.0000
225	172.7274	3451.6809	36.0000	/	226	173.9269	3475.6509	36.0000
227	175.1264	3499.6209	36.0000	/	228	176.3259	3523.5909	36.0000
229	177.5254	3547.5610	36.0000	/	230	182.3234	3643.4410	36.0000
231	183.5229	3667.4110	36.0000	/	232	184.7224	3691.3810	36.0000
233	185.9219	3715.3510	36.0000	/	234	187.1214	3739.3210	36.0000
235	113.5784	3406.1069	0.0000	/	236	114.3783	3430.0935	0.0000
237	115.1781	3454.0802	0.0000	/	238	115.9779	3478.0669	0.0000
239	116.7778	3502.0535	0.0000	/	240	117.5776	3526.0402	0.0000
241	118.3775	3550.0269	0.0000	/	242	119.1773	3574.0135	0.0000
243	119.9772	3598.0002	0.0000	/	244	120.7770	3621.9869	0.0000
245	121.5769	3645.9735	0.0000	/	246	122.3767	3669.9602	0.0000
247	123.1766	3693.9469	0.0000	/	248	123.9764	3717.9335	0.0000
249	124.7763	3741.9202	0.0000	/	250	125.5761	3765.9069	0.0000
251	126.3760	3789.8935	0.0000	/	252	115.1781	3454.0802	9.0000
253	118.3775	3550.0269	9.0000	/	254	121.5769	3645.9735	9.0000
255	124.7763	3741.9202	9.0000	/	256	115.1781	3454.0802	18.0000
257	118.3775	3550.0269	18.0000	/	258	121.5769	3645.9735	18.0000
259	124.7763	3741.9202	18.0000	/	260	115.1781	3454.0802	27.0000
261	118.3775	3550.0269	27.0000	/	262	121.5769	3645.9735	27.0000
263	124.7763	3741.9202	27.0000	/	264	115.1781	3454.0802	36.0000
265	115.9779	3478.0669	36.0000	/	266	116.7778	3502.0535	36.0000
267	117.5776	3526.0402	36.0000	/	268	118.3775	3550.0269	36.0000
269	121.5769	3645.9735	36.0000	/	270	122.3767	3669.9602	36.0000
271	123.1766	3693.9469	36.0000	/	272	123.9764	3717.9335	36.0000
273	124.7763	3741.9202	36.0000	/	274	85.1906	3406.9351	0.0000
275	85.7905	3430.9276	0.0000	/	276	86.3904	3454.9201	0.0000
277	86.9904	3478.9126	0.0000	/	278	87.5903	3502.9051	0.0000
279	88.1902	3526.8976	0.0000	/	280	88.7902	3550.8901	0.0000
281	89.3901	3574.8826	0.0000	/	282	89.9900	3598.8751	0.0000
283	90.5900	3622.8676	0.0000	/	284	91.1899	3646.8601	0.0000
285	91.7898	3670.8526	0.0000	/	286	92.3898	3694.8451	0.0000
287	92.9897	3718.8376	0.0000	/	288	93.5896	3742.8301	0.0000
289	94.1896	3766.8226	0.0000	/	290	94.7895	3790.8151	0.0000
291	86.3904	3454.9201	9.0000	/	292	88.7902	3550.8901	9.0000
293	91.1899	3646.8601	9.0000	/	294	93.5896	3742.8301	9.0000
295	86.3904	3454.9201	18.0000	/	296	88.7902	3550.8901	18.0000
297	91.1899	3646.8601	18.0000	/	298	93.5896	3742.8301	18.0000
299	86.3904	3454.9201	27.0000	/	300	88.7902	3550.8901	27.0000
301	91.1899	3646.8601	27.0000	/	302	93.5896	3742.8301	27.0000
303	86.3904	3454.9201	36.0000	/	304	86.9904	3478.9126	36.0000
305	87.5903	3502.9051	36.0000	/	306	88.1902	3526.8976	36.0000
307	88.7902	3550.8901	36.0000	/	308	91.1899	3646.8601	36.0000
309	91.7898	3670.8526	36.0000	/	310	92.3898	3694.8451	36.0000

311	92.9897	3718.8376	36.0000	/	312	93.5896	3742.8301	36.0000
313	56.7968	3407.5267	0.0000	/	314	57.1968	3431.5234	0.0000
315	57.5968	3455.5200	0.0000	/	316	57.9967	3479.5167	0.0000
317	58.3967	3503.5134	0.0000	/	318	58.7967	3527.5100	0.0000
319	59.1967	3551.5067	0.0000	/	320	59.5967	3575.5034	0.0000
321	59.9966	3599.5000	0.0000	/	322	60.3966	3623.4967	0.0000
323	60.7966	3647.4934	0.0000	/	324	61.1966	3671.4900	0.0000
325	61.5965	3695.4867	0.0000	/	326	61.9965	3719.4834	0.0000
327	62.3965	3743.4800	0.0000	/	328	62.7965	3767.4767	0.0000
329	63.1965	3791.4734	0.0000	/	330	57.5968	3455.5200	9.0000
331	59.1967	3551.5067	9.0000	/	332	60.7966	3647.4934	9.0000
333	62.3965	3743.4800	9.0000	/	334	57.5968	3455.5200	18.0000
335	59.1967	3551.5067	18.0000	/	336	60.7966	3647.4934	18.0000
337	62.3965	3743.4800	18.0000	/	338	57.5968	3455.5200	27.0000
339	59.1967	3551.5067	27.0000	/	340	60.7966	3647.4934	27.0000
341	62.3965	3743.4800	27.0000	/	342	57.5968	3455.5200	36.0000
343	57.9967	3479.5167	36.0000	/	344	58.3967	3503.5134	36.0000
345	58.7967	3527.5100	36.0000	/	346	59.1967	3551.5067	36.0000
347	60.7966	3647.4934	36.0000	/	348	61.1966	3671.4900	36.0000
349	61.5965	3695.4867	36.0000	/	350	61.9965	3719.4834	36.0000
351	62.3965	3743.4800	36.0000	/	352	28.3991	3407.8817	0.0000
353	28.5991	3431.8808	0.0000	/	354	28.7991	3455.8800	0.0000
355	28.9991	3479.8792	0.0000	/	356	29.1991	3503.8783	0.0000
357	29.3991	3527.8775	0.0000	/	358	29.5991	3551.8767	0.0000
359	29.7991	3575.8758	0.0000	/	360	29.9991	3599.8750	0.0000
361	30.1991	3623.8742	0.0000	/	362	30.3991	3647.8733	0.0000
363	30.5990	3671.8725	0.0000	/	364	30.7990	3695.8717	0.0000
365	30.9990	3719.8708	0.0000	/	366	31.1990	3743.8700	0.0000
367	31.3990	3767.8692	0.0000	/	368	31.5990	3791.8683	0.0000
369	28.7991	3455.8800	9.0000	/	370	29.5991	3551.8767	9.0000
371	30.3991	3647.8733	9.0000	/	372	31.1990	3743.8700	9.0000
373	28.7991	3455.8800	18.0000	/	374	29.5991	3551.8767	18.0000
375	30.3991	3647.8733	18.0000	/	376	31.1990	3743.8700	18.0000
377	28.7991	3455.8800	27.0000	/	378	29.5991	3551.8767	27.0000
379	30.3991	3647.8733	27.0000	/	380	31.1990	3743.8700	27.0000
381	28.7991	3455.8800	36.0000	/	382	28.9991	3479.8792	36.0000
383	29.1991	3503.8783	36.0000	/	384	29.3991	3527.8775	36.0000
385	29.5991	3551.8767	36.0000	/	386	30.3991	3647.8733	36.0000
387	30.5990	3671.8725	36.0000	/	388	30.7990	3695.8717	36.0000
389	30.9990	3719.8708	36.0000	/	390	31.1990	3743.8700	36.0000
391	-0.0006	3408.0000	0.0000	/	392	-0.0006	3432.0000	0.0000
393	-0.0006	3456.0000	0.0000	/	394	-0.0006	3480.0000	0.0000
395	-0.0006	3504.0000	0.0000	/	396	-0.0006	3528.0000	0.0000
397	-0.0006	3552.0000	0.0000	/	398	-0.0006	3576.0000	0.0000
399	-0.0006	3600.0000	0.0000	/	400	-0.0006	3624.0000	0.0000
401	-0.0006	3648.0000	0.0000	/	402	-0.0006	3672.0000	0.0000
403	-0.0006	3696.0000	0.0000	/	404	-0.0006	3720.0000	0.0000
405	-0.0006	3744.0000	0.0000	/	406	-0.0006	3768.0000	0.0000
407	-0.0006	3792.0000	0.0000	/	408	-0.0006	3456.0000	9.0000
409	-0.0006	3552.0000	9.0000	/	410	-0.0006	3648.0000	9.0000
411	-0.0006	3744.0000	9.0000	/	412	-0.0006	3456.0000	18.0000
413	-0.0006	3552.0000	18.0000	/	414	-0.0006	3648.0000	18.0000
415	-0.0006	3744.0000	18.0000	/	416	-0.0006	3456.0000	27.0000
417	-0.0006	3552.0000	27.0000	/	418	-0.0006	3648.0000	27.0000
419	-0.0006	3744.0000	27.0000	/	420	-0.0006	3456.0000	36.0000
421	-0.0006	3480.0000	36.0000	/	422	-0.0006	3504.0000	36.0000
423	-0.0006	3528.0000	36.0000	/	424	-0.0006	3552.0000	36.0000
425	-0.0006	3648.0000	36.0000	/	426	-0.0006	3672.0000	36.0000
427	-0.0006	3696.0000	36.0000	/	428	-0.0006	3720.0000	36.0000
429	-0.0006	3744.0000	36.0000	/	430	-28.4002	3407.8817	0.0000
431	-28.6002	3431.8808	0.0000	/	432	-28.8002	3455.8800	0.0000
433	-29.0002	3479.8792	0.0000	/	434	-29.2002	3503.8783	0.0000
435	-29.4002	3527.8775	0.0000	/	436	-29.6002	3551.8767	0.0000
437	-29.8002	3575.8758	0.0000	/	438	-30.0002	3599.8750	0.0000

439	-30.2002	3623.8742	0.0000	/	440	-30.4002	3647.8733	0.0000
441	-30.6002	3671.8725	0.0000	/	442	-30.8002	3695.8717	0.0000
443	-31.0002	3719.8708	0.0000	/	444	-31.2002	3743.8700	0.0000
445	-31.4002	3767.8692	0.0000	/	446	-31.6003	3791.8683	0.0000
447	-28.8002	3455.8800	9.0000	/	448	-29.6002	3551.8767	9.0000
449	-30.4002	3647.8733	9.0000	/	450	-31.2002	3743.8700	9.0000
451	-28.8002	3455.8800	18.0000	/	452	-29.6002	3551.8767	18.0000
453	-30.4002	3647.8733	18.0000	/	454	-31.2002	3743.8700	18.0000
455	-28.8002	3455.8800	27.0000	/	456	-29.6002	3551.8767	27.0000
457	-30.4002	3647.8733	27.0000	/	458	-31.2002	3743.8700	27.0000
459	-28.8002	3455.8800	36.0000	/	460	-29.0002	3479.8792	36.0000
461	-29.2002	3503.8783	36.0000	/	462	-29.4002	3527.8775	36.0000
463	-29.6002	3551.8767	36.0000	/	464	-30.4002	3647.8733	36.0000
465	-30.6002	3671.8725	36.0000	/	466	-30.8002	3695.8717	36.0000
467	-31.0002	3719.8708	36.0000	/	468	-31.2002	3743.8700	36.0000
469	-56.7979	3407.5267	0.0000	/	470	-57.1979	3431.5233	0.0000
471	-57.5979	3455.5200	0.0000	/	472	-57.9979	3479.5167	0.0000
473	-58.3979	3503.5133	0.0000	/	474	-58.7978	3527.5100	0.0000
475	-59.1978	3551.5067	0.0000	/	476	-59.5978	3575.5033	0.0000
477	-59.9978	3599.5000	0.0000	/	478	-60.3978	3623.4967	0.0000
479	-60.7978	3647.4933	0.0000	/	480	-61.1978	3671.4900	0.0000
481	-61.5977	3695.4867	0.0000	/	482	-61.9977	3719.4833	0.0000
483	-62.3977	3743.4800	0.0000	/	484	-62.7977	3767.4767	0.0000
485	-63.1977	3791.4733	0.0000	/	486	-57.5979	3455.5200	9.0000
487	-59.1978	3551.5067	9.0000	/	488	-60.7978	3647.4933	9.0000
489	-62.3977	3743.4800	9.0000	/	490	-57.5979	3455.5200	18.0000
491	-59.1978	3551.5067	18.0000	/	492	-60.7978	3647.4933	18.0000
493	-62.3977	3743.4800	18.0000	/	494	-57.5979	3455.5200	27.0000
495	-59.1978	3551.5067	27.0000	/	496	-60.7978	3647.4933	27.0000
497	-62.3977	3743.4800	27.0000	/	498	-57.5979	3455.5200	36.0000
499	-57.9979	3479.5167	36.0000	/	500	-58.3979	3503.5133	36.0000
501	-58.7978	3527.5100	36.0000	/	502	-59.1978	3551.5067	36.0000
503	-60.7978	3647.4933	36.0000	/	504	-61.1978	3671.4900	36.0000
505	-61.5977	3695.4867	36.0000	/	506	-61.9977	3719.4833	36.0000
507	-62.3977	3743.4800	36.0000	/	508	-85.1917	3406.9350	0.0000
509	-85.7916	3430.9275	0.0000	/	510	-86.3916	3454.9200	0.0000
511	-86.9915	3478.9125	0.0000	/	512	-87.5914	3502.9050	0.0000
513	-88.1914	3526.8975	0.0000	/	514	-88.7913	3550.8900	0.0000
515	-89.3913	3574.8825	0.0000	/	516	-89.9912	3598.8750	0.0000
517	-90.5911	3622.8675	0.0000	/	518	-91.1911	3646.8600	0.0000
519	-91.7910	3670.8525	0.0000	/	520	-92.3910	3694.8450	0.0000
521	-92.9909	3718.8375	0.0000	/	522	-93.5909	3742.8300	0.0000
523	-94.1908	3766.8225	0.0000	/	524	-94.7907	3790.8150	0.0000
525	-86.3916	3454.9200	9.0000	/	526	-88.7913	3550.8900	9.0000
527	-91.1911	3646.8600	9.0000	/	528	-93.5909	3742.8300	9.0000
529	-86.3916	3454.9200	18.0000	/	530	-88.7913	3550.8900	18.0000
531	-91.1911	3646.8600	18.0000	/	532	-93.5909	3742.8300	18.0000
533	-86.3916	3454.9200	27.0000	/	534	-88.7913	3550.8900	27.0000
535	-91.1911	3646.8600	27.0000	/	536	-93.5909	3742.8300	27.0000
537	-86.3916	3454.9200	36.0000	/	538	-86.9915	3478.9125	36.0000
539	-87.5914	3502.9050	36.0000	/	540	-88.1914	3526.8975	36.0000
541	-88.7913	3550.8900	36.0000	/	542	-91.1911	3646.8600	36.0000
543	-91.7910	3670.8525	36.0000	/	544	-92.3910	3694.8450	36.0000
545	-92.9909	3718.8375	36.0000	/	546	-93.5909	3742.8300	36.0000
547	-113.5795	3406.1068	0.0000	/	548	-114.3794	3430.0935	0.0000
549	-115.1792	3454.0802	0.0000	/	550	-115.9791	3478.0668	0.0000
551	-116.7789	3502.0535	0.0000	/	552	-117.5788	3526.0402	0.0000
553	-118.3786	3550.0268	0.0000	/	554	-119.1785	3574.0135	0.0000
555	-119.9784	3598.0002	0.0000	/	556	-120.7782	3621.9868	0.0000
557	-121.5781	3645.9735	0.0000	/	558	-122.3779	3669.9602	0.0000
559	-123.1778	3693.9468	0.0000	/	560	-123.9776	3717.9335	0.0000
561	-124.7775	3741.9202	0.0000	/	562	-125.5773	3765.9068	0.0000
563	-126.3772	3789.8935	0.0000	/	564	-115.1792	3454.0802	9.0000
565	-118.3786	3550.0268	9.0000	/	566	-121.5781	3645.9735	9.0000

567	-124.7775	3741.9202	9.0000	/	568	-115.1792	3454.0802	18.0000
569	-118.3786	3550.0268	18.0000	/	570	-121.5781	3645.9735	18.0000
571	-124.7775	3741.9202	18.0000	/	572	-115.1792	3454.0802	27.0000
573	-118.3786	3550.0268	27.0000	/	574	-121.5781	3645.9735	27.0000
575	-124.7775	3741.9202	27.0000	/	576	-115.1792	3454.0802	36.0000
577	-115.9791	3478.0668	36.0000	/	578	-116.7789	3502.0535	36.0000
579	-117.5788	3526.0402	36.0000	/	580	-118.3786	3550.0268	36.0000
581	-121.5781	3645.9735	36.0000	/	582	-122.3779	3669.9602	36.0000
583	-123.1778	3693.9468	36.0000	/	584	-123.9776	3717.9335	36.0000
585	-124.7775	3741.9202	36.0000	/	586	-170.3296	3403.7409	0.0000
587	-171.5291	3427.7109	0.0000	/	588	-172.7286	3451.6809	0.0000
589	-173.9281	3475.6509	0.0000	/	590	-175.1276	3499.6209	0.0000
591	-176.3271	3523.5909	0.0000	/	592	-177.5266	3547.5609	0.0000
593	-178.7261	3571.5309	0.0000	/	594	-179.9256	3595.5009	0.0000
595	-181.1251	3619.4709	0.0000	/	596	-182.3246	3643.4409	0.0000
597	-183.5241	3667.4109	0.0000	/	598	-184.7236	3691.3809	0.0000
599	-185.9231	3715.3509	0.0000	/	600	-187.1226	3739.3209	0.0000
601	-188.3221	3763.2910	0.0000	/	602	-189.5216	3787.2610	0.0000
603	-172.7286	3451.6809	9.0000	/	604	-177.5266	3547.5609	9.0000
605	-182.3246	3643.4409	9.0000	/	606	-187.1226	3739.3209	9.0000
607	-172.7286	3451.6809	18.0000	/	608	-177.5266	3547.5609	18.0000
609	-182.3246	3643.4409	18.0000	/	610	-187.1226	3739.3209	18.0000
611	-172.7286	3451.6809	27.0000	/	612	-177.5266	3547.5609	27.0000
613	-182.3246	3643.4409	27.0000	/	614	-187.1226	3739.3209	27.0000
615	-172.7286	3451.6809	36.0000	/	616	-173.9281	3475.6509	36.0000
617	-175.1276	3499.6209	36.0000	/	618	-176.3271	3523.5909	36.0000
619	-177.5266	3547.5609	36.0000	/	620	-182.3246	3643.4409	36.0000
621	-183.5241	3667.4109	36.0000	/	622	-184.7236	3691.3809	36.0000
623	-185.9231	3715.3509	36.0000	/	624	-187.1226	3739.3209	36.0000
625	-227.0323	3400.4294	0.0000	/	626	-228.6311	3424.3761	0.0000
627	-230.2299	3448.3228	0.0000	/	628	-231.8287	3472.2695	0.0000
629	-233.4276	3496.2162	0.0000	/	630	-235.0264	3520.1629	0.0000
631	-236.6252	3544.1096	0.0000	/	632	-238.2240	3568.0562	0.0000
633	-239.8228	3592.0029	0.0000	/	634	-241.4217	3615.9496	0.0000
635	-243.0205	3639.8963	0.0000	/	636	-244.6193	3663.8430	0.0000
637	-246.2181	3687.7897	0.0000	/	638	-247.8169	3711.7364	0.0000
639	-249.4157	3735.6830	0.0000	/	640	-251.0146	3759.6297	0.0000
641	-252.6134	3783.5764	0.0000	/	642	-230.2299	3448.3228	9.0000
643	-236.6252	3544.1096	9.0000	/	644	-243.0205	3639.8963	9.0000
645	-249.4157	3735.6830	9.0000	/	646	-230.2299	3448.3228	18.0000
647	-236.6252	3544.1096	18.0000	/	648	-243.0205	3639.8963	18.0000
649	-249.4157	3735.6830	18.0000	/	650	-230.2299	3448.3228	27.0000
651	-236.6252	3544.1096	27.0000	/	652	-243.0205	3639.8963	27.0000
653	-249.4157	3735.6830	27.0000	/	654	-230.2299	3448.3228	36.0000
655	-231.8287	3472.2695	36.0000	/	656	-233.4276	3496.2162	36.0000
657	-235.0264	3520.1629	36.0000	/	658	-236.6252	3544.1096	36.0000
659	-243.0205	3639.8963	36.0000	/	660	-244.6193	3663.8430	36.0000
661	-246.2181	3687.7897	36.0000	/	662	-247.8169	3711.7364	36.0000
663	-249.4157	3735.6830	36.0000	/	664	-283.6719	3396.1735	0.0000
665	-285.6696	3420.0902	0.0000	/	666	-287.6673	3444.0069	0.0000
667	-289.6650	3467.9236	0.0000	/	668	-291.6627	3491.8403	0.0000
669	-293.6604	3515.7570	0.0000	/	670	-295.6581	3539.6738	0.0000
671	-297.6558	3563.5905	0.0000	/	672	-299.6535	3587.5072	0.0000
673	-301.6512	3611.4239	0.0000	/	674	-303.6488	3635.3406	0.0000
675	-305.6465	3659.2573	0.0000	/	676	-307.6442	3683.1740	0.0000
677	-309.6419	3707.0908	0.0000	/	678	-311.6396	3731.0075	0.0000
679	-313.6373	3754.9242	0.0000	/	680	-315.6350	3778.8409	0.0000
681	-287.6673	3444.0069	9.0000	/	682	-295.6581	3539.6738	9.0000
683	-303.6488	3635.3406	9.0000	/	684	-311.6396	3731.0075	9.0000
685	-287.6673	3444.0069	18.0000	/	686	-295.6581	3539.6738	18.0000
687	-303.6488	3635.3406	18.0000	/	688	-311.6396	3731.0075	18.0000
689	-287.6673	3444.0069	27.0000	/	690	-295.6581	3539.6738	27.0000
691	-303.6488	3635.3406	27.0000	/	692	-311.6396	3731.0075	27.0000
693	-287.6673	3444.0069	36.0000	/	694	-289.6650	3467.9236	36.0000

695	-291.6627	3491.8403	36.0000	/	696	-293.6604	3515.7570	36.0000
697	-295.6581	3539.6738	36.0000	/	698	-303.6488	3635.3406	36.0000
699	-305.6465	3659.2573	36.0000	/	700	-307.6442	3683.1740	36.0000
701	-309.6419	3707.0908	36.0000	/	702	-311.6396	3731.0075	36.0000
703	-340.2328	3390.9741	0.0000	/	704	-342.6288	3414.8542	0.0000
705	-345.0248	3438.7343	0.0000	/	706	-347.4208	3462.6144	0.0000
707	-349.8168	3486.4945	0.0000	/	708	-352.2128	3510.3746	0.0000
709	-354.6089	3534.2547	0.0000	/	710	-357.0049	3558.1348	0.0000
711	-359.4009	3582.0149	0.0000	/	712	-361.7969	3605.8950	0.0000
713	-364.1929	3629.7751	0.0000	/	714	-366.5889	3653.6552	0.0000
715	-368.9849	3677.5353	0.0000	/	716	-371.3809	3701.4154	0.0000
717	-373.7769	3725.2955	0.0000	/	718	-376.1729	3749.1756	0.0000
719	-378.5689	3773.0557	0.0000	/	720	-345.0248	3438.7343	9.0000
721	-354.6089	3534.2547	9.0000	/	722	-364.1929	3629.7751	9.0000
723	-373.7769	3725.2955	9.0000	/	724	-345.0248	3438.7343	18.0000
725	-354.6089	3534.2547	18.0000	/	726	-364.1929	3629.7751	18.0000
727	-373.7769	3725.2955	18.0000	/	728	-345.0248	3438.7343	27.0000
729	-354.6089	3534.2547	27.0000	/	730	-364.1929	3629.7751	27.0000
731	-373.7769	3725.2955	27.0000	/	732	-345.0248	3438.7343	36.0000
733	-347.4208	3462.6144	36.0000	/	734	-349.8168	3486.4945	36.0000
735	-352.2128	3510.3746	36.0000	/	736	-354.6089	3534.2547	36.0000
737	-364.1929	3629.7751	36.0000	/	738	-366.5889	3653.6552	36.0000
739	-368.9849	3677.5353	36.0000	/	740	-371.3809	3701.4154	36.0000
741	-373.7769	3725.2955	36.0000	/	742	-396.6992	3384.8329	0.0000
743	-399.4928	3408.6698	0.0000	/	744	-402.2865	3432.5066	0.0000
745	-405.0801	3456.3435	0.0000	/	746	-407.8738	3480.1803	0.0000
747	-410.6675	3504.0172	0.0000	/	748	-413.4611	3527.8540	0.0000
749	-416.2548	3551.6909	0.0000	/	750	-419.0484	3575.5277	0.0000
751	-421.8421	3599.3646	0.0000	/	752	-424.6357	3623.2014	0.0000
753	-427.4294	3647.0383	0.0000	/	754	-430.2231	3670.8751	0.0000
755	-433.0167	3694.7120	0.0000	/	756	-435.8104	3718.5488	0.0000
757	-438.6040	3742.3857	0.0000	/	758	-441.3977	3766.2225	0.0000
759	-402.2865	3432.5066	9.0000	/	760	-413.4611	3527.8540	9.0000
761	-424.6357	3623.2014	9.0000	/	762	-435.8104	3718.5488	9.0000
763	-402.2865	3432.5066	18.0000	/	764	-413.4611	3527.8540	18.0000
765	-424.6357	3623.2014	18.0000	/	766	-435.8104	3718.5488	18.0000
767	-402.2865	3432.5066	27.0000	/	768	-413.4611	3527.8540	27.0000
769	-424.6357	3623.2014	27.0000	/	770	-435.8104	3718.5488	27.0000
771	-402.2865	3432.5066	36.0000	/	772	-405.0801	3456.3435	36.0000
773	-407.8738	3480.1803	36.0000	/	774	-410.6675	3504.0172	36.0000
775	-413.4611	3527.8540	36.0000	/	776	-424.6357	3623.2014	36.0000
777	-427.4294	3647.0383	36.0000	/	778	-430.2231	3670.8751	36.0000
779	-433.0167	3694.7120	36.0000	/	780	-435.8104	3718.5488	36.0000
781	-453.0553	3377.7514	0.0000	/	782	-456.2459	3401.5384	0.0000
783	-459.4364	3425.3254	0.0000	/	784	-462.6269	3449.1124	0.0000
785	-465.8175	3472.8994	0.0000	/	786	-469.0080	3496.6864	0.0000
787	-472.1985	3520.4733	0.0000	/	788	-475.3891	3544.2603	0.0000
789	-478.5796	3568.0473	0.0000	/	790	-481.7701	3591.8343	0.0000
791	-484.9607	3615.6213	0.0000	/	792	-488.1512	3639.4083	0.0000
793	-491.3417	3663.1952	0.0000	/	794	-494.5322	3686.9822	0.0000
795	-497.7228	3710.7692	0.0000	/	796	-500.9133	3734.5562	0.0000
797	-504.1038	3758.3432	0.0000	/	798	-459.4364	3425.3254	9.0000
799	-472.1985	3520.4733	9.0000	/	800	-484.9607	3615.6213	9.0000
801	-497.7228	3710.7692	9.0000	/	802	-459.4364	3425.3254	18.0000
803	-472.1985	3520.4733	18.0000	/	804	-484.9607	3615.6213	18.0000
805	-497.7228	3710.7692	18.0000	/	806	-459.4364	3425.3254	27.0000
807	-472.1985	3520.4733	27.0000	/	808	-484.9607	3615.6213	27.0000
809	-497.7228	3710.7692	27.0000	/	810	-459.4364	3425.3254	36.0000
811	-462.6269	3449.1124	36.0000	/	812	-465.8175	3472.8994	36.0000
813	-469.0080	3496.6864	36.0000	/	814	-472.1985	3520.4733	36.0000
815	-484.9607	3615.6213	36.0000	/	816	-488.1512	3639.4083	36.0000
817	-491.3417	3663.1952	36.0000	/	818	-494.5322	3686.9822	36.0000
819	-497.7228	3710.7692	36.0000					

```
SHELLNODES DIRECTOR=-2 SYSTEM-D=LOCAL
3  -2 G  STEP 39 TO 783 -2 G / 30  -2 G STEP 39 TO 810  -2 G
7  -2 G  STEP 39 TO 787 -2 G / 34  -2 G STEP 39 TO 814  -2 G
11 -2 G  STEP 39 TO 791 -2 G / 35  -2 G STEP 39 TO 815  -2 G
15 -2 G  STEP 39 TO 795 -2 G / 39  -2 G STEP 39 TO 819  -2 G
MATERIAL N=1 ELASTIC E=3000.0E3  NU=0.200 D=0.0 K=.8333333
MATERIAL N=2 ELASTIC E=29000.0E3 NU=0.300 D=0.0 K=.8333333
EGROUP N=1 SHELL D=SMALL M=1 RINT=3 SINT=3 TINT=2 STR=L
THICKNESS 1    6.50
STRESSTABLE 1 17 18 19 20 21
ENODES
ENTRIES EL N3 N6 N2 N7 N13 N5 N4 N8 N1
1    1   2   3   40  41  42  79  80  81
TO
8    15  16  17  54  55  56  93  94  95
EGENERATION 9 8 78
1 TO 8
LIST ENODES 73 80
EDATA
ENTRIES EL NTH TABLE
1    1    1
TO
80   1    1
EGROUP N=2 SHELL D=SMALL M=2 RINT=3 SINT=3 TINT=2 STR=L
THICKNESS 1   0.375
THICKNESS 2   0.500
STRESSTABLE 1 17 18 19 20 21
ENODES
ENTRIES EL N3 N6 N2 N7 N13 N5 N4 N8 N1
1     22  18  3   61  57  42  100 96  81
2     30  26  22  69  65  61  108 104 100
3     30  31  32  69  70  71  108 109 110
4     32  33  34  71  72  73  110 111 112
5     34  27  23  73  66  62  112 105 101
6     23  19  7   62  58  46  101 97  85
7     24  20  11  63  59  50  102 98  89
8     35  28  24  74  67  63  113 106 102
9     35  36  37  74  75  76  113 114 115
10    37  38  39  76  77  78  115 116 117
11    39  29  25  78  68  64  117 107 103
12    25  21  15  64  60  54  103 99  93
EGENERATION 9 12 78
1 TO 12
LIST ENODES 109 120
EDATA
ENTRIES EL NTH TABLE
1     1     1 STEP 12 TO 109    1     1
2     1     1 STEP 12 TO 110    1     1
3     2     1 STEP 12 TO 111    2     1
4     2     1 STEP 12 TO 112    2     1
5     1     1 STEP 12 TO 113    1     1
6     1     1 STEP 12 TO 114    1     1
7     1     1 STEP 12 TO 115    1     1
8     1     1 STEP 12 TO 116    1     1
9     2     1 STEP 12 TO 117    2     1
10    2     1 STEP 12 TO 118    2     1
11    1     1 STEP 12 TO 119    1     1
12    1     1 STEP 12 TO 120    1     1
BOUNDARIES IDOF=001000
30  32  34  35  37  39
810 812 814 815 817 819
BOUNDARIES IDOF=100000
391 TO 429
```

```
CONSTRAINTS
1   1 1   2 -7.455502822
TO
39  1 39  2 -7.455502822
781 1 781 2 +7.455502822
TO
819 1 819 2 +7.455502822
LCASE N=1
LOADS CONCENTRATED
395  3  100000.0
LCASE N=2
LOADS CONCENTRATED
399  3  100000.0
LCASE N=3
LOADS CONCENTRATED
403  3  100000.0
FRAME
MESH NODES=10 ELEMENTS=0
ADINA
END
```

Appendix D

Four Box Girder Bridge ADINA-IN Input File

```
'PLOTSIZE'  30.0  27.5
HEAD STRING='BRIDGE MODEL E1 FINE MESH WITH DIAPH AND CENTER COL SUP.'
MASTER ID=000000
PRINTOUT MIN
PRINTNODES 1 2072 1
COORDINATES
ENTRIES NODE X Y Z
*TOP PLATE CONTROL COORDINATES.
*SECTION 1
1    -2.16142600 +14.63525448 0.120 / 757 +2.16142600 +14.63525448 0.120
3    -2.15558194 +14.59568370 0.120 / 759 +2.15558194 +14.59568370 0.120
19   -2.09714133 +14.19997585 0.120 / 775 +2.09714133 +14.19997585 0.120
21   -2.09129727 +14.16040507 0.120 / 777 +2.09129727 +14.16040507 0.120
*SECTION 2
43   -1.91577150 +14.66943269 0.120 / 715 +1.91577150 +14.66943269 0.120
63   -1.85361317 +14.19347435 0.120 / 735 +1.85361317 +14.19347435 0.120
*SECTION 8
295 -0.27443664 +14.79145431 0.120 / 463 +0.27443664 +14.79145431 0.120
315 -0.26553238 +14.31153690 0.120 / 483 +0.26553238 +14.31153690 0.120
*SECTION 9
379  0.00000000 +14.7940000  0.120 / 399  0.00000000 +14.31400000 0.120
*BOT PLATE CONTROL COORDINATES.
*SECTION 1
778 -2.15558194 +14.59568370 0.000 /1390 +2.15558194 +14.59568370 0.000
794 -2.09714133 +14.19997585 0.000 /1406 +2.09714133 +14.19997585 0.000
*SECTION 2
812 -1.91059164 +14.62976950 0.000 /1356 +1.91059164 +14.62976950 0.000
828 -1.85879303 +14.23313755 0.000 /1372 +1.85879303 +14.23313755 0.000
*SECTION 8
1016 -0.27369462 +14.75146119 0.000/1152 +0.27369462 +14.75146119 0.000
1032 -0.26627441 +14.35153002 0.000/1168 +0.26627441 +14.35153002 0.000
*SECTION 9
1084 0.00000000 +14.7540000  0.000 /1100  0.00000000 +14.35400000 0.000
```

```
*WEBS COORDINATES.
* WEB  B COORDINATES
1407 -2.15558599 14.59568280 0.090 / 1443 2.15558599 14.59568280 0.090
1408 -2.03316240 14.61323914 0.090 / 1442 2.03316240 14.61323914 0.090
1409 -1.91059595 14.62976864 0.090 / 1441 1.91059595 14.62976864 0.090
1410 -1.77481270 14.64686135 0.090 / 1440 1.77481270 14.64686135 0.090
1411 -1.63887675 14.66269383 0.090 / 1439 1.63887675 14.66269383 0.090
1412 -1.50279979 14.67726474 0.090 / 1438 1.50279979 14.67726474 0.090
1413 -1.36659352 14.69057281 0.090 / 1437 1.36659352 14.69057281 0.090
1414 -1.23026967 14.70261691 0.090 / 1436 1.23026967 14.70261691 0.090
1415 -1.09383998 14.71339599 0.090 / 1435 1.09383998 14.71339599 0.090
1416 -0.95731616 14.72290913 0.090 / 1434 0.95731616 14.72290913 0.090
1417 -0.82070998 14.73115551 0.090 / 1433 0.82070998 14.73115551 0.090
1418 -0.68403319 14.73813442 0.090 / 1432 0.68403319 14.73813442 0.090
1419 -0.54729754 14.74384525 0.090 / 1431 0.54729754 14.74384525 0.090
1420 -0.41051480 14.74828753 0.090 / 1430 0.41051480 14.74828753 0.090
1421 -0.27369674 14.75146086 0.090 / 1429 0.27369674 14.75146086 0.090
1422 -0.20527831 14.75257158 0.090 / 1428 0.20527831 14.75257158 0.090
1423 -0.13685546 14.75336497 0.090 / 1427 0.13685546 14.75336497 0.090
1424 -0.06842967 14.75384102 0.090 / 1426 0.06842967 14.75384102 0.090
1425  0.00000000 14.75400000 0.090
* WEB  C COORDINATES
1518 -2.14097589 14.49675641 0.090 / 1554 2.14097589 14.49675641 0.090
1519 -2.01938207 14.51419375 0.090 / 1553 2.01938207 14.51419375 0.090
1520 -1.89764635 14.53061123 0.090 / 1552 1.89764635 14.53061123 0.090
1521 -1.76278341 14.54758808 0.090 / 1551 1.76278341 14.54758808 0.090
1522 -1.62776880 14.56331326 0.090 / 1550 1.62776880 14.56331326 0.090
1523 -1.49261413 14.57778541 0.090 / 1549 1.49261413 14.57778541 0.090
1524 -1.35733104 14.59100328 0.090 / 1548 1.35733104 14.59100328 0.090
1525 -1.22193117 14.60296574 0.090 / 1547 1.22193117 14.60296574 0.090
1526 -1.08642616 14.61367177 0.090 / 1546 1.08642616 14.61367177 0.090
1527 -0.95082768 14.62312043 0.090 / 1545 0.95082768 14.62312043 0.090
1528 -0.81514739 14.63131091 0.090 / 1544 0.81514739 14.63131091 0.090
1529 -0.67939696 14.63824252 0.090 / 1543 0.67939696 14.63824252 0.090
1530 -0.54358807 14.64391465 0.090 / 1542 0.54358807 14.64391465 0.090
1531 -0.40773242 14.64832682 0.090 / 1541 0.40773242 14.64832682 0.090
1532 -0.27184168 14.65147864 0.090 / 1540 0.27184168 14.65147864 0.090
1533 -0.20388698 14.65258183 0.090 / 1539 0.20388698 14.65258183 0.090
1534 -0.13592788 14.65336985 0.090 / 1538 0.13592788 14.65336985 0.090
1535 -0.06796587 14.65384267 0.090 / 1537 0.06796587 14.65384267 0.090
1536  0.00000000 14.65400000 0.090
* WEB  D COORDINATES
1629 -2.12636566 14.39782908 0.090 / 1665 2.12636566 14.39782908 0.090
1630 -2.00560160 14.41514743 0.090 / 1664 2.00560160 14.41514743 0.090
1631 -1.88469662 14.43145286 0.090 / 1663 1.88469662 14.43145286 0.090
1632 -1.75075399 14.44831387 0.090 / 1662 1.75075399 14.44831387 0.090
1633 -1.61666074 14.46393173 0.090 / 1661 1.61666074 14.46393173 0.090
1634 -1.48242838 14.47830512 0.090 / 1660 1.48242838 14.47830512 0.090
1635 -1.34806848 14.49143280 0.090 / 1659 1.34806848 14.49143280 0.090
1636 -1.21359259 14.50331363 0.090 / 1658 1.21359259 14.50331363 0.090
1637 -1.07901228 14.51394659 0.090 / 1657 1.07901228 14.51394659 0.090
1638 -0.94433914 14.52333077 0.090 / 1656 0.94433914 14.52333077 0.090
1639 -0.80958474 14.53146537 0.090 / 1655 0.80958474 14.53146537 0.090
1640 -0.67476068 14.53834967 0.090 / 1654 0.67476068 14.53834967 0.090
1641 -0.53987857 14.54398309 0.090 / 1653 0.53987857 14.54398309 0.090
1642 -0.40495001 14.54836515 0.090 / 1652 0.40495001 14.54836515 0.090
1643 -0.26998661 14.55149547 0.090 / 1651 0.26998661 14.55149547 0.090
1644 -0.20249563 14.55259113 0.090 / 1650 0.20249563 14.55259113 0.090
1645 -0.13500030 14.55337377 0.090 / 1649 0.13500030 14.55337377 0.090
1646 -0.06750206 14.55384336 0.090 / 1648 0.06750206 14.55384336 0.090
1647  0.00000000 14.55400000 0.090
* WEB  E COORDINATES
1740 -2.11175556 14.29890269 0.090 / 1776 2.11175556 14.29890269 0.090
```

```
1741 -1.99182126 14.31610204 0.090 / 1775 1.99182126 14.31610204 0.090
1742 -1.87174701 14.33229545 0.090 / 1774 1.87174701 14.33229545 0.090
1743 -1.73872470 14.34904060 0.090 / 1773 1.73872470 14.34904060 0.090
1744 -1.60555278 14.36455116 0.090 / 1772 1.60555278 14.36455116 0.090
1745 -1.47224273 14.37882579 0.090 / 1771 1.47224273 14.37882579 0.090
1746 -1.33880600 14.39186326 0.090 / 1770 1.33880600 14.39186326 0.090
1747 -1.20525409 14.40366246 0.090 / 1769 1.20525409 14.40366246 0.090
1748 -1.07159847 14.41422237 0.090 / 1768 1.07159847 14.41422237 0.090
1749 -0.93785065 14.42354207 0.090 / 1767 0.93785065 14.42354207 0.090
1750 -0.80402214 14.43162077 0.090 / 1766 0.80402214 14.43162077 0.090
1751 -0.67012445 14.43845777 0.090 / 1765 0.67012445 14.43845777 0.090
1752 -0.53616911 14.44405249 0.090 / 1764 0.53616911 14.44405249 0.090
1753 -0.40216763 14.44840444 0.090 / 1763 0.40216763 14.44840444 0.090
1754 -0.26813155 14.45151325 0.090 / 1762 0.26813155 14.45151325 0.090
1755 -0.20110430 14.45260138 0.090 / 1761 0.20110430 14.45260138 0.090
1756 -0.13407272 14.45337864 0.090 / 1760 0.13407272 14.45337864 0.090
1757 -0.06703826 14.45384501 0.090 / 1759 0.06703826 14.45384501 0.090
1758  0.00000000 14.45400000 0.090
* WEB  F COORDINATES
1851 -2.09714532 14.19997536 0.090 / 1887 2.09714532 14.19997536 0.090
1852 -1.97804080 14.21705572 0.090 / 1886 1.97804080 14.21705572 0.090
1853 -1.85879728 14.23313709 0.090 / 1885 1.85879728 14.23313709 0.090
1854 -1.72669528 14.24976638 0.090 / 1884 1.72669528 14.24976638 0.090
1855 -1.59444472 14.26516963 0.090 / 1883 1.59444472 14.26516963 0.090
1856 -1.46205698 14.27934550 0.090 / 1882 1.46205698 14.27934550 0.090
1857 -1.32954344 14.29229278 0.090 / 1881 1.32954344 14.29229278 0.090
1858 -1.19691551 14.30401034 0.090 / 1880 1.19691551 14.30401034 0.090
1859 -1.06418459 14.31449719 0.090 / 1879 1.06418459 14.31449719 0.090
1860 -0.93136211 14.32375242 0.090 / 1878 0.93136211 14.32375242 0.090
1861 -0.79845949 14.33177522 0.090 / 1877 0.79845949 14.33177522 0.090
1862 -0.66548818 14.33856493 0.090 / 1876 0.66548818 14.33856493 0.090
1863 -0.53245961 14.34412093 0.090 / 1875 0.53245961 14.34412093 0.090
1864 -0.39938522 14.34844278 0.090 / 1874 0.39938522 14.34844278 0.090
1865 -0.26627647 14.35153007 0.090 / 1873 0.26627647 14.35153007 0.090
1866 -0.19971295 14.35261068 0.090 / 1872 0.19971295 14.35261068 0.090
1867 -0.13314513 14.35338256 0.090 / 1871 0.13314513 14.35338256 0.090
1868 -0.06657445 14.35384570 0.090 / 1870 0.06657445 14.35384570 0.090
1869  0.00000000 14.35400000 0.090
*DIAPHRAGMS NODAL COORDINATES
*SECTION 1 DIAPHRAGMS NODES
1962    -2.15191174    14.57095430    0.09
1963    -2.14825916    14.54622270    0.09
1964    -2.14460659    14.52149110    0.09
1965    -2.13730145    14.47202680    0.09
1966    -2.13364887    14.44729610    0.09
1967    -2.12999630    14.42256450    0.09
1968    -2.12269115    14.37310030    0.09
1969    -2.11903858    14.34836860    0.09
1970    -2.11538601    14.32363700    0.09
1971    -2.10808182    14.27417370    0.09
1972    -2.10442924    14.24944210    0.09
1973    -2.10077667    14.22470950    0.09
*
1974    -2.15191174    14.57095430    0.06
1975    -2.14825916    14.54622270    0.06
1976    -2.14460659    14.52149110    0.06
1977    -2.13730145    14.47202680    0.06
1978    -2.13364887    14.44729610    0.06
1979    -2.12999630    14.42256450    0.06
1980    -2.12269115    14.37310030    0.06
1981    -2.11903858    14.34836860    0.06
1982    -2.11538601    14.32363700    0.06
1983    -2.10808182    14.27417370    0.06
```

1984	-2.10442924	14.24944210	0.06
1985	-2.10077667	14.22470950	0.06
*			
1986	-2.15191174	14.57095430	0.03
1987	-2.14825916	14.54622270	0.03
1988	-2.14460659	14.52149110	0.03
1989	-2.13730145	14.47202680	0.03
1990	-2.13364887	14.44729610	0.03
1991	-2.12999630	14.42256450	0.03
1992	-2.12269115	14.37310030	0.03
1993	-2.11903858	14.34836860	0.03
1994	-2.11538601	14.32363700	0.03
1995	-2.10808182	14.27417370	0.03
1996	-2.10442924	14.24944210	0.03
1997	-2.10077667	14.22470950	0.03
*SECTION 9 DIAPHRAGMS NODES			
1998	0.00000000	14.72900000	0.09
1999	0.00000000	14.70400000	0.09
2000	0.00000000	14.67900000	0.09
2001	0.00000000	14.62900000	0.09
2002	0.00000000	14.60400000	0.09
2003	0.00000000	14.57900000	0.09
2004	0.00000000	14.52900000	0.09
2005	0.00000000	14.50400000	0.09
2006	0.00000000	14.47900000	0.09
2007	0.00000000	14.42900000	0.09
2008	0.00000000	14.40400000	0.09
2009	0.00000000	14.37900000	0.09
*			
2010	0.00000000	14.72900000	0.06
2011	0.00000000	14.70400000	0.06
2012	0.00000000	14.67900000	0.06
2013	0.00000000	14.62900000	0.06
2014	0.00000000	14.60400000	0.06
2015	0.00000000	14.57900000	0.06
2016	0.00000000	14.52900000	0.06
2017	0.00000000	14.50400000	0.06
2018	0.00000000	14.47900000	0.06
2019	0.00000000	14.42900000	0.06
2020	0.00000000	14.40400000	0.06
2021	0.00000000	14.37900000	0.06
*			
2022	0.00000000	14.72900000	0.03
2023	0.00000000	14.70400000	0.03
2024	0.00000000	14.67900000	0.03
2025	0.00000000	14.62900000	0.03
2026	0.00000000	14.60400000	0.03
2027	0.00000000	14.57900000	0.03
2028	0.00000000	14.52900000	0.03
2029	0.00000000	14.50400000	0.03
2030	0.00000000	14.47900000	0.03
2031	0.00000000	14.42900000	0.03
2032	0.00000000	14.40400000	0.03
2033	0.00000000	14.37900000	0.03
*SECTION 17 DIAPHRAGMS NODES			
2034	2.15193462	14.57095050	0.09
2035	2.14828205	14.54621980	0.09
2036	2.14462948	14.52148720	0.09
2037	2.13732433	14.47202400	0.09
2038	2.13367176	14.44729230	0.09
2039	2.13001919	14.42256070	0.09
2040	2.12271404	14.37309740	0.09
2041	2.11906147	14.34836480	0.09

```
2042     2.11540890    14.32363320  0.09
2043     2.10810375    14.27416990  0.09
2044     2.10445118    14.24943830  0.09
2045     2.10079861    14.22470570  0.09
*
2046     2.15193462    14.57095050  0.06
2047     2.14828205    14.54621980  0.06
2048     2.14462948    14.52148720  0.06
2049     2.13732433    14.47202400  0.06
2050     2.13367176    14.44729230  0.06
2051     2.13001919    14.42256070  0.06
2052     2.12271404    14.37309740  0.06
2053     2.11906147    14.34836480  0.06
2054     2.11540890    14.32363320  0.06
2055     2.10810375    14.27416990  0.06
2056     2.10445118    14.24943830  0.06
2057     2.10079861    14.22470570  0.06
*
2058     2.15193462    14.57095050  0.03
2059     2.14828205    14.54621980  0.03
2060     2.14462948    14.52148720  0.03
2061     2.13732433    14.47202400  0.03
2062     2.13367176    14.44729230  0.03
2063     2.13001919    14.42256070  0.03
2064     2.12271404    14.37309740  0.03
2065     2.11906147    14.34836480  0.03
2066     2.11540890    14.32363320  0.03
2067     2.10810375    14.27416990  0.03
2068     2.10445118    14.24943830  0.03
2069     2.10079861    14.22470570  0.03
*CENTER COLUMN SUPPORT NODES
2070     0.00000000    14.55400000 -0.10
2071     0.00000000    14.55400000 -0.20
2072     0.00000000    14.55400000 -0.30
2073     0.00000000    14.45400000 -0.15
*FICTIOUS CENTER OF CIRCLE NODES
3000 0.000       0.000          0.120 / 3001 0.000      0.000          0.000
*GENERATE REMAINING NODES OF WEBS
NGENERATION TIMES=2 NSTEP=37 XSTEP=0.0 YSTEP=0.0 ZSTEP=-0.030
1407 TO 1443
1518 TO 1554
1629 TO 1665
1740 TO 1776
1851 TO 1887
SHELLNODES DIRECTOR=-2 SYSTEM-D=LOCAL
3    -2 G  STEP 21 TO 759 -2 G /  778 -2 G STEP 17 TO 1390 -2 G
7    -2 G  STEP 21 TO 763 -2 G /  782 -2 G STEP 17 TO 1394 -2 G
11   -2 G  STEP 21 TO 767 -2 G /  786 -2 G STEP 17 TO 1398 -2 G
15   -2 G  STEP 21 TO 771 -2 G /  790 -2 G STEP 17 TO 1402 -2 G
19   -2 G  STEP 21 TO 775 -2 G /  794 -2 G STEP 17 TO 1406 -2 G
*
3    -2 G  STEP  1 TO  19 -2 G /  778 -2 G STEP  1 TO  794 -2 G
381 -2 G  STEP  1 TO 397 -2 G / 1084 -2 G STEP  1 TO 1100 -2 G
759 -2 G  STEP  1 TO 775 -2 G / 1390 -2 G STEP  1 TO 1406 -2 G
*
1407 -2 G STEP 37 TO 1925 -2 G
1425 -2 G STEP 37 TO 1943 -2 G
1443 -2 G STEP 37 TO 1961 -2 G
*MATERIAL ID : 1=TOP PLATE   2=BOT PLATE   3=WEBS & BEAM   4=DIAPHRAGMS
MATERIAL N=1 ELASTIC E=3.1300E10 NU=0.150 D=0.0 K=.8333333
MATERIAL N=2 ELASTIC E=7.0277E10 NU=0.379 D=0.0 K=.8333333
MATERIAL N=3 ELASTIC E=7.2000E10 NU=0.379 D=0.0 K=.8333333
MATERIAL N=4 ELASTIC E=7.200E10  NU=0.379 D=0.0 K=.8333333
```

```
*ELEMENT GROUP TYPE 1 CONCRETE DECK (TOP PLATE)
EGROUP N=1 SHELL D=SMALL M=1 RINT=3 SINT=3 TINT=2 STR=L
*LINE ARC N1 N2 NC EL MID NF NS RATIO NCOINCIDE
*LINE STR N1 N2 EL MID NF NS RATIO NCOINSIDE
*LINE COM N1 N2 I1 I2 I3 ... IN
LINE A 1    43   3000 1 1 22   21 / LINE A 21   63   3000 1 1 42   21
LINE A 43   295  3000 6 1 64   21 / LINE A 63   315  3000 6 1 84   21
LINE A 295  379  3000 2 1 316  21 / LINE A 315  399  3000 2 1 336  21
LINE A 379  463  3000 2 1 400  21 / LINE A 399  483  3000 2 1 420  21
LINE A 463  715  3000 6 1 484  21 / LINE A 483  735  3000 6 1 504  21
LINE A 715  757  3000 1 1 736  21 / LINE A 735  777  3000 1 1 756  21
LINE C 1 757 43 295 379 463 715   / LINE C 21 777 63 315 399 483 735
LINE S 1    3    1    1   2    1  / LINE S 757  759  1    1    758  1
LINE S 3    19   8    1   4    1  / LINE S 759  775  8    1    760  1
LINE S 19   21   1    1   20   1  / LINE S 775  777  1    1    776  1
LINE C 1    21   3    19          / LINE C 757  777  759 775
*GENERATE TOP PLATE ELEMENTS.
*GSURFACE N1 N2 N3 N4 EL1 EL2 MID NFIRST EFIRST
GSURFACE 1   21   777  757  10   18   9    2    1
LIST ENODES 171 180
THICKNESS 1    .020
STRESSTABLE 1 1 2 3 4 5 6 7 8 9 10 11 12 13 14 15 16
EDATA
ENTRIES EL NTH TABLE
1    1    1
TO
180  1    1
*ELEMENT GROUP TYPE 2 ALUMINUM BOT PLATE.
EGROUP N=2 SHELL D=SMALL M=2 RINT=3 SINT=3 TINT=2 STR=L
LINE A 778  812  3001 1 1 795  17 / LINE A 794  828  3001 1 1 811  17
LINE A 812  1016 3001 6 1 829  17 / LINE A 828  1032 3001 6 1 845  17
LINE A 1016 1084 3001 2 1 1033 17 / LINE A 1032 1100 3001 2 1 1049 17
LINE A 1084 1152 3001 2 1 1101 17 / LINE A 1100 1168 3001 2 1 1117 17
LINE A 1152 1356 3001 6 1 1169 17 / LINE A 1168 1372 3001 6 1 1185 17
LINE A 1356 1390 3001 1 1 1373 17 / LINE A 1372 1406 3001 1 1 1389 17
LINE C 778 1390 812 1016 1084 1152 1356
LINE C 794 1406 828 1032 1100 1168 1372
LINE S 778  794  8    1    779  1 / LINE S 1390 1406 8    1    1391 1
*GENERATE BOTTOM PLATE ELEMENTS.
*GSURFACE N1 N2 N3 N4 EL1 EL2 MID NFIRST EFIRST
GSURFACE 778  794  1406 1390  8   18   9    779  1
LIST ENODES 137 144
THICKNESS 1    .006
STRESSTABLE 1 1 2 3 4 5 6 7 8 9 10 11 12 13 14 15 16
EDATA
ENTRIES EL NTH TABLE
1    1    1
TO
144  1    1
* DELETE FICTIOUS NODES
COORDINATES
DELETE 3000 3001
*ELEMENT GROUP TYPE 3 ALUMINUM WEBS.
EGROUP N=3 SHELL D=SMALL M=3 RINT=3 SINT=3 TINT=2 STR=L
THICKNESS 1    .013
STRESSTABLE 1 1 2 3 4 5 6 7 8 9 10 11 12 13 14 15 16
ENODES
ENTRIES EL N1 N8 N4 N5 N13 N7 N2 N6 N3
1   3    24   45    1407 1408 1409 1444 1445 1446
STEP 36 TO
145 19   40   61    1851 1852 1853 1888 1889 1890
19  1444 1445 1446 1481 1482 1483 778  795  812
STEP 36 TO
```

```
163 1888 1889 1890 1925 1926 1927 794  811  828
EGENERATION TIMES=17 1 42 2 2 42 2 2 2 42 0 0 0 0 2
1    STEP 36 TO 145
EGENERATION TIMES=17 1 2 34 34 2 2 34 2 2 0 0 0 0 2
19   STEP 36 TO 163
LIST ENODES 73 108
EDATA
ENTRIES EL NTH TABLE
1    1    1
TO
180  1    1
*ELEMENT GROUP TYPE 4 ALUMINUM DIAPHRAGMS
EGROUP N=4 SHELL D=SMALL M=3 RINT=3 SINT=3 TINT=2 STR=L
THICKNESS 1     .0092
THICKNESS 2     .0083
STRESSTABLE 1 1 2 3 4 5 6 7 8 9 10 11 12 13 14 15 16
ENODES
ENTRIES EL N2 N5 N1 N6 N13 N8 N3 N7 N4
1   3    4    5    1407 1962 1963 1444 1974 1975
2   5    6    7    1963 1964 1518 1975 1976 1555
3   7    8    9    1518 1965 1966 1555 1977 1978
4   9    10   11   1966 1967 1629 1978 1979 1666
5   11   12   13   1629 1968 1969 1666 1980 1981
6   13   14   15   1969 1970 1740 1981 1982 1777
7   15   16   17   1740 1971 1972 1777 1983 1984
8   17   18   19   1972 1973 1851 1984 1985 1888
9   1444 1974 1975 1481 1986 1987 778  779  780
10  1975 1976 1555 1987 1988 1592 780  781  782
11  1555 1977 1978 1592 1989 1990 782  783  784
12  1978 1979 1666 1990 1991 1703 784  785  786
13  1666 1980 1981 1703 1992 1993 786  787  788
14  1981 1982 1777 1993 1994 1814 788  789  790
15  1777 1983 1984 1814 1995 1996 790  791  792
16  1984 1985 1888 1996 1997 1925 792  793  794
EGENERATION TIMES=2  ESTEP=16 378 378 18 36 378 18 36 36 0 0 0 0 36
1  3  5  7
EGENERATION TIMES=2  ESTEP=16 378 378 36 18 378 36 36 18 0 0 0 0 36
2  4  6  8
EGENERATION TIMES=2  ESTEP=16 36 18 306 306 36 18 306 36 0 0 0 0 36
9  11 13 15
EGENERATION TIMES=2  ESTEP=16 18 36 306 306 36 36 306 18 0 0 0 0 36
10 12 14 16
LIST ENODES 33 48
EDATA
ENTRIES EL NTH TABLE
1    1    1
TO
16   1    1
17   2    1
TO
32   2    1
33   1    1
TO
48   1    1
*EGROUP TYPE 5 ALUMINUM CENTER COLUMN SUPPORT
EGROUP N=5 ISOBEAM D=SMALL M=3
SECTION N=1 SECT1=0.0675 SECT2=0.0675
ENODES
ENTRIES EL AUX N1 N2 N3 N4
1 2073 1092 2072 2070 2071
EDATA
ENTRIES EL SECTION
1   1
```

```
* BC AT EXTREME END SUPPORTS.
BOUNDARIES IDOF=001001
780 786 792 1392 1398 1404
* BC AT CENTER COLUMN SUPPORT.
BOUNDARIES IDOF=111111
2072
LCASE N=1
LOADS CONCENTRATED
* AXLE 3 AT SECTION 4
45   3 -125.1   /48   3 -125.1   /50   3 -125.1   /53  3 -125.1
66   3 -279.9   /69   3 -279.9   /71   3 -279.9   /74  3 -279.9
87   3 -1924.7  /90   3 -1924.7  /92   3 -1924.7  /95  3 -1924.7
129  3 -1369.8  /132  3 -1369.8  /134  3 -1369.8  /137 3 -1369.8
171  3 -870.0   /174  3 -870.0   /176  3 -870.0   /179 3 -870.0
192  3 -225.6   /195  3 -225.6   /197  3 -225.6   /200 3 -225.6
* AXLE 2 AT SECTION 12
507  3 -116.1   /510  3 -125.1   /512  3 -116.1   /515  3 -116.1
528  3 -288.9   /531  3 -288.9   /533  3 -288.9   /536  3 -288.9
549  3 -1924.7  /552  3 -1924.7  /554  3 -1924.7  /557  3 -1924.7
591  3 -1369.8  /594  3 -1369.8  /596  3 -1369.8  /599  3 -1369.8
633  3 -845.9   /636  3 -845.9   /638  3 -845.9   /641  3 -845.9
654  3 -249.7   /657  3 -249.7   /659  3 -249.7   /662  3 -249.7
LCASE N=2
LOADS CONCENTRATED
* AXLE 4 AT SECTION 8
171  3 -208.5   /174  3 -208.5   /176  3 -208.5   /179  3 -208.5
192  3 -635.3   /195  3 -635.3   /197  3 -635.3   /200  3 -635.3
213  3 -1486.0  /216  3 -1486.0  /218  3 -1486.0  /221  3 -1486.0
234  3 -282.0   /237  3 -282.0   /239  3 -282.0   /242  3 -282.0
255  3 -1087.8  /258  3 -1087.8  /260  3 -1087.8  /263  3 -1087.8
297  3 -1095.6  /300  3 -1095.6  /302  3 -1095.6  /305  3 -1095.6
* AXLE 3 AT SECTION 12
465  3 -125.1   /468  3 -125.1   /470  3 -125.1   /473  3 -125.1
486  3 -279.9   /489  3 -279.9   /491  3 -279.9   /494  3 -279.9
507  3 -1924.7  /510  3 -1924.7  /512  3 -1924.7  /515  3 -1924.7
549  3 -1369.8  /552  3 -1369.8  /554  3 -1369.8  /557  3 -1369.8
591  3 -870.0   /594  3 -870.0   /596  3 -870.0   /599  3 -870.0
612  3 -225.6   /615  3 -225.6   /617  3 -225.6   /620  3 -225.6
LCASE N=3
LOADS CONCENTRATED
* AXLE 2 AT SECTION 5
129  3 -116.1   /132  3 -116.1   /134  3 -116.1   /137  3 -116.1
150  3 -288.9   /153  3 -288.9   /155  3 -288.9.  /158  3 -288.9
171  3 -1924.7  /174  3 -1924.7  /176  3 -1924.7  /179  3 -1924.7
213  3 -1369.8  /216  3 -1369.8  /218  3 -1369.8  /221  3 -1369.8
255  3 -845.9   /258  3 -845.9   /260  3 -845.9   /263  3 -845.9
276  3 -249.7   /279  3 -249.7   /281  3 -249.7   /284  3 -249.7
LCASE N=4
LOADS CONCENTRATED
* AXLE 1 AT SECTION 5
171  3 -405.0   /174  3 -405.0   /176  3 -405.0   /179  3 -405.0
192  3 -1372.8  /195  3 -1372.8  /197  3 -1372.8  /200  3 -1372.8
213  3 -551.9   /216  3 -551.9   /218  3 -551.9   /221  3 -551.9
234  3 -946.8   /237  3 -946.8   /239  3 -946.8   /242  3 -946.8
255  3 -423.8   /258  3 -423.8   /260  3 -423.8   /263  3 -423.8
276  3 -531.7   /279  3 -531.7   /281  3 -531.7   /284  3 -531.7
297  3 -563.9   /300  3 -563.9   /302  3 -563.9   /305  3 -563.9
* AXLE 1 AT 78MM FROM SECTION 9
381  3 -172.7   /384  3 -172.7   /386  3 -172.7   /389  3 -172.7
423  3 -501.2   /426  3 -501.2   /428  3 -501.2   /431  3 -501.2
465  3 -1655.8  /468  3 -1655.8  /470  3 -1655.8  /473  3 -1655.8
486  3 -161.2   /489  3 -161.2   /491  3 -161.2   /494  3 -161.2
507  3 -1208.7  /510  3 -1208.7  /512  3 -1208.7  /515  3 -1208.7
```

```
549  3 -998.9   /552  3 -998.9   /554  3 -998.9   /557  3 -998.9
570  3 -96.7    /573  3 -96.7    /575  3 -96.7    /578  3 -96.7
LCASE N=5
LOADS CONCENTRATED
* AXLE 1 AT SECTION 2
45   3 -405.0   /48   3 -408.0   /50   3 -405.0   /53   3 -405.0
66   3 -1372.8  /69   3 -1372.8  /71   3 -1372.8  /74   3 -1372.8
87   3 -551.9   /90   3 -551.9   /92   3 -551.9   /95   3 -551.9
108  3 -946.8   /111  3 -946.8   /113  3 -946.8   /116  3 -946.8
129  3 -423.8   /132  3 -423.8   /134  3 -423.8   /137  3 -423.8
150  3 -531.7   /153  3 -531.7   /155  3 -531.7   /158  3 -531.7
171  3 -629.4   /174  3 -629.4   /176  3 -629.4   /179  3 -629.4
* AXLE 1 AT 114MM FROM SECTION 5
192  3 -339.5   /195  3 -339.5   /197  3 -339.5   /200  3 -339.5
213  3 -1684.1  /216  3 -1684.1  /218  3 -1684.1  /221  3 -1684.1
234  3 -240.6   /237  3 -240.6   /239  3 -240.6   /242  3 -240.6
255  3 -1168.4  /258  3 -1168.4  /260  3 -1168.4  /263  3 -1168.4
276  3 -201.4   /279  3 -201.4   /281  3 -201.4   /284  3 -201.4
297  3 -708.9   /300  3 -708.9   /302  3 -708.9   /305  3 -708.9
339  3 -386.7   /342  3 -386.7   /344  3 -386.7   /347  3 -386.7
LCASE N=6
LOADS CONCENTRATED
* AXLE 3 AT SECTION 13
507  3 -125.1   /510  3 -125.1   /512  3 -125.1   /515  3 -125.1
528  3 -279.9   /531  3 -279.9   /533  3 -279.9   /536  3 -279.9
549  3 -1924.7  /552  3 -1924.7  /554  3 -1924.7  /557  3 -1924.7
591  3 -1369.8  /594  3 -1369.8  /596  3 -1369.8  /599  3 -1369.8
633  3 -870.0   /636  3 -870.0   /638  3 -870.0   /641  3 -870.0
654  3 -225.6   /657  3 -225.6   /659  3 -225.6   /662  3 -225.6
LCASE N=7
LOADS CONCENTRATED
* AXLE 4 AT 49MM FROM SECTION 7
129  3 -354.4   /132  3 -354.4   /134  3 -354.4   /137  3 -354.4
150  3 -1182.8  /153  3 -1182.8  /155  3 -1182.8  /158  3 -1182.8
171  3 -792.5   /174  3 -792.5   /176  3 -792.5   /179  3 -792.5
192  3 -775.6   /195  3 -775.6   /197  3 -775.6   /200  3 -775.6
213  3 -594.3   /216  3 -594.3   /218  3 -594.3   /221  3 -594.3
234  3 -394.7   /237  3 -394.7   /239  3 -394.7   /242  3 -394.7
255  3 -700.9   /258  3 -700.9   /260  3 -700.9   /263  3 -700.9
* AXLE 2 AT SECTION 10
381  3 -116.1   /384  3 -116.1   /386  3 -116.1   /389  3 -116.1
423  3 -288.9   /426  3 -288.9   /428  3 -288.9   /431  3 -288.9
465  3 -1924.7  /468  3 -1924.7  /470  3 -1924.7  /473  3 -1924.7
507  3 -1369.8  /510  3 -1369.8  /512  3 -1369.8  /515  3 -1369.8
549  3 -845.9   /552  3 -845.9   /554  3 -845.9   /557  3 -845.9
570  3 -249.7   /573  3 -249.7   /575  3 -249.7   /578  3 -249.7
FRAME
MESH NODES=0  ELEMENTS=0
LIST COORDINATES 1 2073
LIST BOUNDARIES
ADINA
END
```